DISSERTATION

CROSS-FLOW NON-EQUILIBRIUM MODEL OF AIR SPARGING, NUMERICAL AND ANALYTICAL SOLUTIONS

Submitted by

Osama S. Al-Gahtani

Department of Civil and Environmental Engineering

In partial fulfillment of the requirements

For the Degree of Doctor of Philosophy

Colorado State University

Fort Collins, Colorado

Summer 2006

COLORADO STATE UNIVERSITY

May 26, 2003

WE HEREBY RECOMMEND THAT THE DISSERTATION PREPARED UNDER OUR SUPERVISION BY OSAMA Al-GAHTANI ENTITLED CROSS-FLOW NON-EQUILIBRIUM MODEL OF AIR SPARGING, NUMERICAL AND ANALYTICAL SOLUTIONS BE ACCEPTED AS FULFILLING IN PART REQUIREMENTS FOR THE DEGREE OF DOCTOR OF PHILOSOPHY.

Committee on Graduate Work

Adviser

Department Head

ABSTRACT OF DISSERTATION

CROSS-FLOW, NON-EQUILIBRUIM MODEL OF AIR SPARGING: NUMERICAL AND ANALYTICAL SOLUTIONS

According to the Environmental Protection Agency (EPA), air sparging is the most developed innovative in-situ technology for remediation of sites which have groundwater contaminated by volatile organics. Air sparging systems are easy to implement, and relatively simple to operate. In addition, it is a relatively low cost remediation technology that can be applied in conjunction with other remediation technologies. For these reasons, air sparging has become widely used. However, air sparging is still considered as an unproven technology by the EPA. The objective of this study is to investigate various "rule of thumb" design protocols for air sparging using a cross-flow two-compartment numerical model to improve the efficiency of air sparging. For example, one of the major design elements of an air sparging system is the air-to-water ratio. Too high an air flow rate results in the development of air tubes, which decreases the area of contact between the air and the water. In other cases, it causes desaturation of porous material, which potentially results in the contaminated groundwater flowing around rather than through the active zone of remediation.

In this study, the effective air-to-water ratio in an air sparging application was evaluated. A numerical model developed as a part of this study was concurrently used

with the multiphase flow software Subsurface Transport Over Multiple Phase (STOMP), developed by Pacific Northwest National Laboratory. STOMP was used to calculate the reduction in the hydraulic conductivity of the water phase due to the presence of air and this output was used in the developed model. The developed model for air sparging considers the contaminant concentrations in the two compartments: gas and dissolved phases based on two-film resistance theorem. Mass balance has been applied for deriving a pair of linked partial differential equations in the gas and liquid phases. A numerical technique solution using the finite difference method has been used simultaneously in solving the two differential equations for the contaminant concentration in both gas and liquid phases. Finally, an analytical solution has been derived and verified with the numerical solution.

Osama S. Al-Gahtani

Department of Civil and Environmental Engineering

Colorado State University

Fort Collins, Colorado 80523

Summer 2006

TABLE OF CONTENTS

CHAPTER 1: INTRODUCTION

CHAPTER 2: LITERATURE REVIEW

LIST OF TABLES

LIST OF FIGURES

CHAPTER 1

INTRODUCTION

1.1 Introduction

Groundwater is a major source of public water supply in many parts of the world. Originally groundwater was considered to be immune from contamination and was thought to be a safe clean source of drinking water. To the contrary, accidental spills, improper disposal of wastes and other releases of hazardous chemicals to the environment have resulted in groundwater contamination and have threatened this major natural resource. One lesson learned from past practices is that relatively small quantities of hazardous chemicals can potentially contaminate very large quantities of groundwater. Groundwater moves very slowly and once it is contaminated, several hundred to thousand of years may be required for natural processes to clean the groundwater.

Today, in the United States, groundwater remediation systems are commonplace. As of August 2000, 1,234 current sites and 217 former sites (total of 1,451 sites) are on or have been on EPA's National Proprieties List (EPA's list of the most serious uncontrolled or abandoned hazardous waste sites in the United States). At 835 of these sites (58%), groundwater or source treatment is a required remedial action. The most commonly used technology is "Pump and Treat", where contaminated groundwater is pumped and treated above ground then injected back into the aquifer (Table 1.1). The number of sites used

by all technologies (Table 1.1), is 928, which exceeds the total number of sites (835) because multiple treatment technologies may be used at a single site. According to SAR (2001), there are 117 NPL sites where pump and treat is used with other treatment methods.

Table 1.1: Number of NPL sites requiring groundwater treatment modified from EPA 542/R/01/004 (2001)

Type of Technology	Treatment Technology	No. of sites	% sites used by Technology
Ex-Situ	Pump and Treat	638	76.4
In Situ Technologies	Air Sparging	48	5.7
	Bioremediation	21	2.5
	Dual Phase Extraction	10	1.2
	Permeable Reactive Barrier	8	1.0
	Phytoremediation	4	0.5
	Chemical Treatment	2	0.2
	In-Well Air Stripping	2	0.2
	Monitored Natural Attenuation	109	13.1
	other	86	10.3
	Total	928	

Pump and treat is considered an ex-situ treatment technology in that the contaminated groundwater is removed from the aquifer and treated above ground. With pump and treat, the pumped groundwater is treated by one of several ex-situ treatment technologies. For volatile organic contaminants, the most common treatment method is air stripping (either air stripping tower or shallow tray aeration system (Figure 1.1). Carbon adsorption and reverse osmosis are the most common treatment technologies for non volatile contaminants. Pump and Treat is relatively high in cost and frequently requires long time periods to achieve site remediation.

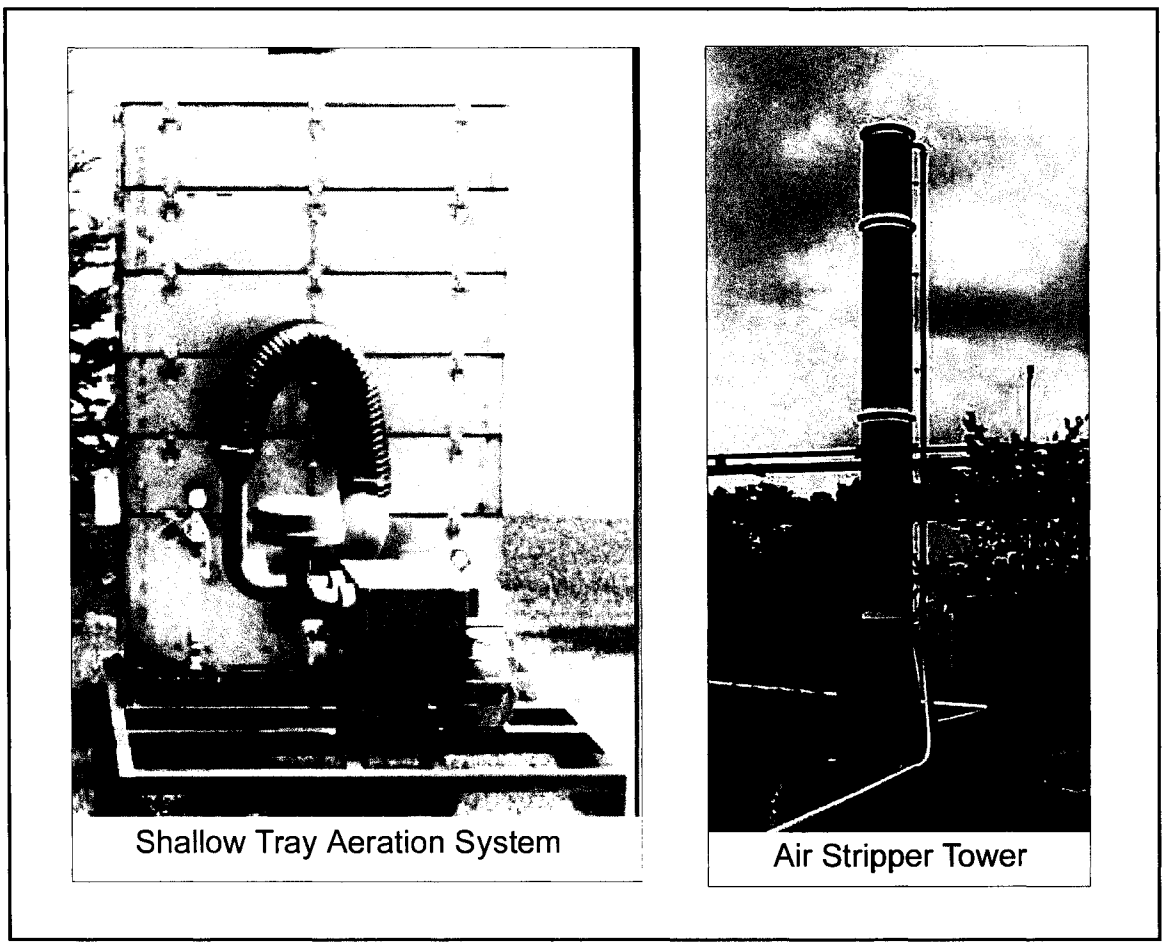

Figure 1.1: Pictures of shallow tray aeration system and air stripper tower

As an alternative to pump and treat, in-situ treatment technologies are gaining popularity and are being increasing implemented. As shown in Table 1.1, the most common in-situ treatment technology used is air sparging (48 sites) and bioremediation (21 sites). Monitored natural attenuation is used at 109 of the NPL sites but is not classified by EPA as either an ex-situ or in-situ treatment technology.

Air sparging is applicable for the case of groundwater contamination by a volatile or semi-volatile organic compound. It has been applied for both LNAPL (Light Non-Aqueous Phase Liquid) contamination (most frequently petroleum hydrocarbons) and also DNAPL (Dense Non-Aqueous Phase Liquid) contamination (e.g. TCE). Air

sparging is applicable to dissolved phase groundwater contamination as well as source control (free phase subsurface volatile compounds). In the case of petroleum hydrocarbons, free phase hydrocarbons may be located in the smear zone above and below the water table (due to past fluctuations in the water table) or as free phase petroleum hydrocarbons floating on the water table. In the case of DNAPLs (e.g. TCE), free phase TCE may exist in pools located at the bottom of the aquifer, commonly in depressions in the underlying bedrock surface.

With air sparging, air is injected into the saturated region in or below the zone of groundwater contamination or zone of the free phase contaminant. The primary purpose of air sparging is to partition the dissolved phase contaminant into the vapor phase and or to volatize the free phase contaminant. The upward migrating air carries the chemical contaminant into the unsaturated zone. Commonly, air sparging is applied in conjunction with soil vapor extraction (SVE). SVE is used to recover subsurface vapors from the unsaturated zone. The recovered vapors are either treated above ground (using carbon adsorption, thermal destruction etc) or discharged directly into the atmosphere. If SVE is not used to recover the air sparging vapors, then it is hoped that natural biological processes in the unsaturated zone will naturally degrade the volatile organic compound.

Bio-sparging is a variation of air sparging. With bio-sparging, air is injected into the subsurface as with air sparging but at a much lower flow rate. With bio-sparging, the primary purpose is to increase the oxygen concentrations of the contaminated groundwater and thus promote natural bioremediation activities. With air sparging, the primary purpose is to volatize the free phase volatile organic compounds or to partition the dissolved phase into the vapor phase. This may also increase subsurface oxygen

concentrations and thus promote bioremediation, but the primary means of recovery is intended to be vapor phase partitioning. Bio-sparging is not considered in this dissertation.

While the EPA considers pump and treat and SVE as proven remediation technologies, air sparging is considered as an unproven experimental or developing technology. Purportedly there are several reasons for these which include:

- Frequently insufficient data are collected when using sir sparging to document the effectiveness of the method, especially when used in conjunction with other remediation technologies;
- Uncertainties exist as to the effect that the injected air has on groundwater flow patterns. Injection at too high a rate may cause the groundwater to bypass the zone of air sparging rather than flow through the zone of air sparging, while too low a rate may allow contaminated groundwater to flow through the zone of air sparging without removing sufficient quantities of the contaminant.
- There is potential for development of preferential air flow pathways (air channels) that may significantly reduce the surface area of contact between the air and the contaminated groundwater, thus allowing contaminated groundwater to flow directly through the zone of aeration.
- Few cases appear in the published literature that document the effectiveness of air sparging.
- Aquifer heterogeneities affect the distribution of injected air; and

- Design protocols are non standardized. Current design protocols do not take into account the chemical properties of the contaminant of concern, the concentration of the contaminant in the incoming contaminated groundwater, the rate of groundwater flow, aquifer properties, and the target concentration of the groundwater exiting the zone of air sparging.

With above ground treatment using air stripping towers or shallow tray aeration, the mathematics is well defined and the design protocols are well established. Design protocols take into account the concentration and chemical properties of the contaminant in the water to be treated, the flow rate of the contaminated water, surficial contact area between the air and the water, and the target concentration of the exiting water. Design factors include the height of the stripping tower (number of trays), air to water ratio (typically in the range of 80 to100), and bubble size (in the case of air stripping towers, hollow particles are used to increase the area of contact between the air and the water). With above ground treatment, it is easy to measure the concentration of the exiting water to ensure that the target concentration is met. In general, design protocols for air sparging systems do not consider these factors.

1.2 Description of Air Sparging

Air sparging is a relatively simple technology and costs less than pump and treat with above groundwater treatment. As seen in Figure 1.2, the two main components of air sparging are the injection well (alternatively a trench) and the compressor. The goal of air

sparging is mass removal primarily by volatilization, i.e. vaporization of free phase and or dissolved phase volatile organic compound (Figure 1.2).

The first step in deciding if air sparging is an appropriate technology for a particular site is a site characterization investigation. The site characterization should identify the concentration and distribution of the chemical contaminant of concern, geologic conditions and aquifer properties. In general, specific conditions required for successful application of air sparging are a relatively homogenous aquifer with adequate hydraulic conductivity to allow for easy injection of the air into the saturated porous media. A major constraint is that no low permeability layers should be present that might adversely affect the distribution of the injected air. Air sparging has had more success for the case of petroleum hydrocarbons (LNAPL) than for DNAPLs (e.g. TCE). In the case of petroleum hydrocarbons, when the depth to groundwater is relatively shallow, an air sparging trench or horizontal wells may be used rather than the more common case using vertical wells.

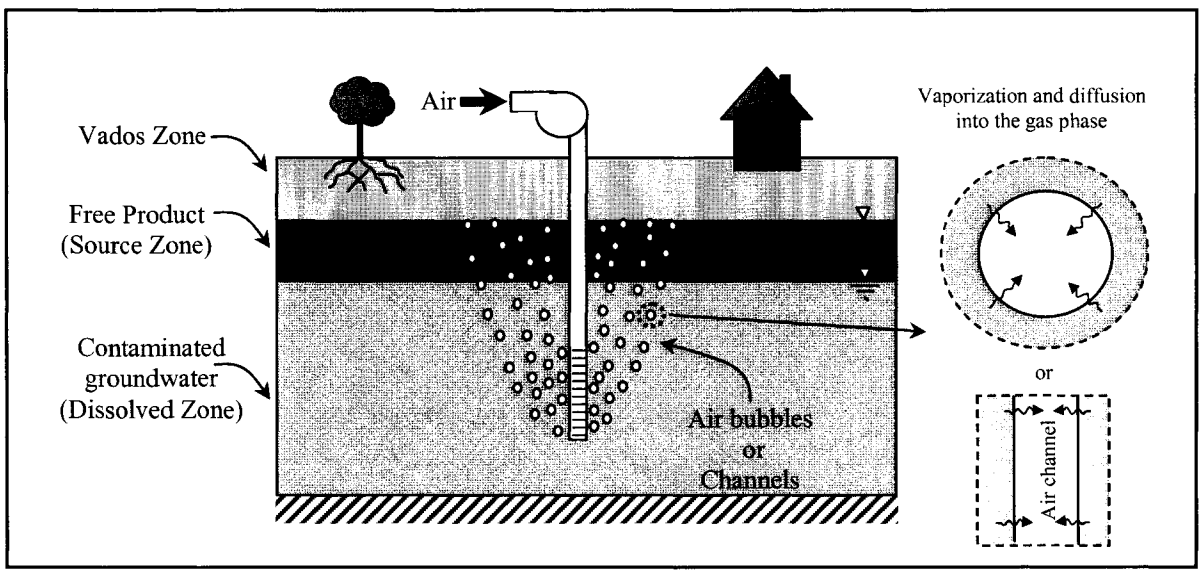

Figure 1.2: Diagram of a typical air sparging system

1.3 Design Elements

The assumption is made here and in the remainder of this dissertation that a site characterization investigation has been conducted and that geologic conditions and aquifer properties are suitable for application of the air sparging technology. The following design elements need to be identified during the design procedure:

- Number and spacing of injection wells,
- Depth, diameter and screened interval for each well,
- Injection pressure and air flow rate for each well,
- Screen size (bubble size generation, microbubbler screen?), and
- Continuous or pulse air injection (if pulsing, then also pulse interval).

Inherent in the determination of the above design elements is:

- Identifying the radius of influence (ROI) versus depth of injection and the air flow rate for the well, and
- Rate of startup during each air injection interval. There is evidence that slow versus fast startup affects the number and distribution of air channels that are formed.

1.4 Typical Design Methodology

In practice there are two main methods used for the design of an air sparging system [Johnson, 2001]:

- Site specific design based on pilot testing, and
- Standardized design based on "rules of thumb" used in previous engineering practice.

The two methods will be discussed here as if they were mutually exclusive, independent methods. Obviously, a combination of the two methods may also be used.

1.4.1 Pilot Testing

Frequently a pilot air sparging test is conducted [Lesson et al., 2002]. This test typically consists of a single sparge well and several monitoring wells located at various distances from the sparge well. The design elements (depth, diameter, screened interval and slot size) of the sparge well should be the same as that planned for the sparge wells to be implemented in the field. Air is injected at various injection pressures and the corresponding air flow rate is measured as well as the radius of influence of the well. The injection pressure must overcome the static water level head and the air entry pressure. Typically 4 or 5 injection pressures are used during the test. The radius of influence is measured in the observation wells by a variety of means. One method is to inject an inert gas such as helium or argon and determine if the gas is detected in the observation well.

1.4.2 Standardized Design

With the standardized design, the design elements are selected based on previous practitioner's experience. With the standardized design, site specific design parameters are not typically included in the design procedure. Table 1.2 has the typical range of values for design parameters for different sites where air sparging has been applied. According to Johnson et al. (2001), many sites using the standardized design may either not be working correctly or not enough data has been provided to evaluate the effectiveness of air sparging.

Johnson (2001) recommends as a standardized design:

- Well depth of 5 feet below water table,
- Air flow rate of 20 cfm/well, and
- Well spacing of 15 feet.

The standardized design presented by Johnson et al. (2001) appears to be overly conservative. A well spacing of 15 feet potentially may result in a large total number of wells. Coupled with the 20 cfm per well recommendation, this standardized design could result in an impractically large total airflow rate. Johnson recommends a well depth of 5 feet below the water table. He is concerned that aquifer heterogeneities could adversely the distribution of the injected air. He does not consider the effect that natural fluctuation of the water table may have on system performance or the potential that the high air flow rate may cause groundwater to bypass the zone of aeration. No recommendation is made as to continuous or pulse injection or screen slot size (microbubbler well screens).

Table1. 2: Typical in situ air sparging design parameters [Marley and Bruell, 1995]

Parameter and Range	Most Often Used Value (# of Sites)	Second Most Often Used Value (# of Sites)	Third Most Often Used Value (# of Sites)	Total # of Sites
Screen Length 0.5 - 10 ft	2 ft (16 sites)	3 ft (8 sites)	5 ft (7 sites)	40
Well Diameter 1 - 4 in	2 inches (17 sites)	4 inches (7 sites)	1 inch (5 sites)	37
Overpressure 0.35 - 18.2 psig	0.35 - 5 psig (14 sites)	5 - 10 psig (9 sites)	10 - 15 psig (5 sites)	31
Well Screen Depth Below Water Table 2 - 26.5 ft	5 - 10 ft (10 sites)	10 - 15 ft (8 sites)	2- 5 ft (6 sites)	31
Air Injection Flowrate 1.3 - 40 scfm	1.3 - 5 scfm (16 sites)	5 - 10 scfm (9 sites)	15 - 20 scfm (5 sites)	39
Air Injection Pressure 3.5 - 25 psig	5 - 10 psig (17 sites)	10 - 15 psig (8 sites)	20 - 25 psig (6 sites)	40
SVE R_I/IAS R_I 0.16 - 7.42	1 - 2 (12 sites)	0.16 - 1 (6 sites)	3 - 4 (3 sites)	26

SVE R_I - radius of influence of vapor extraction wells
IAS R_I - radius of influence of air injection wells

1.5 Subsurface Air Distribution

A key element of the design is to ensure a uniform distribution of airflow in the subsurface. The airflow rate, depth below the water table of the injection point, and the well spacing are all interrelated and affect the distribution of air in the subsurface. Laboratory flume experiments indicate that the injected air will have a zone of influence in a homogenous porous media that varies from 30 degrees to 45 degrees with the vertical. Ideally, if small enough air bubbles are generated (relative to pore size) and the air flow rate is not large, then the air would remain as discrete bubbles (Figure 1.2) which would maximize the surficial area of contact between the air and the water. In practice, the injected air forms air channels in the porous media (Figures 1.3, 1.4). It is desirable to form many smaller air channels rather fewer large air channels (Figure 1.4). This increases the surficial area of contact between the air and the water for a specified flow rate.

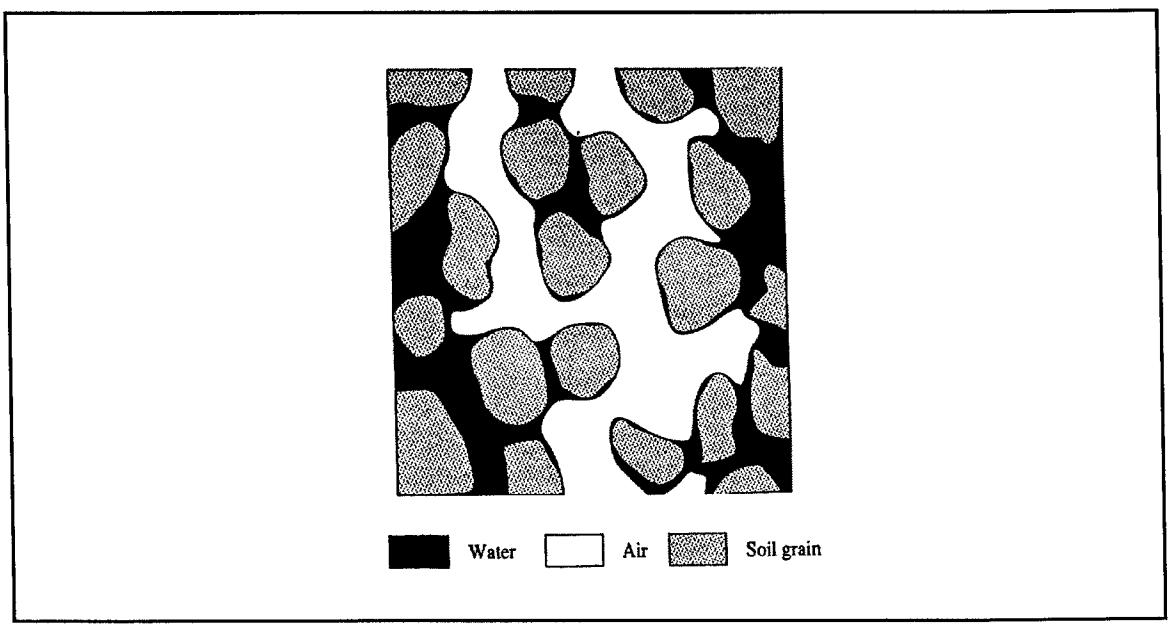

Figure 1.3: Air channel in porous media [Ahlfeld et al., 1994]

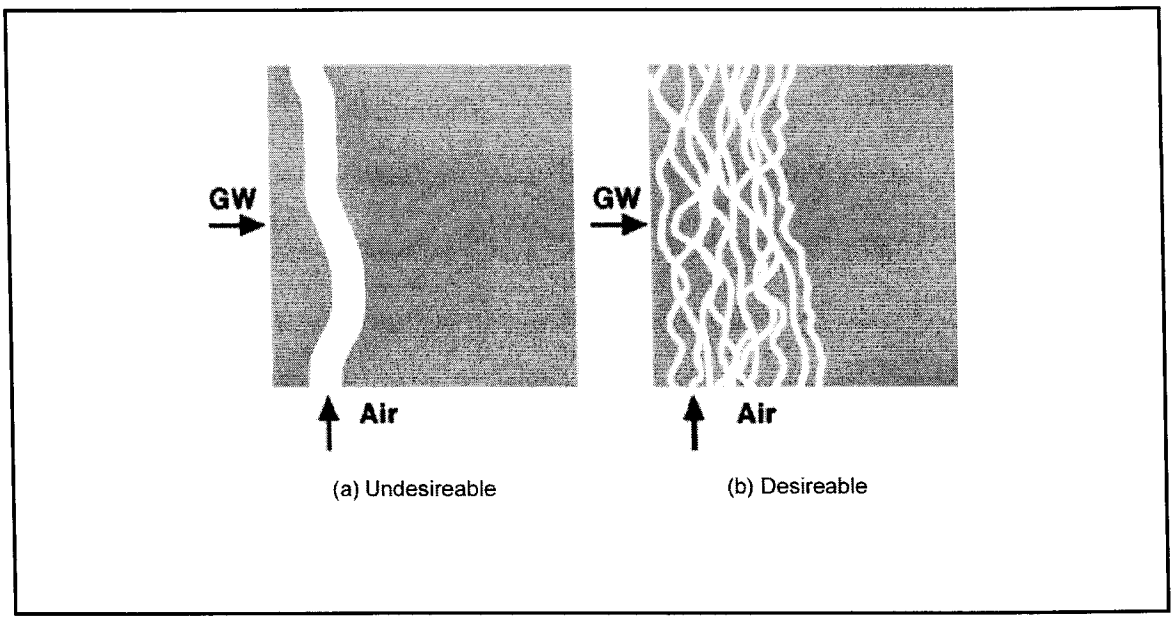

Figure 1.4: Distribution of air channels [U.S. Army Corp of Engineering, 1997]

While the published literature indicates the importance of having a uniform distribution of air channels, the literature is ambiguous on how to accomplish this. With the onset of air sparging, a discrete number of air channels form. Increasing the airflow rate may initially simply strengthen (enlarge) existing air channels (no increase in radius of influence observed). With further increases in the airflow, an increase in the number of air channels and a corresponding increase in the radius of influence is observed.

In general, the radius of influence increases with the depth of injection below the water table. However, field experiments indicate that there may be some limit above which the radius of influence does not increase with either an increase in well depth or an increase in airflow rate.

1.6 Pulsing Versus Continuous Operation

An understanding of the physics of air channel formation is helpful in evaluating the benefits of pulse operation. At early times or "transit phase", air channels form and for the most part determine the number, form and distribution of the air channels. This early time phase is short but important in determining the final total number and distribution of air channels and specifying zone of influence. At longer times or "steady state phase" the second phase of the air sparging operation, little change in shape or size of the radius of influence is expected.

During the transient phase when air channel formation occurs, the injection pressure should lie between two limiting values. Minimum air pressure is the pressure required to overcome hydrostatic pressure and air entry pressure of the soil. On a microscopic level, air entry or "capillary" pressure is dependant on type of soil and is usually measured from the pilot test. For small soil particles, air entry pressure is higher than for relatively large soil particles. Orientation and distribution of soil particles plays an important role since air channels will form along a path corresponding to the path of least resistance [Ahlfeld et al., 1994]. A maximum air pressure limit is necessary for field safety and to avoid failure of injection pipe material.

During the transit state, geologic conditions and airflow rate are major factors affecting zone of influence. Geologic conditions affect the air channel path since airflow will bypass low permeability lenses and seek the path of least resistance [Ahlfeld et al., 1994]. At system startup, air should be injected at a pressure to overcome hydrostatic pressure and the air entry pressure. After the air channels form and reach the water table, a lower injection pressure is required to achieve the same flow rate.

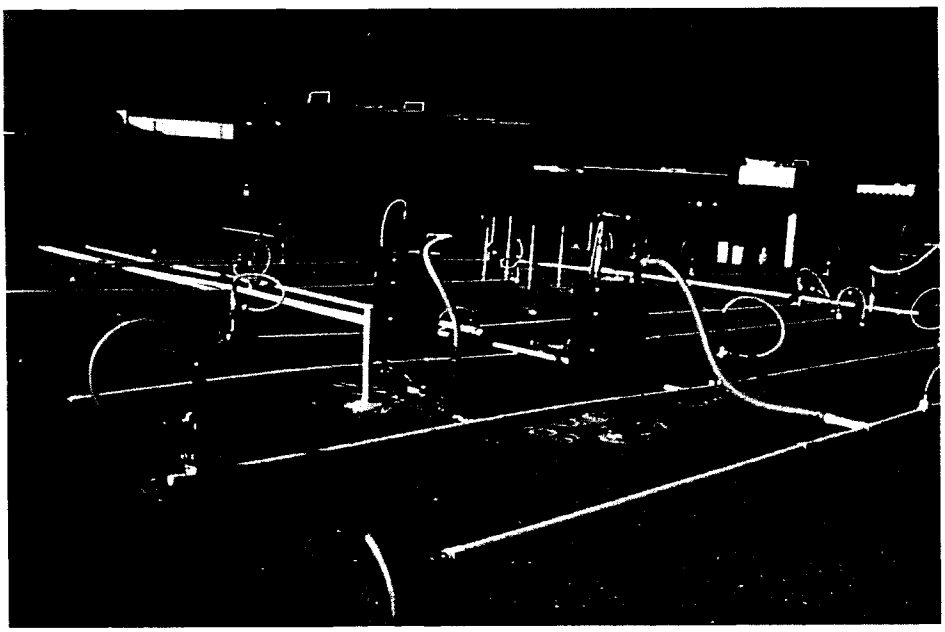

Layout of Air Sparging Sustem

Bubbles caused by air exiting in flooded lagoon.

Figure 1.5: Field experiment [Leeson et al., 2002]

A favorable case for air distribution is when the air channels are evenly distributed and extend laterally as far as possible. For low airflow rate, buoyancy forces are dominant and the horizontal extent of the air channels is limited. [Ji et al., 1992]. At higher initial air flow rates, more air channels will form and will extend more widely. For pulse effect on mass removal, there are two different theories. One theory is that during pulsing when the air channels collapse, surrounding groundwater migrates into the zone of influence of the air sparging system. Another theory is that pulsing results in a new distribution of air channels in the subsurface.

There are three methods to evaluate air distribution in air sparging. The first is lab experimentation which simulates air sparging in a glass tank to visualize channel formation. The second method involves field experimentation at site where the water table is near to the surface or slightly above surface level and setting an injection well to observe air effusion at surface level. Finally, tracer studies have been conducted at several sites using dissolved oxygen sensors, helium, or sulfur hexafluoride (SF_6) for estimating air distribution (Bruce et al., 2001).

The other issue is the effect of airflow rate at steady state level or after air channels are formed. At this phase, some studies suggest that increasing airflow has no effect. Other studies state that increasing flow rate builds a high pressure zone that leads groundwater to bypass the influence zone. However, the pulsing mode of pumping air for one period of time and halting the system for another period of time has reported that it improves system performance. When the pumping is paused, air pressure inside the air channels will drop to atmospheric pressure, which reduce air pressure at the influence zone and allows groundwater to flow through the target zone.

Experimental studies on the effect of airflow rate on mass removing have different results based on the conditions of the experiment. The experimental studies conducted by Johnson et al. (1999), Rogers and Ong (2000), and Reddy and Adams (2000) show that increasing airflow rate has little effect on mass removal during long term continues pumping periods. On the other hand, Reddy and Adams (2000) and Catney and Lynch (2001) experimentally have shown that groundwater flow through the influence zone by air injection into the saturated zone significantly affects the amount of mass removal. To date, no experimental study has yet quantified the reduction in hydraulic conductivity during an air sparging operation.

1.7 Packed Air Stripping Tower Similarity

The technology of air sparging is similar to the air stripping tower that is used in ex-situ groundwater treatment. The air stripping tower is "Counter Current" flow, where water is injected at the top of the tower and air is introduced at the bottom of the tower (Figure 1.8). Packing materials are used to increase the efficiency of removal of volatile contaminants by providing higher interfacial area of contact between the air bubbles and the water. Different size and material types could be used for packing material. Air sparging is conceptually the same as the air stripping tower. However, the mathematical description for each condition is different. Air sparging presents the case of cross current flow and air stripping tower is counter current system. With cross current flow, the groundwater moves in the horizontal direction and air is injected at the bottom.

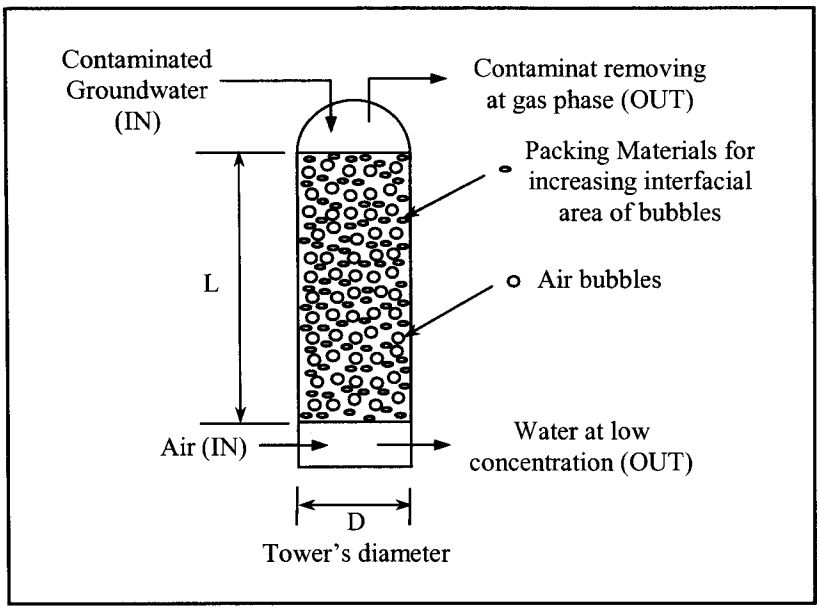

Figure1. 6: Packed air stripping tower

The design parameters for air stripping are the same as mentioned earlier. For the air stripping tower, the air/water ratio is a key element of the design. Typical air/water ratios range between 50 and 100. High air to water ratios (200 or 250) have also been used. In addition, chemical characteristics of contaminant and initial and final concentrations are essential parameters in the equation used to design air stripping towers. Full derivation of the designing equation of the air stripping tower (counter current flow) will be covered in chapter 3 and in appendix C. In air sparging design, the term air to water ratio should be included since an increase in air pressure reduces incoming water flow.

1.8 Objective

Rule of thumb is the method used at most sites for designing an air sparging system. Values shown in Table 1.2 are typical for most system designs. In other words, it

is possible to find two different geologic condition sites with unlike types of contaminants that have the same design output parameters. Recent reports of air sparging design show that practitioners rely on operational site experience most of time for complexity and sensitivity of system behavior. Range of success for this technology is hard to determine because at most sites, source and amount of contaminant is difficult to precisely predict. Some efforts have been made to move from lab experiments to field measurement in an attempt to draw general boundaries for the behavior. Some theoretical models have been created, but lack of understanding of the physical and chemical behavior is slowing the progress in using them. One of the main purposes of this study is to prove and make inside discussion for more incorporation of models in site performance.

As mentioned in section 1.3 and 1.7, some factors should be included in designing air sparging systems that have not been included in current applications of this technology. In addition, these factors should be interpreted for physical and chemical behaviors of the process. For instance, in the beginning of emerging air sparging technology, theoretical studies were focused on bubbling behavior of the system. Later on, experimental studies showed that many sites for this technology are subjected to porous media where air enters the medium in channel fingers. This concept required a change in the way of mathematical derivations used to describe these mechanisms. In conclusion, knowledge of the physical and chemical behavior of the technology is important for better performance and lower cost of the system. Interpreting these concepts in mathematical form is desirable for producing a better system design.

One of the important design factors in air sparging is that the presence of air in porous media will decrease the hydraulic conductivity of the system. Increasing the amount of airflow in the saturated zone will decrease hydraulic conductivity and allow groundwater to bypass the system. Air sparging will act as a barrier system, and groundwater will flow either around or beneath the active zone of the sparge system. Reduction in groundwater passing through zone of influence will reduce the amount of wastewater available for the treatment mechanism. In air sparging modeling, this factor is not considered as a point of interest in some models. In addition, many factors are overlooked and do not play a role in the design process, and it is not discussed how they affect system performance. In this study, incorporating and evaluating different design factors that affect air sparging performance will be discussed.

The following points are the main focus of this study:

- Build a mathematical mode for cross current air sparging taking into account the concentration in the gas and liquid phases, and the reduction in hydraulic conductivity.
- Deriving the differential equations in the dissolved and air phases and finding analytical and numerical solutions for a given model at specific boundary conditions.
- Understanding how type and concentration of contaminant could affect system design even though these are not obvious design parameters.
- Looking for better and more economical way of estimating design factors based on knowledge of site conditions.

- Comparing the developed model with the other published models, and discussing the importance of the assumptions used in these models.

CHAPTER 2

LITERATURE REVIEW

2.1 Mass Transfer Concepts

The main discussion of air sparging is how the contaminant can be transferred efficiently from dissolved to air phase. Air can take different forms that range between bubbles, consecutive bubbles or air channels, and micro-bubbles. Bubbling and channeling differ in mass removal since they have different shapes.

The mass transfer theory should be revised to accommodate air formations in porous medium. The theory of mass transfer used in the air sparging model should include both the characteristic of the contaminant and the shape of air formation. Both these factors have been taken into consideration in the Two-Film theory, since the surface area of the air phase boundary and the concentration gradient between two immiscible fluids are included. The Henry constant is also integrated into the Two-Film theory. The following sections will focus on mass transfer between the air and water solutions.

2.1.1 The Henry Law

For a given substance in a water solution exposed to an air phase, chemical substances tend to partition into the air phase. At equilibrium, Henry's law describes proportional concentrations between both the air and liquid phase, as follows:

$$H_m = \frac{P_{i\ air}}{x_i} \qquad (2.1)$$

where $P_{i\,air}$ = Partial pressure of contaminant (Pa),

x_i = Mole fraction of contaminant in liquid solution,

H_m = Henry's constant (Pa).

If the number of moles in water is much greater than contaminant ($n_w >> n_i$), then $x_i \approx n_i / n_w$. For $C_{i\,w} = n_i / V_w$ (mole/volume) and $C_w = n_w / V_w = \rho_w / MW_w = 1 / v_w$ (mole/volume). ρ_w is water density, MW_w is molecular weight of water, and v_w is molar volume of water, which equals 18×10^{-6} m^3/mol. The second form of Henry's law then becomes

$$H_c = \frac{P_{i\,air}}{C_{i\,w}\,(mol/m^3)} = v_w\,H_m \qquad H_c \text{ in (Pa } m^3\text{/mol)} \quad (2.2\text{ a})$$

or

$$H_c = \frac{P_{i\,air}}{C_{i\,w}\,(mg/l \text{ or } gm/m^3)} = v_w\,MW_i\,H_m \qquad H_c \text{ in (Pa } m^3\text{/gm)} \quad (2.2\text{ b}),$$

where MW_i is the molecular weight of the contaminant constituent.

Equation (2.2 b) is most widely used in environmental application for estimation of H_c. This value can be estimated by dividing vapor pressure or saturated partial pressure, and concentration of contaminant at water phase (solubility). The accuracy of this value depends on the estimation of vapor pressure and water solubility.

Figure 2.1 shows the contaminant distribution in the three phases. First, the concentration is constant during the liquid phase, in which it reaches the limit of solubility. At the liquid and vapor region, the concentration increases as a result of a sudden change in water density and mole fractions. At the two solid circle points, measurements of solubility and vapor pressure are conducted at the equilibrium interface.

From the liquid and vapor region, the concentration of the contaminant increases until it approaches a hypothetical constant value.

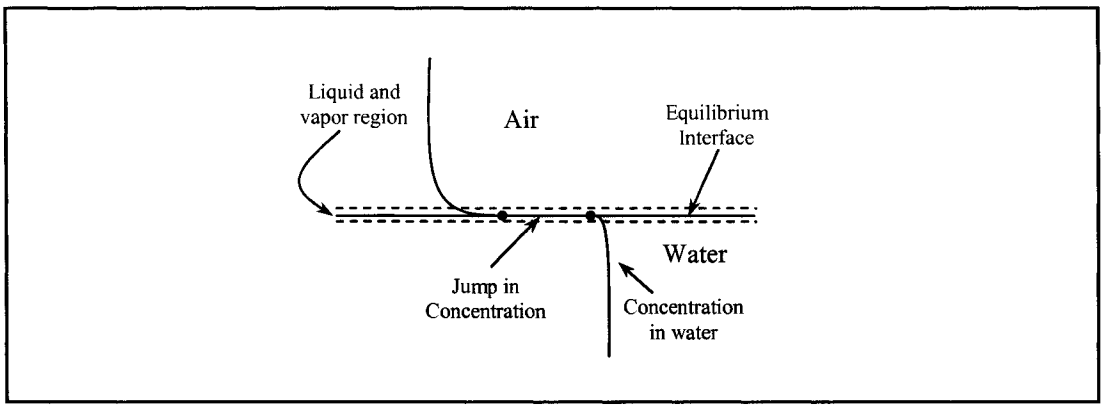

Figure 2.1: Concentration profile of contaminant in air-water interface

As mentioned above, the emphasis here is on the material behavior during the three phases. The behavior of a chemical substance in these three phases is represented in Figure 2.2. For our purposes, the discussion will focus on the liquid and vapor phases.

In Figure 2.2, which shows the transition of the material behavior during the three phases, liquid is clearly shown by the dashed line boundary where pressure changes with specific volume and temperature.

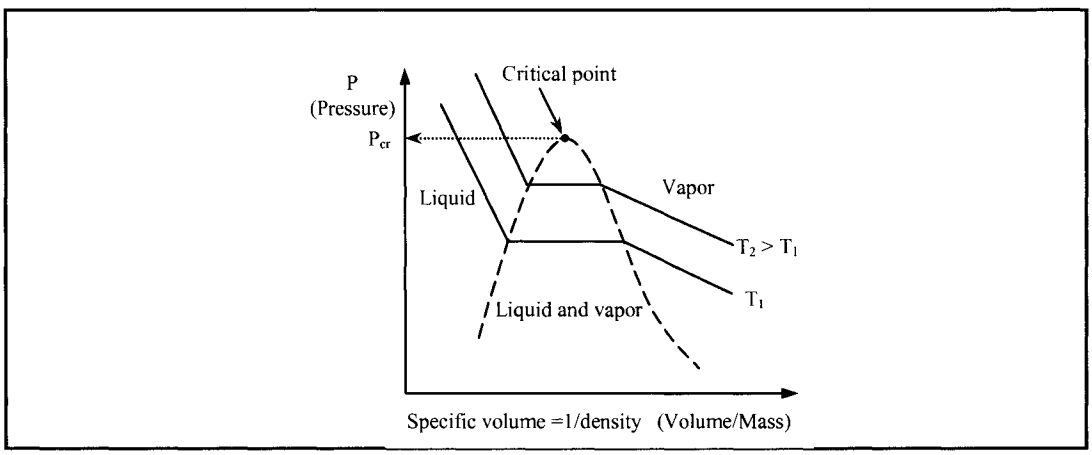

Figure 2.2: Material behaviors during the three phases

For the same material, different values of vapor pressure are expected at different values of temperature. Vapor pressures for the different materials tabulated in Appendix A represent the average values of the vapor pressure within a range of temperatures. Antoine's equation for the estimation of the vapor pressure was presented by Mackay and Shiu (1981) as follows:

$$\log(P_v) = A - \frac{B}{(T + C)} \qquad (2.3)$$

where P_v is vapor pressure, T is temperature, and A, B, and C are fitting constants.

Solubility is temperature dependent. Its values, tabulated in Appendix A, are estimated at T = 25°C. The most acceptable values are measured using liquid chromatography. Schwartz (1977) reported that the solubility of aromatic hydrocarbons could be doubled at temperatures ranging from 10°C to 24°C. Moreover, solubility is highly dependent on the sorption of experimental glassware equipment. May et al (1978) experimentally measure the solubility of various chemicals using a column packed with glass beads in order to eliminate errors from sorption. Finally, reported values of solubility may vary due to variations in experimental conditions.

Another way of estimating Henry's law constant is by chemical activity and vapor pressure, as described in the following formula:

$$H_m = \gamma_i P_{v,} \qquad (2.4)$$

where γ_i is the activity coefficient of the solute.

The full derivation of equation (2.4) is shown in Appendix B, with the following assumptions:

- The reaction proceeds under a reversible process.
- The reaction is time invariant and chemically stable at equilibrium condition.

- The system is isolated.
- The gas behavior is ideal.

According to Mackay and Shiu (1981), this method is acceptable for solubility of less than 0.55 mol/l. This is an acceptable value since the solubility of benzene, which has one of the highest solubility values in environmental application, is 0.02 mol/l. In addition, this method is used for the estimation of chemical activity of solutes, even in the presence of cosolvents or surfactants in the solution.

The dimensionless form of Henry's law for ideal gas is

$$H = \frac{H_c}{RT} = \frac{C_{i\,air}}{C_{i\,w}} \qquad (2.5)$$

Equation 2.5 is the third form of Henry's law, conveniently utilized by eliminating the complexity of the units. Appendix A shows the values of dimensional and non-dimensional values of Henry's constant.

2.1.2 The Two-Film Theory and Overall Mass Transfer

The Two-Film theory is used in many environmental applications. This theory was formulated by Whitman (1923), and it describes the mass transfer mechanism between two phases of immiscible fluids which dissolved in water. This theory demonstrates the transport of chemicals either from or into water solution. The transport follows the direction of decreasing concentration gradient (Figure 2.3). The mass transfer in both phases is derived using the process of diffusion across the two films. At the interface between the two phases, the resistance resulting from the jump in the concentrations is neglected. The extent of this jump is controlled by Henry's constant.

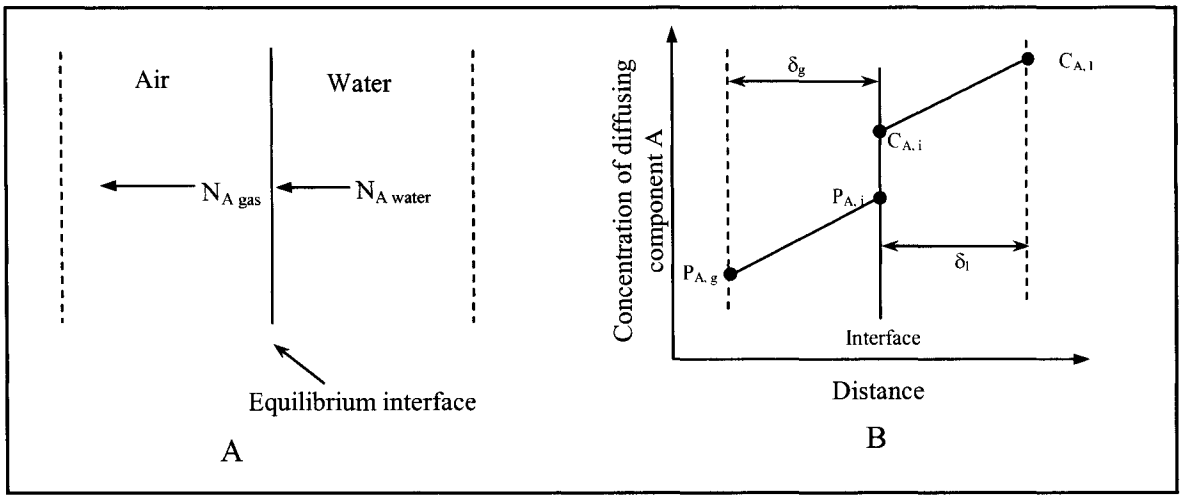

Figure 2.3: Concentrations and deriving forces across aqueous and gas films

At the equilibrium interface, the deriving forces $N_{A,g}$ and $N_{A,l}$ (Mass/Time/Area) are those forces that transfer constituent A from liquid to gas phase (Figure 2.3), as described below:

$$N_{A,\ g} = k_g\ (P_{A,\ i}\ - P_{A,\ g})\ /\ RT \qquad (2.6)$$

and

$$N_{A,\ l} = k_l\ (C_{A,\ l} - C_{A,\ i}). \qquad (2.7)$$

where k_g = Convection mass transfer coefficient in the gas phase (Length/Time),

P_{Ai} = Partial pressure of A at equilibrium interface, vapor pressure (Pressure),

$P_{A,\ g}$ = Partial pressure of component A in gas phase (Pressure),

k_l = Convection mass transfer coefficient in the liquid phase (Length/Time),

$C_{A,\ l}$ = Concentration of component A in liquid phase (Mass),

$C_{A,\ i}$ = Concentration of component A at equilibrium interface (Mass),

SA = Interfacial area at interface (Length^2).

At steady state, the flux of overall mass transferred N_A (Mass./Time/Area) is described by the following equations:

$$N_A = N_{A,l} = N_{A,g} \tag{2.8}$$

and

$$N_A = K_L (C_{A,l} - C^*_A) = K_L [(C_{A,l} - C_{A,i}) + (C_{A,i} - C^*_A)] \tag{2.9}$$

At the equilibrium curve where Henry's law applies (Figure 2.4), we have

$$C^*_A = \frac{P_{A,g}}{H_c} \quad \text{and} \quad C_{A,i} = \frac{P_{A,i}}{H_c} \tag{2.10}$$

By combining (2.6), (2.7), (2.8), (2.9), (2.10), and (2.3), the overall mass transfer coefficient will be

$$\frac{1}{K_L} = \frac{1}{k_l} + \frac{1}{H k_g} \tag{2.11}$$

The Two-Film theory can then be written in the form of mass rate of component A for flux formula as:

$$N_A SA = \frac{\partial m_A}{\partial t} = K_L SA (C_{A,l} - C^*_A) \tag{2.12}$$

where SA is the interfacial surface area at the interface (Length^2) and m_A is the mass of the contaminant.

Appendix A shows the values of k_l, k_g, and K_L for some environmentally selected chemicals. As discussed in Chapter 3 and Appendix C, the Two-Film theory has been used in designing air stripping towers. Here, the Two-Film theory will be used in air-sparging modeling.

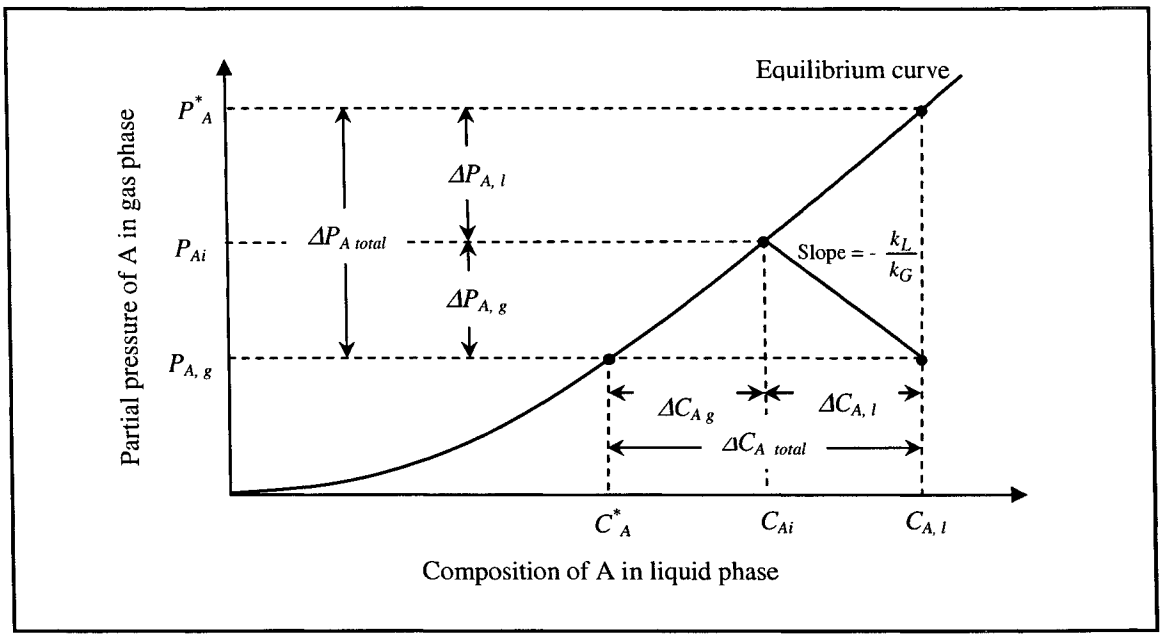

Figure 2.4: Concentrations of the Two-Film Theory

2.2 Bubble Flow

The behavior of air bubbles in a water solution depends on many factors. Fluid characteristics such as surface tension, viscosity, and density can affect bubble movement, especially when the temperature changes. Physical characteristics such as air injection rate and orifice size are also important factors that affect bubble formation and behavior in water. The boundary thickness around a bubble can affect mass transfer and bubble size. In constructing an air sparging model (bubble behavior), all of these factors should be studied and incorporated into the mathematical model. However, due to complexity in some processes, an empirical equation may be necessary to achieve the design purpose.

2.2.1 Bubble Formation and Behavior in Free Water

There are two studies of the formation and behavior of rising bubbles in a column of water [Soo, 1990]. At low injection rate, air forms in water as a single bubble under the equilibrium forces around the orifice. Conversely, at high airflow rate, multiple bubbles form at the orifice. In this section, we will investigate the size and velocity of bubbles for different airflow rates.

2.2.1.1 Bubbles at Low Injection Airflow

Buoyancy and surface tension forces govern the mechanism of bubble formation at low airflow rates. For a circular orifice with diameter R, the buoyancy and surface tension forces (Equations (2.13) and (2.14)) are equal at the moment of release.

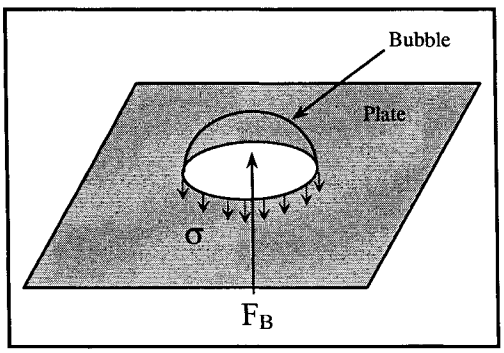

Figure 2.5: Single bubble formation

F_B (Buoyancy force) = $\frac{4}{3} \pi r^3 \rho_w g$, (2.13)

W_{air} (air weight) = $\rho_a g$ $(4/3 \pi r^3)$, (2.14)

Surface Tension force = $2 \pi R \sigma (\cos\theta)$, (2.15)

where θ is equal zero for perfect wetting.

From the equilibrium of the forces

$$r = \sqrt[3]{\frac{3\,R\,\sigma}{2\,\Delta\rho\,g}} \qquad (2.16)$$

where $\Delta\rho = \rho_w - \rho_{air}$,

ρ_w = water density,

ρ_a = air density,

r = air bubble radius,

R = orifice diameter.

From Equation (2.16), the radius of bubble is independent of the flow rate and depends mainly on the orifice diameter. In practice, Equation (2.16) can be rewritten as follows:

$$r = C_c \sqrt[3]{\frac{3\,R\,\sigma}{2\,\Delta\rho\,g}} \qquad (2.17)$$

where C_c = coefficient of chemical.

Takahashi and Miahara (1981) suggested a formula for the coefficient of a chemical, as follows:

$C_c = 0.89\ (\mu_w / \mu_{w1})$, where μ_{w1} is the viscosity of water at liquid temperature.

After the air bubble is released, it may move in water under balanced forces in a steady motion (terminal velocity). During this stage, there are two forces that control bubble movement. Buoyancy force is equal to the volume of the bubble times the

specific weight of water (Equation 2.13). In the motion of small bubbles, the tension force becomes smaller in its value and usually is neglected.

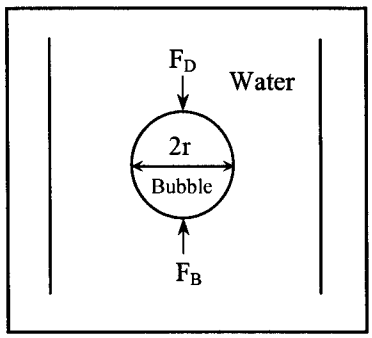

Figure 2.6: Force balance on bubble

$$F_D \text{ (Dragging Force)} = \tfrac{1}{2}\, \rho_w\, v_b^2\, C_D\, \pi r^2, \qquad (2.18)$$

where C_D is the dragging coefficient.

$C_D = 24/N_{Re}$ for laminar flow (2.19 a)

N_{Re} is Renold number $= v_b\, 2r\, \rho_w/\mu_w$. (2.19.b),

Where v_b is the velocity of the bubble.

In addition, the weight of air is quite small. Due to the equilibrium of the forces, the terminal velocity will be as shown in Equation 2.20. This equation is called Stoke's law and is valid for low injection air and small bubble diameter (Re < 1).

$$v_b = \frac{2\, g\, r^2 \Delta\rho}{9\, \mu_w} \qquad (2.20)$$

By combining Equations 2.16 and 2.20 and solving for the orifice diameter where Reynold's number equal to 1, the maximum radius of orifice is equal to 2.06×10^{-5} mm. This value is very small and impractical, indicating that the application of Stoke's law in free water is limited.

2.2.1.2 Bubble at High Injection Airflow

With increasing airflow, the number of bubbles increases and their velocity depends on the airflow rate. At this stage, "chain bubbles" may form and the bubble's diameter remains constant and independent of the orifice diameter. In the other words, the only response to the increasing airflow is the increase in the bubbles velocity [Soo, 1990].

The distance between the centers of two bubbles is the bubble diameter, r as shown in Figure 2.7. The volume between two halves of the two successive bubbles is $4/3\ \pi r^3$ and the velocity is $2r/t$, where t is the travel time between the two centers of the bubbles. Airflow rate can be expressed as follows:

$$Q_{air} = \frac{Volume\ of\ air}{t} = \frac{2}{3}\ \pi\pi\ ^2 v_b \qquad (2.21)$$

By rearranging of Equation (2.21), the velocity of a bubble as a function of the air injected becomes.

$$v_b = \frac{3}{2}\ \frac{Q_{air}}{\pi r^2}. \qquad (2.22)$$

As shown in Figure 2.8, the relationship between the Reynold's number (Equation (2.19a)) and the Farud number (Equation (2.23)) for bubble motion can be established. If a Reynold's number is greater than 10 (turbulent region), the bubbles are independent of the Reynold's number (Figure 2.8).

$$N_{Fr}^{`} = \frac{2g\ r\ \Delta}{v_b^2 \rho} \qquad (2.23)$$

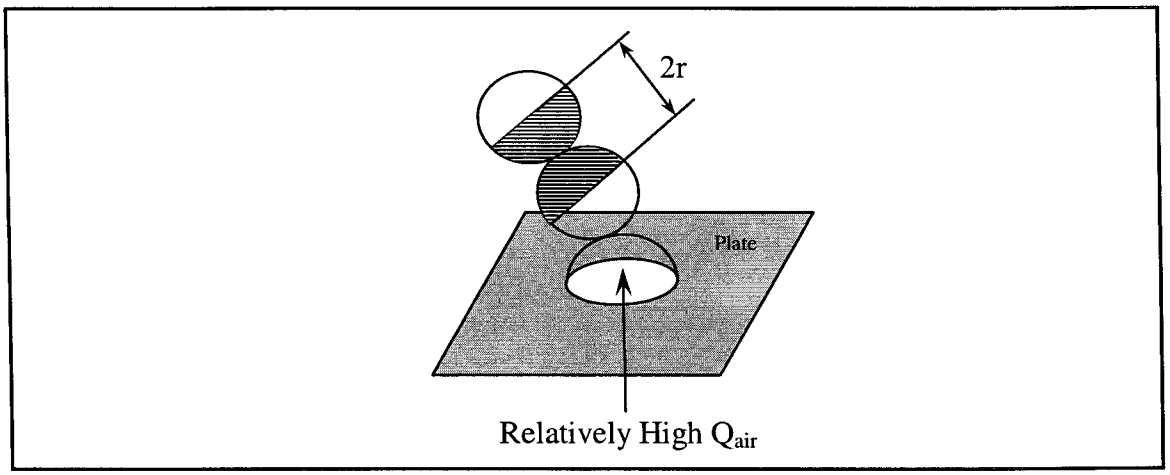

Figure 2.7: Velocity between two successive bubbles

At the turbulent region, the Fraud number is equal to a constant value of 2. After substitution of Equation (2.22) in (2.23), the raduis of the bubble as a function of the airflow rate is given by Equation (2.24) [Soo, 1990], as follows:

$$r = \left(\frac{9\, Q_{air}^2\, \rho}{4\, \pi^2 \Delta\rho} \right)^{\frac{1}{5}} \qquad (2.24)$$

At the critical point, Equations (2.16) and (2.24) are equal and the critical airflow rate becomes.

$$(Q_{air})_{critical} = \frac{\pi (R\sigma)^{\frac{5}{6}}}{\sqrt{6\rho}} \sqrt[3]{\frac{12}{g\Delta\rho}} \qquad (2.25)$$

At high airflow rate, the bubble size and velocity are functions of the airflow rate and are independent of the orifice size. Figure 2.9 represents the change of bubble radius (Equation (2.24)) and bubble velocity (Equation (2.22)).

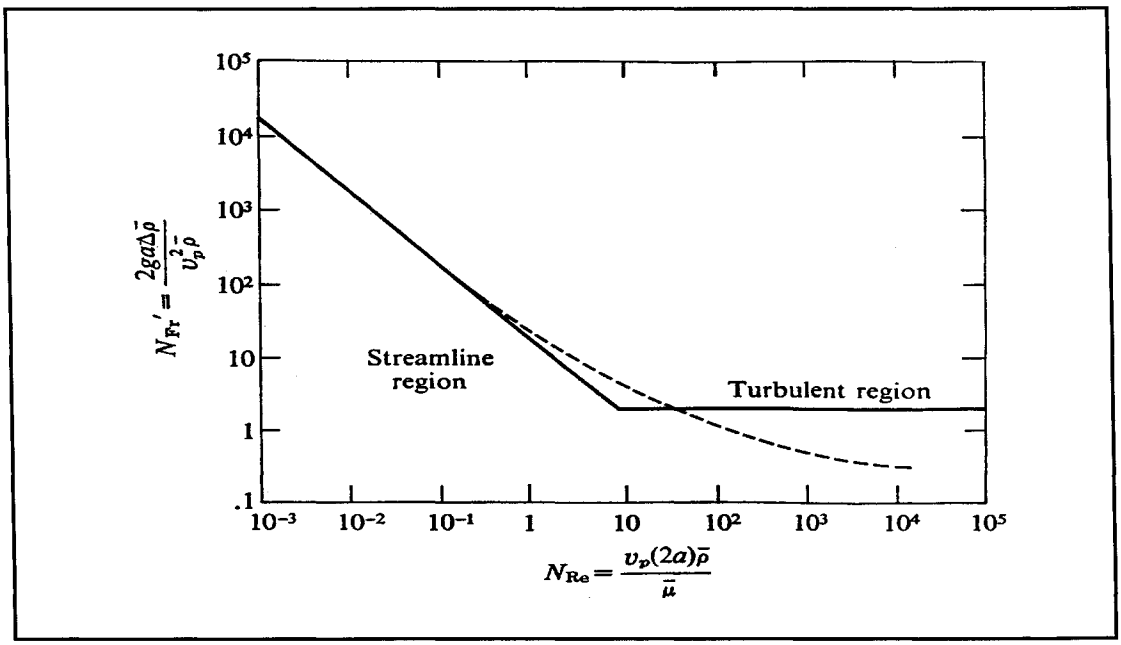

Figure 2.8: Fraud number verses Reynold's number (U.S. Weather Bureau Meteorology and Atomic Energy, Report AECU-3066, U.S. AEC, Washington, D.C. (1955). See also Soo (1990))

Figure 2.10 shows some experimental results. By comparing Figures 2.9 and 2.10, it becomes clear that Equations (2.22) and (2.24) are not valid for high Reynold's numbers. The reason is that large size bubbles tend to elongate and flatten under unbalanced interfacial forces, resulting in a change of the bubble's motion and behavior.

As shown in Figure 2.10, in the case of contaminated water, viscosity and surface tension are key factors due to the change in shear stress over the bubble surface. For a bubble radius of more than 2.6 mm, an approximate formula for the terminal velocity as a function of the surface tension and liquid density is:

$$v_b = \sqrt{\frac{1.07\,\sigma}{\rho\, r_b} + 1.01\, g\, r_b} \qquad (2.26)$$

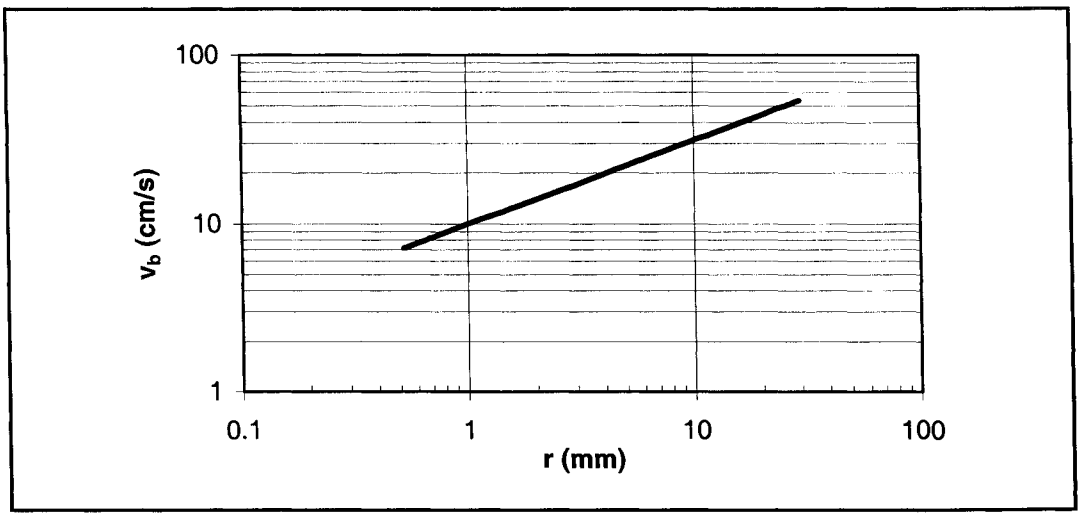

Figure 2.9: Velocity of bubble verses bubble radius

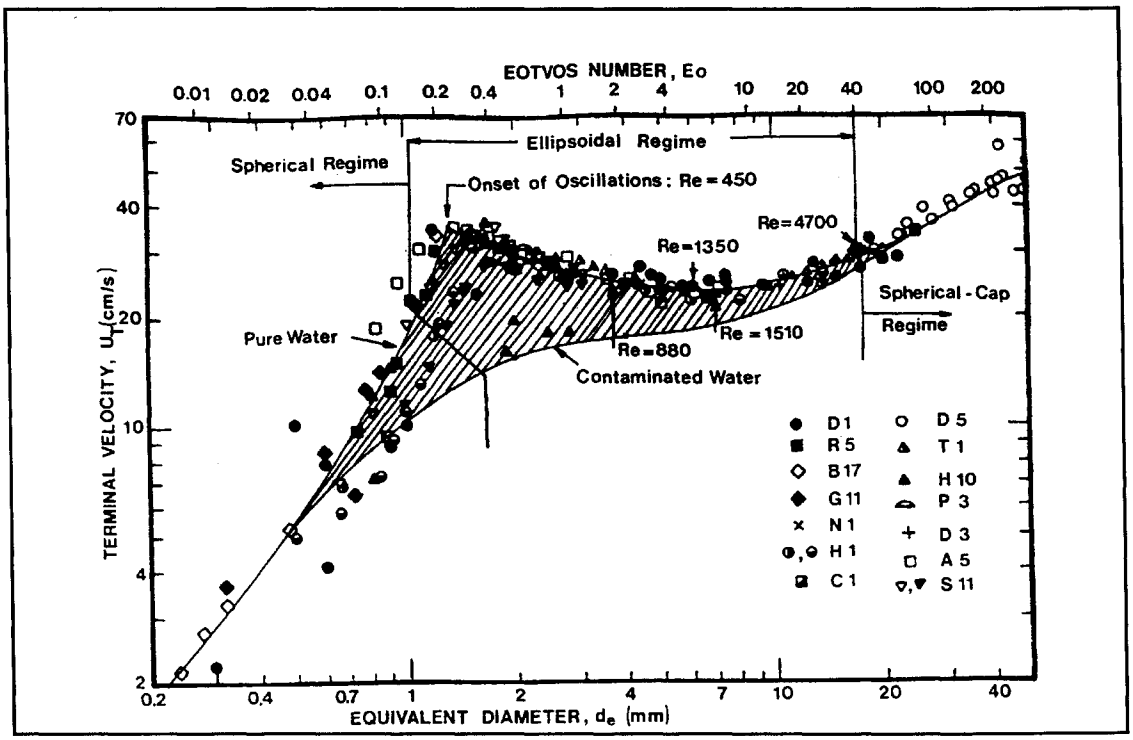

Figure 2.10: Experimental results of velocity and bubble radius (Clift et al., 1978)

2.2.2 Factors Affecting Bubble Rising

Air bubbles rise in water due to the change in pressure between the water and the air inside the bubble. However, the circular shape of the bubble suggests that air pressure inside the bubble is greater than the external water pressure. This mechanism of rising can be affected by many factors. First, a bubble's rising in a cylinder in the lab is different from one in an infinite boundary, which is termed the "wall effect" factor. As the bubble diameter increases, the tangential stresses around the bubble surface change and cause different patterns in the shape and the path of the bubbles. At a very high rate of air injection, bubbles can coalesce into one large bubble that subsequently collapses due to a decrease in pressure.

2.2.2.1 Bubble Size and Shape

Bubbles have different shapes and hydrodynamics paths due to changes in interfacial stresses at the bubble boundary. Figure 2.11 shows these different pathologies with changes in effective bubble diameter and Reynold's number. Since the shape of bubbles is not spherical, d_e represents an average or effective bubble diameter.

At high Reynold's numbers, surface tension and dragging forces create a significant imbalance of forces around a bubble. The forms of the dragging coefficient are changed due to the distribution of tangential stresses at the interface between the liquid and the bubble [Levich, 1962]. In addition, pressure distribution and shear stress cause the bubble to flatten and elongate, thereby causing a change in the shape of the bubble from spherical to ellipsoidal and then to "spherical cap" [Darby, 1996].

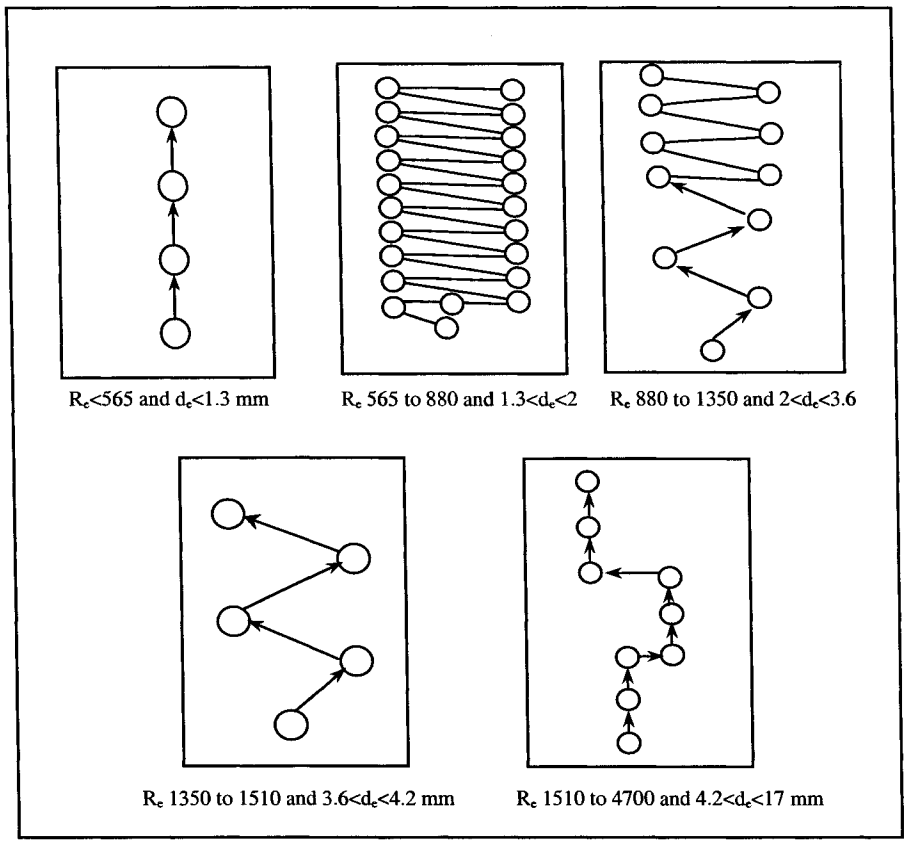

Figure 2.11: Bubble pathologies at different Reynold's number values (modified from Clift et al., 1978)

2.2.2.2 Wall Effect

The essential physical appearance of a bubble emerging in water indicates that the air gas is displaced by an equivalent volume of water. The displaced water responds to this by trying to travel away from the bubble. When a wall barrier exists near the bubble, displaced water will hit the wall and rebound back, thereby affecting the relative velocity of the bubble. In most groundwater applications, it is necessary to evaluate the infinite velocity, unless other structures located next to the injection well, such as a barrier or cutoff wall, are located near the injection point.

Several studies have focused on evaluating the wall effects on an air bubble traveling through water. Chhabra (1993) presented a correction factor, K_w, that can be multiplied by the infinite velocity of the bubble to yield the terminal velocity, as follows:

$$K_w = \frac{v_b}{v_\infty} = \left(\frac{1 - r/D}{1 - 0.475\ r/D} \right)^4 \qquad (2.27)$$

where v_b is the velocity of bubble in a container,

v_∞ is the velocity of bubble in an infinite medium,

r is the equivalent bubble diameter,

D is the distance between the bubble to the wall of the container.

Equation (2.27) is valid when r/D is less than 0.97 and Reynold's number is less than 1. For a large Reynold's number, (N_{Re}>1000) and r/D <0.8, the correction factor is independent of the Reynold's number and is given by the following equation:

$$K_w = \frac{v_b}{v_\infty} = 1 - \left(\frac{r}{D} \right)^{1.5} \qquad (2.28)$$

For a Reynold's number between 1 and 1000, the correction factor (K_w) should be a function of the Reynold's number [Chhabra, 1992; also see Darby, 1996]. In the study of bubble velocity in porous media, Roosevelt and Corapcioglu (1998) used the formula developed by Uno and Kintner (1956), as shown in Equation (2.29):

$$K_w = \frac{v_b}{v_\infty} = \left[\frac{1}{0.825} (1 - r/D) \right]^{0.769} \qquad (2.29)$$

2.3 Bubble Behavior in Porous Media

The mechanism of bubble migration in a saturated porous medium has been studied using many different porous media. Roosevelt and Corapcioglu, (1998) conducted a column experiment for measuring bubble velocity in pours media using spherical glass beads. The study showed that bubble velocity in a porous medium is linearly dependent on time. An experimental study carried by Burns and Zhang (1999) showed that the size of a soil particle has an inverse effect on the size of bubbles produced in a porous medium.

An increase in air pressure increases bubble diameter. At low air pressure, micro-bubbles can be produced having a size less than the void space between soil particles. Recently, micro-bubbles produced by using KVA C-sparge^{TM} have been utilized under tight soil conditions (hydraulic conductivity 10^{-1} ~ 10^{-5} cm/s) [Kerfoot, 2003]. Varhegyi et al. (1986) developed a formula of micro-bubble velocity in porous media by modifying Stoke's law (Equation 2.20). The formula employed is that of Stokes, with modified bubble radius (r) as follows:

$$r = 0.63\ \phi(\phi + 0.21)\ d_g, \qquad (2.30)$$

where ϕ = soil porosity and

d_g = average grain diameters of soil.

Eatiope and Lombardi (1996) conducted an experimental study confirming the above Equations 2.20 and 2.30. Their experiments were conducted for two types of sand, coarse and fine. In this study, results began to deviate from the theoretical results when air pressure exceeded 20 kPa (93.33 psi).

2.4 Air Channel Spacing and Size

Discrete air channels may form in saturated porous media as a result of advection air pressure's overcoming capillary pressure between soil particles. Ji et al. (1993) experimentally demonstrated this phenomenon, which has changed the fundamental concept of air sparging behavior.

The surface area of air channels differs from that of bubbles, and the behavoir of air in porous media is dissimilar in bubbling and channeling. For example, increasing the airflow rate increases the number of bubbles. For air channels, an increase in the airflow rate increases the number of air channels up to certain values. At high airflow rates, increasing the airflow rate strengthens the air channels rather than increasing their density or extending their zone of influence [Rutherford and Johnson, 1996]. In stratified heterogeneous soils, increasing airflow rate allows air channels to break through the soil layers [Ji et al., 1993]. Table 2.1 presents a summary of the experimental studies done in this field.

One may ask if an increase in the number of air channels improves the amount of mass removal of the contaminant. To date, there is no clear answer to this due to the lack of theoretical, experimental and field studies. However, to avoid confusion on this point, one should take into account the differences in experimental conditions. Some of the experimental studies targeted source zones and others considered dissolved zones. Experimental studies are usually carried out with homogenous soils and a fixed volume tank containing polluted water, whereas field studies are usually done with heterogeneous soils and moving groundwater. Finally, an increase in the number of air channels reduces

hydraulic conductivity and consequently the amount of contaminant flow that passes through the treatment zone.

The other issue is the extent and depth of the influence zone that yields optimal air distribution. Experimental work carried out by Ji et al. (1993), using a Plexiglas tank of 2 ft depth with a homogenous porous medium, demonstrated that the air zone had conical shapes. The extent of the zone of influence reached approximately the same depth. Similar conclusions were drawn from field studies carried out by Leeson et al. (1995) and Lundegard and LaBreque (1998). More field studies for evaluating air distribution using pilot tests were done with tracer indicators and pressure transducers [Bruce et al., 2001].

In channeling, the pilot study is very important for specifying the zone of influence because the air channels are sometimes unpredictable. From the perspective of experience, either pulsing or cycling the airflow rate during an air sparging operation can help increase the number of air channels. The difference between pulsing and cycling is the shutting off of the system and then turning it back on over a period of hours for pulsing, and a week or months for cycling. Bass et al. (2000) stated that pulsing does not change the size of the zone of influence. Gorden (1998) argued that when shutting off the system and turning it back on for pulsing, air channels followed the same path formed during the early time of operation. In addition, initial formation of air channels plays a key role in long-term operation. Finally, Gorden et al. (1998) stated that a hasty increase in airflow operation rate would not help increase the number of air channels.

2.5 Application of Air Sparging

Air sparging is an innovative technology used for sites that have been contaminated by chlorinated solvent or petroleum hydrocarbons or both. The primary mass transfer mechanisms of air sparging are volatilization and aerobic bioremediation. For hydrocarbons of concentrations greater than 1 mg/l, volatilization is the dominant mechanism [Johnson, 1998], while for concentrations less than 1 mg/l, aerobic biodegradation is applied.

The average dissolved oxygen in groundwater is between 5-6 mg/l and the average percentage of concentration of oxygen in atmospheric air is 21%. At low contaminant concentrations, the oxygen gradient between the dissolved and gas phase is high, and oxygen diffusion in the dissolved phase increases. With oxygen, aerobica bioremediation enhances and promotes the degradation process.

Air sparging performs best when applied to homogenous and sandy formations. For soil of low hydraulic conductivity, pulsing with low airflow rates works well [Kirtland and Aelion, 2000]. The following section describes the type of air sparging that can be applied under various site conditions.

Table 2.1: Summary of experimental studies [Peterson et al., 2001]

Reference	Grain size (mm)	Medium	Flow (L/min)	Pressure (kPa)	Overall geometry	Characteristics
Peterson et al. (2000)	0.841–1.00	Natural	1.0–1.3	8.3–8.9	Mosaic pattern of meandering channels	Discrete channels with distinct boundaries
	1.00–1.19	Natural	1.0–1.3	8.3–8.9		
Peterson et al. (1999)	1.1[a]	Natural	0.2–1.1	4.8–8.9	Mosaic pattern of meandering channels	Discrete channels with distinct boundaries
	1.3[a]	Natural	0.2–1.1	4.8–8.9		
	1.84[a]	Natural	0.2–1.1	4.8–8.9	Symmetrical cone around injection point	Pervasive bubbly flow
	2.61[a]	Natural	0.2–1.1	4.8–8.9		
	4.38[a]	Natural	0.2–1.1	4.8–8.9		
Wehrle (1990)	3[b]	Natural			Limited area around injection point	Flow as discrete, non-continuous pulsating air bubbles
	0.8[b]	Natural				
Ji et al. (1993)	4	Glass beads	0.6–10	1.6–22.4	Symmetrical parabolic cone around injection point	Bubble flow
	2	Glass beads	3	4	Dense, parabolic plume of bubble streams	Bubble flow and Channel flow
	0.75	Glass beads	0.6–10	4.7–27.1	Few, narrow channel paths	Channel flow
Adams and Reddy (1997)	2.5[b] (1.88)[c]	Natural	2.23	6.9	Uniform flow throughout soil	Bubble flow
	0.43[b] (1.28)[c]	Natural	2.23	6.9	Extensive network of channels	Channel flow
	0.20[b] (3.25)[c]	Natural	2.23	6.9		Channel flow
	0.18[b] (1.39)[c]	Natural	2.23	6.9		Channel flow
	0.08[b] (1.38)[c]	Natural	2.23	6.9	One or two channels only	Channel flow
Brooks et al. (1999)	3.0	Glass beads	0.023–2.1	6.6–12.9		Bubble flow
	2.0	Glass beads	0.020-0.90	6.2–7.2	Pervasive flow	Slugs of air
	2.0	Glass beads	0.175-0.45	7.8–8.6	Transitional	Mix of bubbles or slugs and channels
	2.0	Glass beads	1.15–1.625	10.2–12.1		Channel flow
	1.5	Glass beads	0.020	6.8	Pervasive flow	Slugs of air
	1.5	Glass beads	0.080	7.2	Transitional	Mix of bubbles or slugs and channels
	1.5	Glass beads	0.30–2.05	8.4–12.1		Channel flow
	1.0	Glass beads	0.020	6.4	Pervasive flow	Slugs of air
	1.0	Glass beads	0.070–1.825	7.2–12.7		Channel flow
	0.71–0.80	Glass beads	0.02–1.93	6.6–13		Channel flow
	0.42–0.50	Glass beads				Channel flow
Elder and Benson (1999)	2[d]	Glass beads	0.35–11.1	4.1–11.0	Channelized flow	Tortuous pore-scale channels, discontinuous and continuous slugs of air
	0.6[d]	Glass beads	4.4	4.8	Channelized flow	Straight pore-scale channels, discontinuous and continuous slugs of air
	0.2[d]	Glass beads	12.0–17.1	10.3–17.2	Widely spaced channels	Straight pore-scale channels, discontinuous and continuous slugs of air

[a] Average modal grain diameter
[b] d_{10}
[c] $(=d_{50}/d_{10})$
[d] Approximate d_{50} from published particle-size distribution curve

2.6 Types of Air Sparging

Different techniques have been carried out using air sparging as remediation for volatile contaminants of groundwater. For deep water, well air sparging is a valid method, where the well pipes are drilled vertically to the appropriate distance below the water table (Figure (2.12)). For a shallow water table (less than 25ft), air sparging utilizes a horizontal well for soil remediation.

The horizontal well is more efficient and economical than the vertical well for the following reasons:

- Although cost per foot for horizontal wells is more than for vertical wells, the horizontal wells cover more horizontal area than the vertical wells. As a result, one horizontal well can take the place of several vertical wells and reduce the overall system cost.
- Air distribution (channels or bubbles) above injection line in horizontal wells is evenly distributed. In vertical wells, there is a dead zone between two adjacent vertical wells.
- Horizontal wells are more visible where homogenous soil layers exist above the well and,.
- The remediation time for horizontal wells is less than vertical (about 1/5).

There are two types of horizontal wells. First, the trench air sparging well involves excavating a trench with variable trench depth and width. High permeability backfill (coarse sand or crushed rock) fills the trench for better performance. The pattern flow behavior of air bubbles is involved in this method. In general, air bubbles have more surface area than air channels. In addition, a low permeability porous medium contaminant diffuses slowly between air channels, thus limiting the remediation time.

The second type of horizontal well is directly drilled into the subsurface at some angle and then extended horizontally. This method has the advantage of avoiding any obstacle, structural or utility, that hampers or limits the project.

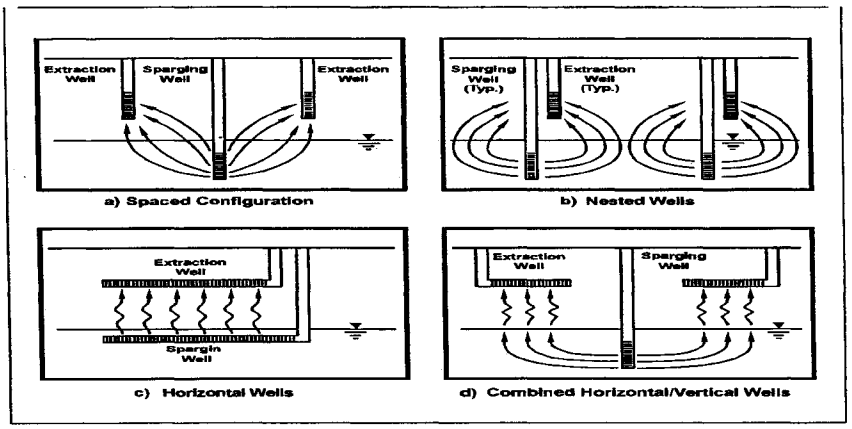

Source: "Advances in Air Sparging Design." The Hazardous Waste Consultant, Vol. 11, Issue 1, January/February 1993, p. 1-4.

Figure 2.12: In situ air sparging types

2.7 Air Sparging Modeling

In modeling air sparging, two principle models have been applied: air bubbles and air channels. These air formations are different in surface area and air residency in the subsurface. The residence time for air bubbles depends on bubble velocity, while for air channels it depends on advection of air velocity within the channel tube. Obviously, modeling air sparging is different for bubbling and channeling. The following sections present both models.

2.7.1 Bubble-Flow Models

Seller and Schreiber (1992) suggested simple analytical exponential terms for concentration in an aqueous phase using diffusion and Fick's first law. However, the model neglected to take into consideration moving groundwater and assumed the

concentration in the aqueous phase to be completely mixed. Wilson et al. (1994) modified the Seller and Schreiber model to determine bubble velocity. Marley et al. (1994) extended Seller and Schreiber's work by considering the reduction in hydraulic conductivity due to an increase in airflow within the air sparging zone. Pankow et al. (1993) developed an analytical model using mass balance in an aqueous phase utilizing Henry's law and assuming the dissolved phase to be completely mixed. Pankow et al. (1993) also assumed that building cutoff walls would control contaminant plumes. Wilson et al. (1992) used a similar method but considered bubble volume changes due to changes in hydrostatic pressure.

2.7.2 Air-Channel Models

Many physical models have been developed to utilize air sparging for the purpose of air channeling. The two most common procedures for modeling air sparging are equilibrium (Henry's law) and non-equilibrium (the Two Film theorem) mass transfer process.

Wilson (1992) developed an analytical model for air channels in vertical wells. This model is based on the conservation of mass. A similar approach was used by May et al. (2002) to obtain a numerical solution for air sparging. Dijke et al. (1995), Landegard and Anderson (1996), McCray and Falta (1997) used a multiphase flow model and applied it to air sparging. All the above work assumed the validity of Darcian flow in advection of air phase. Moreover, local equilibrium was applied for each cell. Rabideau and Blaydon (1998) developed an analytical solution considering contaminant sorption and non-equilibrium mass transfer of aqueous phase only. However, the model neglected mass

inflow due to advection and assumed complete mixing of the contaminant. Elder et al. (1999) tried to solve the non-equilibrium mass transfer of the aqueous phase numerically, assuming diffusion to be a controlling mechanism. An excellent literature review has been presented by McCray (2000), stating that most models consider mass-transfer for either aqueous or gas phases. To date, there has been no model considering both phases. In this study, a two-compartments model will be presented without assuming complete mix.

CHAPTER 3

MASS BALANCE DERIVATIONS OF SPARGING SYSTEMS

3.1 Introduction

Mass balance is the most common way for establishing a model procedure for stripping systems. The equation used for designing air stripping towers is derived by using enthalpy balance over controlled volume element and mass balance of represented element volume (REV). The full derivation of designing air stripping towers is shown in Appendix C. In this chapter, the focus is deriving the deferential equations for the two phases using the mass balance within an REV in three different cases of air stripping applications: fixed volume, counter-current flow, and cross-current flow.

3.2 Fixed Volume Case

The first case is where contaminated water is stagnant within a fixed volume size. The stripping method is to introduce air or bubbled air either from the bottom or top. For this case, balance equations are formed for three phases: dissolved, vapor, and material balance for both air and water.

3.2.1 Dissolved Phase Mass Balance (Fixed Volume)

The general mass balance for the dissolved phase is (Figure 3.1)

$$(m^o_{out} - m^o_{In})_{dissolved} + m^o_{IPT} = -\frac{\partial m_{Box}}{\partial t} \qquad (3.1)$$

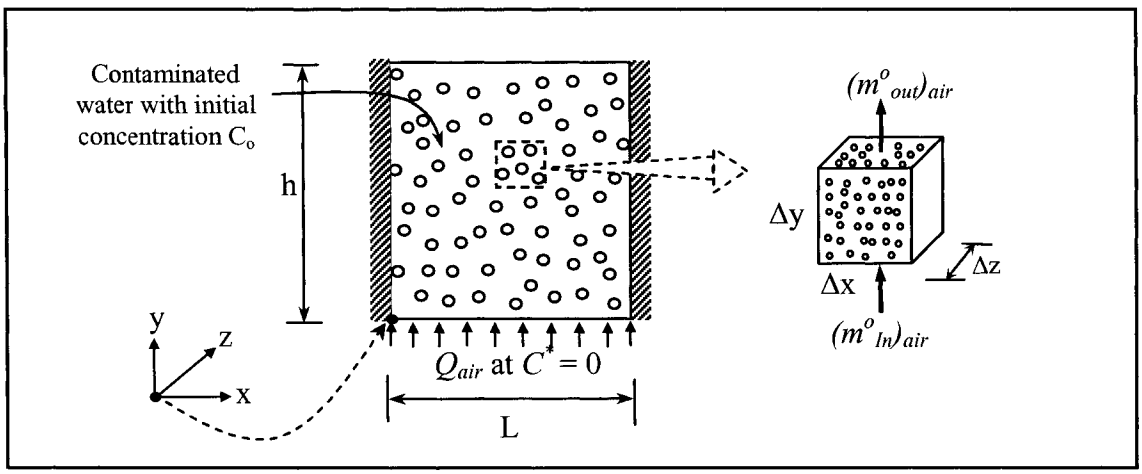

Figure 3.1: Fixed volume condition

Where m^o_{out} = contaminant mass rate entering REV box as dissolved phase (M/T).

m^o_{In} = contaminant mss rate leaving REV box as dissolved phase (M/T).

m^o_{IPT} = contaminant mass rate loss within REV box as dissolved phase (M/T).

m_{Box} = contaminant mass in dissolved phase (M/T).

Now, $m^o_{out} = m^o_{In}$ and is equal to zero since no water flux enters or leaves REV and m_{Box} is equal to:

$$m_{Box} = C\,\phi\,(\Delta x\,\Delta y\,\Delta z) = C\phi\,V_{Box}$$

Applying tow-film theory m^o_{IPT} can be written as

$$m^o_{IPT} = K_L\,(SA)\,(C - C^*)$$

Where K_L= Overall mass transfer coefficient.

SA = surface area of gas boundary.

C= Concentration of contaminant in dissolved phase.

C^* = Equivalent dissolve concentration in (mg/l).

ϕ = media porosity.

By defining $a = SA/V_{Box}$, Equation (3.1) then can be rewritten as

$$\frac{\partial C}{\partial t} = -\frac{K_L a}{\phi}(C - C^*) \qquad (3.2)$$

3.2.2 Vapor Phase Mass Balance (Fixed Volume)

The mass balance gas phase is

$$\left(m^o_{Out} - m^o_{In}\right)_{air} - m^o_{IPT} = -\frac{\partial m_{Box}}{\partial t}$$

Where $m^o_{In} = Q_{air} G$ and $m^o_{Out} = Q_{air} G_{Out}$

G_{In} = the concentration of gas phase entering REV (M/ V_{air}).

Q_{air} = Air flow rate in L^3/T.

G_{Out} = Concentration of gas phase leaving REV (M/V_{air}).

Then

$$\left(m^o_{Out} - m^o_{In}\right)_{air} = Q_{air}(G_{out} - G_{In})$$

Using Forward Taylor series and neglecting second term and above

$$G_{Out} = G_{In} + \frac{\partial G}{\partial y}\Delta y$$

Then using Henry's law as Equation 2.3

$$\left(m^o_{Out} - m^o_{In}\right)_{air} = q_{air} H \frac{\partial C^*}{\partial y}$$

Where $q_{air} = Q_{air}/(\Delta x\, \Delta z)$

Mass balance of vapor phase of fixed volume condition will be

$$q_{air}H\frac{\partial C^*}{\partial y} - K_L a\,(C - C^*) = \phi\frac{\partial C^*}{\partial t} \qquad (3.3)$$

At steady state

$$\frac{\partial C^*}{\partial y} = \frac{K_L a}{q_{air}H}(C - C^*) \qquad (3.4)$$

3.2.3 Material Balance (Fixed volume)

Using the mass balance approach based on the control volume, the mass rate entering and leaving the system can be written for fixed volume water case as:

$$(m^o_{out} - m^o_{In})_{dissolved} + (m^o_{out} - m^o_{In})_{air} = -\frac{\partial m_{Box}}{\partial t} \qquad (3.5)$$

For a fixed volume, m^o_{In} and m^o_{out} for a stagnant water solution equal to zero. Mass of vapor in comparison to mass of solution is very small, so total mass in box (m_{Box}) in REV is equal to the mass of water solution.

$$m_{Box} = C\,\phi\,(\Delta x\,\Delta y\,\Delta z) = C\phi V_B$$

Using Forward Taylor series as in section 1.2

$$\frac{\partial C}{\partial t} = -\frac{q_{air}H}{\phi}\frac{\partial C^*}{\partial y}$$

3.3 Counter-Current Flow

Counter-current flow is the case where contaminated water and air are injected in opposite directions (Figure 3.2). An air stripping tower is an example of application of counter current.

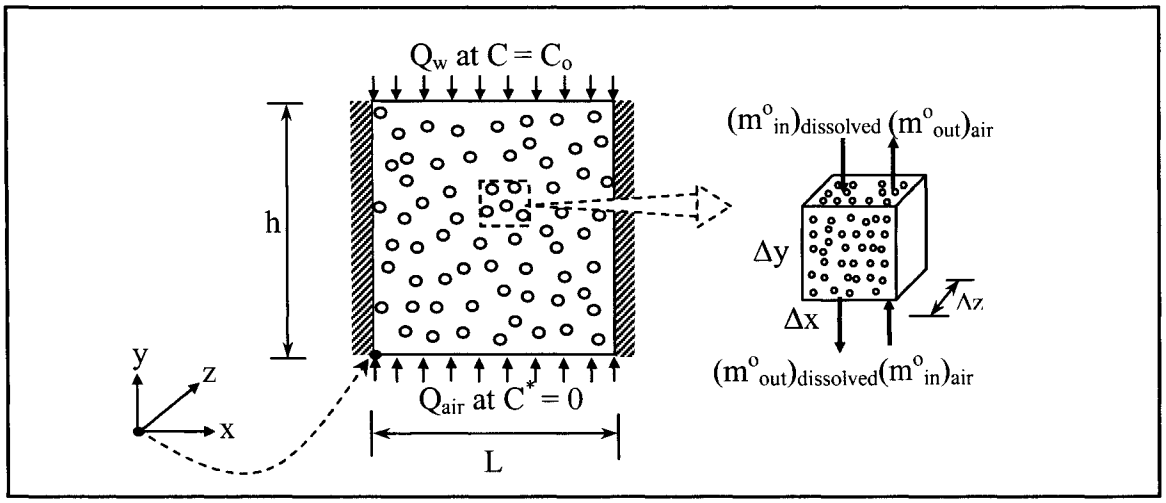

Figure 3.2: Counter-current flow

3.3.1 Dissolved Phase Mass Balance (Counter-Current flow)

General mass balance dissolved phase is

$$(m^o_{out} - m^o_{In})_{dissolved} + m^o_{IPT} = -\frac{\partial m_{Box}}{\partial t} \qquad (3.6)$$

Where $(m^o_{in})_{dissolved} = Q_w C_{in}$ and $(m^o_{out})_{dissolved} = Q_w C_{out}$

Q_w = flow rate of water effluent into system.

C_{in} = Concentration of contaminant entering REV.

C_{out} = Concentration of contaminant leaving REV.

Backward Taylor expansion of concentration in dissolved phase and neglecting higher order terms will be as

$$C_{out} = C_{in} - \frac{\partial C}{\partial y}\Delta y$$

Then

$$(m^o_{out} - m^o_{In})_{dissolved} = -q_w V_{Box} \frac{\partial C}{\partial x}$$

Using vales of m_{Box} and m^{o}_{IPT}

$$m_{Box} = C\,\phi\,(\Delta x\,\Delta y\,\Delta z) = C\phi V_{Box}$$

$$m^{o}_{IPT} = K_L\,(SA)\,(C - C^*)$$

Again using the same definitions of a ($a=SA/V_{Box}$) mass balance of counter-current in dissolved phase will be

$$q_w \frac{\partial C}{\partial y} - K_L\,a\,(C - C^*) = \phi \frac{\partial C}{\partial t} \qquad (3.7)$$

Steady state of mass balance in counter-current condition yields

$$\frac{\partial C}{\partial y} = \frac{K_L\,a}{q_w}(C - C^*) \qquad (3.8)$$

3.3.2 Vapor Phase Mass Balance (Counter-Current)

Derivation procedures of this case are similar to mass balance in air phase of fixed volume.

$$\frac{q_{air}}{\phi}\frac{\partial C^*}{\partial y} - \frac{K_L\,a}{\phi H}(C - C^*) = \frac{\partial C^*}{\partial t} \qquad (3.9)$$

Where $q_{air} = Q_{air}/(\Delta x\,\Delta z)$

And again at steady state

$$\frac{\partial C^*}{\partial y} = \frac{K_L\,a}{q_{air}H}(C - C^*) \qquad (3.10)$$

3.3.3 Material Balance (Counter-Current)

General material balance is

$$(m^o_{out} - m^o_{In})_{dissolved} + (m^o_{out} - m^o_{In})_{air} = -\frac{\partial m_{Box}}{\partial t} \qquad (3.11)$$

Where $(m^o_{out} - m^o_{In})_{dissolved} = -q_w V_{Box} \frac{\partial C}{\partial y}$ (Backward Taylor series)

$$(m^o_{out} - m^o_{In})_{air} = q_{air} V_{Box} H \frac{\partial C^*}{\partial y} \qquad \text{(Forward Taylor series)}$$

$$m_{Box} = C\,\phi V_{Box}, \quad V_{Box} = \Delta x\,\Delta y\,\Delta z, \quad q_w = \frac{Q_w}{\Delta y \Delta z}, \text{ and } q_{air} = \frac{Q_{air}}{\Delta x \Delta z}$$

Then Equation (3.11) can be written as

$$q_w \frac{\partial C}{\partial y} - q_{air} H \frac{\partial C^*}{\partial y} = \phi \frac{\partial C}{\partial t} \qquad (3.12)$$

Steady state material mass balance of counter current condition is

$$\frac{\partial C}{\partial y} = \frac{q_{air} H}{q_w} \frac{\partial C^*}{\partial y} \qquad (3.13)$$

3.4 Cross-Current Flow

Injecting air which crosses a polluted water solution current is the case called cross current. An application of cross current is an air sparging system (Figure 3.3), and (Figure 1.1). For this case, Air Sparging would be an application case of cross current since injection air crosses groundwater current.

3.4.1 Dissolved Phase Mass Balance (Cross Current)

General Mass Balance in dissolved phase written as

$$(m^o_{out} - m^o_{In})_{dissolved} + m^o_{IPT} = -\frac{\partial m_{Box}}{\partial t} \qquad (3.14)$$

Where $(m^o_{out} - m^o_{In})_{dissolved} = q_w V_{Box} \dfrac{\partial C}{\partial x}$ (Forward Taylor Series)

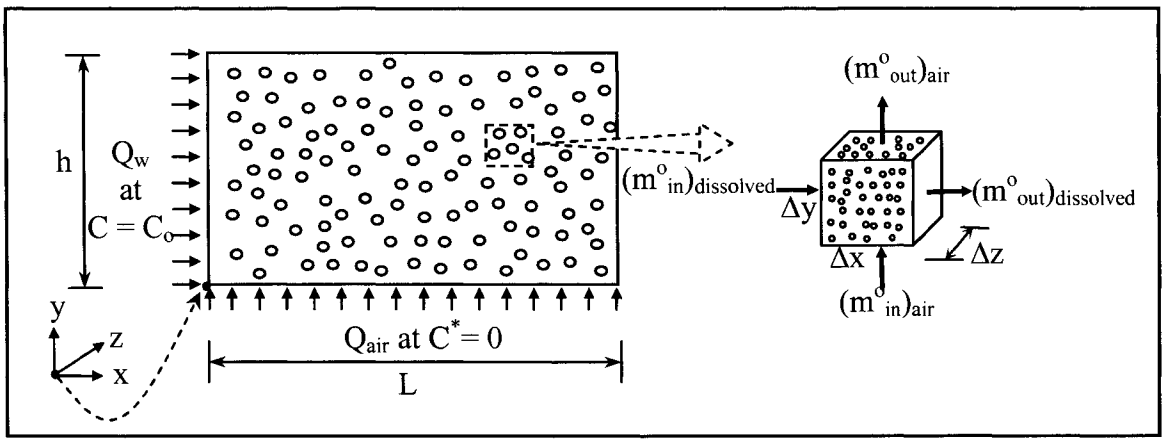

Figure 3.3: Cross-current flow condition

$$m^o_{IPT} = K_L\, SA\,(C - C^*)$$

$$m_{Box} = C\,\phi\, V_{Box}, \quad V_{Box} = \Delta x\,\Delta y\,\Delta z, \quad a = \frac{SA}{V_{Box}}, \text{ and } q_w = \frac{Q_w}{\Delta y \Delta z}$$

Equation (3.14) can be written as

$$q_w \frac{\partial C}{\partial x} + K_L\, a\,(C - C^*) = -\phi \frac{\partial C}{\partial t} \tag{3.15}$$

Steady state mass balance of dissolved phase is

$$\frac{\partial C}{\partial x} = -\frac{K_L a}{q_w}(C - C^*) \tag{3.16}$$

3.4.2 Vapor Phase Mass Balance (Cross-Current)

General mass balance in vapor phase is

$$\left(m^o_{Out} - m^o_{In}\right)_{air} - m^o_{IPT} = -\frac{\partial m_{Box}}{\partial t} \tag{3.17}$$

Where $(m^o_{out} - m^o_{In})_{air} = q_{air} V_{Box} H \dfrac{\partial C^*}{\partial y}$ (Forward Taylor series)

$$m^{o}_{lPT} = K_L\, SA\,(C - C^*)$$

$$m_{Box} = C\,\phi\, V_{Box}, \quad V_{Box} = \Delta x\,\Delta y\,\Delta z, \quad a = \frac{SA}{V_{Box}}, \text{ and } q_{air} = \frac{Q_{air}}{\Delta x \Delta z}$$

Equation (3.17) can be written as

$$q_{air}\, H \frac{\partial C^*}{\partial y} - K_L\, a\,(C - C^*) = \phi \frac{\partial C}{\partial t} \tag{3.18}$$

Steady state mass balance of dissolved phase is

$$\frac{\partial C^*}{\partial y} = \frac{K_L a}{q_{air} H} K_L\, a\,(C - C^*) \tag{3.19}$$

3.4.3 Material Balance (Cross-Current)

General material balance is

$$(m^{o}_{out} - m^{o}_{In})_{dissolved} + (m^{o}_{out} - m^{o}_{In})_{air} = -\frac{\partial m_{Box}}{\partial t} \tag{3.20}$$

Where $(m^{o}_{out} - m^{o}_{In})_{dissolved} = q_w V_{Box} \frac{\partial C}{\partial x}$ (Forward Taylor series)

$(m^{o}_{out} - m^{o}_{In})_{air} = q_{air} V_{Box} H \frac{\partial C^*}{\partial y}$ (Forward Taylor series)

$$m_{Box} = C\,\phi\, V_{Box}, \quad V_{Box} = \Delta x\,\Delta y\,\Delta z, \quad q_w = \frac{Q_w}{\Delta y \Delta z}, \text{ and } q_{air} = \frac{Q_{air}}{\Delta x \Delta z}$$

Then Equation (11) can be written as

$$q_w \frac{\partial C}{\partial x} + q_{air} H \frac{\partial C^*}{\partial y} = -\phi \frac{\partial C}{\partial t} \tag{3.21}$$

Steady state material mass balance of counter-current flow is

$$\frac{\partial C}{\partial x} = -\frac{q_{air} H}{q_w} \frac{\partial C^*}{\partial y} \tag{3.22}$$

CHAPTER 4

NUMERICAL SIMULATION OF CROSS CURRENT FLOW

4.1 Air Sparging Basic Mechanisms

There are three main mechanisms to remove the contaminant in the source and dissolved zones using air sparging (Figure 4.1). The first mechanism is volatilization to remove the hydrocarbons present in the dissolved phase by vaporization of the contaminant from the dissolved to the air phase. The second mechanism is direct vaporization from the hydrocarbon phase to the air phase, which exists in the source zone. The final process is enhanced biodegradation in the dissolved phase, which is achieved by increasing the oxygen content. The contaminant dissolved from source to the dissolved zone can be removed either by volatilization or biodegradation.

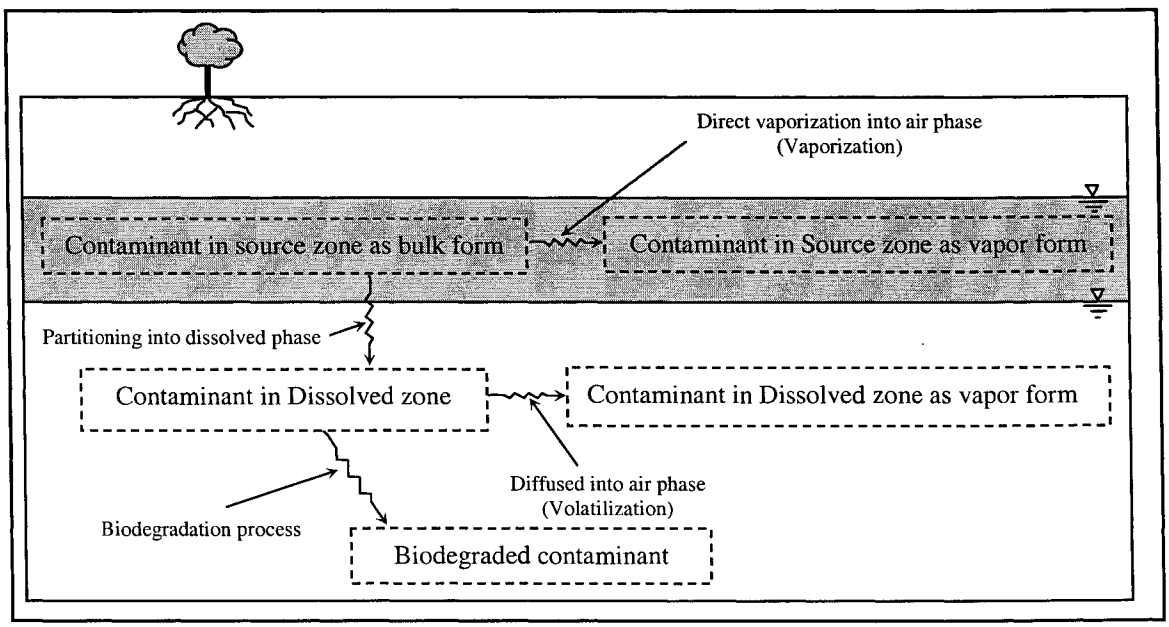

Figure 4.1: Possible mechanisms of mass removal using air sparging

Experimental and field studies done by Johnson, (1998), Johnston et al., (1998), and Aelion and Kirtland, (2000), showed that biodegradation is much less effective than volatilization. Mass removal from the dissolved zone by volatilization is the focus of this study.

There are two cases where the air sparging system could be modeled. Some models assume the contaminant plume to be stagnant "fixed-volume". In this case, it is reasonable to apply the unsteady state model, especially for the sites where contaminant is trapped by the aquifer formation or the plume is contained by barrier wells. However, remediation time is highly dependent on the volume of the plume in the stagnant area where plume migration is neglected. For coarse sandy sites, groundwater moves relatively faster and air sparging wells are installed to remediate the plume as it crosses the air phase as shown in Figure 5.2. It would be reasonable use steady state to estimate the number of wells needed to capture the plume and clean the site. The system design is highly dependant on the contaminant type, its concentration in the dissolved phase, and groundwater and air flow rates. Practitioner's experience is needed to deliver a reasonable amount of air for better air distribution. The second case, where contaminated groundwater passes through the zone of influence, is the focus in this study.

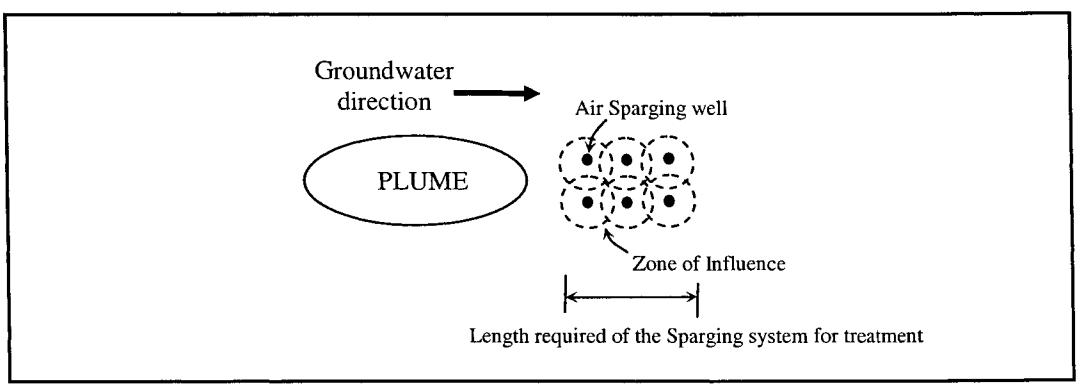

Figure 4.2: In situ air sparging system applications for cross current flow

4.2 Governing Equations and Boundary Conditions

The governing equations to be used in the modeling of air sparging was derived in chapter 3 and rewritten here as shown in equation (4.1), and equation (4.2).

$$\frac{\partial C}{\partial x} = -\frac{K_L a}{q_w}(C\text{-}C^*) \qquad (4.1)$$

$$\frac{\partial C^*}{\partial y} = \frac{K_L a}{q_{air} H}(C\text{-}C^*) \qquad (4.2)$$

Where

q_w and q_{air} can be approximated as $q_w = Q_w/(Height*Width)$ and $q_{air} = Q_{air}/(Length*Width)$

Equation (4.1) is the differential equation of the concentration changes in the dissolved phase. The differential equation describes the change in the concentration of the air phase shown in equation (4.2). The pair of equations (4.1) and (4.2) were written for cross-current flow and used as a basis for developing the numerical solution of air sparging. The concentration changes in these two equations vary in the two dimensional domain. This means that the concentrations in the two phases of dissolved and air are treated as not completely mixed. The other considerations in this system of equations are the concentration gradient, surface area, and mass transfer coefficient. When the physical process combines all these considerations together it is called non-equilibrium mass transfer. More discussion in how these parameters effect on the physical remove of the contaminant in the dissolved phase will be covered in detail in this and the next chapters.

The boundary conditions simulation for the air sparging system will be written using the system shown in Figure 3.3. As shown in this figure, the concentration of the dissolved phase reaches a certain value upon entering the system ($C\ (0,y) = C_o$) and a zero concentration of air phase where air is injected at the bottom of the system

($C^*(x,0)= 0$). For simplification, Equations (4.1) and (4.2) with the boundary conditions can be rewritten in the following form:

$$\frac{\partial C}{\partial x} = -K_1 (C\text{-}C^*) \quad C(0,y) = C_o \quad (4.3)$$

$$\frac{\partial C^*}{\partial y} = K_2 (C\text{-}C^*) \quad C^*(x,0) = 0 \quad (4.4)$$

Where $K_1 = K_L a / q_w$ and $K_2 = K_L a / (q_{air} H)$.

Equations (4.3) and (4.4) contain two dependent variables and two independent variables. These two equations should be solved simultaneously for the concentration in the air and dissolved phases. The solution for these two differential equations will be solved numerically and analytically as will be shown in this chapter and chapter 6. The focus here is to solve for the concentration in the dissolved phase. However, the concentration in the gas phase has been used for checking the program result using mass balance. In this chapter, a numerical solution using the finite difference math technique will be presented and discussed.

4.3 Finite Difference Procedure for Numerical Solution

The procedures used to solve equation (4.3) and (4.4) are to write backward the Taylor derivative for concentration in the dissolved and vapor phase as follows:

$$\frac{\partial C}{\partial x} = \frac{C_{i-1,j} - C_{ij}}{\Delta x} \quad (4.5)$$

and for vapor phase as

$$\frac{\partial C^*}{\partial y} = \frac{C^*_{i,j-1} - C^*_{i,j}}{\Delta y} \quad (4.6)$$

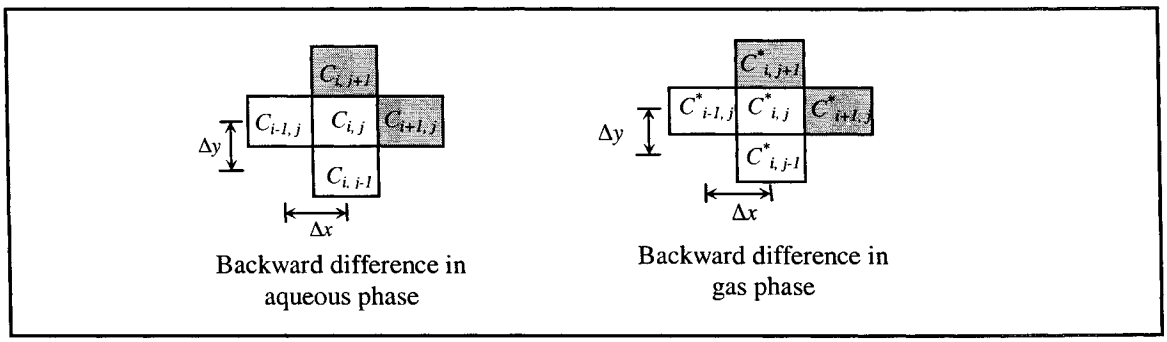

Figure 4.3: Schematic for the notation used for simulating the finite difference cells

Values of concentrations at cell i,j assumed to be an average of the two consecutive cells then equation (4.5) and (4.6) will be:

$$\frac{C_{i-1,j} - C_{i,j}}{\Delta x} = -K_1 \left(\frac{C_{i-1,j} + C_{i,j}}{2} - \frac{C^*_{i,j-1} + C^*_{i,j}}{2}\right) \qquad (4.7)$$

$$\frac{C^*_{i,j-1} - C^*_{i,j}}{\Delta y} = K_2 \left(\frac{C_{i-1,j} + C_{i,j}}{2} - \frac{C^*_{i,j-1} + C^*_{i,j}}{2}\right) \qquad (4.8)$$

For the first cell in the bottom row, $C_{i-1,j}$ and $C^*_{i,j-1}$ are known from the boundary condition. For other cells, values from previous computations are used. Computational procedures explicitly solve equation (4.7) and (4.8) simultaneously for each cell row by row. The iteration scheme for each cell is first to assume the initial value for $C_{i,j}$ and $C^*_{i,j}$ and as denoted by $C_{i,j}^{(0)}$ and $C^{*(0)}_{i,j}$ then correct the estimation by solving the following equations:

$$C_{i,j}^{(r)} = C_{i-1,j} + \tfrac{1}{2} K_1 \Delta x (C_{i-1,j} + C_{i,j}^{(r-1)} - C^*_{i,j-1} - C^{*(r-1)}_{i,j}) \qquad (4.9)$$

$$C^{*(r)}_{i,j} = C^*_{i-1,j} + \tfrac{1}{2} K_2 \Delta y (-C_{i-1,j} - C_{i,j}^{(r-1)} + C^*_{i,j-1} + C^{*(r-1)}_{i,j}) \qquad (4.10)$$

Where $r = 0, 1, 2 \ldots$

The iteration r stops when previous corrected values are less thatn new by 0.001. the source program is shown in Appendix D and written using Visual Basic program language. Software of spreadsheet (Excel) is used for running the Macro program. The

program solves for the concentration in the dissolve and gas phases for every point in the Sparging system. The program results are shown in the next section at different air sparging application.

4.4 Numerical Solution Applications

4.4.1 Plume Interception with Air Sparging Trench

The common assumption in modeling of air sparging is treating the zone of influence as a completely mixed zone. For a deep penetration air sparging well, this assumption doesn't represent the actual situation in field sites. The complete mixing assumption is basically taking into account the average of the concentrations in the vertical depth. For bubbling or channeling behavior, the contaminant concentration of air formation starts from zero concentration of the air phase as released from the air sparging well and increases in its concentration as it rises to the top of the aquifer. Apparently, the increase in the concentration of the hydrocarbon in the air phase decreases the concentration gradient and limits the mass transfer process. Consequently, the concentration of the contaminant at the bottom of the air sparging zone is less than the concentration at the top. In most models of air sparging, the concentration of the dissolved phase is calculated based on the average of the concentrations in a vertical direction. The average of concentrations in the vertical direction would be ambiguous especially for deeper sparging wells. In this study, a numerical solution has been developed to account for both non-equilibrium process of mass transfer diffusion and the concentration changes in two dimensional domains.

A hypothetical case has been simulated for a site contaminated with Benzene. The air sparging trench with a size of 1 m depth and 2 m length was set for capturing the Benzene plume (Figure 4.4). Site conditions and chemical properties used are summarized in Table 1. The trench was packed with crushed gravel so that bubbles would form in the trench. The bubble size was assumed to be 1 mm in diameter and bubble velocity is 0.1 m/s.

The unit surface area per dissolved volume (a) was calculated based on the assumption of a linear relationship between the surface area of one air bubble and its volume to the total surface area to the overall water volume in the trench (Equation (4.11)).

$$\frac{A_{bubble}}{V_{bubble}} = \frac{SA}{V_{air\ total}} \qquad (4.11)$$

Where A_{bubble} = Surface area of one bubble = $4\ \pi r^2$

V_{bubble} = Volume of one bubble = $4/3\ \pi r^3$

r = bubble radius.

$V_{air\ total}$= total air volume in the trench

SA = total surface of bubbles within the trench

The total air volume can be estimated from giving the total airflow rate, trench height, and bubble velocity (equation (4.12)).

$$V_{air\ total} = Q_{air}\ t = Q_{air}\ \frac{h}{v_b} \qquad (4.12)$$

Where Q_{air} = total airflow rate.

t = time of bubble to reach the top the trench.

h = trench height

v_b = bubble velocity

Combining equations 4.11 and 4.12 for total surface area (SA) is then written as

$$SA = \frac{3Q_{air}h}{r\,v_b} \qquad (4.13)$$

Using equation (4.13), the surface area per unit of dissolved volume a can be estimated now as

$$a = \frac{SA}{V_{dissolved}} = \frac{3\,q_{air}}{r\,v_b\,\phi} \qquad (4.14)$$

Where $V_{dissolve} = \phi h L w$

$q_{air} = Q_{air} / (w L)$

w, and L, are width, and length, of trench respectively.

ϕ = packed medium porosity of the trench.

The program has been found be stable for space steps in x and y directions of about 0.005 m in each direction. The program output gives Benzene concentrations in liquid and gas phases at each point in the trench. The program results for the concentration in the dissolved phase have been drawn in the colored contour graphs presented in Figure 4.5.

Figure 4.5 represents the concentration distribution in the dissolved phase along the trench. The color index shows the red color for high concentrations and blue for clean groundwater. The concentration distribution indicates that the top part of the trench is the part which has high concentration values in the dissolved phase. The physical interpretation for that is that the concentrations in the air phase are either in the form of air bubbles or the air channel is getting closer to the saturation limit at the top part of the sparging zone. As a result, the mass transfer mechanism is limited at the top part of the

Table 4.1: Chemical and soil properties

K_L (cm/hr)	H	ϕ	i Groundwater Gradient	K hydraulic conductivity (cm/s)	Q_w(m^3/s)	Q_{air} (m^3/s)	A/W air to water ratio
20.4	0.42	0.4	0.001	0.001	0.26	0.96	3.7

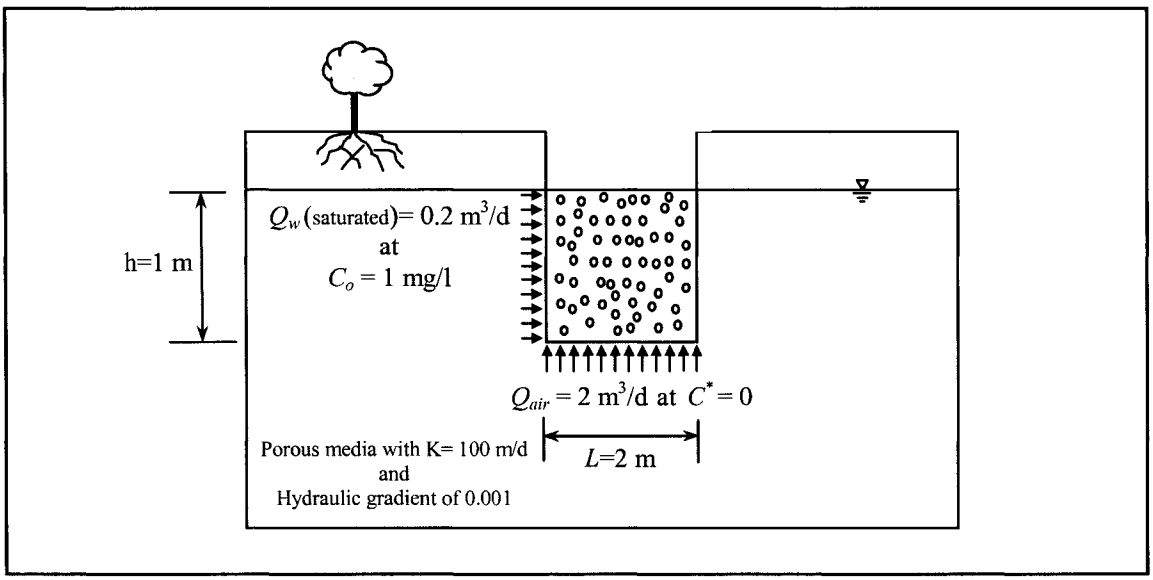

Figure 4.4: Hypothetical air sparging trench example cases

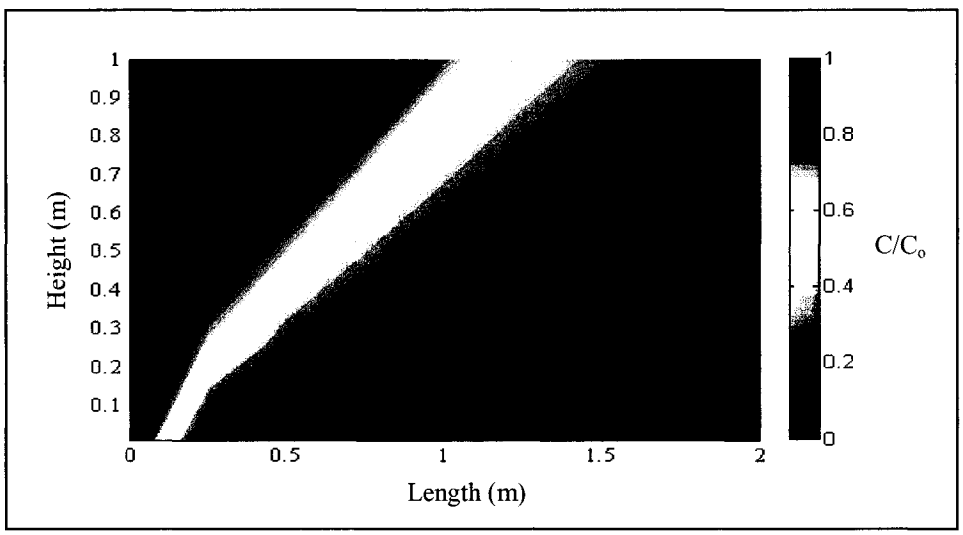

Figure 4.5: Numerical solution results at different points of the air sparging system

trench because the concentration deficit between the concentrations in the gas and dissolved phases is approaching zero. This is what is described by the resistance theory, which states that the concentration in the air phase increases, the concentration gradient will decrease and limit the mass transfer process. It is concluded from this concept, the increase in the values of the overall mass transfer coefficient and surface area are not necessary reduces the dissolved concentrations at every where in the air sparging domain.

4.4.2 Nonlinear Boundary Conditions Simulation

The availability of the chemical concentration in the dissolved phase as a result of contaminant dissociation from the source zone is controlled by the chemical characteristics of the contaminant such as solubility and molecular weight. In most cases, the concentrations in the dissolved phase as a result of source zone dissociation are not distributed evenly. One of the advantages of using a numerical solution is to handle more complicated cases of nonlinear boundary conditions. These include the case described in Figure 4.6. The source program has been modified for such simulation. The program results for the dissolved concentration distribution for nonlinear boundary condition is shown in Figure 4.7. The site and chemical conditions for the hypothetical case used for the run here were the same as the conditions described in section 4.4.1. The modified program is shown in appendix D. The concentration distribution at the boundary is assumed to be polynomial to the second degree.

The purpose of this section is to demonstrate the capability of the numerical program to handle more complicated cases. As will be presented later, the numerical program presented here can run with other multiphase contaminant transport software.

The advantage of this is to show that the program is numerically flexible and can run with other software to consider other physical and chemical reactions besides volatilization, such as biodegradation and reduction in hydraulic conductivity.

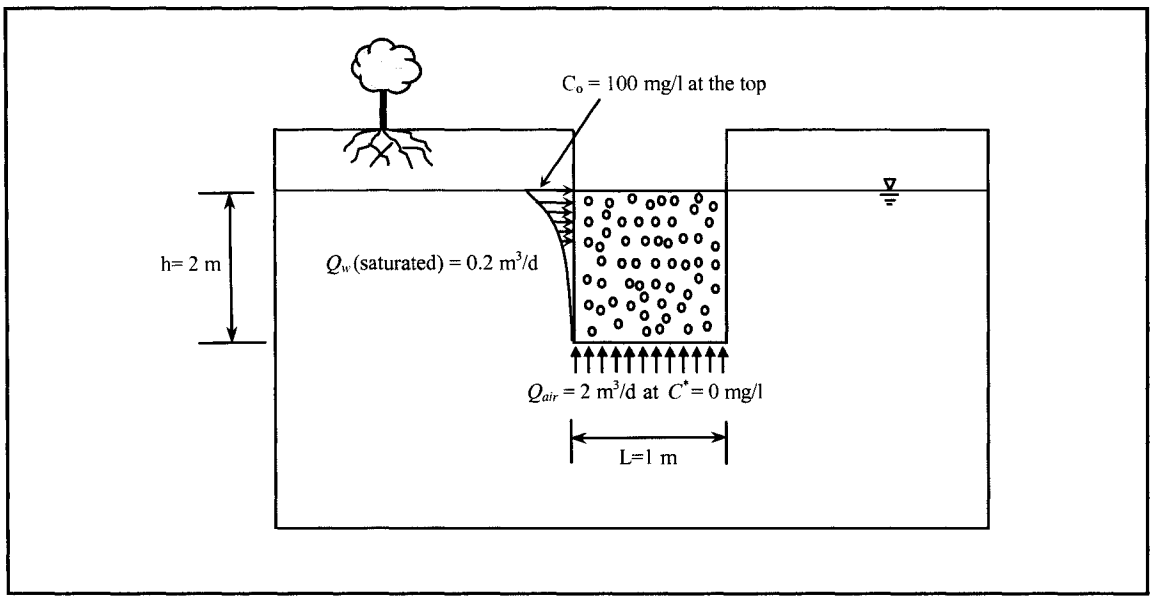

Figure 4.6: Non-linear distribution of the contaminant

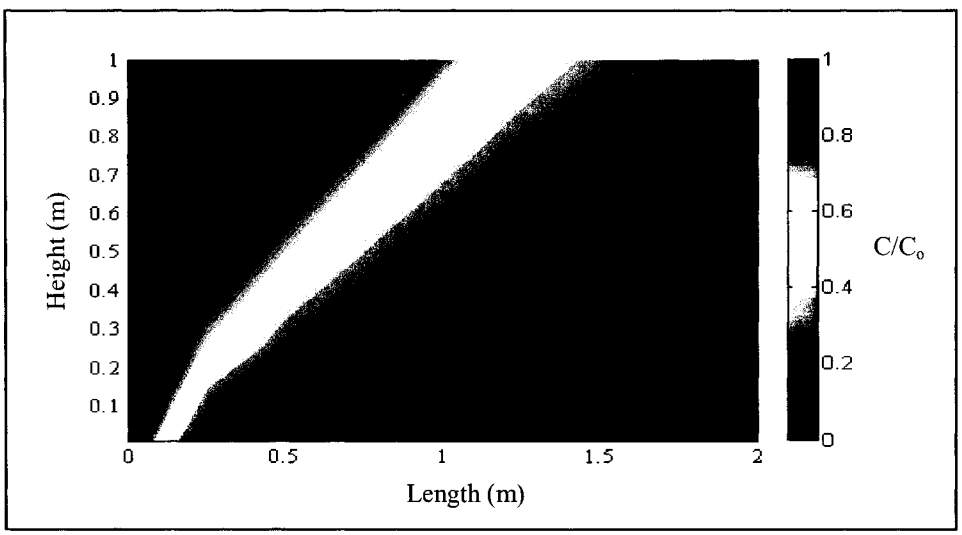

Figure 4.7: Program results for nonlinear boundary condition

4.5 Model Sensitivity for the Parameters

The cross flow model presented in this chapter is used to test the sensitivity of the physical and chemical design parameters. The dissolved concentration profile along the far top of the trench was used as a basis for comparing the program results at different parameters. By looking at the differential equations used in this model, equations (4.3) and (4.4) have two group parameters, K_1 and K_2. K_1 and K_2 are two groups of designing parameters which control the concentration removal in the dissolved and air phases. If we divide K_1 by K_2, the mass transfer coefficient and surface area will cancel out. Equation (4.15) presented K_1/K_2 ratio and this equation will be used to study the effect of the design parameters of Henry's constant, air to water ratio and trench size.

$$K_1 / K_2 = H(A/W)\frac{L}{h} \qquad (4.15)$$

Where A/W is air to water flow rate ratio (Q_{air}/Q_{water}), H Henry constant, and L and h are the length and height of air sparging system. For the given system of 5 ft ($\approx$ 1.5 m) depth, the concentration ratio profile at the top of the sparging system for different values of K_1/K_2 ratios is shown in Figure 4.8. As K_1/K_2 ratio increase in its value, the concentration ratio rapidly decreases.

Figure 4.9 demonstrates the change in the concentration ratio profile at the same group parameters ratio where K_1/K_2 equals 5 but at different magnitude of each group parameters values (K_1 and K_2). The Figure 4.9 shows the sensitivity of three parameters. These parameters are mass transfer coefficient, specific surface area, and width of the air sparging system. These parameters will increase each group parameters K_1 and K_2 by the same amount when they have the same value of K_1/K_2. Since we don't consider the change in concentration in the z direction, the value of width is always assumed on unit

length. The only two parameters left with no effect on the profiles of Figure 4.9 are mass transfer coefficient and specific surface area. As shown in Figure 4.9, the change in the mass transfer coefficient time specific surface area doesn't make major changes in the dissolved concentration when K_1 and K_2 reach high values. This means that increases in the values of the mass transfer coefficient and surface area will not necessarily cause a big change in the air sparging mass removal.

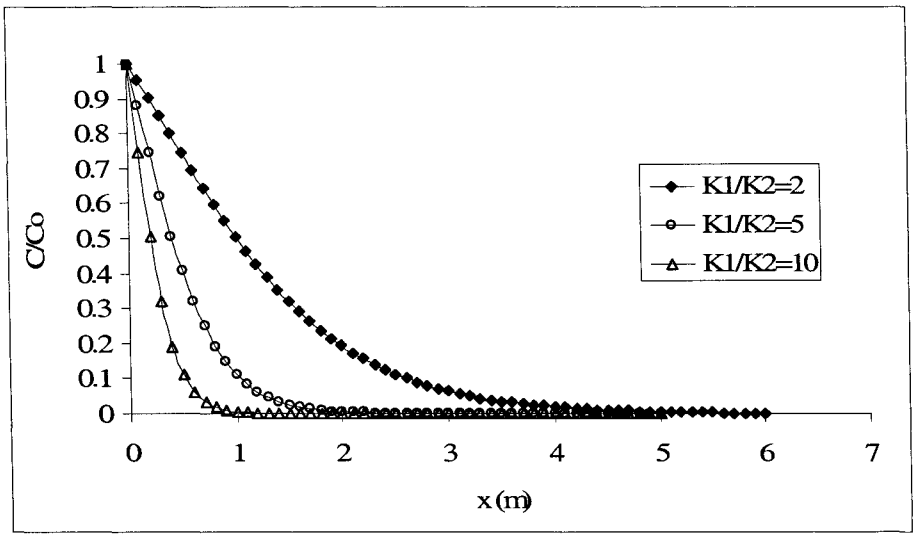

Figure 4.8: Concentration profile at different K_1/K_2 ratios

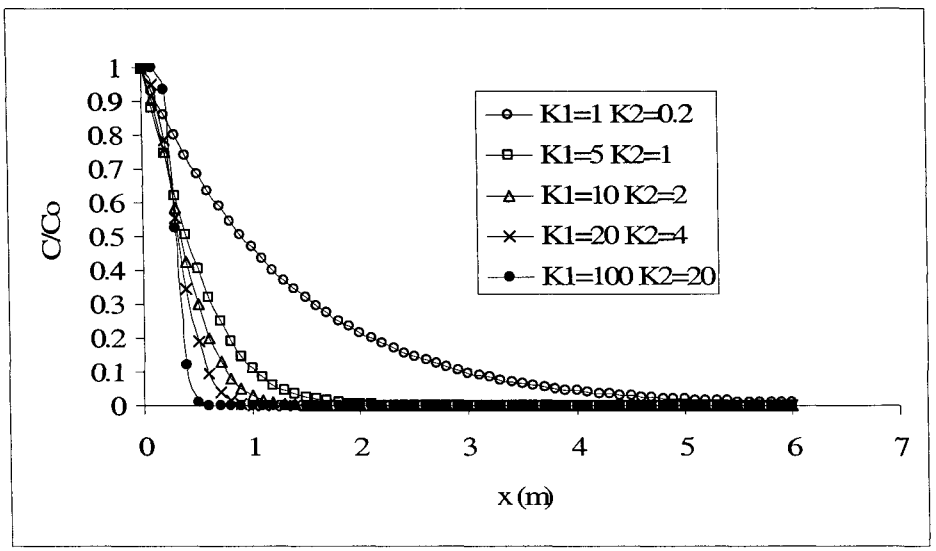

Figure 4.8: Concentrations changes at different K_1 and K_2 values and same K_1/K_2 ratio

As we conclude, the dimensions of the air sparging system, air to water ratio, and Henry's constant have a more direct effect on the air sparging mass removal mechanism than do the mass transfer coefficient and the specific surface area. The only designing parameter which could change during the air sparging operation is air to water ratio, which is believed to be the most important designing parameter. In section 4.6, the effect of the air to water ratio on mass removal will be discussed.

Finally, the only parameter not tested here is the initial contaminant concentration. Usually groundwater contaminants exist as a mix of chemical constituents which dissociate into the dissolved phase. Contaminants existing in the dissolved phase are highly dependent on their solubility. For this purpose, a sensitivity analysis for the model has been done to study the effect of initial concentrations on concentration profile. A selection of chemicals with properties needed in this model sensitivity study is shown in Table 4.2.

Chemicals with low solubility such as isooctane are unlikely to be found in the dissolved phase. However, because isooctane is lighter it can be expected to exist in the source zone. Air sparging could be helpful treating isooctane by direct vaporization since its vapor pressure is high. The effects of initial concentrations are clearly shown by comparing the concentration profiles of Benzene and Toluene since they have similar properties except for their solubility (Figure 4.9). Toluene with less solubility can be removed much faster than Benzene despite of similarities in other chemical properties.

Table 4.2: Chemical properties*

Chemical	TCE	o-Xylene	Benzene	Toluene	2,2,4-Trimethyl pentane (isooctane)
H	0.42	0.22	0.24	0.28	129
K_L(cm/hr)	20.4	22	26	24	22
K_L/H	48.6	100	108.3	85.7	0.2
Solubility (mg/l)	1000	175	1780	515	2.44
MCL (mg/l)	0.005	10	0.005	1	-----

* Bedient et al., 1994

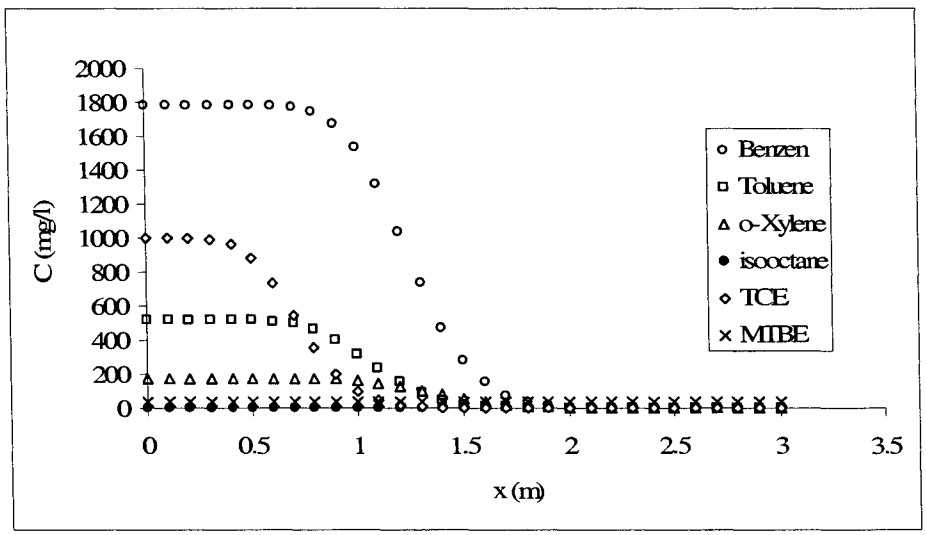

Figure 4.9: Concentration distributions for different chemicals at different solubility

4.6 The Effect of the Air to Water Ratio on Reduction of Hydraulic Conductivity

Opinions vary about what the airflow rate should be used in designing air sparging in the field. Table 1.2 in chapter 1, shows a range of airflow rates between 5 to 20 cfm which are used in the field. Some studies looked at the effect of the air flow rate on air distribution. Other experiments focused on the effect of airflow rate on the mass removal of the fixed volume tank. Overall, an insufficient number of theoretical, experimental, and field studies have led to confusion for air sparging parameters estimation.

Standard design protocol of air sparging does not consider the different application types of air sparging. As mentioned at the beginning of this chapter, air sparging can be treated as cross current flow where the contaminant plume crosses the air sparging wells, or fixed volume where the contaminant plume is contained by the barrier system. In the cross current flow application type, the increase in the airflow rate would decrease in the hydraulic conductivity and cause the contaminant to flow around the sparging zone rather than pass through it (Figure 4.10). This section focuses on the impact of the increase of airflow rate on the mass removal using the developed model with multiphase contaminant transport software.

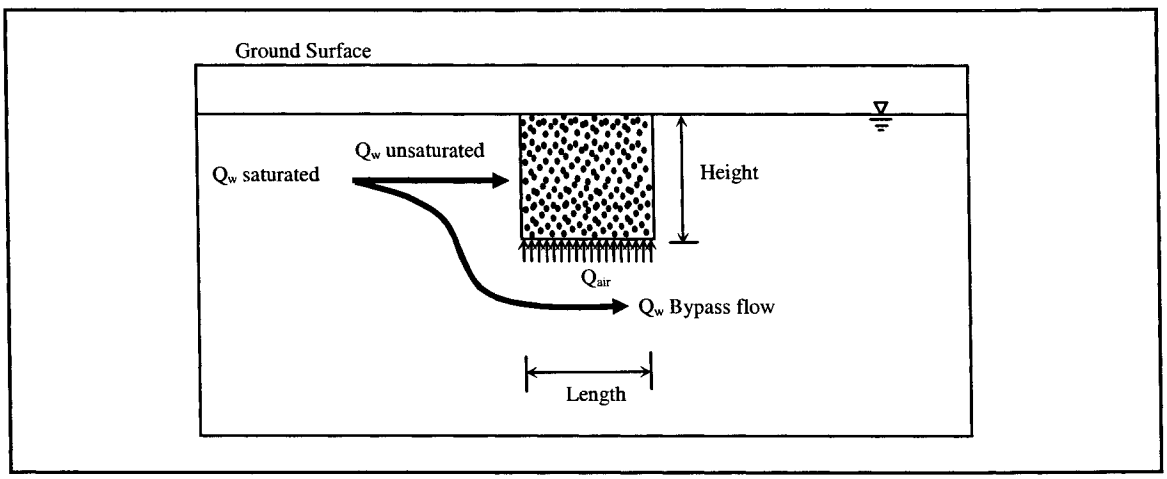

Figure 4.10: Schematic for the reduction in the hydraulic conductivity

In order to estimate the amount of the contaminant removed from the migrant plume, multiphase software is used for estimating the reduction in the hydraulic conductivity. The software used here is Subsurface Transport Over Multiple Phases (STOMP) developed by Pacific Northwest National Laboratory (PNNL) [White and Oostrom, 2003]. Input file script presents in appendix E. More discussion about the input file of the STOMP simulation will be covered in detail in Chapter 5. The STOMP simulation results for the reduction of the groundwater reduction with the increase of the

air to water ratio is graphically presented in Figure 4.11. The definition for air to water ratio is total airflow rate divided by the reduced value of the groundwater flow rate (Figure 4.10). The STOMP included an air sparging trench filled with coarse sand with porosity of 0.4 and with Van Genuchten parameters of α and n at 2.5 1/m and 2.0 respectively. From Figure 4.11, the most groundwater reduction rate occurs within an air to water ratio range of 50.

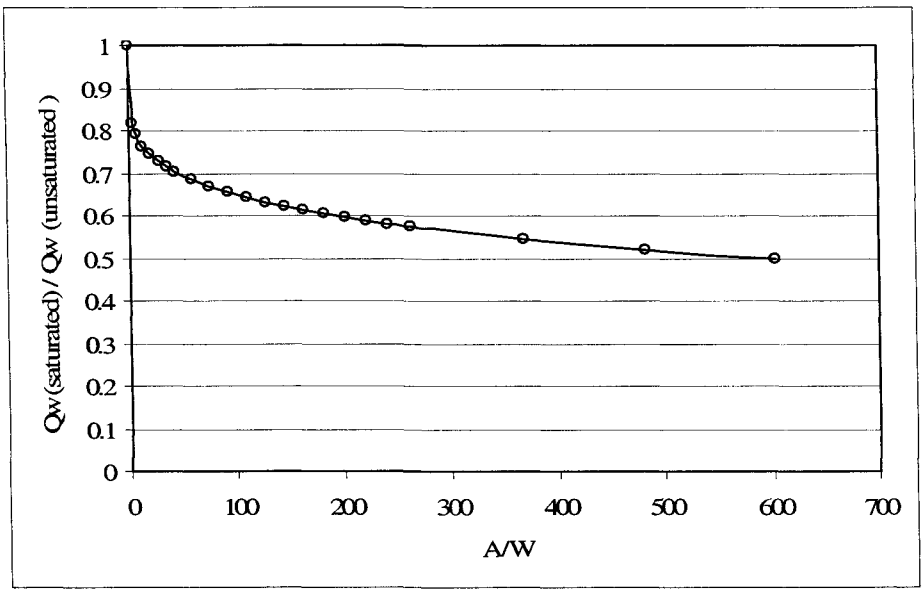

Figure 4.11: STOMP results for the groundwater reduction due to increase in airflow rate

Figure 4.12 presents the typical design of air sparging followed by the standard procedure for air sparging. As illustrated in Figure 4.12, the typical air to water ratio used in the field is over 200. At this value, the groundwater flow would be reduced by more than 40% and only less than 60 % of the groundwater would pass through the air sparging zone. It is worth mentioning here that low air to water ratio is not sufficient for plume cleaning as it outflows from the air sparging zone. At a very low airflow rate, few air channels are created, and that does not allow a sufficient surface area for cleanup.

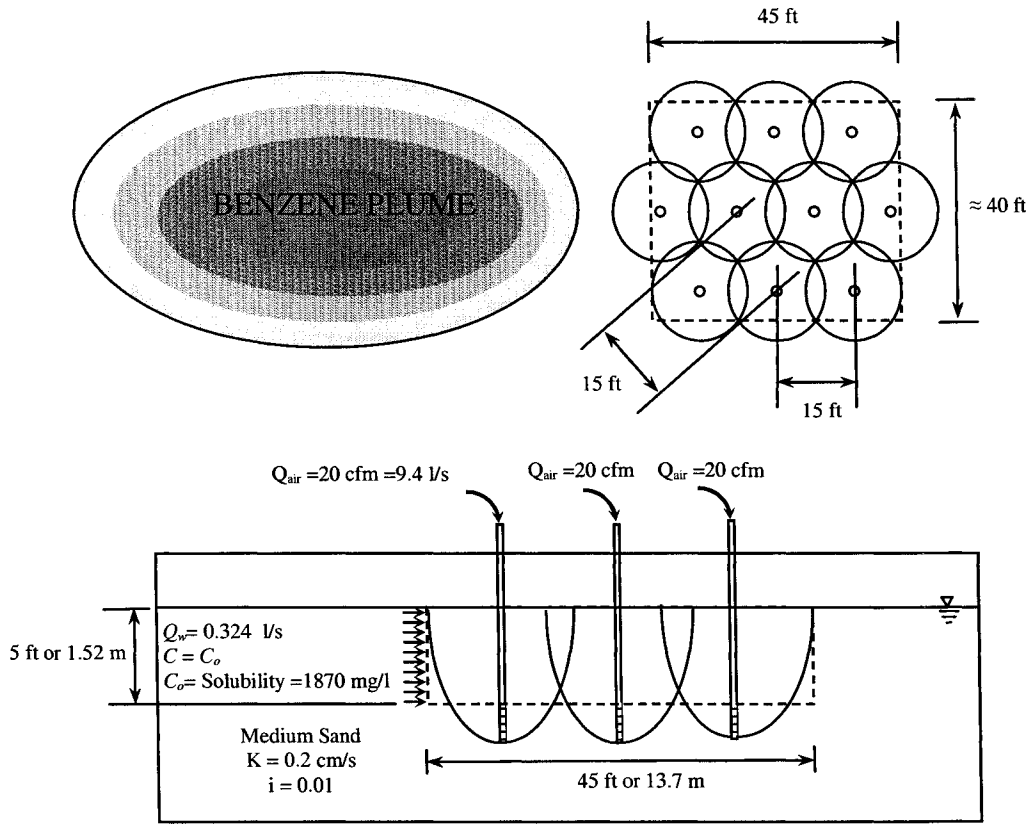

Area of contamination = A = assumed 5500 ft^2

R_w = 15 ft

$$\text{Number of wells} = \frac{1.3 \times A}{\pi R_w^2} = 10.1 \text{ well}$$

A/W = Q_w (unsaturated) /Q_{air} > Qw (saturated)/Q_{air} ≈ (7 wells × 9.41 l/s/well)/0.324 l/s

or A/W > 200

Figure 4.12: Typical Standard air sparging design

The objective in designing air sparging is to operate the system at maximum mass removal at lowest possible cost. Both computer programs, STOMP and the non-equilibrium model developed in this study, are used for optimizing the air sparging system for cross current flow application type. STOMP was run first to determine the amount of groundwater flux reduction. Then, the developed model used the results of STOMP to determine the concentration of the dissolved phase. The typical mass removal curve of the air sparging system of cross current curve is shown in Figure 4.13. The formula to calculate the mass removal is described by equations (4.22) and (4.23).

At low air-water ratio, mass removal is controlled by the non-equilibrium model. At this stage, the dissolved phase outflow concentration does not reach the clean level. The optimal mass removal would occur at the moment when the concentration of the dissolved phase reaches zero upon leaving the trench. After the outflow of dissolved concentration reaches the clean level, increasing the airflow rate would not be beneficial and cause to reduce the amount of treated water as shown later in Figure 4.13. Identifying the optimal air to water ratio is an important designing parameter for optimizing the operation of an air sparging system.

$$\text{Mass Removal ratio} = \frac{Q_w unsaturated\ C_o - Q_w unsaturted\ C_{out}}{Q_w saturated\ C_o} \qquad (4.22)$$

$$\text{Mass Removal ratio} = \frac{\text{mass rate entering the effective zone - mass rate leaving the effective zone}}{\text{Total mass rate}} \qquad (4.21)$$

The simulation result of the STOMP and non-equilibrium mass transfer has been applied for two different chemicals (Figure 4.14). The chemicals used are Benzene and MTBE. The estimated mass transfer coefficient and Henry's constant of the Benzene is presented in Table 4.2. The recent study shows that the MTBE can be removed from groundwater

using one of above ground treatment with an air stripping tower (reference). In this study the estimation of the mass transfer coefficient times the surface area per unit volume as they combined into one parameter is equal 0.004 [Ramakrishnan et al, 2004]. The Henry constant of the MTBE is estimated at 25°C and equal to 0.03 [Fischer, 2004].

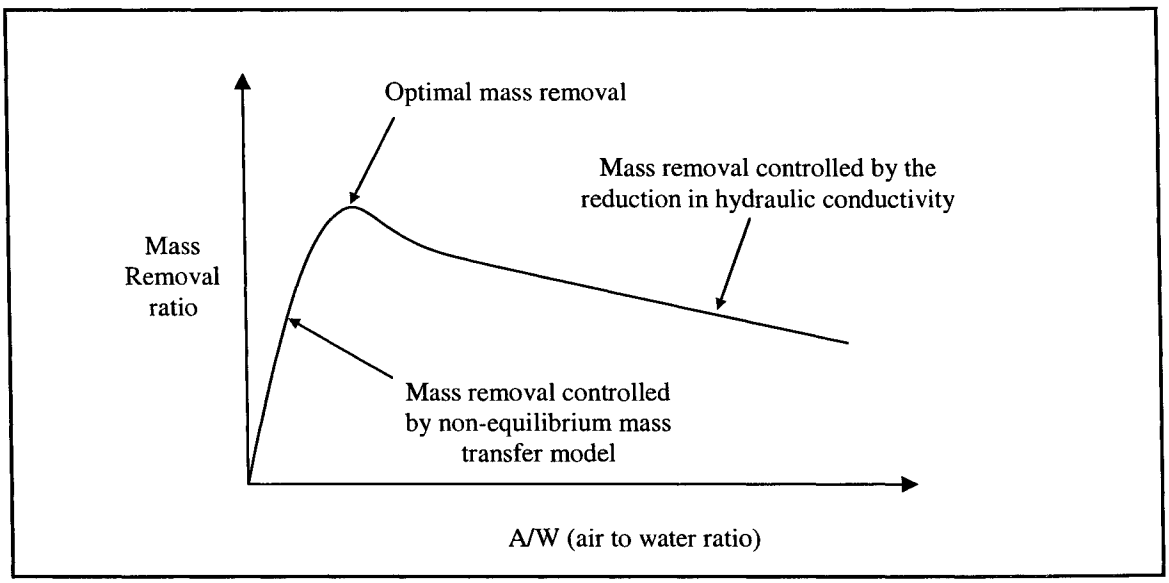

Figure 4.13: A typical curve for the effect of air to water ratio on mass removal

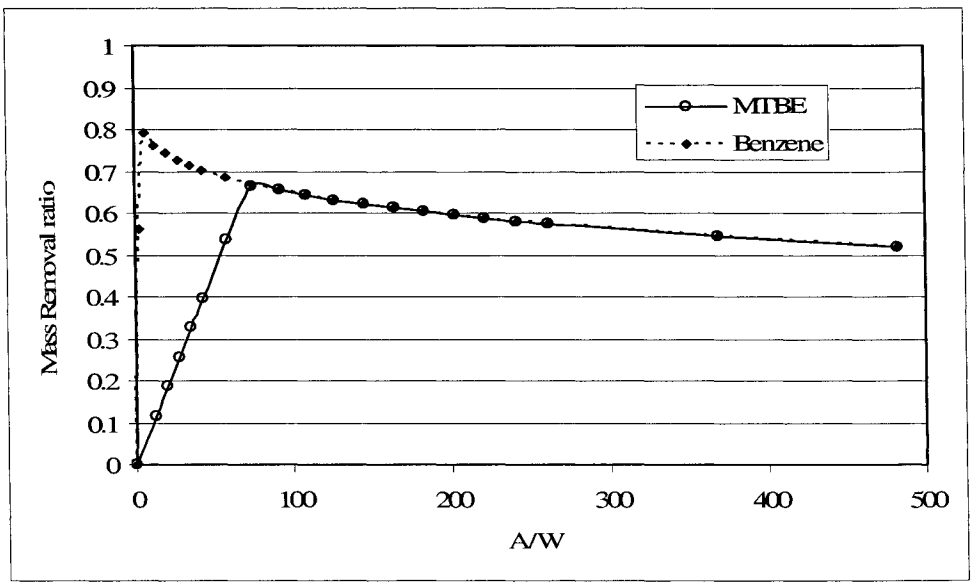

Figure 4.14: Mass removal ratio profile for Benzene (high volatile chemical) verses MTBE (low volatility chemical)

From Figure 4.14, the mass removal of Benzene reaches its optimum level at air to water ratio around 3.7. The concentration distribution of the contaminant in the dissolved phase at an air to water ratio of 3.7 is shown in Figure 4.5. Air to water ratio of 3.7 presents the maximum air to water ratio where the concentrations of the dissolved phase at far end of trench reach to the cleaning level. Benzene is considered to have high volatility level, and it is expected to be removed at a very low airflow rate. MTBE has low value of mass transfer coefficient and high value of Henry constant. For these reasons, the optimum mass removal occurred at an air to water ratio of around 90. A conclusion can be made that with most volatile chemicals, a low air to water ratio would be more efficient more than using high value of airflow rate. At a very low air to water ratio, air distribution is expected to be under the developing range, and the surface area per unit volume (a) would not be constant as assumed in Figure 4.14. In addition, more experimental studies are recommended for better estimation of the mass transfer coefficient and the surface area at low airflow rates.

CHAPTER 5

COMPARISON BETWEEN THE EQUILIBRIUM AND NON-EQUILIBRIUM MODEL

5.1 Introduction

In modeling multiphase contaminant transport, equilibrium mass transfer is always assumed in all phases. The model presented in this study was built based on the assumption of non-equilibrium mass transfer between the dissolved and air phases. In air sparging applications, removal of the contaminant is relatively high in a short time. For this reason, the non-equilibrium model is more appropriate to consider for interchangeable concentrations between the dissolved and air phase. The focus in this chapter is to study of how this assumption will make a difference in the physical removal. In order to do this, a multiphase contaminant transport software which was programmed based on equilibrium mass transfer has been used for the comparison. The chosen software is Subsurface Transport Over Multiple Phases (STOMP) developed by Pacific Northwest National Laboratory (www.stomp.pnl.gov). The version of the STOMP software used for the comparison study presented here is STOMP5.

STOMP5 was developed for the study of contaminant transport in three phases (water-air-oil). The fluid phases used for the model developed and presented in chapter 3 and 4 are dissolved and air phases. The bulk form of oil was not investigated nor

considered for this study. For this reason, the input file was written in a way which eliminated the contaminant existing as a bulk phase or source zone. Before explaining how STOMP5 handled this environmental case, the background of the theoretical description which will help to understand the STOMP5 input file written for the hypothetical case will be presented.

5.2 Preliminary Investigation of Air Sparging Need for STOMP Runs

The hypothetical case of air sparging used for comparing equilibrium and non-equilibrium mass transfer is similar to the one used in section 4.4.1. Figure 4.3 presents the description of the boundary and parameters of the air sparging trench which will be used for the input file. On the left side, groundwater flux is 0.1 m/day, a value chosen based on having soil with 100 m/day in hydraulic conductivity and 0.001 in hydraulic gradient. Figure 4.3 does not show how to handle boundary conditions for fluxes in water and air phases.

In STOMP5, there are two ways for dealing with such fluxes. The first way is to create constant head boundaries or "hydraulic gradient", at the left and right sides, sufficient to allow for a specific flux. The advantage of using this type of boundary condition is to allow for the reduction in hydraulic conductivity of the dissolved phase due to the presence of air pressure. The second way is to specify a constant flux for all the cells on the left side. On the right side, constant pressure head must be used to accommodate the constant flux on the left side. This is because the cells at the boundary which are not declared in their boundary conditions are considered as inactive cells or zero flux boundary type. This method way is different from the one previously mentioned

in that it does not allow the flow to be reduced due to the presence of the air or the non-wetting fluid pressure. This method works by adjusting the pressure between the two consecutive cells to maintain constant flux. Evaluating pressure distribution for understanding these types of boundary conditions will be presented next.

To simulate the boundary conditions as shown in Figure 4.3, head and pressure distribution were calculated with groundwater flow of 0.1 m/day and air flow of 2 m/day using a steady state form of Darcy's law in water and air phases. Water pressure head and air pressure distribution along the boundary condition are presented in Figure 5.1. Figure 5.2 shows the grid of the air sparging domain used by STOMP5 and numerical model presented in chapter 4. STOMP defines the z axis in the vertical direction as shown in Figure 5.1 and 5.2, while the model presented in chapter 4 used y axis in the vertical direction. To simulate the boundary condition, pressure distribution needs to be evaluated at the boundaries. The pressures are calculated at every cell for water and air.

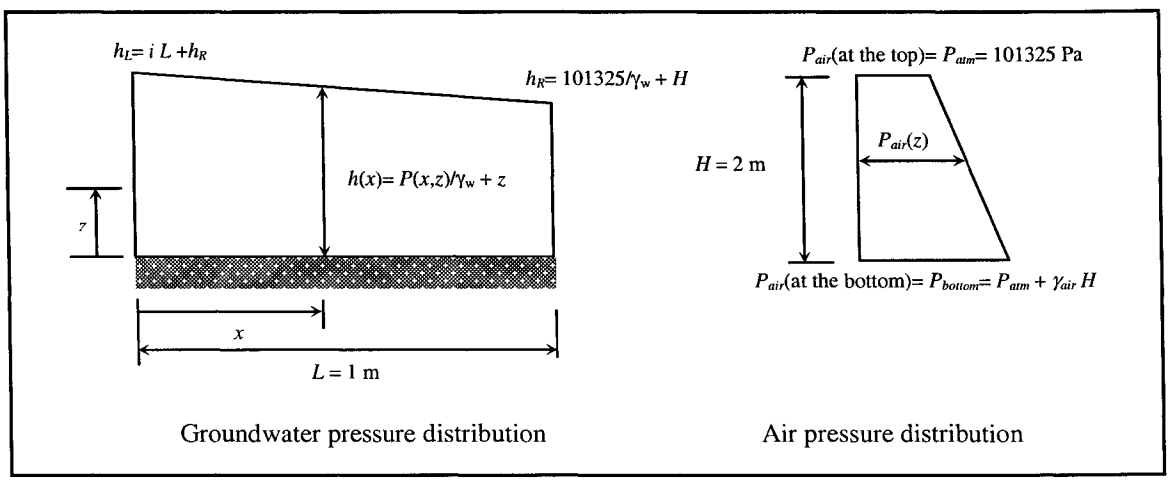

Figure 5.1 initial condition of pressure distribution used in the input file of STOMP5

To calculate the pressure in the air and water phases, a general formula was written using Darcy's law to evaluate the air and water pressure at every point in the

domain. For the groundwater head distribution and from the similarity of triangle in Figure 5.1,

$$h(x) = h_L - \frac{x}{L}(h_L - h_R) \qquad (5.1)$$

and

$$h(x) = \frac{P_{water}(x,z)}{\gamma_w} + z \qquad (5.2)$$

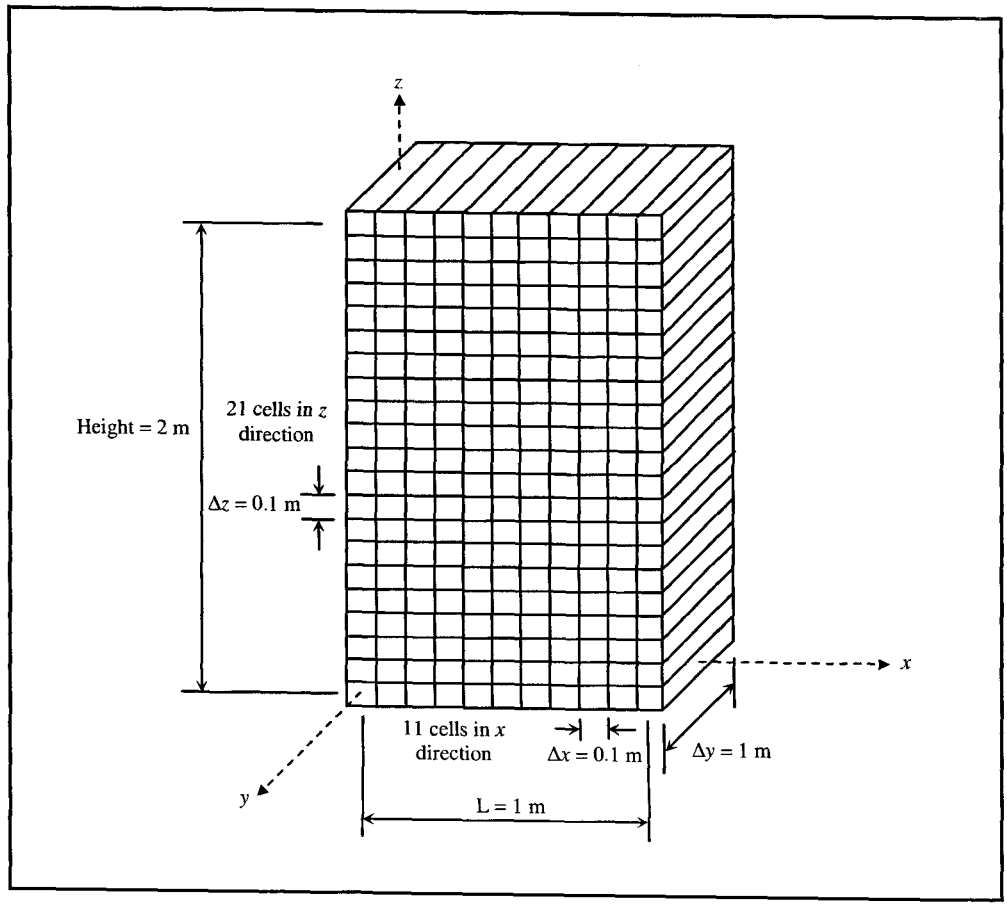

Figure 5.2 Grid cells used in simulating air sparging trench

Comparing equation 5.1 and 5.2

$$P_{water}(x,z) = \gamma_w\left(h_L - \frac{x}{L}(h_L - h_R) - z\right) \qquad (5.3)$$

$$P_{water}(x,z) = \gamma_w\left(h_L - \frac{x}{L}(h_L - h_R) - z\right)$$

Equation 5.3 is used for evaluating the groundwater pressure at every point, and that will be used in simulating the boundary condition of STOMP5.

Similarly, the air pressure can be written as follow:

$$P_{air}(z) = P_{air\ bottom} - \frac{z}{H}\left(P_{air\ bottom} - P_{air\ top}\right) \qquad (5.4)$$

The formulas of h_L, h_R, $P_{air\ bottom}$, and $P_{air\ top}$ are shown in Figure 5.1. These formulas were written using Darcy's law in air and maintaining water and keeping the air pressure in the top row cells equal to the atmospheric pressure and water pressure at the far top right cell equal to the atmospheric pressure. In addition, there is no air gradient, and air flux is assumed to be zero at the initial condition. If the height and length of the trench and the hydraulic gradient of the groundwater are known then the h_L, h_R, $P_{air\ bottom}$, and $P_{air\ top}$ can be determined using the formula shown in Figure 5.1.

Equations (5.3) and (5.4) are used to calculate the water and air pressure at the center of each cell. The main reason for air and water pressure calculation is that STOMP accepts only total pressure values instead of pressure heads for simulating boundary and initial condition.

5.3 STOMP5 Input File Description

The user guide [White and Oostrom, 2003] contains details explaining the input file. Here, a general description of the input file will be presented focusing on the parameters used. The input file used for this run is shown in Appendix E. The input file showed that the size of the air sparging trench is 2 m depth and 1 m in length per unit width in y direction. The distance increment and x and z direction used is 0.1 m. Twenty

one cells are in the z direction and eleven cells are in the x direction for simulating the trench domain (Figure 5.3).

The soil parameters used for the simulation are the same used in chapter 4 (Figure 4.4). The chemical properties for the Benzene are evaluated using the method followed by Reid et al. (1985). Table A.2 in appendix A shows the chemical properties used in the input file oil properties card. Table A.3 in appendix A presents the method of evaluating the vapor pressure, liquid density, and liquid viscosity in the simulation.

The important part of the input file is how STOMP5 evaluates the initial condition and boundary condition for each case. The initial condition should be evaluated for the three phases, water, air, and oil. Since there is no oil phase for the simulated case, the oil pressure is assigned to negative values which will not any change in oil pressure to cause oil to move within the domain. For the air phase, the pressure at the bottom is assigned using the formula shown in Figure 5.1, and this value is calculated assuming no air flow with the air pressure in the upper domain equal to the atmospheric pressure. For initial condition with no air flow, the hydraulic gradient in the z direction is equal to zero and pressure gradient per unit length can be derived. By doing that, the pressure gradient per unit length in the z direction for the air phase is equal to the specific weight of air pressure, which equals to -11.74 Pascal per meter.

The hydraulic gradient of the water phase used for the initial condition is 0.01, and the pressure distribution used is based on the formulas shown in Figure 5.1 and equation 5.3. The boundary condition used for the water flux is constant heads at both sides and for the air is constant flux at the bottom of the domain and constant pressure at top of the domain. In this way, the reduction in hydraulic conductivity allows the air flux to be kept

almost constant along the domain. Constant air pressure is assigned for all the cells at the top of the domain. The air is injected at the rate of 2 m/day at the bottom of the domain, and the groundwater flow rate is 0.2 m^3/day.

The contaminant flux is introduced to the domain using a source card. The contaminant flux rate slowly enters the domain and increases in its value until it reaches its solubility limit. For the purpose of comparing the program results with the non-equilibrium model, the input file was written to make sure there would be no chemical reactions other than the equilibrium partitioning of the mass contaminate from dissolved to air phases. The Van Genuchten formula [Van Genuchten, 1980] used for the calculations of the reduction in the hydraulic conductivity due to the increase in the air pressure.

The output file format shows the values of the water and air pressure, concentrations in the dissolved phase, and air and water fluxes at each cell. The air and water fluxes are used as input data for the program developed in chapter 3 and 4. The program runs for unsteady state for ten days at which point the run is assumed to reach a steady state. The program results at the last time step were compared with the non-equilibrium model.

5.4 Program Result and Comparison Discussion

To conduct a comparison study between the equilibrium and non-equilibrium model, the STOMP program was run for the hypothetical case shown in Figure 4.4. The developed model presented in this study was run with STOMP5. STOMP5 used the reduction in the hydraulic conductivity to perform its calculations. This run represents the non-equilibrium result and behavior of mass transfer in air sparging. For equilibrium

mass transfer results, STOMP5 executed with the option of equilibrium mass transfer between the dissolved and gas phases. Figure 5.3 and 5.4 show the result of both models. The difference between the results becomes obvious in the top part of the trench where the expected concentration of benzene vapor reaches the saturation limit. In the equilibrium run, the contaminant is expected to be removed at about 0.4 m in trench length, where in the non-equilibrium model it is expected that the contaminant would be clean with 0.6 m of trench length. The greater the increase in the depth of the air source, the more noticeable the difference between the two models.

As shown in Figure 5.3, the contaminant is free to transfer from the dissolved phase to the gas phase without any limit on resistance. That is obvious from the decreases in the dissolved concentrations from the left to the right side of the trench (Figure 5.3). This is explained by Henry's law, which describes the mass transfer from the liquid phase into infinite space without a deficit term or resistance from the contaminant concentration in the gas phase. Figure 5.4 shows the effect of the resistance of the vapor concentration in the gas phase that is observable at the top part of the trench. At the upper part of the trench, the vapor concentration is high, and that brings the deficit term to zero. Consequently, the mass transfer at the upper part of the trench is limited, and the concentration in the dissolved phase does not change. It is clear that the non-equilibrium model must make major changes for the equilibrium run, especially for modeling of air sparging where mass transfer is expected to be relatively fast.

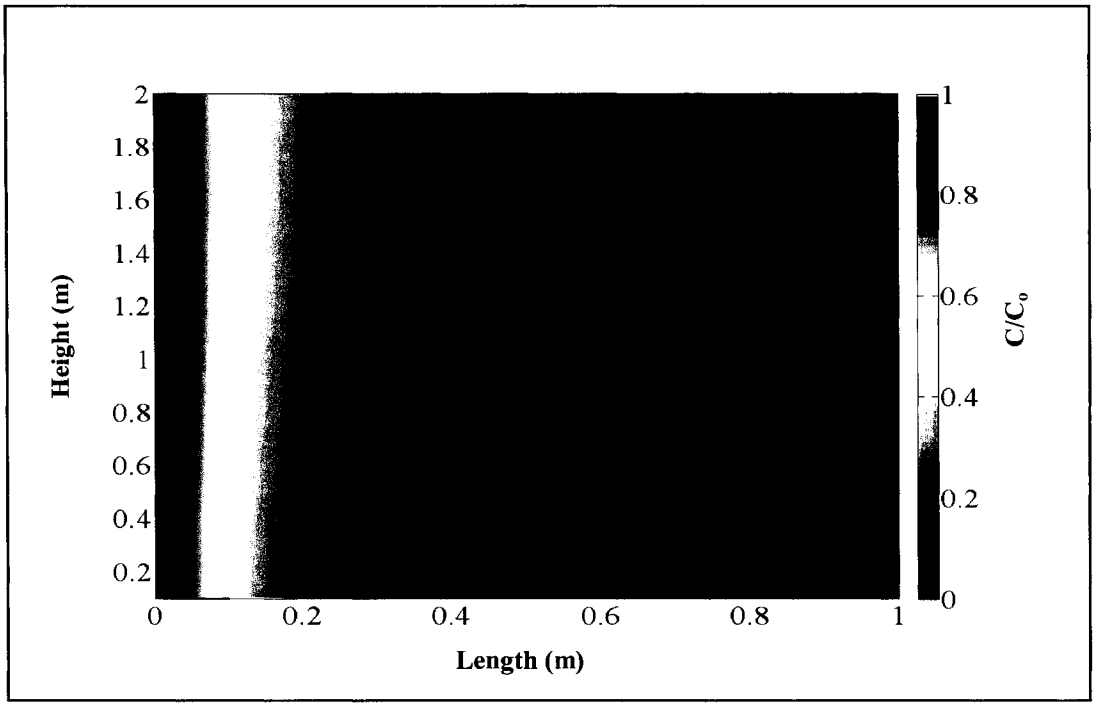

Figure 5.3: STOMP5 result with equilibrium mass transfer assumption

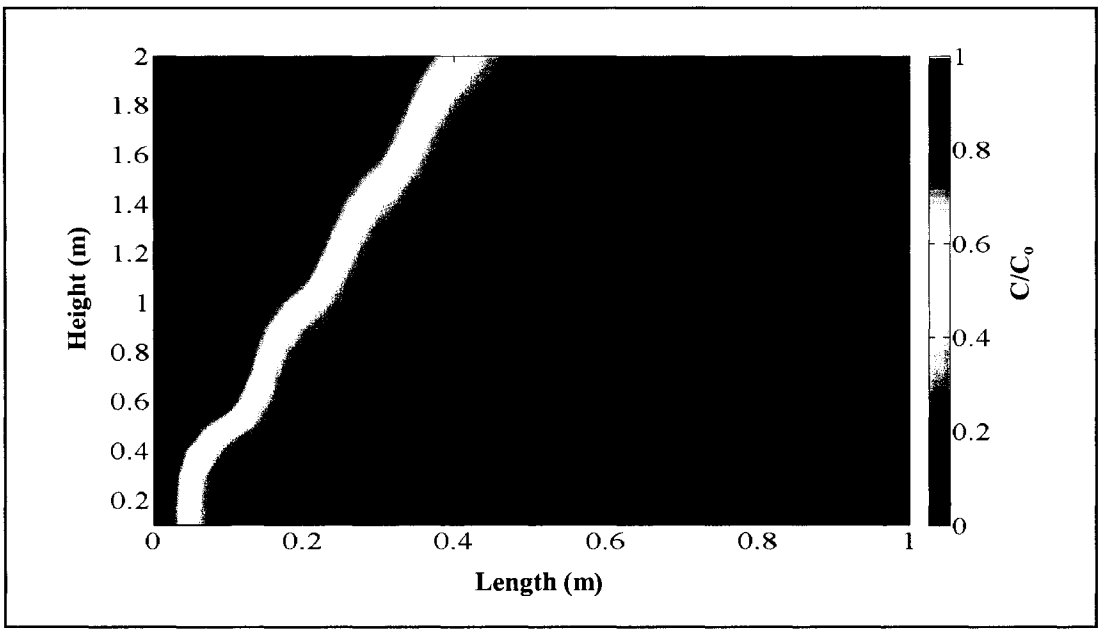

Figure 5.4: STOMP5 with non-equilibrium numerical mass transfer model results

CHAPTER 6

ANALYTICAL SOLUTION DERIVATION FOR AIR SPARGING

6.1 Introduction

An analytical solution for multiphase flow is always attractive to designers as it gives an easy and simple solution. In most cases, the required assumptions for the analytical solutions are homogenous with simple boundary conditions. For multiphase flow, finding the exact solution is always challenging because more than one equation needs to be solved for the same number of unknowns. Most analytical solutions for air sparging are developed based on the assumption of one phase, a completely mixed zone, and equilibrium partitioning from one phase to another. The analytical solution presented in this chapter is not based on the above assumptions, and it also includes the fluxes of the water and air phases as they cross each other.

6.2 Analytical Derivations

The analytical solution presented in this section was developed based on solving the differential equations presented in chapters 3 and 4. The equations (4.3) and (4.4) are a coupled system of first order linear partial differential equations with two starting boundary conditions. This system behaves essentially like two ordinary differential equations that are weakly coupled through the solution. Since each equation applies on a

semi infinite interval and is subject to an initial boundary condition, the Laplace transform can be used to solve these equations. Transforming using both variables reduces the system to a system of two linear algebraic equations, but there is then some difficulty in inverting.

On the other hand, transforming in just one variable or the other leads to a simple ordinary differential equation problem in the untransformed variable. In order to easily invert the transform, it is necessary to use a Taylor series to expand the exponential term which appears in the solution of the ordinary differential equation. Whether transforming in x or y seems to make little difference, and both approaches are shown here. Note also that changing variables eliminates the parameters K_1 and K_2 from the two equations. The solution will be as functions of K_1x and K_2y, and the parameters K_1 and K_2 describe the soil and fluids properties.

6.2.1 Solution Using Laplace Transformation in x Direction

Letting $C_\ell(s,y) = L_x[C(x,y)]$ and $C_\ell^*(s,y) = L_x[C^*(x,y)]$ are Laplace transformed of the independent variables C and C^*, the Laplace transform of equation (4.3) in x direction and solving C_ℓ in terms C_ℓ^* as

$$C_\ell(s,y) = \frac{C_o}{s+K_1} + \frac{K_1}{s+K_1} C_\ell^*(s,y) \qquad (6.1)$$

Now the Laplace transform of equation (4.4) will be

$$\frac{\partial C_\ell^*(s,y)}{\partial y} = K_2(C_\ell - C_\ell^*) \qquad (6.2)$$

The transform of the boundary condition of equation (4.4) is

$$C_\ell^*(s,0) = L_x\left[C^*(x,0)\right] = 0 \qquad (6.3)$$

The algebraic combination of equation (6.1) and (6.2) becomes

$$\frac{\partial C_\ell^*(s,y)}{\partial y} = -\frac{K_2 s}{s+K_1} C_\ell^*(s,y) + \frac{K_2 C_o}{s+K_1} \qquad (6.4)$$

Solving the ordinary differential equation of (6.4) with boundary condition of equation (6.3) will get

$$C_\ell^*(s,y) = \frac{C_o}{s}\left[1 - e^{-K_2 y\left(\frac{s}{s+K_1}\right)}\right] \qquad (6.5)$$

Using the expansion of exponential series (i.e. $e^y = \sum_{n=0}^{\infty} \frac{y^n}{n!}$) of equation (6.5) and substituting that into equation (6.1), the term C_ℓ(s,y) becomes

$$C_\ell(s,y) = \frac{C_o}{s+K_1} - K_1 C_o \sum_{n=1}^{\infty} \frac{(-K_2 y)^n}{n!} \frac{s^{n-1}}{(s+K_1)^{n+1}} \qquad (6.6)$$

Since

$$L_x^{-1}\left[\frac{1}{(s+a)^n}\right] = \frac{1}{(s-1)!} x^{n-1} e^{-K_1 x} \text{ and } L_x^{-1}\left[\frac{s^{n-1}}{(s+K_1)^{n+1}}\right] = \left(\frac{d}{dx}\right)^{n-1}\left[\frac{1}{n!} x^n e^{-K_1 x}\right]$$

The inverse of Laplace will hold the concentration of the contaminant in the aqueous phase in the form of

$$C(x,y) = C_o e^{-K_1 x} + C_o \sum_{n=1}^{\infty} \frac{(-K_2 y)^n}{n!} \phi_n(K_1 x)(-K_1 x) e^{-K_1 x}$$

where

$$L_x^{-1}\left[\frac{1}{(s+K_1)^2}\right] = x e^{-K_1 x} = \phi_0(K_1 x) x e^{-K_1 x}$$

$$L_x^{-1}\left[\frac{s}{(s+K_1)^3}\right]=\frac{1}{2!}\frac{d}{dx}\left(x^2e^{-K_1x}\right)=\left(1-\frac{1}{2}K_1x\right)xe^{-K_1x}=\phi_1(K_1x)xe^{-K_1x}$$

$$L_x^{-1}\left[\frac{s^2}{(s+K_1)^4}\right]=\frac{1}{3!}\frac{d^2}{dx^2}\left(x^3e^{-K_1x}\right)=\left(1-K_1x+\frac{1}{6}(K_1x)^2\right)xe^{-K_1x}=\phi_2(K_1x)xe^{-K_1x}$$

and in general

$$L_x^{-1}\left[\frac{s^{n-1}}{(s+K_1)^{n+1}}\right]=\frac{1}{(n-1)!}\frac{d^{n-1}}{dx^{n-1}}\left(x^ne^{-K_1x}\right)=\phi_{n-1}(K_1x)xe^{-K_1x}\quad\text{for } n=1,2,\ldots \quad (6.6)$$

$\phi_m(x)$ is a polynomial of degree m in x such that $\phi_m(0) = 1$ for every m then

$$C(x,y)=C_oe^{-K_1x}\left[1+\sum_{n=1}^{\infty}\frac{(-K_2y)^n}{n!}(-K_1x)\,\phi_{n-1}(K_1x)\right] \quad (6.7\text{ a})$$

or

$$C(x,y)=C_oe^{-K_1x}\left[1+\Phi(K_1x,K_2y)\right] \quad (6.7\text{ b})$$

where

$$\Phi(K_1x,K_2y)=\sum_{n=1}^{\infty}\frac{(-K_2y)^n}{n!}(-K_1x)\,\phi_{n-1}(K_1x) \quad (6.8)$$

The Φ function evaluation is shown in appendix F. Φ function as presented in equation (6.8) has stability value up to the K_2y value of 20. Another way evaluating Φ as shown in the following equation:

$$\Phi(K_1x,K_2y)=\sum_{n=1}^{\infty}\frac{(-K_2y)^n}{n!}\sum_{m=0}^{n-1}\binom{n-1}{m}\frac{(-K_1x)^{m+1}}{(m+1)!} \quad (6.9)$$

6.2.2 Solution Using the Laplace Transform in *y* Direction

Let $C_\ell(s,y) = L_y[C(x,y)]$ and $C_\ell^*(s,y) = L_y[C^*(x,y)]$

The Laplace formula in *y* direction of equation (4.4) will be as

$$C_l^*(x,s) = \frac{K_2}{s+K_2} C_l(x,s) \quad (6.10)$$

and equation (4.3) with the boundary condition will be

$$\frac{\partial C_l(x,s)}{\partial x} = -K_1\left(C_l(x,s) - C_l^*(x,s)\right) \quad (6.11)$$

and from the boundary condition

$$C_l(0,s) = \frac{C_o}{s} \quad (6.12)$$

Combing equation (6.10) and (6.11) becomes

$$\frac{\partial C_l(x,s)}{\partial x} = -\frac{K_1 s}{s+K_2} C_l(x,s) \quad (6.13)$$

Solving the ordinary differential equation of equation (6.13) with boundary condition of equation (6.12) will lead to

$$C_l(x,s) = \frac{C_o}{s} e^{-K_1 x\left(\frac{s}{s+K_2}\right)} \quad (6.14)$$

The expansion of the exponential term will be

$$e^{-K_1 x\left(\frac{s}{s+K_2}\right)} = \sum_{n=0}^{\infty} \frac{(-K_1 x)^n}{n!}\left(\frac{s}{s+K_2}\right)^n \quad (6.15)$$

The transformed concentration in the dissolved phase will be

$$C_l(x,s) = \frac{C_o}{s} e^{-K_1 x\left(\frac{s}{s+K_2}\right)} = \frac{C_o}{s} + C_o \sum_{n=1}^{\infty} \frac{(-K_1 x)^n}{n!} \frac{s^{n-1}}{(s+K_2)^n} \quad (6.16)$$

or

$$C_l(x,s)=\frac{C_o}{s}+C_o\left[(-K_1x)\frac{1}{s+b}+\frac{(-K_1x)^2}{2!}\frac{s}{(s+K_2)^2}+\frac{(-K_1x)^3}{3!}\frac{s^2}{(s+K_2)^3}+\ldots\right] \quad (6.17)$$

Since

$$L_y^{-1}\left[\frac{s^{n-1}}{(s+K_1)^n}\right]=\left(\frac{d}{dy}\right)^{n-1}\left[\frac{1}{(n-1)!}y^{n-1}e^{-K_1y}\right]=e^{-K_1y}\psi_{n-1}(K_2y) \quad (6.18)$$

The inverse Laplace will bring the concentration in the dissolved phase in the form of:

$$C(x,y)=C_o\left(1+e^{-K_2y}\sum_{n=1}^{\infty}\frac{(K_1x)^n}{n!}\psi_{n-1}(K_2y)\right) \qquad (6.19\text{ a})$$

or

$$C(x,y)=C_o\left(1+e^{-K_2y}\Psi(K_1x,K_2y)\right) \qquad (6.19\text{ b})$$

where

$$\Psi(K_1x,K_2y)=\sum_{n=1}^{\infty}\frac{(K_1x)^n}{n!}\psi_{n-1}(K_2y) \qquad (6.20)$$

The equation of (6.19) is the concentration of the contaminant in the dissolved phase using the Laplace transform in the y direction. The evolution of the Ψ function as it is presented in equation (6.20) is shown in Appendix F. In the next section, stability of the equation (6.7) ad (6.19) will be discussed and general formula to evaluate the polynomial function will be presented.

6.3 Stability Analysis for the Solutions

This section will focus on studying the stability of equations (6.7) and (6.19). Equation (6.7) is derived from taking the Laplace transform in the x direction. The Φ function evaluated in appendix F. This function has evaluated and given a stable value up

to the value of K_1x of 20. Equation (6.19) is a similar form of evaluating the concentration in the dissolved phase, and it is derived by taking the Laplace transform in the y direction. By comparing equation (6.7 b) and (6.19b), the Φ function can be written in the following equation.

$$\Phi(K_1x, K_2y) = e^{K_1x}\left[1 - e^{-K_2y}\Psi(K_1x, K_2y)\right] - 1 \quad (6.21)$$

where the $\Psi(K_1x,K_2y)$ evaluation shown in appendix F.

Another form of equation (6.21) can be written in binomial terms:

$$\Phi(K_1x, K_2y) = e^{K_1x}\left[1 - e^{-K_2y}\sum_{n=1}^{\infty}\frac{(-K_1x)^n}{n!}(-K_2y)\sum_{m=0}^{n-1}\binom{n-1}{m}\frac{(-K_2y)^m}{m!}\right] - 1 \quad (6.22)$$

The Φ function, as they are written in equations (6.21) and (6.22), have stability up to the K_2y value of 20. A similar stability form is shown in equation (6.8) and (6.9), where Φ runs for a stable solution up to K_1x equal to 20. Figure 6.1 shows the schematic of the stability domain with ranges in both x and y directions. From Figure 6.1, there is a range where the analytical solution can not evaluate. This range includes where both K_1x and K_2y are greater than 20.

The numerical solution developed in chapter 4 has a stable solution on a more extended range than does the analytical solution. The focus here is how to evaluate the Φ function in table format in similar way that error function and error complementary function. For this reason, Φ function will be rewritten in numerical form. Using equation (6.7b), the third form of Φ function based on a numerical solution is

$$\Phi(K_1x, K_2y) = \left(\frac{C}{C_o}\right)_{numerical} e^{K_1x} - 1 \quad (6.23)$$

The C/C_o term of equation (6.23) can be evaluated by running the numerical program at different K_1x and K_2y values. In this way, a table for different Φ values can be generated at different K_1x and K_2y. The table can be used for evaluation of the analytical solution for any homogenous case and constant boundary condition. A table of evaluating the Φ function at different values of K_1x and K_2y based on numerical solution has been written in appendix G.

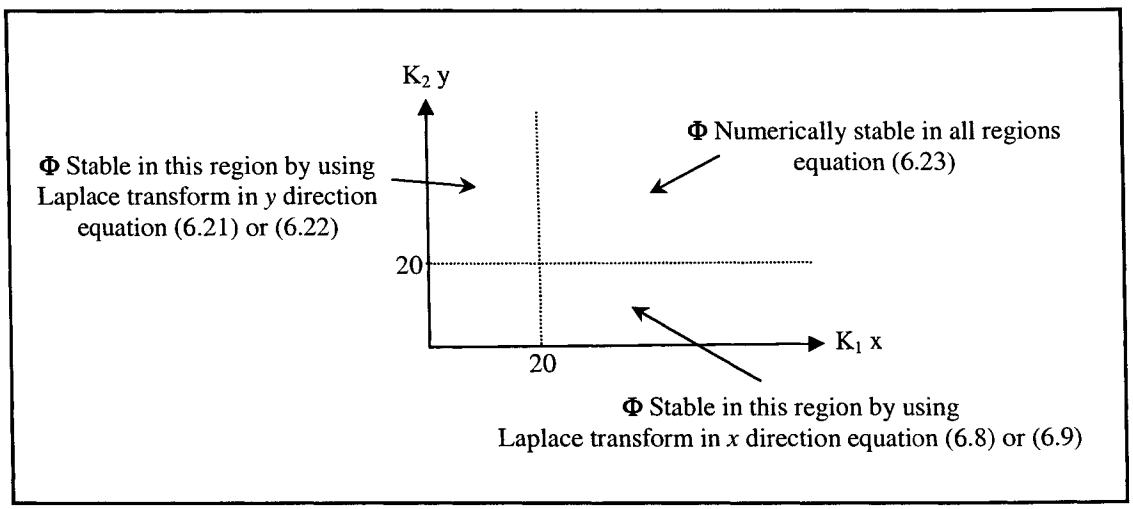

Figure 6.1: Stability of $\Phi(K_1x,K_2y)$ function

6.4 Solution Comparison with Numerical Solution

For comparing the analytical solution of the equation (6.7), and the numerical solution, a hypothetical case for a site contaminated with TCE is used. The problem consists of a 1 m depth and 2 m length air sparging trench. Site conditions and chemical properties used are summarized in Table 6.1. The trench is packed with crushed gravel, which assumes that bubbles will form in the trench. The bubble size was assumed to be 1 mm in diameter with bubble velocity of 0.1 m/s.

The concentration profile is shown in Figure 6.2 and 6.3 for numerical and analytical results. More details of comparison between the numerical and analytical solutions are shown in Figures 6.4 and 6.5 for different section profiles along the trench's length and depth. Figures 6.2-5 show that the numerical and analytical solutions developed in this study are matched well at all the points on the domain.

Table 6.1: Chemical and soil properties

K_L (cm/hr)	H	ϕ	i Groundwater Gradient	K hydraulic conductivity (cm/s)	$Q_w(m^3/s)$	Q_{air} (m^3/s)	A/W air to water ratio
20.4	0.42	0.5	0.003	0.001	0.26	0.96	3.7

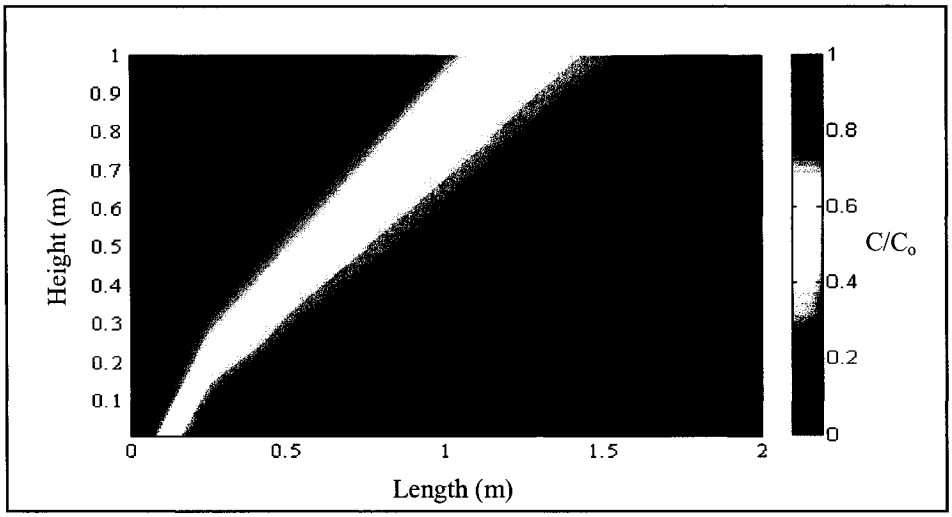

Figure 6.2: Program results for numerical solution

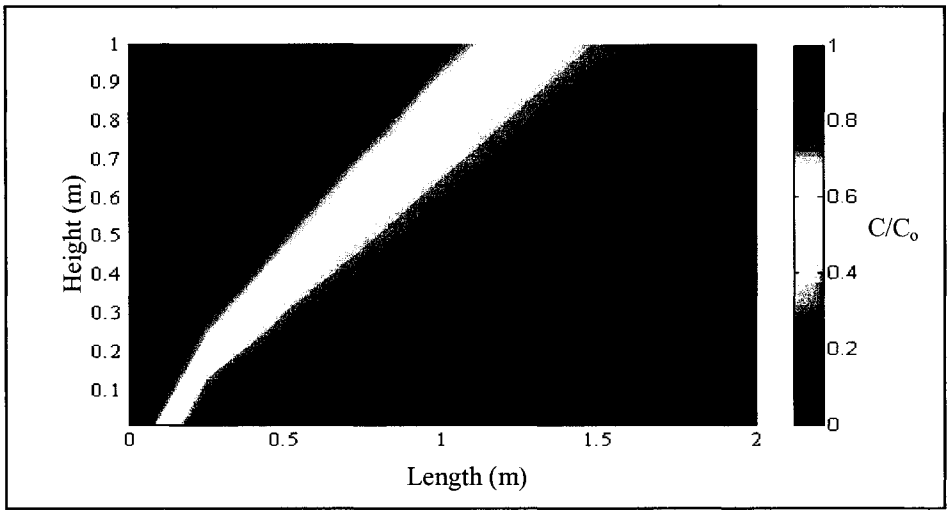

Figure 6.3: Analytical solution results

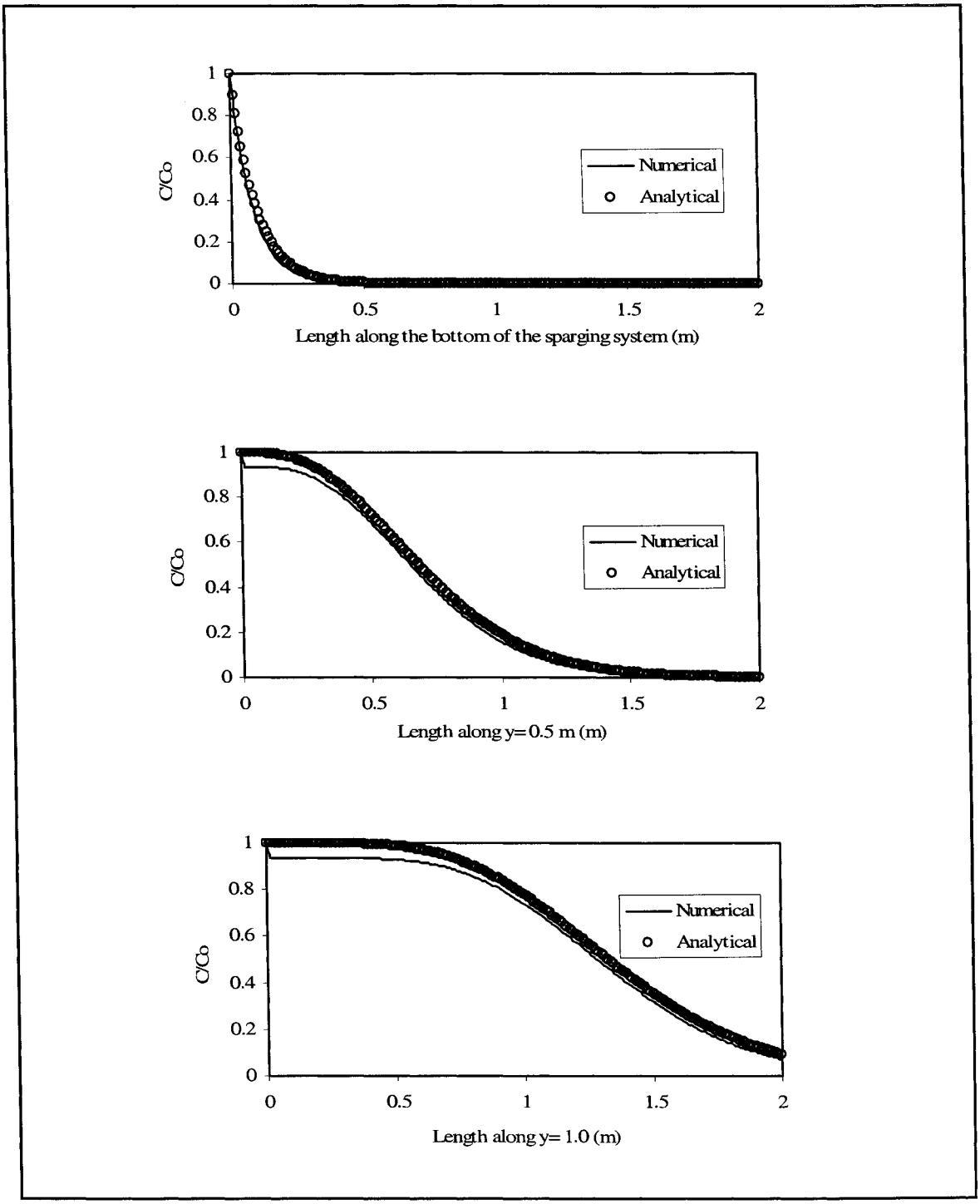

Figure 6.4: Analytical and numerical developed in chapter 4 comparison along different trench elevations

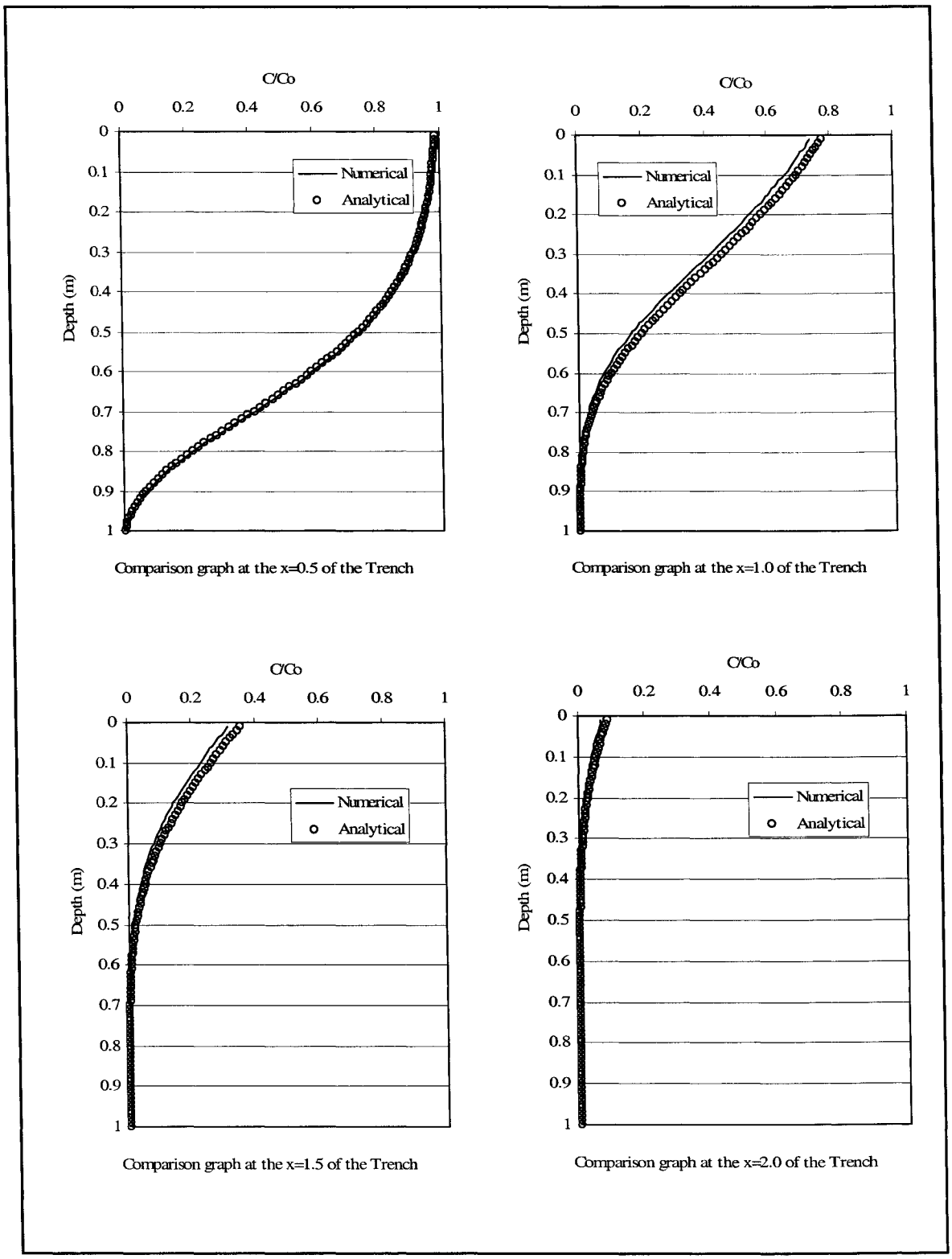

Figure 6.5: Analytical and numerical comparison along the trench depth

CHAPTER 7

SUMMARY, CONCLUSION, AND RECOMMENDATION

7.1 Summary

The model developed in this study is the first non-equilibrium model developed for cross-current flow of air sparging. The model developed is based on assuming that the mass transfer between the dissolved and gas phase will follow a two-film theorem. The two film theorem [Whitman,1923] is used for deriving a pair of differential equations in the dissolved and gas phases using the mass balance of the represented element volume (REV). The system of partial differential equations is solved numerically using the finite difference method. The analytical solution is derived using the Laplace transform in the two dependent variables x and y. The numerical and analytical solutions are compared, and it shows that they correspond. The developed model program is used with multiphase flow software. The advantage of using multiphase flow software is to consider other physical and chemical processes in the porous media. These processes include the reduction in the hydraulic conductivity, biodegradation, dispersion, and adsorption.

The multiphase flow software used in this study is called Subsurface Transport Over Multiple Phases (STOMP) [White and Oostrom, 2000]. STOMP is written assuming equilibrium partitioning at all phases. In this study, non-equilibrium is assumed between the dissolved and gas phases. The discussion comparison between equilibrium

and non-equilibrium is made to show the effect of using this assumption. Using the non-equilibrium mass transfer model developed in this study, some parameters were added to design the air sparging system. These parameters included mass transfer coefficient of the contaminant and surface area of the gas phase.

Finally, a sensitivity analysis for the parameters of the developed model was performed. From the sensitivity analysis, the air to water ratio and Henry's constant, the air sparging effective zone dimensions are more sensitive than the mass transfer coefficient and surface area. STOMP was run to calculate the reduction in the hydraulic conductivity. The STOMP results were used as input for the developed model, and the developed model was run for the mass removal taking into an account the reduction in the groundwater due to the increase in the air flow rate. The optimal air to water ratio was evaluated at the maximum mass removal.

7.2 Conclusion

In this study, the numerical solution was applied to several cases to study model sensitivity. It showed that this model can work with other models to compensate for additional chemical and physical reactions. From this study, the following conclusions can be drawn:

1. Equilibrium mass transfer is used in most multiphase models. This study shows that there is a significant difference in the value of the dissolved concentration between the equilibrium and non-equilibrium models (Figure 5.3 and 5.4).
2. There are differences in the physical processes between the equilibrium and non-equilibrium mass transfer. The physical process involved in the non-equilibrium

is concentration deficit or a gradient between the concentration in the dissolved and gas phases. Some design parameters are added when using a non-equilibrium model, such as mass transfer coefficient, surface area, air to water ratio. This study shows that these parameters are significant in the modeling of air sparging.

3. From the sensitivity analysis of the developed model, mass transfer coefficient and surface area are less significant than the other design parameters.
4. The program run with STOMP shows that the air-water ratio is a key parameter in designing the air sparging. Increasing the air flow rate enhances the mass removal and reduces the amount of groundwater flow into the effective zone at the same time. In this study, optimal air-water ratio was determined at maximum mass removal.
5. A simple analytical solution was derived and used for simple boundary conditions. The analytical solution gives a simple solution and an approximate estimation for the air sparging system.

7.3 Future research

Many experiments and field studies have been done on air sparging with limited contributions in finding efficient design tools. One of the reasons for that is that there still are not mathematical models capable of describing the physical removal of air sparging. For example, there have not been enough studies which evaluate the mass transfer coefficient and surface area of the air sparging. That is because few mathematical models assume the non-equilibrium model of air sparging. In conclusion, experimental and field measurements should be compatible with mathematical models for better estimation of

design parameters. For these reasons, future work on air sparging should include the following:

- Evaluate the mass transfer coefficient and surface area at different chemical and soil by using an appropriate experiments and mathematical models.
- Applying the same mathematical concept of non-equilibrium for other phase partitioning. This should include air sparging modeling for source zone.
- Incorporating the proposed model with other chemical and physical processes of multiphase flow in one software program.
- Evaluating the air distribution for surface area and flow rate distribution within the zone of influence.

References

[1] Adams J.A., K. R. Reddy. The effect of grain size distribution on air sparging efficiency. In: Alleman BC, Leeson A (eds) In situ and on-site bioremediation, vol 1. Battelle Press, Columbus, Ohio, 1997

[2] Aelion, C., and B. Kirtland, Physical versus biological hydrocarbon removal during air sparging and soil vapor extraction. Environmental Science and technology. 34: 3167-3173. 2002

[3] Ahlfeld, D.P., M. A. Dahmani, and W. Ji. A conceptual model of field behavior of air sparging and its implications for application. Ground Water Monitor and Remediation, 14 : 132–139. 1994.

[4] Bass, D.H., N.A. Hastings, and R.A. Brown. Performance of air sparging systems: a review of case studies. Journal of Hazardous Materials, 72(2-3): 101-119. 2000.

[5] Bedient, P. B. , H. S. Rifai, and C. J. Newell. Ground Water Contamination: Transport and Remediation. Prentice Hall,1994.

[6] Brooks M.C., W. R. Wise, M. D. Annable. Fundamental changes in in-situ air sparging flow patterns. Ground Water Monitor Remediation. 19:105–113. 1999.

[7] Brooks, R.H., and A. J. Corey. Hydraulic properties of porous media. Hydrology Day. Paper 3, Colorado State University, Fort Collins, CO. 1964

[8] Bruce, C. L., I. L. Amerson, , R. L. Johnson, , and P. C. Johnson. Use of an SF_6-based diagnostic tool for assessing air distributions and oxygen transfer rates during IAS operation. Bioremediation Journal. 5(4): 337-347. 2001.

[9] Burns, S.E. and M. Zhang. Digital image analysis to assess microbubble behavior in porous media. Journal of Computing in Civil Engineering. 13(1): 43-48. 1999

[10] Catney, S.F., and R. J. Lynch.. Experimental investigations of air sparging to control contaminated groundwater. Geotechnical Engineering, 149(4): 253-258. 2001

[11] Chhabra, R. P. Bubbles, drops, and particles in non-Newtonian fluids. Boca Raton, Fla: CRC Press, 1993

[12] Clift, R., J. R. Grace, and M. E. Weber. Bubbles, Drops, and Particles. San Diego, California: Academic press Inc., 1978

[13] Darby, R. Chemical Engineering Fluid Mechanics. New York, New York: Marcel Dekker Inc., 1996

[14] Elder C.R., C. H. Benson. Air channel formation, size, spacing, and tortuosity during air sparging. Ground Water Monitor Remediation. 19:171–181, 1999.

[15] Elder, C.R., C. H. Benson, and G. R. Eykholt. Modeling mass removal during in situ air sparging. Journal of Geotechnical and Geoenvironmental Engineering, V.125, No.11, PP 947-958, 1999.

[16] Etiope G and S. Lombardi. Laboratory simulation of geogas microbubble flow. Environmental Geology. 27 (3): 226-232, 1996.

[17] Fischer, A., M. Muller, and J. Klasmeier. Determination of Henry's law constant for methyl tert-butyl ether (MTBE) at groundwater temperatures . Chemosphere, V 54, p. 689–694, 2004.

[18] Gordon, M.J. Case history of a large-scale air sparging/soil vapor extraction system for remediation of chlorinated volatile organic compounds in groundwater. Ground Water Monitoring and Remediation. *18*(2):137-149, 1998.

[19] Ji, W., Dahmani, A., and D. P. Ahlfeld. Laboratory study of air sparging: Air flow visualization. Ground Water Monitoring and Remediation, 12(4): 115-126, 1993.

[20] Johnson, P. Assessment of the contributions of volatilization and biodegradation to in-situ air sparging performance. Environmental science and technology. 32: 276-281, 1998.

[21] Johnson, P.C., A. Das, and C. Bruce. Effect of flow rate changes and pulsing on the treatment of source zones by in situ air sparging. *Environmental Science and Technology*, 33(10): 1726-1731, 1999.

[22] Johnson, P.C., R. L. Johnson, C. L. Bruce, and A. Leeson. Advances in in situ air sparging/biosparging. Bioremediation Journal. V5 No.4: 251-362, 2001.

[23] Johnston, C., J. Rayne, B. Patterson, and G. Davis. Volatilization and biodegradation during air sparging of dissolved BTEX-contaminated groundwater. Journal of Contaminant Hydrology. 33 (3-4): 377- 404, 1998.

[24] Johnston, C.D., J. L. Rayne, B. M. Patterson, and G.B. Davis. Volatilization and biodegradation during air sparging of dissolved BTEX-contaminated Groundwater. Journal of Contaminant Hydrology, 33 (3-4):377-404, 1998.

[25] Kavanaugh, M. C., and R. R. Trussell. Design of Aeration Towers to Strip Volatile Contaminants from Drinking Water. Journal of the American Water Works Association, Vol 72, No. 12, pp 684-692, 1980.

[26] Kerfoot, W. B., Microbubble ozone sparging for chlorinated ethane spill remediation. In: Henry, S. M. and S. D. Warner, Chlorinated solvent and DNAPL remediation innovative strategies for subsurface cleanup. Washington, DC: American Chemical Society Series *837*: Distributed by Oxford University Press, pp. 86-108, 2003.

[27] Kirtland, B.C., and C. M. Aelion, Petroleum mass removal from low permeability sediment using air sparging/soil vapor extraction: impact of continuous or pulsed operation. Journal of Contaminant Hydrology, (41)367-383, 2000.

[28] Leeson, A., P. C. Johnson, R. L. Johnson, C. M. Vogel, R. E. Hinchee, M. Marley , T. Peargin, C. L. Bruce, I. L. Amerson, C. T. Coonfare, R. D. Gillespie, and D. B. McWhorter. Air sparging design paradigm. Prepared for Battelle, Columbus, OH. August 12. 2002.

[29] Leeson, A., R.E. Hinchee, G.L. Headington, and C.M. Vogel. Air channel distribution during air sparging: a field experiment. In: Hinchee, R.E., R.N. Miller, and P.C. Johnson. In Situ Aeration: Air Sparging, Bioventing, and Related Remediation Processes. pp. 215-222. Battelle Press: Columbus, Ohio, 1995.

[30] Levich, V.G. Physicochemical Hydrodynamics. Englewood Cliffs, New Jersey: Prentice- Hall, 1962.

[31] Lundegard, P.D. and. LaBreque, D. J., Geophysical and hydrologic monitoring of air sparging flow behavior: comparison of two extreme sites. Remediation Journal. 8(3):59 -71, 1998.

[32] Lundegard, P.D., and G. Anderson, Multiphase numerical simulation of air sparging performance. Ground Water, 34, No.3, PP 451-460, 1996.

[33] Mackay, D. and W. Y. Shiu., A critical review of Henry's law constants for chemicals of environmental interest. Journal of Physical and Chemical Reference Data, 10(4): 1175-1199, 1981.

[34] MaCray, J.E., Mathematical modeling of air sparging for subsurface remediation: state of the art. Journal of Hazardous Materials. V. 72: 237-263, 2000.

[35] Marley, M., F.L. Droste, and R. Cody., The design of an in situ sparging trench. Conference proceedings of the 1994 petroleum hydrocarbons and organic chemicals in ground water: prevention, detection, and restoration. Houston, Texas, PP. 579-590, 1994.

[36] Marley, M.C. and C. J. Bruell, In situ air sparging: evaluation of petroleum industry sites and considerations for applicability, design, and operation. Washington, D.C. API, American Petroleum Institute, Publication 4609, 1995.

[37] May,W. E., S. P. Waisk, , and D. H. Freeman. Determination of the Solubility Behavior of Some Polycyclic Aromatic Hydrocarbons in Water. Analytical Chemistry, 50(7): 997-1000, 1978.

[38] May,W. E., S. P. Waisk, and D. H. Freeman, Determination of the aqueous solubility of polynuclear aromatic hydrocarbons by a coupled column liquid chromatographic technique. Analytical Chemistry, 50(1): 175-179, 1978.

[39] McCray, J. E., and R. W. Falta, Numerical simulation of air sparging for remediation of NAPL contamination. Ground Water. V.35 No.1: 99-110, 1997.

[40] McQuarrie, D. A., and J. D. Simon. Physical Chemistry: A Molecular Approach. University Science Books, 1997.

[41] Mei , C. C., Z. Cheng, and C.O. Ng, A model for flow induced by steady air venting and air spaging. Applies Mathematical Modelling. 26: 727-750, 2002.

[42] Pankow, J. F., R. F. Johnson, J. A. Cherry, Air sparging in gate wells in cutoff walls and trenches for control of plume of volatile organic compounds (VOCs). Ground Water, 31(4): 654-663, 1993.

[43] Peterson J. W., M. J. DeBoer, and K. L. Lake. A laboratory simulation of toluene cleanup by air sparging of water-saturated sands. Journal of Hazardous Materials 72:167–178, 2000.

[44] Peterson J.W., Lepczyk P.A., Lake K.L. Effect of sediment size on area of influence during groundwater remediation by air sparging: a laboratory approach. Environmental Geology. 38(1): 1–6, 1999.

[45] Peterson, J. W., K. S. Murray, Y. I. Tulu, B. D. Peuler, and D. A. Wilkens, Air-flow geometry in air sparging of fine-grained sands. Hydrogeology Journal. 9 (2):168-176, 2001.

[46] Rabideau, A.J., and J. M. Blayden, Analytical model for contaminant mass removal by air sparging. Ground Water Monitoring and Remediation, 18(4): 120-130, 1998.

[47] Ramakrishnan, B., G. A. Sorial, , T. F. Speth, P. Clark, A. Zaffiro, C. Patterson, and D. W. Hand, Remediation of MTBE from drinking water: air stripping followed by off-gas adsorption. Journal of the Air and Waste Management Association. V 54 (5): p.529–539, 2004.

[48] Reddy, K.R., and J. A. Adams, Effect of groundwater flow on remediation of dissolved-phase VOC contamination using air sparging. *Journal of Hazardous Materials*, 72(2-3): 147-165, 2000.

[49] Reid, R. C., J. M. Prausnitz, and B. E. Poling. The properties of gases and liquids. Fourth edition, McGraw-Hill Book Company, New York, 1987.

[50] Rogers, S.W., and S. K. Ong. Influence of porous media, airflow rate, and air channel spacing on benzene NAPL removal during air sparging. *Environmental Science and Technology*, 34(5):.764-770, 2000.

[51] Roosevelt, S.E. and M. T. Corapcioglu. Air bubble migration in a granular porous medium: experimental study. Water Resources Research. 34(5): 1131-1142, 1998.

[52] Rutherford, K. and P.C. Johnson. Effects of process control changes on aquifer oxygenation rates during in situ air sparging in homogeneous aquifers. Ground Water Monitoring and Remediation. 16(4):132-141, 1996.

[53] Schwartz, F.P. Determination of temperature dependence of solubilities of polycyclic aromatic hydrocarbons in aqueous solutions by a fluorescence method. Journal of chemical and engineering data, 22(3): 273-277, 1977.

[54] Sellers, K.L., and R. P. Schreiber. Air sparging model for predicting groundwater cleanup rate. Conference proceedings of the 1992 petroleum hydrocarbons and organic chemicals in groundwater: prevention, detection, and restoration, the Weston Galleria, Houston, Texas, November 4-6, pp. 365-376, 1992.

[55] Soo, S. L. Multiphase Fluid Dynamics. Beijing, China: Science Press, 1990.

[56] Takahashi, T. and T. Miahara. Volume of bubble formed at a single circular, submerges orifice. International Chemical Engineering, 21(2): 224-228, 1981.

[57] U.S. Army Corp of Engineering, Engineering and design in-situ air sparging. EM 1110-l -4005, 1997.

[58] U.S. Environmental Protection Agency. Treatment technologies for site cleanup: annual status report (tenth edition). EPA 542/R/01/004, 2001.

[59] Uno, S., and R.C. Kintner, Effect of wall proximity on the rate of rise of single air bubles in a quiescent liquid, American Institute of Chemical Engineers Journal. 2: 420-425, 1956.

[60] Valsaraj, K. T., Elements of Environmental Engineering: Thermodynamics and Kinetics. CRC., 2000.

[61] Van Dijke, M. I., S. E. van der Zee, and C. J. van Duijn. Multi-phase flow modeling of air sparging. Advances in Water Resources, 18(6): 319-333, 1995.

[62] van Genuchten, M.T., A closed-form equation for predicting the hydraulic conductivity of unsaturated soils. Soil Science Society of America Journal, v. 44, pp. 892-898, 1980.

[63] Varhegyi A., I. Baranyi, and G. Somogyi, A model for the vertical subsurface radon transport in "geogas" microbubbles. Geophys. Trans. 32(3):235-253, 1986.

[64] Varhegyi A., J. Hakl, M. Monnin, J. P. Morin, and J. L. Seidel, Experimental study of radon transport in water as test for a transportation microbubble model. Journal of Applied Geophysics. 29(1):37-46, 1992.

[65] Wehrle K., In situ cleaning of CHC contaminated sites: model-scale experiments using air-injection (in-situ stripping) method in granular soils. In: Arendt F., M. Hinsenveld, W. J. Van Den Brink. Contaminated Soil '90: Kluwer acadmic publisher. Netherlands, pp 1061–1062, 1990.

[66] White, M.D., and M. Oostrom. STOMP Subsurface Transport Over Multiple Phase: Theory Guide PNNL-11216 (UC-2010), Pacific Northwest National Laboratory, Richland, Washington, 2000.

[67] White, M.D., and M. Oostrom. STOMP Subsurface Transport Over Multiple Phase: User's Guide PNNL-14286 (UC-2010), Pacific Northwest National Laboratory, Richland, Washington, 2003.

[68] Whitman, W.G., The Two-Film theory of gas absorption. *Chemical and Metallurgical Engineering*, 29(4): 146-148, 1923.

[69] Wilson, D.J., C. Gomez-Lahoz, and J. M. Rodriguez-Maroto. Groundwater cleanup by in-situ sparging. VIII. Effect of air channeling on dissolved volatile organic compounds removal efficiency. Separation science and technology, 29(18): 2387-2418, 1994

[70] Wilson, D.J., S. Kayano, R. D. Mutch, and A. N. Clarke, A.N. Groundwater cleanup by in-situ sparging. I. Mathematical modeling. Separation Science and Technology, 27: 1023-1041, 1992.

Appendix A

Volatilization Parameters for Selected Chemical

Chemical	M (g/mol)	Solubility[a] mg/L	Solubility[a] mol/m³	Vapor pressure at 20°C mm Hg	Vapor pressure at 20°C atm	Henry's law Const. H Atm-m³/mol	Henry's law Const. H Non-dim	Phase Exchange Coeff. (cm/hr) Liquid k_l	Phase Exchange Coeff. (cm/hr) Gas k_g	Mass Transfer Coefficient K_L (cm/hr)	Half-life $\tau_{1/2}$ (hr)
					Low volatility ($H < 3 \times 10^{-7}$)						
3-Bromo-*f*-propanol	139	1.7×10^{-5}	1233	0.1	1.3×10^{-4}	1.1×10^{-7}	4.6×10^{-6}	16	1600	7.4×10^{-3}	9400
Dieldrin	381	0.25	6.6×10^{-4}	1×10^{-7}	1.3×10^{-0}	2×10^{-7}	8.9×10^{-6}	12	990	8.8×10^{-3}	7840
					Middle range ($3 \times 10^{-7} < H < 10^{-3}$)						
Lindane	290.9	7.3	2.5×10^{-2}	9.4×10^{-6}	1.2×10^{-8}	4.8×10^{-7}	2.2×10^{-5}	14	1130	0.025	2760
m-Bromonitrobenzene	170	104	58.8	0.07	9.2×10^{-5}	1.6×10^{-6}	7.4×10^{-5}	16	1500	0.11	626
Pentachlorophenol	266	14	5.3×10^{-2}	1.4×10^{-4}	1.8×10^{-7}	3.4×10^{-6}	1.5×10^{-4}	12	1150	0.17	406
4-*t*-Butylphenol	150	10^3	6.7	0.046	6.1×10^{-5}	9.1×10^{-6}	3.8×10^{-4}	17	1600	0.59	117
Aldrin	365	0.2	5.5×10^{-4}	6×10^{-6}	7.9×10^{-9}	1.4×10^{-5}	6.1×10^{-4}	12	1810	1.0	68
Nitrobenzene	123	2×10^3	16.3	0.27	3.5×10^{-4}	2.2×10^{-5}	9.3×10^{-4}	20	1700	1.5	45
DDT	354.5	1.2×10^{-3}	3.4×10^{-6}	1×10^{-7}	1.3×10^{-10}	3.8×10^{-5}	1.7×10^{-3}	13	1025	1.5	45
Phenanthrene	178	1.29	7×10^{-3}	2.1×10^{-4}	2.8×10^{-7}	3.9×10^{-5}	1.7×10^{-3}	18	1450	2.2	31
Acetylene tetrabromide	344	650	1.9	0.3	3.9×10^{-4}	2.1×10^{-4}	8.9×10^{-3}	13	1000	5.3	13.1
Aroclor 1242	254	0.24	9.5×10^{-4}	4.1×10^{-4}	5.3×10^{-7}						
Ethylene dibromide	188	4.3×10^3	22.9	11.6	1.5×10^{-2}	5.6×10^{-4}	2.4×10^{-2}	15	1210	9.9	7
					High volatility ($H > 10^{-3}$)	6.6×10^{-4}	2.8×10^{-2}	16	1400	11.4	6.1
Ethylene dichloride	99	8.0×10^3	80.8	67	0.09						
Naphthalene	128	33	0.026	0.23	3×10^{-4}	1.1×10^{-3}	4×10^{-2}	22	1900	17.1	4
Biphenyl	154	7.5	0.05	0.06	7.5×10^{-5}	1.15×10^{-3}	4.9×10^{-2}	21	1765	16.9	4.1
Methylene chloride	85	1.3×10^4	155	349	0.46	1.5×10^{-3}	6.8×10^{-2}	19	1554	16.2	4.3
Chlorobenzene	113	472	4.2	11.8	1.6×10^{-2}	3×10^{-3}	0.13	25	2000	22.8	3
Chloroform	119	8×10^3	67	246	0.32	3.7×10^{-3}	0.165	22	1820	15.1	4.6
o-Xylene	106	175	1.7	6.6	8.7×10^{-3}	4.8×10^{-3}	0.2	20	1700	18.9	3.7
Benzene	78	1780	22.8	95.2	1.25×10^{-1}	5.1×10^{-3}	0.22	23	1870	22	3.2
Toluene	92	515	5.6	28.4	3.7×10^{-2}	5.5×10^{-3}	0.24	27	2180	26	2.7
Perchloroethylene	166	400	2.4	14.3	2×10^{-2}	6.6×10^{-3}	0.28	25	2010	24	2.9
Ethyl benzene	106	152	1.43	9.5	1.25×10^{-2}	8.3×10^{-3}	0.34	17	1450	16.4	4.2
Trichloroethylene	131	1×10^3	7.6	60	8×10^{-2}	8.7×10^{-3}	0.37	23	1870	22.3	3.1
Mercury	201	3×10^{-2}	1.5×10^{-4}	1.3×10^{-3}	1.7×10^{-6}	1×10^{-2}	0.42	21	1700	20.4	3.4
Methyl bromide	95	1.3×10^4	137	1.4×10^3	1.8	1.1×10^{-2}	0.48	17	1360	16.6	4.2
Cumene (isopropyl benzene)	120	50	0.416	4.6	6.1×10^{-3}	1.3×10^{-2}	0.56	23	2000	22.5	3.1
1,1,1-Trichloroethane	133	950	7.1	100	0.13	1.5×10^{-2}	0.62	22	1760	21.6	3.2
Carbon tetrachloride	154	800	5.2	91	0.12	1.8×10^{-2}	0.77	19	1650	18.7	3.7
Methyl chloride	50.5	7.4×10^3	146	3.6×10^3	4.74	2.3×10^{-2}	0.97	19	1500	18.8	3.7
Ethyl bromide	109	900	8.3	460	6.1×10^{-1}	2.4×10^{-2}	0.36	30	2600	29	2.4
Vinyl chloride	62.5	90	1.44	2580	3.4	7.3×10^{-2}	3.1	22	1800	22	3.1
2,2,4-Trimethyl pentane	114	2.44	2.1×10^{-2}	49.3	6.5×10^{-2}	2.4	99	28	2400	28	2.5
n-Octane	114	0.66	5.8×10^{-3}	14.1	1.85×10^{-2}	3.1	129	22	1810	22	3.1
Fluoro-trichloromethane	137					3.2	136	22	1810	22	3.1
Ethylene	28	131	4.7		>40	5		11.3	1090	11.3	6.1
						>8.6	~360	40	3700	40	1.7

[a] Source: Mackay and Leinonen, 1975; Mackay et al., 1979; Mackay and Wolkoff, 1973; Verschueren, 1977.
Source: Lyman et al., 1990.

Appendix B

Henry Law Analysis (Derivation and Assumptions)

[McQuarrie, and Simon, 1997, and Valsaraj, , 2000]

- From First Law of thermodynamics

$$dU = \delta q - \delta w \qquad (1)$$

Were:

dU = Change in energy of the system

δq = Change (at a certain path) in head absorbance energy

δw = Change (at a certain path) in external work

$$\delta w = P_{external}\, dV \qquad (2)$$

For a closed system of volume V, $P_{external}$ is external pressure that subject on the system.

- From Second law

$$dS = d_iS + d_eS \qquad (3)$$

Were:

dS= The total entropy change within isolated system

d_iS= Internal change of entropy.

d_eS= The entropy change between the system and surround.

$$d_eS = \frac{\delta q}{T} \qquad (4)$$

T = Temperature of the system.

For system disorder under only heat exchange between system and surround (reversible process), the change in internal entropy will diminish ($d_iS = 0$) (reference P 828) and total entropy equation (3) will be as

$$dS = \frac{\delta q}{T} \qquad (5)$$

This condition apply for only when the system chemically under equilibrium process. Combining equations (1), (2), and (5)

$$dU = T\,dS + P\,dV \qquad (6)$$

After rearrange

$$dU - T\,dS + P\,dV = 0$$

For isolated system, the changes in pressure and temperature at equilibrium are constant ($dT = dP = 0$) and we can rewrite this expression as (P 884)

$$d(U - TS + PV) = 0$$

By definition, *Gibbs free energy* is defined as

$$G = U - TS + PV$$

This mean for closed system under equilibrium condition and constant T and P, the change of Gibbs energy is zero ($dG = 0$). Figure A1 shows the processes where for reactions tend proceed spontaneously then settle down at minimum values of Gibbs values at equilibrium state.

1) Gibbs Relation for single phase

As written above

$$G = U - TS + PV$$

The total derivates of G written as

$$dG = dU + P\,dV + V\,dP - T\,dS - S\,dT$$

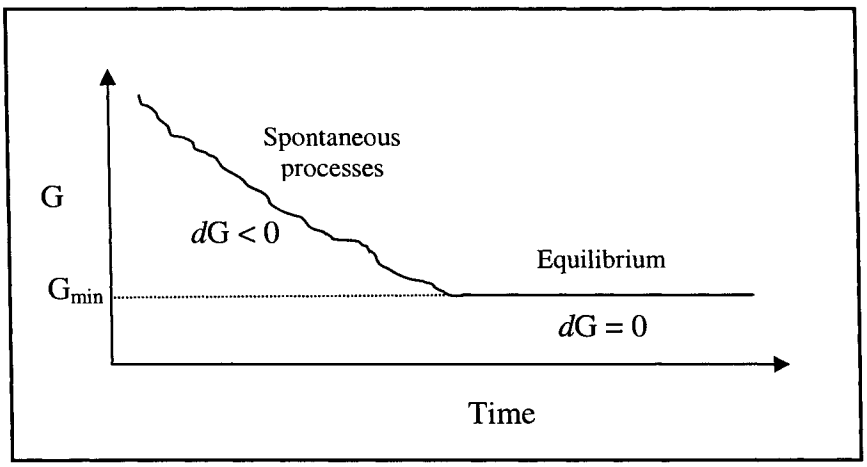

Figure A1 Changes in Gibbs free energy with reaction time at constant T and P

By substitution of equation (6)

$$dG = V\,dP - S\,dT \qquad (7)$$

The above equation shows that G is function of P, T, and number of moles (n). Therefore total derivative of G can be written as

$$dG = \left(\frac{\partial G}{\partial P}\right) dP + \left(\frac{\partial G}{\partial T}\right) dT - \sum \left(\frac{\partial G}{\partial n}\right) dn \qquad (8)$$

By definition $\frac{\partial G}{\partial n}$ called *chemical potential* and has a symbol of μ_i.

By comparing equation (7) and (8) then

$$\frac{\partial G}{\partial P} = V \;,\; \frac{\partial G}{\partial T} = S \text{, and } \sum \mu_i\, dn = 0$$

Also dG can be written as

$$dG = \sum n_i\, d\mu_i + \sum \mu_i dn_i \qquad (9)$$

By Comparing (7), (8), and (9)

$$\sum n_i \, d\mu_i = V \, dP - S \, dT$$

The above equation called *Gibbs-Duhem relationship* and for constant temperature within the system, change in chemical potential is

$$d\mu_i = \frac{V}{n_i} dP$$

Using *Ideal Gas law* (PV = nRT) for vapor phase and separate variables and integrate.

$$\mu_i^{vap} = \mu_{standard} + RT \ln\left(\frac{P_i}{P_i^o}\right) \qquad (10)$$

Were $\mu_{standard}$ and P_i^o are chemical potential and Pressure at standard conditions.
For solution, Rault Law ($P = x_i P_i^o$) is using and equation (10) becomes

$$\mu_i^{sln} = \mu_{standard} + RT \ln(x_i) \qquad (11)$$

were x_i is molar fraction of species i.

2) Gibbs Relation for gas and solution phases

The formula of Gibbs energy between solution and gas is

$$G = G^{sln} + G^{vap}$$

The total derivatives of G is

$$dG = dG^{sln} + dG^{vap}$$

$$dG = \left(\frac{\partial G^{sln}}{\partial n_j^{sln}}\right) dn_j^{sln} + \left(\frac{\partial G^{vap}}{\partial n_j^{vap}}\right) dn_j^{vap}$$

and

$$dG = \mu_j^{sln}\, dn_j^{sln} + \mu_j^{vap}\, dn_j^{sln}$$

For isolated system

$$dn_j = dn_j^{vap} \text{ and } dn_j = -dn_j^{sln}$$

Then

$$dG = (\mu_j^{sln} - \mu_j^{vap})\, dn_j$$

At equilibrium and the change of number on moles is not zero then

$$\mu_j^{sln} = \mu_j^{vap} \qquad (12)$$

Substitution equations (10) and (11) into equation (12) and by taking P_i^o at 1 atm as standard reference, Henry law can be written for ideal behaviors of solution and gas mixture as.

$$\frac{P_i}{x_i} = \exp\left[\frac{\mu_i^{sln,o} - \mu_i^{vap,o}}{RT}\right]$$

Hence H_i (Henry constant) as $H_i = \exp\left[\frac{\mu_i^{sln,o} - \mu_i^{vap,o}}{RT}\right]$

Noted that this form of Henry for ideal behavior and accepted when $P_i < 10$ bar and $x_i < 3\%$.

For nonideal gas and solution, Lewis (Mackay 1979) defined potential chemical fugacity for gases as

$$\mu_i^{vap} = \mu_{standard}^{vap} + RT \ln\left(\frac{f_i^{vap}}{f_i^{vap,\,o}}\right) \qquad (13)$$

and for solutions

$$\mu_i^{sln} = \mu_{standard}^{sln} + RT \ln\left(\frac{f_i^{sln}}{f_i^{sln,\,o}}\right) \qquad (14)$$

By chosen same standard states, substitution of equation (13) and (14) into (12) then

$$f_i^{sln} = f_i^{vap} \qquad (15)$$

For gases $f_i^{vap} = \chi_i P_i$ where χ_i is *fugacity coefficient* indicate for nonideality of the gas mixture. For liquid solution $f_i^{sln} / f_i^{sln,\,o}$ is called activity and symboled as a_i. Activity coefficient (γ_i) is defending to the departure from ideality as this form.

$$\gamma_i = a_i / x_i$$

Combined these equations with equation (15) and for ideal gas ($\chi_i = 1$)

$$H_i = \frac{P_i}{x_i} = \gamma_i f_i^{sln,\,o}$$

$f_i^{sln,\,o}$ is fugacity at reference condition and is assumed is equal to vapor pressure P_v.

Appendix C

Air Stripping Design Equation Derivation [Kavanaugh , and Trussell, 1980]

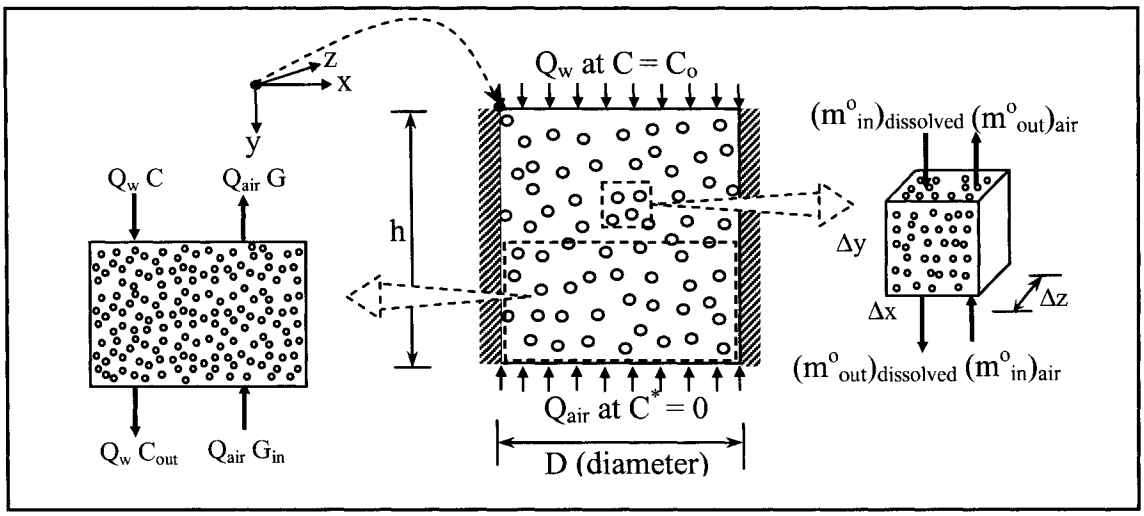

Figure 1 Air Stripping Tower

1. Mass balance in dissolved phase of Counter Current

General mass balance dissolved phase for Represent Element Volume (REV) is

$$(m^o_{out} - m^o_{In})_{dissolved} + m^o_{IPT} = -\frac{\partial m_{Box}}{\partial t} \qquad (1)$$

Where $(m^o_{in})_{dissolved} = Q_w C_{in}$ and $(m^o_{out})_{dissolved} = Q_w C_{out}$

Q_w = flow rate of water effluent into system.

C_{in} = Concentration of contaminant entering REV.

C_{out} = Concentration of contaminant leaving REV.

Forward Taylor expansion of concentration in dissolved phase and neglecting higher order terms will be as

$$C_{out} = C_{in} + \frac{\partial C}{\partial y}\Delta y$$

Then

$$(m^o_{out} - m^o_{In})_{dissolved} = q_w V_{Box} \frac{\partial C}{\partial x}$$

Using vales of m_{Box} and m^o_{IPT}

$$m_{Box} = C\,\phi\,(\Delta x\,\Delta y\,\Delta z) = C\phi V_{Box}$$

$$m^{o}_{IPT} = K_L\,(SA)\,(C - C^*)$$

and again using same definitions of a ($a=SA/V_{Box}$) mass balance of counter current in dissolved phase of counter current as

$$q_w \frac{\partial C}{\partial y} + K_L a\,(C - C^*) = -\phi \frac{\partial C}{\partial t} \qquad (3)$$

Steady state of mass balance in counter current condition yield to

$$\frac{\partial C}{\partial y} = -\frac{K_L a}{q_w}(C - C^*) \qquad (4)$$

Equation (4) can be written in integral form

$$\int_0^h dy = \frac{q_w}{K_L\, a} \int_{C_{IN}}^{C_{OUT}} \frac{dC}{(C^* - C)} \qquad (5)$$

2. Enthalpy balance of Counter Current

Mass balance of the bottom part of element (Figure B1) will be as:

$$\text{IN} = \text{OUT}$$

$$Q_w C + Q_{air} G_{IN} = Q_w C_{OUT} + Q_{air} G \qquad (6)$$

Using Henry's law ($G=H\,C^*$) and $G_{in}= 0$ (clean air entering the system)

$$C^* = \frac{Q_w}{Q_{air} H}(C - C_{OUT}) \qquad (7)$$

Let $R = H\left(\frac{Q_{air}}{Q_w}\right)$ (sparge factor) and solving Equation (5) and (7)

$$h = \frac{q_w}{K_L \mathrm{a}} \frac{R}{R-1} \ln\left(\frac{C_{IN} / C_{OUT}(R-1)+1)}{R}\right) \qquad (8)$$

Let $NTU = \frac{R}{R-1} \ln\left(\frac{C_{in} / C_{out}(R-1)+1)}{R}\right)$ (number of transfer units) and

$HTU = \frac{q_w}{K_L \mathrm{a}}$ (Height of transfer unit) where $q_w = \frac{Q_w}{\text{Surface area of tower}}$ then

$$h \text{ (height of tower)} = HTU * NTU \qquad (9)$$

Appendix D

Program Code

1. Symbols Reference

$Ci1j = C_{i-1,j}$

$Cij1 = C_{i,j-1}$

$Cai1j = \hat{C}_{i-1,j}$

$Caij1 = \hat{C}_{i,j-1}$

$Cijr = C_{i-1,j}^{(r)}$

$Caijr = \hat{C}_{i,j-1}^{(r)}$

$Cijr1 = C_{i-1,j}^{(r-1)}$

$Caijr1 = \hat{C}_{i,j-1}^{(r-1)}$

2. Program Code for constant boundary condition

```
Private Sub CommandButton1_Click()

Sheets("sheet2").Select
Range("D1:IV1000").Select
Selection.ClearContents

' Start of setting Input data
dx = Worksheets("sheet2").Cells(15, 2).Value
dy = Worksheets("sheet2").Cells(16, 2).Value
h = Worksheets("sheet2").Cells(2, 2).Value
L = Worksheets("sheet2").Cells(3, 2).Value
Co = Worksheets("sheet2").Cells(1, 2).Value
k1 = Worksheets("sheet2").Cells(21, 2).Value
k2 = Worksheets("sheet2").Cells(22, 2).Value
' End of setting Input data

' Start of setting Number of steps in x and y
m = L / dx
n = h / dy
' End of setting Number of steps in x and y

' Start of setting Boundary Condition for Aqueous phase
For I = 1 To n Step 1
Worksheets("sheet2").Cells(3 + I, 4).Value = Co
Next I
'End of setting boundary condition of Aqueous phase
```

```
' Start of setting Boundary Condition for gas phase
For I = 1 To m Step 1
Worksheets("sheet2").Cells(7 + 2 * n, 4 + I).Value = 0
Next I
'End of setting boundary condition for gas phase

' Start of FDM calculations and output
For I = 1 To n Step 1
   For J = 1 To m Step 1
   Ci1j = Worksheets("sheet2").Cells(4 + n - I, 3 + J).Value
   Cij1 = Worksheets("sheet2").Cells(5 + n - I, 4 + J).Value
   Cai1j = Worksheets("sheet2").Cells(7 + 2 * n - I, 3 + J).Value
   Caij1 = Worksheets("sheet2").Cells(8 + 2 * n - I, 4 + J).Value

'Initial values for Cij and Caij
   Cijn1 = Ci1j
   Caijn1 = Caij1
'End of initial values for Cij and Caij

      Diff = 0.002
      Do Until Diff <= 0.0001

      Cijn = Ci1j - k1 * dx / 2 * (Cijn1 + Ci1j - Caijn1 - Cai1j)
      Caijn = Caij1 + k2 * dy / 2 * (Cijn1 + Cij1 - Caijn1 - Caij1)

      Diff1 = Cijn - Caijn
      Diff2 = Caijn1 - Caijn

      If Diff1 >= Diff2 Then Diff = Diff2 Else:  Diff = Diff1

      Cijn1 = Cijn
      Caijn1 = Caijn
      Loop

   Worksheets("sheet2").Cells(4 + n - I, 4 + J).Value = Cijn
   Worksheets("sheet2").Cells(7 + 2 * n - I, 4 + J).Value = Caijn

   Next J
Next I
'End of FDM Calculations and output

End Sub
```

Appendix E
Input file for STOMP5 run

1. Input file for equilibrium run of air sparging

```
#-------------------------------------------------------------
~Simulation Title Card
#-------------------------------------------------------------
1,
Air Sprging multiphase for dissolved Benzen,
James Warner/Osama AlGahtan,
CSU,
Feb 24,
10:00,
2,
Air Sparging Tench STOMP Simulation,

#-------------------------------------------------------------
~Solution Control Card
#-------------------------------------------------------------
Normal,
Water-Oil-Air,
1,
0,s,10,d,10,s,5,d,1.25,8,1e-1,
1000000,
Variable,
Constant,0.9e-6,m^2/s,0.9e-6,m^2/s,
0,

#-------------------------------------------------------------
~Grid Card
#-------------------------------------------------------------
Uniform Cartesian,
11,1,21,
0.1,m,
1,m,
0.1,m,

#-------------------------------------------------------------
~Rock/Soil Zonation Card
#-------------------------------------------------------------
1,
Sand,1,11,1,1,1,21,

#-------------------------------------------------------------
~Mechanical Properties Card
#-------------------------------------------------------------
Sand,2650,kg/m^3,0.4,0.4,,,Millington and Quirk,

#-------------------------------------------------------------
~Hydraulic Properties Card
#-------------------------------------------------------------
Sand,100.0,hc m/day,,,100.0,hc m/day,

#-------------------------------------------------------------
~Saturation Function Card
```

```
#-------------------------------------------------------------
72.0,dynes/cm,,,35.43,dynes/cm,
Sand,Van Genuchten,2.5,1/m,2.0,0.10,72.0,dynes/cm,,

#-------------------------------------------------------------
~Aqueous Relative Permeability Card
#-------------------------------------------------------------
Sand,Mualem,,

#-------------------------------------------------------------
~NAPL Relative Permeability Card
#-------------------------------------------------------------
Sand,Constant,0.0,

#-------------------------------------------------------------
~Gas Relative Permeability Card
#-------------------------------------------------------------
Sand,Mualem,,

#-------------------------------------------------------------
~Oil Properties Card
#-------------------------------------------------------------
Benzen,
78.114,g/mol,278.7,K,353.2,K,562.2,K,
48.9,bar,259,cm^3/mol,0.271,0.212,0.0,debyes,
-33.92,0.4739,-3.02e-4,7.13e-8,
Constant,9326,Pa,
Constant,875,kg/m^3,
Constant,0.652e-3,Pa s,
0.316e8,Pa,

#-------------------------------------------------------------
~Dissolved Oil Transport Card
#-------------------------------------------------------------
Sand,0.0,cm,0.00,cm,linear kd,0.0,m^3/kg,

#-------------------------------------------------------------
~Solute/Fluid Interaction Card
#-------------------------------------------------------------
1,
Benzen,,,,,,,Constant,0.24,m^3/m^3,,,,,
0,

#-------------------------------------------------------------
~Solute/Porous Media Interaction Card
#-------------------------------------------------------------
Sand,0.0,cm,0.00,cm,
Benzen,0.0,m^3/kg,

#-------------------------------------------------------------
~Initial Conditions Card
#-------------------------------------------------------------
4,
Aqueous Pressure,120921.8319,Pa,-9.7935192,1/m,,,-
9793.5192,1/m,1,11,1,1,1,21,
Gas Pressure,101348.42,Pa,,,,,-11.71,1/m,1,11,1,1,1,21,
NAPL Pressure,-1.e9,Pa,,,,,,,1,11,1,1,1,21,
```

```
Aqueous Oil Conc,100.0,mg/l,,,,,,1,11,1,1,1,21,

#-------------------------------------------------------------
~Boundary Conditions Card
#-------------------------------------------------------------
4,
West,hydraulic gradient,zero flux,zero flux,
1,1,1,1,1,21,1,
0,d,120921.8319,Pa,,,,,,,,
East,hydraulic gradient,zero flux,zero flux,
11,11,1,1,1,21,1,
0,d,120912.0384,,,,,,,,,
bottom,zero flux,Neumann,zero flux,
1,11,1,1,1,1,1,
0,d,,,,,2.0,m/day,,,,,,,
top,zero flux,dirichlet,zero flux,
1,11,1,1,21,21,1,
0,d,,,,,101325,Pa,,,,,

#-------------------------------------------------------------
~Source Card
#-------------------------------------------------------------
1,
Aqueous Mass,1,1,1,1,1,21,1,
0,d,1.0,kg/d,,1,

#-------------------------------------------------------------
~Output Options Card
#-------------------------------------------------------------
231,
1,1,21,
1,1,20,
1,1,19,
1,1,18,
1,1,17,
1,1,16,
1,1,15,
1,1,14,
1,1,13,
1,1,12,
1,1,11,
1,1,10,
1,1,9,
1,1,8,
1,1,7,
1,1,6,
1,1,5,
1,1,4,
1,1,3,
1,1,2,
1,1,1,
2,1,21,
2,1,20,
2,1,19,
2,1,18,
2,1,17,
2,1,16,
```

```
2,1,15,
2,1,14,
2,1,13,
2,1,12,
2,1,11,
2,1,10,
2,1,9,
2,1,8,
2,1,7,
2,1,6,
2,1,5,
2,1,4,
2,1,3,
2,1,2,
2,1,1,
3,1,21,
3,1,20,
3,1,19,
3,1,18,
3,1,17,
3,1,16,
3,1,15,
3,1,14,
3,1,13,
3,1,12,
3,1,11,
3,1,10,
3,1,9,
3,1,8,
3,1,7,
3,1,6,
3,1,5,
3,1,4,
3,1,3,
3,1,2,
3,1,1,
4,1,21,
4,1,20,
4,1,19,
4,1,18,
4,1,17,
4,1,16,
4,1,15,
4,1,14,
4,1,13,
4,1,12,
4,1,11,
4,1,10,
4,1,9,
4,1,8,
4,1,7,
4,1,6,
4,1,5,
4,1,4,
4,1,3,
4,1,2,
4,1,1,
```

```
5,1,21,
5,1,20,
5,1,19,
5,1,18,
5,1,17,
5,1,16,
5,1,15,
5,1,14,
5,1,13,
5,1,12,
5,1,11,
5,1,10,
5,1,9,
5,1,8,
5,1,7,
5,1,6,
5,1,5,
5,1,4,
5,1,3,
5,1,2,
5,1,1,
6,1,21,
6,1,20,
6,1,19,
6,1,18,
6,1,17,
6,1,16,
6,1,15,
6,1,14,
6,1,13,
6,1,12,
6,1,11,
6,1,10,
6,1,9,
6,1,8,
6,1,7,
6,1,6,
6,1,5,
6,1,4,
6,1,3,
6,1,2,
6,1,1,
7,1,21,
7,1,20,
7,1,19,
7,1,18,
7,1,17,
7,1,16,
7,1,15,
7,1,14,
7,1,13,
7,1,12,
7,1,11,
7,1,10,
7,1,9,
7,1,8,
7,1,7,
```

```
7,1,6,
7,1,5,
7,1,4,
7,1,3,
7,1,2,
7,1,1,
8,1,21,
8,1,20,
8,1,19,
8,1,18,
8,1,17,
8,1,16,
8,1,15,
8,1,14,
8,1,13,
8,1,12,
8,1,11,
8,1,10,
8,1,9,
8,1,8,
8,1,7,
8,1,6,
8,1,5,
8,1,4,
8,1,3,
8,1,2,
8,1,1,
9,1,21,
9,1,20,
9,1,19,
9,1,18,
9,1,17,
9,1,16,
9,1,15,
9,1,14,
9,1,13,
9,1,12,
9,1,11,
9,1,10,
9,1,9,
9,1,8,
9,1,7,
9,1,6,
9,1,5,
9,1,4,
9,1,3,
9,1,2,
9,1,1,
10,1,21,
10,1,20,
10,1,19,
10,1,18,
10,1,17,
10,1,16,
10,1,15,
10,1,14,
10,1,13,
```

```
10,1,12,
10,1,11,
10,1,10,
10,1,9,
10,1,8,
10,1,7,
10,1,6,
10,1,5,
10,1,4,
10,1,3,
10,1,2,
10,1,1,
11,1,21,
11,1,20,
11,1,19,
11,1,18,
11,1,17,
11,1,16,
11,1,15,
11,1,14,
11,1,13,
11,1,12,
11,1,11,
11,1,10,
11,1,9,
11,1,8,
11,1,7,
11,1,6,
11,1,5,
11,1,4,
11,1,3,
11,1,2,
11,1,1,
1,1,day,m,6,6,6,
5,
aqueous pressure, Pa,
Gas pressure, Pa,
Oil aqueous conc, mg/L,
x aqueous Volumetric Flux, m/day,
z gas Volumetric Flux, m/day,
1,
10,d,
6,
no restart,,
aqueous pressure, Pa,
Gas pressure, Pa,
Oil aqueous conc, mg/L,
x aqueous Volumetric Flux, m/day,
z gas Volumetric Flux, m/day,
```

2. Input file for hydraulic conductivity reduction

```
#-------------------------------------------------------------
~Simulation Title Card
#-------------------------------------------------------------
1,
Air Sprging,
James Warner/Osama AlGahtan,
CSU,
April 05,
10:00,
2,
STOMP Simulation for the reduction in hydraulic conductivity of Air
Sparging Tench,

#-------------------------------------------------------------
~Solution Control Card
#-------------------------------------------------------------
Normal,
Water-Oil-Air,
1,
0,s,10,d,10,s,5,d,1.25,8,1e-1,
1000000,
Variable,
Constant,0.9e-6,m^2/s,0.9e-6,m^2/s,
0,

#-------------------------------------------------------------
~Grid Card
#-------------------------------------------------------------
Uniform Cartesian,
11,1,21,
0.1,m,
1,m,
0.1,m,

#-------------------------------------------------------------
~Rock/Soil Zonation Card
#-------------------------------------------------------------
1,
Sand,1,11,1,1,1,21,

#-------------------------------------------------------------
~Mechanical Properties Card
#-------------------------------------------------------------
Sand,2650,kg/m^3,0.4,0.4,,,Millington and Quirk,

#-------------------------------------------------------------
~Hydraulic Properties Card
#-------------------------------------------------------------
Sand,100.0,hc m/day,,,100.0,hc m/day,

#-------------------------------------------------------------
~Saturation Function Card
#-------------------------------------------------------------
72.0,dynes/cm,,,35.43,dynes/cm,
```

```
Sand,Van Genuchten,2.5,1/m,2.0,0.10,72.0,dynes/cm,,

#-------------------------------------------------------------
~Aqueous Relative Permeability Card
#-------------------------------------------------------------
Sand,Mualem,,

#-------------------------------------------------------------
~NAPL Relative Permeability Card
#-------------------------------------------------------------
Sand,Constant,0.0,

#-------------------------------------------------------------
~Gas Relative Permeability Card
#-------------------------------------------------------------
Sand,Mualem,,

#-------------------------------------------------------------
~Oil Properties Card
#-------------------------------------------------------------
Benzene,
78.114,g/mol,278.7,K,353.2,K,562.2,K,
48.9,bar,259,cm^3/mol,0.271,0.212,0.0,debyes,
-33.92,0.4739,-3.02e-4,7.13e-8,
Constant,9326,Pa,
Constant,875,kg/m^3,
Constant,0.652e-3,Pa s,
0.316e8,Pa,

#-------------------------------------------------------------
~Dissolved Oil Transport Card
#-------------------------------------------------------------
Sand,0.0,cm,0.00,cm,linear kd,0.0,m^3/kg,

#-------------------------------------------------------------
~Solute/Fluid Interaction Card
#-------------------------------------------------------------
1,
Benzen,,,,,,,Constant,0.24,m^3/m^3,,,,,
0,

#-------------------------------------------------------------
~Solute/Porous Media Interaction Card
#-------------------------------------------------------------
Sand,0.0,cm,0.00,cm,
Benzen,0.0,m^3/kg,

#-------------------------------------------------------------
~Initial Conditions Card
#-------------------------------------------------------------
4,
Aqueous Pressure,120921.8319,Pa,-9.7935192,1/m,,,-
9793.5192,1/m,1,11,1,1,1,21,
Gas Pressure,101348.42,Pa,,,,,-11.71,1/m,1,11,1,1,1,21,
NAPL Pressure,-1.e9,Pa,,,,,,,1,11,1,1,1,21,
Aqueous Oil Conc,0.0,mg/l,,,,,,,1,11,1,1,1,21,
```

```
#-------------------------------------------------------------
~Boundary Conditions Card
#-------------------------------------------------------------
4,
West,hydraulic gradient,zero flux,zero flux,
1,1,1,1,1,21,1,
0,d,120921.8319,Pa,,,,,,,,
East,hydraulic gradient,zero flux,zero flux,
11,11,1,1,1,21,1,
0,d,120912.0384,,,,,,,,,
bottom,zero flux,Neumann,zero flux,
1,11,1,1,1,1,1,
0,d,,,,,2.0,m/day,,,,,,,
top,zero flux,dirichlet,zero flux,
1,11,1,1,21,21,1,
0,d,,,,,101325,Pa,,,,,

#-------------------------------------------------------------
~Output Options Card
#-------------------------------------------------------------
231,
1,1,21,
1,1,20,
1,1,19,
1,1,18,
1,1,17,
1,1,16,
1,1,15,
1,1,14,
1,1,13,
1,1,12,
1,1,11,
1,1,10,
1,1,9,
1,1,8,
1,1,7,
1,1,6,
1,1,5,
1,1,4,
1,1,3,
1,1,2,
1,1,1,
2,1,21,
2,1,20,
2,1,19,
2,1,18,
2,1,17,
2,1,16,
2,1,15,
2,1,14,
2,1,13,
2,1,12,
2,1,11,
2,1,10,
2,1,9,
2,1,8,
2,1,7,
```

```
2,1,6,
2,1,5,
2,1,4,
2,1,3,
2,1,2,
2,1,1,
3,1,21,
3,1,20,
3,1,19,
3,1,18,
3,1,17,
3,1,16,
3,1,15,
3,1,14,
3,1,13,
3,1,12,
3,1,11,
3,1,10,
3,1,9,
3,1,8,
3,1,7,
3,1,6,
3,1,5,
3,1,4,
3,1,3,
3,1,2,
3,1,1,
4,1,21,
4,1,20,
4,1,19,
4,1,18,
4,1,17,
4,1,16,
4,1,15,
4,1,14,
4,1,13,
4,1,12,
4,1,11,
4,1,10,
4,1,9,
4,1,8,
4,1,7,
4,1,6,
4,1,5,
4,1,4,
4,1,3,
4,1,2,
4,1,1,
5,1,21,
5,1,20,
5,1,19,
5,1,18,
5,1,17,
5,1,16,
5,1,15,
5,1,14,
5,1,13,
```

```
5,1,12,
5,1,11,
5,1,10,
5,1,9,
5,1,8,
5,1,7,
5,1,6,
5,1,5,
5,1,4,
5,1,3,
5,1,2,
5,1,1,
6,1,21,
6,1,20,
6,1,19,
6,1,18,
6,1,17,
6,1,16,
6,1,15,
6,1,14,
6,1,13,
6,1,12,
6,1,11,
6,1,10,
6,1,9,
6,1,8,
6,1,7,
6,1,6,
6,1,5,
6,1,4,
6,1,3,
6,1,2,
6,1,1,
7,1,21,
7,1,20,
7,1,19,
7,1,18,
7,1,17,
7,1,16,
7,1,15,
7,1,14,
7,1,13,
7,1,12,
7,1,11,
7,1,10,
7,1,9,
7,1,8,
7,1,7,
7,1,6,
7,1,5,
7,1,4,
7,1,3,
7,1,2,
7,1,1,
8,1,21,
8,1,20,
8,1,19,
```

```
8,1,18,
8,1,17,
8,1,16,
8,1,15,
8,1,14,
8,1,13,
8,1,12,
8,1,11,
8,1,10,
8,1,9,
8,1,8,
8,1,7,
8,1,6,
8,1,5,
8,1,4,
8,1,3,
8,1,2,
8,1,1,
9,1,21,
9,1,20,
9,1,19,
9,1,18,
9,1,17,
9,1,16,
9,1,15,
9,1,14,
9,1,13,
9,1,12,
9,1,11,
9,1,10,
9,1,9,
9,1,8,
9,1,7,
9,1,6,
9,1,5,
9,1,4,
9,1,3,
9,1,2,
9,1,1,
10,1,21,
10,1,20,
10,1,19,
10,1,18,
10,1,17,
10,1,16,
10,1,15,
10,1,14,
10,1,13,
10,1,12,
10,1,11,
10,1,10,
10,1,9,
10,1,8,
10,1,7,
10,1,6,
10,1,5,
10,1,4,
```

```
10,1,3,
10,1,2,
10,1,1,
11,1,21,
11,1,20,
11,1,19,
11,1,18,
11,1,17,
11,1,16,
11,1,15,
11,1,14,
11,1,13,
11,1,12,
11,1,11,
11,1,10,
11,1,9,
11,1,8,
11,1,7,
11,1,6,
11,1,5,
11,1,4,
11,1,3,
11,1,2,
11,1,1,
1,1,day,m,6,6,6,
4,
aqueous pressure, Pa,
Gas pressure, Pa,
x aqueous Volumetric Flux, m/day,
z gas Volumetric Flux, m/day,
1,
10,d,
5,
no restart,,
aqueous pressure, Pa,
Gas pressure, Pa,
x aqueous Volumetric Flux, m/day,
z gas Volumetric Flux, m/day,
```

Appendix F
Evaluating Φ and Ψ functions

1. Evaluating of Φ function

The general formula of ϕ as shown in equation (6.6) and rewritten here is

$$\phi_{n-1}(K_1x) = \frac{1}{xe^{-K_1x}} \frac{1}{(n-1)!} \frac{d^{n-1}}{dx^{n-1}} \left(x^n e^{-K_1x}\right) \qquad \text{for } n = 1, 2, \ldots$$

By evaluating the derivative to the forth degree (n up to 5) ϕ values will be as:

$\phi_0 = 1$
$\phi_1 = 1\text{-}1/2\ (K_1x)$
$\phi_2 = 1\text{-}\quad (K_1x) + 1/6\ (K_1x)^2$
$\phi_3 = 1\text{-}\ 3/2\ (K_1x) + 1/2\ (K_1x)^2 - 1/24\ (K_1x)^3$
$\phi_4 = 1\text{-}\ 2\quad (K_1x) + 1/2\ (K_1x)^2 - 1/6\ (K_1x)^3 + 1/120\ (K_1x)^4$

After rearrange
$\phi_0 = 1$
$\phi_1 = 1\text{-}1/2!\ (K_1x)$
$\phi_2 = 1\text{-}\ 2/2!\ (K_1x) + 1/3!\ (K_1x)^2$
$\phi_3 = 1\text{-}\ 3/2!\ (K_1x) + 3/3!\ (K_1x)^2 - 1/4!\ (K_1x)^3$
$\phi_4 = 1\text{-}\ 4/2!\ (K_1x) + 6/3!\ (K_1x)^2 - 4/4!\ (K_1x)^3 + 1/5!\ (K_1x)^4$

In matrix form

$$\begin{bmatrix} \phi_0 \\ \phi_1 \\ \phi_2 \\ \phi_3 \\ \phi_4 \end{bmatrix} = \begin{bmatrix} 1 & 0 & 0 & 0 & 0 \\ 1 & -1 & 0 & 0 & 0 \\ 1 & -2 & 1 & 0 & 0 \\ 1 & -3 & 3 & -1 & 0 \\ 1 & -4 & 6 & -4 & 1 \end{bmatrix} \begin{bmatrix} (K_1x)^0/1! \\ (K_1x)^1/2! \\ (K_1x)^2/3! \\ (K_1x)^3/4! \\ (K_1x)^4/5! \end{bmatrix}$$

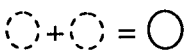

As noticed the first column of the matrix has the value of 1 and alternates the sign as marching to the next columns. As shown above, adding any two absolute consequences number in row (dashed circles) gives the second number's position in column and next row's position (solid circle). By this way and using spreadsheet, the middle matrix can be generated to the desired terms. After that the Φ term as mentioned in equation (6.7) can be evaluated for any values of K_1 and K_2 and point location x and y.

2. Evaluating of Ψ function.

Evaluating of $\Psi(K_1x,K_2y)$ function

$\psi_0 = 1$

$\psi_1 = 1- (K_2y)$

$\psi_2 = 1- 2\ (K_2y) + 1/2\ (\ K_2y)^2$

$\psi_3 = 1- 3\ (K_2y) + 3/2\ \ (K_2y)^2 - 1/6\ \ (K_2y)^3$

$\psi_4 = 1- 4\ (K_2y) +\ \ 3\ \ (K_2y)^2 - 4/6\ \ (K_2y)^3 + 1/24\ \ (K_2y)^4$

$\psi_5 = 1- 5\ (K_2y) +\ \ 5\ \ (K_2y)^2 - 5/3\ \ (K_2y)^3 + 5/24\ \ (K_2y)^4\ -1/120\ \ \ (K_2y)^5$

After rearrange

$\psi_0 = 1$

$\psi_1 = 1-1/1!\ \ (K_2y)$

$\psi_2 = 1- 2/1!\ \ (K_2y) + 1/2!\ \ (K_2y)^2$

$\psi_3 = 1- 3/1!\ \ (K_2y) + 3/2!\ \ (K_2y)^2\ - 1/3!\ \ (K_2y)^3$

$\psi_4 = 1- 4/1!\ \ (K_2y) + 6/2!\ \ (K_2y)^2\ - 4/3!\ \ (K_2y)^3\ + 1/4!\ \ \ (K_2y)^4$

$\psi_5 = 1- 5/1!\ \ (K_2y) + 10/2!\ (K_2y)^2\ - 10/3!\ (K_2y)^3\ + 5/4!\ \ \ (K_2y)^4\ - 1/5!\ \ \ (K_2y)^5$

In matrix form

$$\begin{bmatrix}\psi_0\\ \psi_1\\ \psi_2\\ \psi_3\\ \psi_4\\ \psi_5\end{bmatrix} = \begin{bmatrix}1 & 0 & 0 & 0 & 0 & 0\\ 1 & -1 & 0 & 0 & 0 & 0\\ 1 & -2 & 1 & 0 & 0 & 0\\ 1 & -3 & 3 & -1 & 0 & 0\\ 1 & -4 & 6 & -4 & 1 & 0\\ 1 & -5 & 10 & -10 & 5 & -1\end{bmatrix}\begin{bmatrix}(K_2y)^0/0!\\ (K_2y)^1/1!\\ (K_2y)^2/2!\\ (K_2y)^3/3!\\ (K_2y)^4/4!\\ (K_2y)^5/5!\end{bmatrix}$$

Again the process ends up same middle matrix has been developed for Φ function as shown in the previous section.

Appendix G
Tables for evaluating $\Phi(K_1x, K_2y)$ function

K_{2y} \ K_{1x}	1	2	3	4	5	6	7	8	9	10	11	12	13	14	15	16	17	18	19	20	21	22	23	24	25
1	1.718282	6.389056	19.08554	53.59815	147.4132	402.4288	1095.633	2979.958	8102.084	2.2E+04	6.0E+04	1.6E+05	4.4E+05	1.2E+06	3.3E+06	8.9E+06	2.4E+07	6.6E+07	1.8E+08	4.9E+08	1.3E+09	3.6E+09	9.7E+09	2.6E+10	7.2E+10
2	1.718282	6.389056	19.08554	53.59815	147.4132	402.4288	1095.633	2979.958	8102.084	2.2E+04	6.0E+04	1.6E+05	4.4E+05	1.2E+06	3.3E+06	8.9E+06	2.4E+07	6.6E+07	1.8E+08	4.9E+08	1.3E+09	3.6E+09	9.7E+09	2.6E+10	7.2E+10
3	1.718282	6.389056	19.08554	53.59815	147.4132	402.4288	1095.633	2979.958	8102.084	2.2E+04	6.0E+04	1.6E+05	4.4E+05	1.2E+06	3.3E+06	8.9E+06	2.4E+07	6.6E+07	1.8E+08	4.9E+08	1.3E+09	3.6E+09	9.7E+09	2.6E+10	7.2E+10
4	1.718282	6.389056	19.08554	53.59815	147.4132	402.4288	1095.633	2979.958	8102.084	2.2E+04	6.0E+04	1.6E+05	4.4E+05	1.2E+06	3.3E+06	8.9E+06	2.4E+07	6.6E+07	1.8E+08	4.9E+08	1.3E+09	3.6E+09	9.7E+09	2.6E+10	7.2E+10
5	1.718282	6.389056	19.08554	53.59815	147.4132	402.4288	1095.633	2979.958	8102.084	2.2E+04	6.0E+04	1.6E+05	4.4E+05	1.2E+06	3.3E+06	8.9E+06	2.4E+07	6.6E+07	1.8E+08	4.9E+08	1.3E+09	3.6E+09	9.7E+09	2.6E+10	7.2E+10
6	1.718282	6.389056	19.08554	53.59815	147.4132	402.4288	1095.633	2979.958	8102.084	2.2E+04	6.0E+04	1.6E+05	4.4E+05	1.2E+06	3.3E+06	8.9E+06	2.4E+07	6.6E+07	1.8E+08	4.9E+08	1.3E+09	3.6E+09	9.7E+09	2.6E+10	7.2E+10
7	1.718282	6.389056	19.08554	53.59815	147.4132	402.4288	1095.633	2979.958	8102.084	2.2E+04	6.0E+04	1.6E+05	4.4E+05	1.2E+06	3.3E+06	8.9E+06	2.4E+07	6.6E+07	1.8E+08	4.9E+08	1.3E+09	3.6E+09	9.7E+09	2.6E+10	7.2E+10
8	1.718282	6.389056	19.08554	53.59815	147.4132	402.4288	1095.633	2979.958	8102.084	2.2E+04	6.0E+04	1.6E+05	4.4E+05	1.2E+06	3.3E+06	8.9E+06	2.4E+07	6.6E+07	1.8E+08	4.9E+08	1.3E+09	3.6E+09	9.7E+09	2.6E+10	7.2E+10
9	1.718282	6.389056	19.08554	53.59815	147.4132	402.4288	1095.633	2979.958	8102.084	2.2E+04	6.0E+04	1.6E+05	4.4E+05	1.2E+06	3.3E+06	8.9E+06	2.4E+07	6.6E+07	1.8E+08	4.9E+08	1.3E+09	3.6E+09	9.7E+09	2.6E+10	7.2E+10
10	1.718282	6.389056	19.08554	53.59815	147.4132	402.4288	1095.633	2979.958	8102.084	2.2E+04	6.0E+04	1.6E+05	4.4E+05	1.2E+06	3.3E+06	8.9E+06	2.4E+07	6.6E+07	1.8E+08	4.9E+08	1.3E+09	3.6E+09	9.7E+09	2.6E+10	7.2E+10
11	1.718282	6.389056	19.08554	53.59815	147.4132	402.4288	1095.633	2979.958	8102.084	2.2E+04	6.0E+04	1.6E+05	4.4E+05	1.2E+06	3.3E+06	8.9E+06	2.4E+07	6.6E+07	1.8E+08	4.9E+08	1.3E+09	3.6E+09	9.7E+09	2.6E+10	7.2E+10
12	1.718282	6.389056	19.08554	53.59815	147.4132	402.4288	1095.633	2979.958	8102.084	2.2E+04	6.0E+04	1.6E+05	4.4E+05	1.2E+06	3.3E+06	8.9E+06	2.4E+07	6.6E+07	1.8E+08	4.9E+08	1.3E+09	3.6E+09	9.7E+09	2.6E+10	7.2E+10
13	1.718282	6.389056	19.08554	53.59815	147.4132	402.4288	1095.633	2979.958	8102.084	2.2E+04	6.0E+04	1.6E+05	4.4E+05	1.2E+06	3.3E+06	8.9E+06	2.4E+07	6.6E+07	1.8E+08	4.9E+08	1.3E+09	3.6E+09	9.7E+09	2.6E+10	7.2E+10
14	1.718282	6.389056	19.08554	53.59815	147.4132	402.4288	1095.633	2979.958	8102.084	2.2E+04	6.0E+04	1.6E+05	4.4E+05	1.2E+06	3.3E+06	8.9E+06	2.4E+07	6.6E+07	1.8E+08	4.9E+08	1.3E+09	3.6E+09	9.7E+09	2.6E+10	7.2E+10
15	1.718282	6.389056	19.08554	53.59815	147.4132	402.4288	1095.633	2979.958	8102.084	2.2E+04	6.0E+04	1.6E+05	4.4E+05	1.2E+06	3.3E+06	8.9E+06	2.4E+07	6.6E+07	1.8E+08	4.9E+08	1.3E+09	3.6E+09	9.7E+09	2.6E+10	7.2E+10
16	1.718282	6.389056	19.08554	53.59815	147.4132	402.4288	1095.633	2979.958	8102.084	2.2E+04	6.0E+04	1.6E+05	4.4E+05	1.2E+06	3.3E+06	8.9E+06	2.4E+07	6.6E+07	1.8E+08	4.9E+08	1.3E+09	3.6E+09	9.7E+09	2.6E+10	7.2E+10
17	1.718282	6.389056	19.08554	53.59815	147.4132	402.4288	1095.633	2979.958	8102.084	2.2E+04	6.0E+04	1.6E+05	4.4E+05	1.2E+06	3.3E+06	8.9E+06	2.4E+07	6.6E+07	1.8E+08	4.9E+08	1.3E+09	3.6E+09	9.7E+09	2.6E+10	7.2E+10
18	1.718282	6.389056	19.08554	53.59815	147.4132	402.4288	1095.633	2979.958	8102.084	2.2E+04	6.0E+04	1.6E+05	4.4E+05	1.2E+06	3.3E+06	8.9E+06	2.4E+07	6.6E+07	1.8E+08	4.9E+08	1.3E+09	3.6E+09	9.7E+09	2.6E+10	7.2E+10
19	1.718282	6.389056	19.08554	53.59815	147.4132	402.4288	1095.633	2979.958	8102.084	2.2E+04	6.0E+04	1.6E+05	4.4E+05	1.2E+06	3.3E+06	8.9E+06	2.4E+07	6.6E+07	1.8E+08	4.9E+08	1.3E+09	3.6E+09	9.7E+09	2.6E+10	7.2E+10
20	1.718282	6.389056	19.08554	53.59815	147.4132	402.4288	1095.633	2979.958	8102.084	2.2E+04	6.0E+04	1.6E+05	4.4E+05	1.2E+06	3.3E+06	8.9E+06	2.4E+07	6.6E+07	1.8E+08	4.9E+08	1.3E+09	3.6E+09	9.7E+09	2.6E+10	7.2E+10
21	1.718282	6.389056	19.08554	53.59815	147.4132	402.4288	1095.633	2979.958	8102.084	2.2E+04	6.0E+04	1.6E+05	4.4E+05	1.2E+06	3.3E+06	8.9E+06	2.4E+07	6.6E+07	1.8E+08	4.9E+08	1.3E+09	3.6E+09	9.7E+09	2.6E+10	7.2E+10
22	1.718282	6.389056	19.08554	53.59815	147.4132	402.4288	1095.633	2979.958	8102.084	2.2E+04	6.0E+04	1.6E+05	4.4E+05	1.2E+06	3.3E+06	8.9E+06	2.4E+07	6.6E+07	1.8E+08	4.9E+08	1.3E+09	3.6E+09	9.7E+09	2.6E+10	7.2E+10
23	1.718282	6.389056	19.08554	53.59815	147.4132	402.4288	1095.633	2979.958	8102.084	2.2E+04	6.0E+04	1.6E+05	4.4E+05	1.2E+06	3.3E+06	8.9E+06	2.4E+07	6.6E+07	1.8E+08	4.9E+08	1.3E+09	3.6E+09	9.7E+09	2.6E+10	7.2E+10
24	1.718282	6.389056	19.08554	53.59815	147.4132	402.4288	1095.633	2979.958	8102.084	2.2E+04	6.0E+04	1.6E+05	4.4E+05	1.2E+06	3.3E+06	8.9E+06	2.4E+07	6.6E+07	1.8E+08	4.9E+08	1.3E+09	3.6E+09	9.7E+09	2.6E+10	7.2E+10
25	1.718282	6.389056	19.08554	53.59815	147.4132	402.4288	1095.633	2979.958	8102.084	2.2E+04	6.0E+04	1.6E+05	4.4E+05	1.2E+06	3.3E+06	8.9E+06	2.4E+07	6.6E+07	1.8E+08	4.9E+08	1.3E+09	3.6E+09	9.7E+09	2.6E+10	7.2E+10
26	1.718282	6.389056	19.08554	53.59815	147.4132	402.4288	1095.633	2979.958	8102.084	2.2E+04	6.0E+04	1.6E+05	4.4E+05	1.2E+06	3.3E+06	8.9E+06	2.4E+07	6.6E+07	1.8E+08	4.9E+08	1.3E+09	3.6E+09	9.7E+09	2.6E+10	7.2E+10
27	1.718282	6.389056	19.08554	53.59815	147.4132	402.4288	1095.633	2979.958	8102.084	2.2E+04	6.0E+04	1.6E+05	4.4E+05	1.2E+06	3.3E+06	8.9E+06	2.4E+07	6.6E+07	1.8E+08	4.9E+08	1.3E+09	3.6E+09	9.7E+09	2.6E+10	7.2E+10
28	1.718282	6.389056	19.08554	53.59815	147.4132	402.4288	1095.633	2979.958	8102.084	2.2E+04	6.0E+04	1.6E+05	4.4E+05	1.2E+06	3.3E+06	8.9E+06	2.4E+07	6.6E+07	1.8E+08	4.9E+08	1.3E+09	3.6E+09	9.7E+09	2.6E+10	7.2E+10
29	1.718282	6.389056	19.08554	53.59815	147.4132	402.4288	1095.633	2979.958	8102.084	2.2E+04	6.0E+04	1.6E+05	4.4E+05	1.2E+06	3.3E+06	8.9E+06	2.4E+07	6.6E+07	1.8E+08	4.9E+08	1.3E+09	3.6E+09	9.7E+09	2.6E+10	7.2E+10
30	1.718282	6.389056	19.08554	53.59815	147.4132	402.4288	1095.633	2979.958	8102.084	2.2E+04	6.0E+04	1.6E+05	4.4E+05	1.2E+06	3.3E+06	8.9E+06	2.4E+07	6.6E+07	1.8E+08	4.9E+08	1.3E+09	3.6E+09	9.7E+09	2.6E+10	7.2E+10
31	1.718282	6.389056	19.08554	53.59815	147.4132	402.4288	1095.633	2979.958	8102.084	2.2E+04	6.0E+04	1.6E+05	4.4E+05	1.2E+06	3.3E+06	8.9E+06	2.4E+07	6.6E+07	1.8E+08	4.9E+08	1.3E+09	3.6E+09	9.7E+09	2.6E+10	7.2E+10
32	1.718282	6.389056	19.08554	53.59815	147.4132	402.4288	1095.633	2979.958	8102.084	2.2E+04	6.0E+04	1.6E+05	4.4E+05	1.2E+06	3.3E+06	8.9E+06	2.4E+07	6.6E+07	1.8E+08	4.9E+08	1.3E+09	3.6E+09	9.7E+09	2.6E+10	7.2E+10
33	1.718282	6.389056	19.08554	53.59815	147.4132	402.4288	1095.633	2979.958	8102.084	2.2E+04	6.0E+04	1.6E+05	4.4E+05	1.2E+06	3.3E+06	8.9E+06	2.4E+07	6.6E+07	1.8E+08	4.9E+08	1.3E+09	3.6E+09	9.7E+09	2.6E+10	7.2E+10
34	1.718282	6.389056	19.08554	53.59815	147.4132	402.4288	1095.633	2979.958	8102.084	2.2E+04	6.0E+04	1.6E+05	4.4E+05	1.2E+06	3.3E+06	8.9E+06	2.4E+07	6.6E+07	1.8E+08	4.9E+08	1.3E+09	3.6E+09	9.7E+09	2.6E+10	7.2E+10
35	1.718282	6.389056	19.08554	53.59815	147.4132	402.4288	1095.633	2979.958	8102.084	2.2E+04	6.0E+04	1.6E+05	4.4E+05	1.2E+06	3.3E+06	8.9E+06	2.4E+07	6.6E+07	1.8E+08	4.9E+08	1.3E+09	3.6E+09	9.7E+09	2.6E+10	7.2E+10
36	1.718282	6.389056	19.08554	53.59815	147.4132	402.4288	1095.633	2979.958	8102.084	2.2E+04	6.0E+04	1.6E+05	4.4E+05	1.2E+06	3.3E+06	8.9E+06	2.4E+07	6.6E+07	1.8E+08	4.9E+08	1.3E+09	3.6E+09	9.7E+09	2.6E+10	7.2E+10
37	1.718282	6.389056	19.08554	53.59815	147.4132	402.4288	1095.633	2979.958	8102.084	2.2E+04	6.0E+04	1.6E+05	4.4E+05	1.2E+06	3.3E+06	8.9E+06	2.4E+07	6.6E+07	1.8E+08	4.9E+08	1.3E+09	3.6E+09	9.7E+09	2.6E+10	7.2E+10
38	1.718282	6.389056	19.08554	53.59815	147.4132	402.4288	1095.633	2979.958	8102.084	2.2E+04	6.0E+04	1.6E+05	4.4E+05	1.2E+06	3.3E+06	8.9E+06	2.4E+07	6.6E+07	1.8E+08	4.9E+08	1.3E+09	3.6E+09	9.7E+09	2.6E+10	7.2E+10
39	1.718282	6.389056	19.08554	53.59815	147.4132	402.4288	1095.633	2979.958	8102.084	2.2E+04	6.0E+04	1.6E+05	4.4E+05	1.2E+06	3.3E+06	8.9E+06	2.4E+07	6.6E+07	1.8E+08	4.9E+08	1.3E+09	3.6E+09	9.7E+09	2.6E+10	7.2E+10
40	1.718282	6.389056	19.08554	53.59815	147.4132	402.4288	1095.633	2979.958	8102.084	2.2E+04	6.0E+04	1.6E+05	4.4E+05	1.2E+06	3.3E+06	8.9E+06	2.4E+07	6.6E+07	1.8E+08	4.9E+08	1.3E+09	3.6E+09	9.7E+09	2.6E+10	7.2E+10
41	1.718282	6.389056	19.08554	53.59815	147.4132	402.4288	1095.633	2979.958	8102.084	2.2E+04	6.0E+04	1.6E+05	4.4E+05	1.2E+06	3.3E+06	8.9E+06	2.4E+07	6.6E+07	1.8E+08	4.9E+08	1.3E+09	3.6E+09	9.7E+09	2.6E+10	7.2E+10
42	1.718282	6.389056	19.08554	53.59815	147.4132	402.4288	1095.633	2979.958	8102.084	2.2E+04	6.0E+04	1.6E+05	4.4E+05	1.2E+06	3.3E+06	8.9E+06	2.4E+07	6.6E+07	1.8E+08	4.9E+08	1.3E+09	3.6E+09	9.7E+09	2.6E+10	7.2E+10
43	1.718282	6.389056	19.08554	53.59815	147.4132	402.4288	1095.633	2979.958	8102.084	2.2E+04	6.0E+04	1.6E+05	4.4E+05	1.2E+06	3.3E+06	8.9E+06	2.4E+07	6.6E+07	1.8E+08	4.9E+08	1.3E+09	3.6E+09	9.7E+09	2.6E+10	7.2E+10
44	1.718282	6.389056	19.08554	53.59815	147.4132	402.4288	1095.633	2979.958	8102.084	2.2E+04	6.0E+04	1.6E+05	4.4E+05	1.2E+06	3.3E+06	8.9E+06	2.4E+07	6.6E+07	1.8E+08	4.9E+08	1.3E+09	3.6E+09	9.7E+09	2.6E+10	7.2E+10
45	1.718282	6.389056	19.08554	53.59815	147.4132	402.4288	1095.633	2979.958	8102.084	2.2E+04	6.0E+04	1.6E+05	4.4E+05	1.2E+06	3.3E+06	8.9E+06	2.4E+07	6.6E+07	1.8E+08	4.9E+08	1.3E+09	3.6E+09	9.7E+09	2.6E+10	7.2E+10
46	1.718282	6.389056	19.08554	53.59815	147.4132	402.4288	1095.633	2979.958	8102.084	2.2E+04	6.0E+04	1.6E+05	4.4E+05	1.2E+06	3.3E+06	8.9E+06	2.4E+07	6.6E+07	1.8E+08	4.9E+08	1.3E+09	3.6E+09	9.7E+09	2.6E+10	7.2E+10
47	1.718282	6.389056	19.08554	53.59815	147.4132	402.4288	1095.633	2979.958	8102.084	2.2E+04	6.0E+04	1.6E+05	4.4E+05	1.2E+06	3.3E+06	8.9E+06	2.4E+07	6.6E+07	1.8E+08	4.9E+08	1.3E+09	3.6E+09	9.7E+09	2.6E+10	7.2E+10
48	1.718282	6.389056	19.08554	53.59815	147.4132	402.4288	1095.633	2979.958	8102.084	2.2E+04	6.0E+04	1.6E+05	4.4E+05	1.2E+06	3.3E+06	8.9E+06	2.4E+07	6.6E+07	1.8E+08	4.9E+08	1.3E+09	3.6E+09	9.7E+09	2.6E+10	7.2E+10
49	1.718282	6.389056	19.08554	53.59815	147.4132	402.4288	1095.633	2979.958	8102.084	2.2E+04	6.0E+04	1.6E+05	4.4E+05	1.2E+06	3.3E+06	8.9E+06	2.4E+07	6.6E+07	1.8E+08	4.9E+08	1.3E+09	3.6E+09	9.7E+09	2.6E+10	7.2E+10
50	1.718282	6.389056	19.08554	53.59815	147.4132	402.4288	1095.633	2979.958	8102.084	2.2E+04	6.0E+04	1.6E+05	4.4E+05	1.2E+06	3.3E+06	8.9E+06	2.4E+07	6.6E+07	1.8E+08	4.9E+08	1.3E+09	3.6E+09	9.7E+09	2.6E+10	7.2E+10

K_2y \ K_1x	1	2	3	4	5	6	7	8	9	10	11	12	13	14	15	16	17	18	19	20	21	22	23	24	25
51	1.718282	6.389056	19.08554	53.59815	147.4132	402.4288	1095.633	2979.958	8102.084	2.2E+04	6.0E+04	1.6E+05	4.4E+05	1.2E+06	3.3E+06	8.9E+06	2.4E+07	6.6E+07	1.8E+08	4.9E+08	1.3E+09	3.6E+09	9.7E+09	2.6E+10	7.2E+10
52	1.718282	6.389056	19.08554	53.59815	147.4132	402.4288	1095.633	2979.958	8102.084	2.2E+04	6.0E+04	1.6E+05	4.4E+05	1.2E+06	3.3E+06	8.9E+06	2.4E+07	6.6E+07	1.8E+08	4.9E+08	1.3E+09	3.6E+09	9.7E+09	2.6E+10	7.2E+10
53	1.718282	6.389056	19.08554	53.59815	147.4132	402.4288	1095.633	2979.958	8102.084	2.2E+04	6.0E+04	1.6E+05	4.4E+05	1.2E+06	3.3E+06	8.9E+06	2.4E+07	6.6E+07	1.8E+08	4.9E+08	1.3E+09	3.6E+09	9.7E+09	2.6E+10	7.2E+10
54	1.718282	6.389056	19.08554	53.59815	147.4132	402.4288	1095.633	2979.958	8102.084	2.2E+04	6.0E+04	1.6E+05	4.4E+05	1.2E+06	3.3E+06	8.9E+06	2.4E+07	6.6E+07	1.8E+08	4.8E+08	1.3E+09	3.6E+09	9.7E+09	2.6E+10	7.2E+10
55	1.718282	6.389056	19.08554	53.59815	147.4132	402.4288	1095.633	2979.958	8102.084	2.2E+04	6.0E+04	1.6E+05	4.4E+05	1.2E+06	3.3E+06	8.9E+06	2.4E+07	6.6E+07	1.8E+08	4.8E+08	1.3E+09	3.6E+09	9.7E+09	2.6E+10	7.2E+10
56	1.718282	6.389056	19.08554	53.59815	147.4132	402.4288	1095.633	2979.958	8102.084	2.2E+04	6.0E+04	1.6E+05	4.4E+05	1.2E+06	3.3E+06	8.9E+06	2.4E+07	6.6E+07	1.8E+08	4.8E+08	1.3E+09	3.6E+09	9.7E+09	2.6E+10	7.1E+10
57	1.718282	6.389056	19.08554	53.59815	147.4132	402.4288	1095.633	2979.958	8102.084	2.2E+04	6.0E+04	1.6E+05	4.4E+05	1.2E+06	3.3E+06	8.9E+06	2.4E+07	6.6E+07	1.8E+08	4.8E+08	1.3E+09	3.6E+09	9.7E+09	2.6E+10	7.1E+10
58	1.718282	6.389056	19.08554	53.59815	147.4132	402.4288	1095.633	2979.958	8102.083	2.2E+04	6.0E+04	1.6E+05	4.4E+05	1.2E+06	3.3E+06	8.9E+06	2.4E+07	6.6E+07	1.8E+08	4.8E+08	1.3E+09	3.6E+09	9.7E+09	2.6E+10	7.1E+10
59	1.718282	6.389056	19.08554	53.59815	147.4132	402.4288	1095.633	2979.958	8102.083	2.2E+04	6.0E+04	1.6E+05	4.4E+05	1.2E+06	3.3E+06	8.9E+06	2.4E+07	6.6E+07	1.8E+08	4.8E+08	1.3E+09	3.6E+09	9.7E+09	2.6E+10	7.1E+10
60	1.718282	6.389056	19.08554	53.59815	147.4132	402.4288	1095.633	2979.958	8102.081	2.2E+04	6.0E+04	1.6E+05	4.4E+05	1.2E+06	3.3E+06	8.9E+06	2.4E+07	6.6E+07	1.8E+08	4.8E+08	1.3E+09	3.6E+09	9.6E+09	2.6E+10	7.0E+10
61	1.718282	6.389056	19.08554	53.59815	147.4132	402.4288	1095.633	2979.958	8102.079	2.2E+04	6.0E+04	1.6E+05	4.4E+05	1.2E+06	3.3E+06	8.9E+06	2.4E+07	6.6E+07	1.8E+08	4.8E+08	1.3E+09	3.5E+09	9.6E+09	2.6E+10	7.0E+10
62	1.718282	6.389056	19.08554	53.59815	147.4132	402.4288	1095.633	2979.957	8102.076	2.2E+04	6.0E+04	1.6E+05	4.4E+05	1.2E+06	3.3E+06	8.9E+06	2.4E+07	6.6E+07	1.8E+08	4.8E+08	1.3E+09	3.5E+09	9.5E+09	2.6E+10	6.9E+10
63	1.718282	6.389056	19.08554	53.59815	147.4132	402.4288	1095.633	2979.956	8102.07	2.2E+04	6.0E+04	1.6E+05	4.4E+05	1.2E+06	3.3E+06	8.9E+06	2.4E+07	6.5E+07	1.8E+08	4.8E+08	1.3E+09	3.5E+09	9.5E+09	2.5E+10	6.8E+10
64	1.718282	6.389056	19.08554	53.59815	147.4132	402.4288	1095.633	2979.955	8102.059	2.2E+04	6.0E+04	1.6E+05	4.4E+05	1.2E+06	3.3E+06	8.9E+06	2.4E+07	6.5E+07	1.8E+08	4.8E+08	1.3E+09	3.5E+09	9.4E+09	2.5E+10	6.7E+10
65	1.718282	6.389056	19.08554	53.59815	147.4132	402.4288	1095.633	2979.953	8102.04	2.2E+04	6.0E+04	1.6E+05	4.4E+05	1.2E+06	3.3E+06	8.9E+06	2.4E+07	6.5E+07	1.8E+08	4.8E+08	1.3E+09	3.5E+09	9.3E+09	2.5E+10	6.6E+10
66	1.718282	6.389056	19.08554	53.59815	147.4132	402.4287	1095.632	2979.949	8102.008	2.2E+04	6.0E+04	1.6E+05	4.4E+05	1.2E+06	3.3E+06	8.9E+06	2.4E+07	6.5E+07	1.8E+08	4.7E+08	1.3E+09	3.4E+09	9.1E+09	2.4E+10	6.4E+10
67	1.718282	6.389056	19.08554	53.59815	147.4131	402.4287	1095.632	2979.942	8101.952	2.2E+04	6.0E+04	1.6E+05	4.4E+05	1.2E+06	3.3E+06	8.9E+06	2.4E+07	6.5E+07	1.7E+08	4.7E+08	1.3E+09	3.4E+09	9.0E+09	2.4E+10	6.2E+10
68	1.718282	6.389056	19.08554	53.59815	147.4131	402.4285	1095.63	2979.93	8101.858	2.2E+04	6.0E+04	1.6E+05	4.4E+05	1.2E+06	3.3E+06	8.8E+06	2.4E+07	6.4E+07	1.7E+08	4.7E+08	1.2E+09	3.3E+09	8.8E+09	2.3E+10	6.0E+10
69	1.718282	6.389056	19.08554	53.59815	147.4131	402.4283	1095.628	2979.909	8101.698	2.2E+04	6.0E+04	1.6E+05	4.4E+05	1.2E+06	3.2E+06	8.8E+06	2.4E+07	6.4E+07	1.7E+08	4.6E+08	1.2E+09	3.2E+09	8.5E+09	2.2E+10	5.8E+10
70	1.718282	6.389056	19.08554	53.59815	147.4131	402.4279	1095.624	2979.873	8101.431	2.2E+04	6.0E+04	1.6E+05	4.4E+05	1.2E+06	3.2E+06	8.8E+06	2.4E+07	6.3E+07	1.7E+08	4.5E+08	1.2E+09	3.2E+09	8.3E+09	2.1E+10	5.5E+10
71	1.718282	6.389056	19.08554	53.59814	147.413	402.4271	1095.616	2979.811	8100.987	2.2E+04	6.0E+04	1.6E+05	4.4E+05	1.2E+06	3.2E+06	8.8E+06	2.4E+07	6.3E+07	1.7E+08	4.4E+08	1.2E+09	3.1E+09	7.9E+09	2.0E+10	5.2E+10
72	1.718282	6.389056	19.08554	53.59813	147.4129	402.4256	1095.602	2979.705	8100.256	2.2E+04	6.0E+04	1.6E+05	4.4E+05	1.2E+06	3.2E+06	8.7E+06	2.3E+07	6.3E+07	1.7E+08	4.4E+08	1.2E+09	2.9E+09	7.6E+09	1.9E+10	4.9E+10
73	1.718282	6.389056	19.08554	53.59812	147.4126	402.423	1095.579	2979.526	8099.063	2.2E+04	6.0E+04	1.6E+05	4.4E+05	1.2E+06	3.2E+06	8.6E+06	2.3E+07	6.2E+07	1.6E+08	4.3E+08	1.1E+09	2.8E+09	7.2E+09	1.8E+10	4.6E+10
74	1.718282	6.389056	19.08553	53.59808	147.4122	402.4182	1095.538	2979.227	8097.133	2.2E+04	6.0E+04	1.6E+05	4.4E+05	1.2E+06	3.2E+06	8.5E+06	2.3E+07	6.0E+07	1.6E+08	4.2E+08	1.1E+09	2.8E+09	7.2E+09	1.8E+10	4.6E+10
75	1.718282	6.389056	19.08553	53.59801	147.4113	402.4096	1095.468	2978.732	8094.045	2.2E+04	6.0E+04	1.6E+05	4.4E+05	1.2E+06	3.2E+06	8.4E+06	2.2E+07	5.9E+07	1.5E+08	4.0E+08	1.0E+09	2.7E+09	6.7E+09	1.7E+10	4.2E+10
76	1.718282	6.389056	19.08552	53.59788	147.4097	402.3945	1095.348	2977.919	8089.154	2.2E+04	5.9E+04	1.6E+05	4.3E+05	1.2E+06	3.1E+06	8.3E+06	2.2E+07	5.7E+07	1.5E+08	3.8E+08	9.8E+08	2.5E+09	6.2E+09	1.5E+10	3.8E+10
77	1.718282	6.389055	19.08551	53.59763	147.4068	402.3678	1095.146	2976.599	8081.496	2.2E+04	5.9E+04	1.6E+05	4.3E+05	1.1E+06	3.1E+06	8.1E+06	2.1E+07	5.5E+07	1.4E+08	3.6E+08	9.2E+08	2.3E+09	5.7E+09	1.4E+10	3.4E+10
78	1.718282	6.389054	19.08548	53.59715	147.4015	402.3213	1094.809	2974.479	8069.647	2.2E+04	5.9E+04	1.6E+05	4.3E+05	1.1E+06	3.0E+06	7.9E+06	2.0E+07	5.3E+07	1.3E+08	3.4E+08	8.5E+08	2.1E+09	5.1E+09	1.2E+10	3.0E+10
79	1.718282	6.389051	19.08541	53.59623	147.3918	402.241	1094.252	2971.116	8051.544	2.2E+04	5.9E+04	1.6E+05	4.2E+05	1.1E+06	2.9E+06	7.6E+06	2.0E+07	5.0E+07	1.3E+08	3.1E+08	7.8E+08	1.9E+09	4.6E+09	1.1E+10	2.6E+10
80	1.718282	6.389046	19.08529	53.59449	147.3745	402.1042	1093.342	2965.848	8024.256	2.2E+04	5.8E+04	1.5E+05	4.1E+05	1.1E+06	2.8E+06	7.3E+06	1.9E+07	4.7E+07	1.2E+08	2.9E+08	7.0E+08	1.7E+09	4.0E+09	9.4E+09	2.2E+10
81	1.718281	6.389034	19.08504	53.59124	147.3438	401.8733	1091.876	2957.703	7983.716	2.1E+04	5.7E+04	1.5E+05	4.0E+05	1.0E+06	2.7E+06	6.9E+06	1.7E+07	4.3E+07	1.1E+08	2.6E+08	6.2E+08	1.5E+09	3.4E+09	7.9E+09	1.8E+10
82	1.718281	6.389009	19.08454	53.58522	147.2901	401.4887	1089.543	2945.296	7924.41	2.1E+04	5.6E+04	1.5E+05	3.9E+05	1.0E+06	2.5E+06	6.4E+06	1.6E+07	3.9E+07	9.5E+07	2.3E+08	5.3E+08	1.2E+09	2.9E+09	6.5E+09	1.5E+10
83	1.71828	6.388957	19.08357	53.57417	147.1971	400.8562	1085.886	2926.686	7839.085	2.1E+04	5.5E+04	1.4E+05	3.7E+05	9.5E+05	2.4E+06	5.9E+06	1.4E+07	3.5E+07	8.3E+07	2.0E+08	4.5E+08	1.0E+09	2.3E+09	5.2E+09	1.2E+10
84	1.718277	6.388847	19.0817	53.55415	147.038	399.8309	1080.241	2899.238	7723.649	2.0E+04	5.3E+04	1.4E+05	3.5E+05	8.8E+05	2.2E+06	5.3E+06	1.3E+07	3.1E+07	7.1E+07	1.6E+08	3.7E+08	8.4E+08	1.9E+09	4.1E+09	8.8E+09
85	1.718271	6.388618	19.0781	53.5183	146.7699	398.1944	1071.672	2860.557	7568.459	2.0E+04	5.1E+04	1.3E+05	3.3E+05	8.1E+05	2.0E+06	4.7E+06	1.1E+07	2.6E+07	6.0E+07	1.4E+08	3.0E+08	6.6E+08	1.4E+09	3.1E+09	6.6E+09
86	1.718258	6.388146	19.07128	53.45493	146.3246	395.6259	1059.022	2808.086	7359.725	1.9E+04	4.9E+04	1.2E+05	3.0E+05	7.3E+05	1.7E+06	4.1E+06	9.5E+06	2.2E+07	4.9E+07	1.1E+08	2.4E+08	5.1E+08	1.1E+09	2.3E+09	4.7E+09
87	1.718226	6.387182	19.0585	53.34453	145.5973	391.6681	1041.634	2735.839	7085.115	1.8E+04	4.5E+04	1.1E+05	2.7E+05	6.4E+05	1.5E+06	3.5E+06	7.9E+06	1.8E+07	3.8E+07	8.3E+07	1.8E+08	3.7E+08	7.8E+08	1.6E+09	3.2E+09
88	1.718155	6.385231	19.03486	53.15523	144.4308	386.0262	1017.08	2638.708	6732.532	1.7E+04	4.2E+04	1.0E+05	2.4E+05	5.5E+05	1.3E+06	2.8E+06	6.3E+06	1.4E+07	2.9E+07	6.2E+07	1.3E+08	2.7E+08	5.3E+08	1.1E+09	2.1E+09
89	1.717995	6.38133	18.99178	52.83631	142.6612	377.8836	983.1873	2511.313	6291.638	1.5E+04	3.7E+04	8.8E+04	2.0E+05	4.6E+05	1.0E+06	2.2E+06	4.8E+06	1.0E+07	2.1E+07	4.4E+07	9.0E+07	1.8E+08	3.5E+08	6.7E+08	1.3E+09
90	1.717636	6.373624	18.91455	52.31249	140.053	366.2807	937.5925	2348.774	5756.303	1.4E+04	3.2E+04	7.4E+04	1.7E+05	3.7E+05	8.0E+05	1.7E+06	3.6E+06	7.3E+06	1.5E+07	3.0E+07	5.8E+07	1.1E+08	2.1E+08	4.0E+08	7.3E+08
91	1.716838	6.358615	18.7786	51.52305	136.1943	350.1905	878.0038	2147.726	5127.459	1.2E+04	2.7E+04	6.1E+04	1.3E+05	2.8E+05	6.0E+05	1.2E+06	2.5E+06	5.0E+06	9.8E+06	1.9E+07	3.5E+07	6.6E+07	1.2E+08	2.2E+08	3.9E+08
92	1.715082	6.329839	18.55537	50.29544	130.6352	328.5305	802.6171	1907.629	4416.026	1.0E+04	2.2E+04	4.7E+04	1.0E+05	2.1E+05	4.2E+05	8.4E+05	1.7E+06	3.2E+06	6.0E+06	1.1E+07	2.0E+07	3.6E+07	6.4E+07	1.1E+08	2.0E+08
93	1.711259	6.276049	18.19383	48.44004	122.8703	300.3528	710.7434	1632.256	3645.253	7.9E+03	1.7E+04	3.5E+04	7.1E+04	1.4E+05	2.8E+05	5.4E+05	1.0E+06	1.8E+06	3.3E+06	5.9E+06	1.0E+07	1.8E+07	3.1E+07	5.3E+07	8.9E+07
94	1.703034	6.183838	17.61044	45.72057	112.4023	265.1228	603.5524	1330.988	2851.407	5.9E+03	1.2E+04	2.4E+04	4.7E+04	9.0E+04	1.7E+05	3.1E+05	5.5E+05	9.8E+05	1.7E+06	2.9E+06	4.9E+06	8.2E+06	1.4E+07	2.2E+07	3.6E+07
95	1.686107	6.021505	16.69871	41.87876	98.87286	223.1052	484.8096	1019.408	2081.659	4.1E+03	8.0E+03	1.5E+04	2.9E+04	5.2E+04	9.2E+04	1.6E+05	2.7E+05	4.6E+05	7.6E+05	1.3E+06	2.0E+06	3.2E+06	5.2E+06	8.1E+06	1.3E+07
96	1.653137	5.742674	15.32389	36.6847	82.25564	175.7842	361.3208	718.5199	1388.276	2.6E+03	4.8E+03	8.7E+03	1.5E+04	2.6E+04	4.3E+04	7.2E+04	1.2E+05	1.9E+05	3.0E+05	4.6E+05	7.1E+05	1.1E+06	1.7E+06	2.5E+06	3.7E+06
97	1.587405	5.279622	13.34162	30.03728	63.10796	126.1904	242.7008	451.9945	819.0759	1.4E+03	2.5E+03	4.2E+03	6.8E+03	1.1E+04	1.7E+04	2.7E+04	4.1E+04	6.2E+04	9.4E+04	1.4E+05	2.0E+05	3.0E+05	4.3E+05	6.1E+05	8.7E+05
98	1.458636	4.541328	10.64267	22.11404	42.80791	78.89038	140.045	241.2714	405.6597	6.6E+02	1.0E+03	1.6E+03	2.4E+03	3.6E+03	5.3E+03	7.8E+03	1.1E+04	1.6E+04	2.2E+04	3.1E+04	4.3E+04	5.9E+04	8.1E+04	1.1E+05	1.5E+05
99	1.214053	3.427573	7.244305	13.55239	23.63763	39.34119	63.28825	99.26336	147.6251	2.2E+02	3.1E+02	4.3E+02	6.0E+02	8.3E+02	1.1E+03	1.5E+03	2.0E+03	2.6E+03	3.5E+03	4.5E+03	5.8E+03	7.4E+03	9.4E+03	1.2E+04	1.5E+04
100	0.764956	1.872488	3.431922	5.577776	8.4826	12.3771	17.03946	22.67405	29.58994	3.8E+01	4.8E+01	6.0E+01	7.5E+01	9.2E+01	1.1E+02	1.3E+02	1.6E+02	1.9E+02	2.3E+02	2.7E+02	3.2E+02	3.7E+02	4.3E+02	5.0E+02	5.8E+02

K_{2y}	26	27	28	29	30	31	32	33	34	35	36	37	38	39	40	41	42	43	44	45	46	47	48	49	50
1.0E+00	2.0E+11	5.3E+11	1.4E+12	3.9E+12	1.1E+13	2.9E+13	7.9E+13	2.1E+14	5.8E+14	1.6E+15	4.3E+15	1.2E+16	3.2E+16	8.7E+16	2.4E+17	6.4E+17	1.7E+18	4.7E+18	1.3E+19	3.5E+19	9.5E+19	2.6E+20	7.0E+20	1.9E+21	5.2E+21
2.0E+00	2.0E+11	5.3E+11	1.4E+12	3.9E+12	1.1E+13	2.9E+13	7.9E+13	2.1E+14	5.8E+14	1.6E+15	4.3E+15	1.2E+16	3.2E+16	8.7E+16	2.4E+17	6.4E+17	1.7E+18	4.7E+18	1.3E+19	3.5E+19	9.5E+19	2.6E+20	7.0E+20	1.9E+21	5.2E+21
3.0E+00	2.0E+11	5.3E+11	1.4E+12	3.9E+12	1.1E+13	2.9E+13	7.9E+13	2.1E+14	5.8E+14	1.6E+15	4.3E+15	1.2E+16	3.2E+16	8.7E+16	2.4E+17	6.4E+17	1.7E+18	4.7E+18	1.3E+19	3.5E+19	9.5E+19	2.6E+20	7.0E+20	1.9E+21	5.2E+21
4.0E+00	2.0E+11	5.3E+11	1.4E+12	3.9E+12	1.1E+13	2.9E+13	7.9E+13	2.1E+14	5.8E+14	1.6E+15	4.3E+15	1.2E+16	3.2E+16	8.7E+16	2.4E+17	6.4E+17	1.7E+18	4.7E+18	1.3E+19	3.5E+19	9.5E+19	2.6E+20	7.0E+20	1.9E+21	5.2E+21
5.0E+00	2.0E+11	5.3E+11	1.4E+12	3.9E+12	1.1E+13	2.9E+13	7.9E+13	2.1E+14	5.8E+14	1.6E+15	4.3E+15	1.2E+16	3.2E+16	8.7E+16	2.4E+17	6.4E+17	1.7E+18	4.7E+18	1.3E+19	3.5E+19	9.5E+19	2.6E+20	7.0E+20	1.9E+21	5.2E+21
6.0E+00	2.0E+11	5.3E+11	1.4E+12	3.9E+12	1.1E+13	2.9E+13	7.9E+13	2.1E+14	5.8E+14	1.6E+15	4.3E+15	1.2E+16	3.2E+16	8.7E+16	2.4E+17	6.4E+17	1.7E+18	4.7E+18	1.3E+19	3.5E+19	9.5E+19	2.6E+20	7.0E+20	1.9E+21	5.2E+21
7.0E+00	2.0E+11	5.3E+11	1.4E+12	3.9E+12	1.1E+13	2.9E+13	7.9E+13	2.1E+14	5.8E+14	1.6E+15	4.3E+15	1.2E+16	3.2E+16	8.7E+16	2.4E+17	6.4E+17	1.7E+18	4.7E+18	1.3E+19	3.5E+19	9.5E+19	2.6E+20	7.0E+20	1.9E+21	5.2E+21
8.0E+00	2.0E+11	5.3E+11	1.4E+12	3.9E+12	1.1E+13	2.9E+13	7.9E+13	2.1E+14	5.8E+14	1.6E+15	4.3E+15	1.2E+16	3.2E+16	8.7E+16	2.4E+17	6.4E+17	1.7E+18	4.7E+18	1.3E+19	3.5E+19	9.5E+19	2.6E+20	7.0E+20	1.9E+21	5.2E+21
9.0E+00	2.0E+11	5.3E+11	1.4E+12	3.9E+12	1.1E+13	2.9E+13	7.9E+13	2.1E+14	5.8E+14	1.6E+15	4.3E+15	1.2E+16	3.2E+16	8.7E+16	2.4E+17	6.4E+17	1.7E+18	4.7E+18	1.3E+19	3.5E+19	9.5E+19	2.6E+20	7.0E+20	1.9E+21	5.2E+21
1.0E+01	2.0E+11	5.3E+11	1.4E+12	3.9E+12	1.1E+13	2.9E+13	7.9E+13	2.1E+14	5.8E+14	1.6E+15	4.3E+15	1.2E+16	3.2E+16	8.7E+16	2.4E+17	6.4E+17	1.7E+18	4.7E+18	1.3E+19	3.5E+19	9.5E+19	2.6E+20	7.0E+20	1.9E+21	5.2E+21
1.1E+01	2.0E+11	5.3E+11	1.4E+12	3.9E+12	1.1E+13	2.9E+13	7.9E+13	2.1E+14	5.8E+14	1.6E+15	4.3E+15	1.2E+16	3.2E+16	8.7E+16	2.4E+17	6.4E+17	1.7E+18	4.7E+18	1.3E+19	3.5E+19	9.5E+19	2.6E+20	7.0E+20	1.9E+21	5.2E+21
1.2E+01	2.0E+11	5.3E+11	1.4E+12	3.9E+12	1.1E+13	2.9E+13	7.9E+13	2.1E+14	5.8E+14	1.6E+15	4.3E+15	1.2E+16	3.2E+16	8.7E+16	2.4E+17	6.4E+17	1.7E+18	4.7E+18	1.3E+19	3.5E+19	9.5E+19	2.6E+20	7.0E+20	1.9E+21	5.2E+21
1.3E+01	2.0E+11	5.3E+11	1.4E+12	3.9E+12	1.1E+13	2.9E+13	7.9E+13	2.1E+14	5.8E+14	1.6E+15	4.3E+15	1.2E+16	3.2E+16	8.7E+16	2.4E+17	6.4E+17	1.7E+18	4.7E+18	1.3E+19	3.5E+19	9.5E+19	2.6E+20	7.0E+20	1.9E+21	5.2E+21
1.4E+01	2.0E+11	5.3E+11	1.4E+12	3.9E+12	1.1E+13	2.9E+13	7.9E+13	2.1E+14	5.8E+14	1.6E+15	4.3E+15	1.2E+16	3.2E+16	8.7E+16	2.4E+17	6.4E+17	1.7E+18	4.7E+18	1.3E+19	3.5E+19	9.5E+19	2.6E+20	7.0E+20	1.9E+21	5.2E+21
1.5E+01	2.0E+11	5.3E+11	1.4E+12	3.9E+12	1.1E+13	2.9E+13	7.9E+13	2.1E+14	5.8E+14	1.6E+15	4.3E+15	1.2E+16	3.2E+16	8.7E+16	2.4E+17	6.4E+17	1.7E+18	4.7E+18	1.3E+19	3.5E+19	9.5E+19	2.6E+20	7.0E+20	1.9E+21	5.2E+21
1.6E+01	2.0E+11	5.3E+11	1.4E+12	3.9E+12	1.1E+13	2.9E+13	7.9E+13	2.1E+14	5.8E+14	1.6E+15	4.3E+15	1.2E+16	3.2E+16	8.7E+16	2.4E+17	6.4E+17	1.7E+18	4.7E+18	1.3E+19	3.5E+19	9.5E+19	2.6E+20	7.0E+20	1.9E+21	5.2E+21
1.7E+01	2.0E+11	5.3E+11	1.4E+12	3.9E+12	1.1E+13	2.9E+13	7.9E+13	2.1E+14	5.8E+14	1.6E+15	4.3E+15	1.2E+16	3.2E+16	8.7E+16	2.4E+17	6.4E+17	1.7E+18	4.7E+18	1.3E+19	3.5E+19	9.5E+19	2.6E+20	7.0E+20	1.9E+21	5.2E+21
1.8E+01	2.0E+11	5.3E+11	1.4E+12	3.9E+12	1.1E+13	2.9E+13	7.9E+13	2.1E+14	5.8E+14	1.6E+15	4.3E+15	1.2E+16	3.2E+16	8.7E+16	2.4E+17	6.4E+17	1.7E+18	4.7E+18	1.3E+19	3.5E+19	9.5E+19	2.6E+20	7.0E+20	1.9E+21	5.2E+21
1.9E+01	2.0E+11	5.3E+11	1.4E+12	3.9E+12	1.1E+13	2.9E+13	7.9E+13	2.1E+14	5.8E+14	1.6E+15	4.3E+15	1.2E+16	3.2E+16	8.7E+16	2.4E+17	6.4E+17	1.7E+18	4.7E+18	1.3E+19	3.5E+19	9.5E+19	2.6E+20	7.0E+20	1.9E+21	5.2E+21
2.0E+01	2.0E+11	5.3E+11	1.4E+12	3.9E+12	1.1E+13	2.9E+13	7.9E+13	2.1E+14	5.8E+14	1.6E+15	4.3E+15	1.2E+16	3.2E+16	8.7E+16	2.4E+17	6.4E+17	1.7E+18	4.7E+18	1.3E+19	3.5E+19	9.5E+19	2.6E+20	7.0E+20	1.9E+21	5.2E+21
2.1E+01	2.0E+11	5.3E+11	1.4E+12	3.9E+12	1.1E+13	2.9E+13	7.9E+13	2.1E+14	5.8E+14	1.6E+15	4.3E+15	1.2E+16	3.2E+16	8.7E+16	2.4E+17	6.4E+17	1.7E+18	4.7E+18	1.3E+19	3.5E+19	9.5E+19	2.6E+20	7.0E+20	1.9E+21	5.2E+21
2.2E+01	2.0E+11	5.3E+11	1.4E+12	3.9E+12	1.1E+13	2.9E+13	7.9E+13	2.1E+14	5.8E+14	1.6E+15	4.3E+15	1.2E+16	3.2E+16	8.7E+16	2.4E+17	6.4E+17	1.7E+18	4.7E+18	1.3E+19	3.5E+19	9.5E+19	2.6E+20	7.0E+20	1.9E+21	5.2E+21
2.3E+01	2.0E+11	5.3E+11	1.4E+12	3.9E+12	1.1E+13	2.9E+13	7.9E+13	2.1E+14	5.8E+14	1.6E+15	4.3E+15	1.2E+16	3.2E+16	8.7E+16	2.4E+17	6.4E+17	1.7E+18	4.7E+18	1.3E+19	3.5E+19	9.5E+19	2.6E+20	7.0E+20	1.9E+21	5.2E+21
2.4E+01	2.0E+11	5.3E+11	1.4E+12	3.9E+12	1.1E+13	2.9E+13	7.9E+13	2.1E+14	5.8E+14	1.6E+15	4.3E+15	1.2E+16	3.2E+16	8.7E+16	2.4E+17	6.4E+17	1.7E+18	4.7E+18	1.3E+19	3.5E+19	9.5E+19	2.6E+20	7.0E+20	1.9E+21	5.1E+21
2.5E+01	2.0E+11	5.3E+11	1.4E+12	3.9E+12	1.1E+13	2.9E+13	7.9E+13	2.1E+14	5.8E+14	1.6E+15	4.3E+15	1.2E+16	3.2E+16	8.7E+16	2.4E+17	6.4E+17	1.7E+18	4.7E+18	1.3E+19	3.5E+19	9.5E+19	2.6E+20	7.0E+20	1.9E+21	5.1E+21
2.6E+01	2.0E+11	5.3E+11	1.4E+12	3.9E+12	1.1E+13	2.9E+13	7.9E+13	2.1E+14	5.8E+14	1.6E+15	4.3E+15	1.2E+16	3.2E+16	8.7E+16	2.4E+17	6.4E+17	1.7E+18	4.7E+18	1.3E+19	3.5E+19	9.5E+19	2.6E+20	7.0E+20	1.9E+21	5.1E+21
2.7E+01	2.0E+11	5.3E+11	1.4E+12	3.9E+12	1.1E+13	2.9E+13	7.9E+13	2.1E+14	5.8E+14	1.6E+15	4.3E+15	1.2E+16	3.2E+16	8.7E+16	2.4E+17	6.4E+17	1.7E+18	4.7E+18	1.3E+19	3.5E+19	9.4E+19	2.6E+20	7.0E+20	1.9E+21	5.1E+21
2.8E+01	2.0E+11	5.3E+11	1.4E+12	3.9E+12	1.1E+13	2.9E+13	7.9E+13	2.1E+14	5.8E+14	1.6E+15	4.3E+15	1.2E+16	3.2E+16	8.7E+16	2.4E+17	6.4E+17	1.7E+18	4.7E+18	1.3E+19	3.5E+19	9.4E+19	2.6E+20	6.9E+20	1.9E+21	5.1E+21
2.9E+01	2.0E+11	5.3E+11	1.4E+12	3.9E+12	1.1E+13	2.9E+13	7.9E+13	2.1E+14	5.8E+14	1.6E+15	4.3E+15	1.2E+16	3.2E+16	8.7E+16	2.4E+17	6.4E+17	1.7E+18	4.7E+18	1.3E+19	3.5E+19	9.4E+19	2.5E+20	6.9E+20	1.9E+21	5.1E+21
3.0E+01	2.0E+11	5.3E+11	1.4E+12	3.9E+12	1.1E+13	2.9E+13	7.9E+13	2.1E+14	5.8E+14	1.6E+15	4.3E+15	1.2E+16	3.2E+16	8.7E+16	2.4E+17	6.4E+17	1.7E+18	4.7E+18	1.3E+19	3.5E+19	9.4E+19	2.5E+20	6.9E+20	1.9E+21	5.0E+21
3.1E+01	2.0E+11	5.3E+11	1.4E+12	3.9E+12	1.1E+13	2.9E+13	7.9E+13	2.1E+14	5.8E+14	1.6E+15	4.3E+15	1.2E+16	3.2E+16	8.6E+16	2.3E+17	6.4E+17	1.7E+18	4.7E+18	1.3E+19	3.5E+19	9.4E+19	2.5E+20	6.9E+20	1.9E+21	5.0E+21
3.2E+01	2.0E+11	5.3E+11	1.4E+12	3.9E+12	1.1E+13	2.9E+13	7.9E+13	2.1E+14	5.8E+14	1.6E+15	4.3E+15	1.2E+16	3.2E+16	8.6E+16	2.3E+17	6.4E+17	1.7E+18	4.7E+18	1.3E+19	3.5E+19	9.4E+19	2.5E+20	6.9E+20	1.8E+21	5.0E+21
3.3E+01	2.0E+11	5.3E+11	1.4E+12	3.9E+12	1.1E+13	2.9E+13	7.9E+13	2.1E+14	5.8E+14	1.6E+15	4.3E+15	1.2E+16	3.2E+16	8.6E+16	2.3E+17	6.4E+17	1.7E+18	4.7E+18	1.3E+19	3.5E+19	9.4E+19	2.5E+20	6.8E+20	1.8E+21	4.9E+21
3.4E+01	2.0E+11	5.3E+11	1.4E+12	3.9E+12	1.1E+13	2.9E+13	7.9E+13	2.1E+14	5.8E+14	1.6E+15	4.3E+15	1.2E+16	3.2E+16	8.6E+16	2.3E+17	6.4E+17	1.7E+18	4.7E+18	1.3E+19	3.4E+19	9.3E+19	2.5E+20	6.8E+20	1.8E+21	4.9E+21
3.5E+01	2.0E+11	5.3E+11	1.4E+12	3.9E+12	1.1E+13	2.9E+13	7.9E+13	2.1E+14	5.8E+14	1.6E+15	4.3E+15	1.2E+16	3.2E+16	8.6E+16	2.3E+17	6.3E+17	1.7E+18	4.7E+18	1.3E+19	3.4E+19	9.3E+19	2.5E+20	6.7E+20	1.8E+21	4.8E+21
3.6E+01	2.0E+11	5.3E+11	1.4E+12	3.9E+12	1.1E+13	2.9E+13	7.9E+13	2.1E+14	5.8E+14	1.6E+15	4.3E+15	1.2E+16	3.2E+16	8.6E+16	2.3E+17	6.3E+17	1.7E+18	4.6E+18	1.3E+19	3.4E+19	9.2E+19	2.5E+20	6.7E+20	1.8E+21	4.8E+21
3.7E+01	2.0E+11	5.3E+11	1.4E+12	3.9E+12	1.1E+13	2.9E+13	7.9E+13	2.1E+14	5.8E+14	1.6E+15	4.3E+15	1.2E+16	3.2E+16	8.6E+16	2.3E+17	6.3E+17	1.7E+18	4.6E+18	1.3E+19	3.4E+19	9.1E+19	2.5E+20	6.6E+20	1.8E+21	4.7E+21
3.8E+01	2.0E+11	5.3E+11	1.4E+12	3.9E+12	1.1E+13	2.9E+13	7.9E+13	2.1E+14	5.8E+14	1.6E+15	4.3E+15	1.2E+16	3.2E+16	8.6E+16	2.3E+17	6.3E+17	1.7E+18	4.6E+18	1.2E+19	3.4E+19	9.1E+19	2.4E+20	6.5E+20	1.7E+21	4.6E+21
3.9E+01	2.0E+11	5.3E+11	1.4E+12	3.9E+12	1.1E+13	2.9E+13	7.9E+13	2.1E+14	5.8E+14	1.6E+15	4.3E+15	1.2E+16	3.2E+16	8.6E+16	2.3E+17	6.3E+17	1.7E+18	4.6E+18	1.2E+19	3.3E+19	9.0E+19	2.4E+20	6.4E+20	1.7E+21	4.5E+21
4.0E+01	2.0E+11	5.3E+11	1.4E+12	3.9E+12	1.1E+13	2.9E+13	7.9E+13	2.1E+14	5.8E+14	1.6E+15	4.3E+15	1.2E+16	3.2E+16	8.5E+16	2.3E+17	6.2E+17	1.7E+18	4.5E+18	1.2E+19	3.3E+19	8.9E+19	2.4E+20	6.3E+20	1.7E+21	4.4E+21
4.1E+01	2.0E+11	5.3E+11	1.4E+12	3.9E+12	1.1E+13	2.9E+13	7.9E+13	2.1E+14	5.8E+14	1.6E+15	4.3E+15	1.2E+16	3.1E+16	8.5E+16	2.3E+17	6.2E+17	1.7E+18	4.5E+18	1.2E+19	3.3E+19	8.7E+19	2.3E+20	6.2E+20	1.6E+21	4.4E+21
4.2E+01	2.0E+11	5.3E+11	1.4E+12	3.9E+12	1.1E+13	2.9E+13	7.9E+13	2.1E+14	5.8E+14	1.6E+15	4.3E+15	1.2E+16	3.1E+16	8.5E+16	2.3E+17	6.2E+17	1.7E+18	4.5E+18	1.2E+19	3.2E+19	8.6E+19	2.3E+20	6.1E+20	1.6E+21	4.2E+21
4.3E+01	2.0E+11	5.3E+11	1.4E+12	3.9E+12	1.1E+13	2.9E+13	7.9E+13	2.1E+14	5.8E+14	1.6E+15	4.3E+15	1.2E+16	3.1E+16	8.4E+16	2.3E+17	6.1E+17	1.6E+18	4.4E+18	1.2E+19	3.2E+19	8.4E+19	2.2E+20	5.9E+20	1.6E+21	4.1E+21
4.4E+01	2.0E+11	5.3E+11	1.4E+12	3.9E+12	1.1E+13	2.9E+13	7.9E+13	2.1E+14	5.8E+14	1.6E+15	4.3E+15	1.2E+16	3.1E+16	8.4E+16	2.2E+17	6.0E+17	1.6E+18	4.3E+18	1.1E+19	3.1E+19	8.3E+19	2.2E+20	5.8E+20	1.5E+21	4.0E+21
4.5E+01	2.0E+11	5.3E+11	1.4E+12	3.9E+12	1.1E+13	2.9E+13	7.9E+13	2.1E+14	5.8E+14	1.6E+15	4.2E+15	1.1E+16	3.1E+16	8.3E+16	2.2E+17	6.0E+17	1.6E+18	4.2E+18	1.1E+19	3.0E+19	8.1E+19	2.1E+20	5.6E+20	1.5E+21	3.8E+21
4.6E+01	2.0E+11	5.3E+11	1.4E+12	3.9E+12	1.1E+13	2.9E+13	7.9E+13	2.1E+14	5.8E+14	1.6E+15	4.2E+15	1.1E+16	3.1E+16	8.2E+16	2.2E+17	5.9E+17	1.6E+18	4.1E+18	1.1E+19	2.9E+19	7.8E+19	2.1E+20	5.4E+20	1.4E+21	3.6E+21
4.7E+01	2.0E+11	5.3E+11	1.4E+12	3.9E+12	1.1E+13	2.9E+13	7.8E+13	2.1E+14	5.8E+14	1.6E+15	4.2E+15	1.1E+16	3.0E+16	8.1E+16	2.2E+17	5.8E+17	1.5E+18	4.0E+18	1.1E+19	2.8E+19	7.6E+19	2.0E+20	5.2E+20	1.3E+21	3.5E+21
4.8E+01	2.0E+11	5.3E+11	1.4E+12	3.9E+12	1.1E+13	2.9E+13	7.8E+13	2.1E+14	5.7E+14	1.5E+15	4.2E+15	1.1E+16	3.0E+16	8.0E+16	2.2E+17	5.7E+17	1.5E+18	3.9E+18	1.0E+19	2.7E+19	7.3E+19	1.9E+20	5.0E+20	1.3E+21	3.3E+21
4.9E+01	2.0E+11	5.3E+11	1.4E+12	3.9E+12	1.1E+13	2.9E+13	7.8E+13	2.1E+14	5.7E+14	1.5E+15	4.1E+15	1.1E+16	2.9E+16	7.9E+16	2.1E+17	5.6E+17	1.5E+18	3.8E+18	1.0E+19	2.6E+19	7.1E+19	1.8E+20	4.7E+20	1.2E+21	3.1E+21
5.0E+01	2.0E+11	5.3E+11	1.4E+12	3.9E+12	1.1E+13	2.9E+13	7.8E+13	2.1E+14	5.7E+14	1.5E+15	4.1E+15	1.1E+16	2.9E+16	7.8E+16	2.1E+17	5.5E+17	1.5E+18	3.8E+18	1.0E+19	2.6E+19	6.7E+19	1.7E+20	4.5E+20	1.1E+21	2.9E+21

K_{2y}	$K_{1}x$																								
	26	27	28	29	30	31	32	33	34	35	36	37	38	39	40	41	42	43	44	45	46	47	48	49	50
5.1E+01	2.0E+11	5.3E+11	1.4E+12	3.9E+12	1.1E+13	2.9E+13	7.7E+13	2.1E+14	5.6E+14	1.5E+15	4.1E+15	1.1E+16	2.9E+16	7.7E+16	2.0E+17	5.4E+17	1.4E+18	3.7E+18	9.6E+18	2.5E+19	6.4E+19	1.6E+20	4.2E+20	1.1E+21	2.7E+21
5.2E+01	2.0E+11	5.3E+11	1.4E+12	3.9E+12	1.1E+13	2.9E+13	7.7E+13	2.1E+14	5.6E+14	1.5E+15	4.0E+15	1.1E+16	2.8E+16	7.5E+16	2.0E+17	5.2E+17	1.4E+18	3.5E+18	9.2E+18	2.4E+19	6.1E+19	1.5E+20	3.9E+20	9.9E+20	2.5E+21
5.3E+01	2.0E+11	5.3E+11	1.4E+12	3.9E+12	1.1E+13	2.8E+13	7.6E+13	2.1E+14	5.5E+14	1.5E+15	3.9E+15	1.0E+16	2.8E+16	7.3E+16	1.9E+17	5.0E+17	1.3E+18	3.4E+18	8.7E+18	2.2E+19	5.7E+19	1.4E+20	3.6E+20	9.1E+20	2.3E+21
5.4E+01	1.9E+11	5.3E+11	1.4E+12	3.9E+12	1.0E+13	2.8E+13	7.6E+13	2.0E+14	5.4E+14	1.5E+15	3.9E+15	1.0E+16	2.7E+16	7.1E+16	1.9E+17	4.8E+17	1.2E+18	3.2E+18	8.2E+18	2.1E+19	5.3E+19	1.3E+20	3.4E+20	8.4E+20	2.1E+21
5.5E+01	1.9E+11	5.3E+11	1.4E+12	3.9E+12	1.0E+13	2.8E+13	7.5E+13	2.0E+14	5.4E+14	1.4E+15	3.8E+15	1.0E+16	2.6E+16	6.8E+16	1.8E+17	4.6E+17	1.2E+18	3.0E+18	7.7E+18	2.0E+19	4.9E+19	1.2E+20	3.1E+20	7.6E+20	1.9E+21
5.6E+01	1.9E+11	5.2E+11	1.4E+12	3.8E+12	1.0E+13	2.8E+13	7.4E+13	2.0E+14	5.3E+14	1.4E+15	3.7E+15	9.7E+15	2.5E+16	6.6E+16	1.7E+17	4.4E+17	1.1E+18	2.9E+18	7.2E+18	1.8E+19	4.5E+19	1.1E+20	2.8E+20	6.8E+20	1.7E+21
5.7E+01	1.9E+11	5.2E+11	1.4E+12	3.8E+12	1.0E+13	2.7E+13	7.3E+13	1.9E+14	5.1E+14	1.4E+15	3.6E+15	9.3E+15	2.4E+16	6.3E+16	1.6E+17	4.1E+17	1.1E+18	2.7E+18	6.7E+18	1.7E+19	4.1E+19	1.0E+20	2.5E+20	6.1E+20	1.5E+21
5.8E+01	1.9E+11	5.2E+11	1.4E+12	3.8E+12	1.0E+13	2.7E+13	7.2E+13	1.9E+14	5.0E+14	1.3E+15	3.4E+15	9.0E+15	2.3E+16	6.0E+16	1.5E+17	3.9E+17	9.8E+17	2.5E+18	6.1E+18	1.5E+19	3.7E+19	9.2E+19	2.2E+20	5.4E+20	1.3E+21
5.9E+01	1.9E+11	5.2E+11	1.4E+12	3.7E+12	9.9E+12	2.6E+13	7.0E+13	1.9E+14	4.9E+14	1.3E+15	3.3E+15	8.6E+15	2.2E+16	5.6E+16	1.4E+17	3.6E+17	9.1E+17	2.3E+18	5.6E+18	1.4E+19	3.4E+19	8.2E+19	2.0E+20	4.7E+20	1.1E+21
6.0E+01	1.9E+11	5.1E+11	1.4E+12	3.7E+12	9.8E+12	2.6E+13	6.8E+13	1.8E+14	4.7E+14	1.2E+15	3.2E+15	8.1E+15	2.1E+16	5.3E+16	1.3E+17	3.3E+17	8.3E+17	2.1E+18	5.0E+18	1.2E+19	3.0E+19	7.2E+19	1.7E+20	4.1E+20	9.7E+20
6.1E+01	1.9E+11	5.1E+11	1.4E+12	3.6E+12	9.6E+12	2.5E+13	6.6E+13	1.7E+14	4.5E+14	1.2E+15	3.0E+15	7.7E+15	1.9E+16	4.9E+16	1.2E+17	3.1E+17	7.5E+17	1.8E+18	4.5E+18	1.1E+19	2.6E+19	6.3E+19	1.5E+20	3.5E+20	8.2E+20
6.2E+01	1.9E+11	5.0E+11	1.3E+12	3.5E+12	9.3E+12	2.5E+13	6.4E+13	1.7E+14	4.3E+14	1.1E+15	2.8E+15	7.2E+15	1.8E+16	4.5E+16	1.1E+17	2.8E+17	6.8E+17	1.7E+18	4.0E+18	9.6E+18	2.3E+19	5.4E+19	1.3E+20	3.0E+20	6.9E+20
6.3E+01	1.8E+11	4.9E+11	1.3E+12	3.4E+12	9.1E+12	2.4E+13	6.2E+13	1.6E+14	4.1E+14	1.0E+15	2.6E+15	6.7E+15	1.7E+16	4.1E+16	1.0E+17	2.5E+17	6.0E+17	1.5E+18	3.5E+18	8.3E+18	2.0E+19	4.6E+19	1.1E+20	2.5E+20	5.7E+20
6.4E+01	1.8E+11	4.8E+11	1.3E+12	3.3E+12	8.8E+12	2.3E+13	5.9E+13	1.5E+14	3.8E+14	9.7E+14	2.5E+15	6.1E+15	1.5E+16	3.7E+16	9.1E+16	2.2E+17	5.3E+17	1.3E+18	3.0E+18	7.1E+18	1.7E+19	3.9E+19	9.0E+19	2.1E+20	4.6E+20
6.5E+01	1.8E+11	4.7E+11	1.2E+12	3.2E+12	8.4E+12	2.2E+13	5.6E+13	1.4E+14	3.6E+14	9.0E+14	2.3E+15	5.6E+15	1.4E+16	3.3E+16	8.1E+16	1.9E+17	4.6E+17	1.1E+18	2.6E+18	6.0E+18	1.4E+19	3.2E+19	7.4E+19	1.7E+20	3.7E+20
6.6E+01	1.7E+11	4.6E+11	1.2E+12	3.1E+12	8.0E+12	2.1E+13	5.2E+13	1.3E+14	3.3E+14	8.3E+14	2.0E+15	5.0E+15	1.2E+16	3.0E+16	7.1E+16	1.7E+17	4.0E+17	9.4E+17	2.2E+18	5.0E+18	1.2E+19	2.6E+19	5.9E+19	1.3E+20	2.9E+20
6.7E+01	1.7E+11	4.4E+11	1.1E+12	3.0E+12	7.6E+12	1.9E+13	4.9E+13	1.2E+14	3.1E+14	7.5E+14	1.8E+15	4.5E+15	1.1E+16	2.6E+16	6.1E+16	1.4E+17	3.4E+17	7.9E+17	1.8E+18	4.2E+18	9.4E+18	2.1E+19	4.7E+19	1.0E+20	2.3E+20
6.8E+01	1.6E+11	4.2E+11	1.1E+12	2.8E+12	7.1E+12	1.8E+13	4.5E+13	1.1E+14	2.8E+14	6.8E+14	1.6E+15	4.0E+15	9.4E+15	2.2E+16	5.3E+16	1.2E+17	2.8E+17	6.5E+17	1.5E+18	3.4E+18	7.5E+18	1.7E+19	3.6E+19	7.9E+19	1.7E+20
6.9E+01	1.6E+11	4.1E+11	1.0E+12	2.6E+12	6.7E+12	1.7E+13	4.1E+13	1.0E+14	2.5E+14	6.0E+14	1.4E+15	3.4E+15	8.1E+15	1.9E+16	4.4E+16	1.0E+17	2.3E+17	5.3E+17	1.2E+18	2.7E+18	5.9E+18	1.3E+19	2.8E+19	6.0E+19	1.3E+20
7.0E+01	1.5E+11	3.8E+11	9.8E+11	2.5E+12	6.1E+12	1.5E+13	3.7E+13	9.1E+13	2.2E+14	5.3E+14	1.3E+15	3.0E+15	6.9E+15	1.6E+16	3.7E+16	8.4E+16	1.9E+17	4.3E+17	9.4E+17	2.1E+18	4.5E+18	9.7E+18	2.1E+19	4.5E+19	9.4E+19
7.1E+01	1.4E+11	3.6E+11	9.1E+11	2.3E+12	5.6E+12	1.4E+13	3.3E+13	8.1E+13	1.9E+14	4.6E+14	1.1E+15	2.5E+15	5.8E+15	1.3E+16	3.0E+16	6.8E+16	1.5E+17	3.3E+17	7.3E+17	1.6E+18	3.4E+18	7.3E+18	1.5E+19	3.2E+19	6.8E+19
7.2E+01	1.3E+11	3.3E+11	8.4E+11	2.1E+12	5.1E+12	1.2E+13	3.0E+13	7.0E+13	1.7E+14	3.9E+14	9.0E+14	2.1E+15	4.8E+15	1.1E+16	2.4E+16	5.4E+16	1.2E+17	2.6E+17	5.5E+17	1.2E+18	2.5E+18	5.3E+18	1.1E+19	2.3E+19	4.7E+19
7.3E+01	1.2E+11	3.1E+11	7.6E+11	1.9E+12	4.5E+12	1.1E+13	2.6E+13	6.0E+13	1.4E+14	3.3E+14	7.5E+14	1.7E+15	3.9E+15	8.6E+15	1.9E+16	4.2E+16	9.0E+16	1.9E+17	4.1E+17	8.7E+17	1.8E+18	3.8E+18	7.8E+18	1.6E+19	3.3E+19
7.4E+01	1.1E+11	2.8E+11	6.8E+11	1.6E+12	3.9E+12	9.4E+12	2.2E+13	5.1E+13	1.2E+14	2.7E+14	6.1E+14	1.4E+15	3.1E+15	6.7E+15	1.5E+16	3.1E+16	6.7E+16	1.4E+17	3.0E+17	6.2E+17	1.3E+18	2.6E+18	5.4E+18	1.1E+19	2.2E+19
7.5E+01	1.0E+11	2.5E+11	6.0E+11	1.4E+12	3.4E+12	8.0E+12	1.9E+13	4.3E+13	9.7E+13	2.2E+14	4.9E+14	1.1E+15	2.4E+15	5.1E+15	1.1E+16	2.3E+16	4.9E+16	1.0E+17	2.1E+17	4.3E+17	8.9E+17	1.8E+18	3.6E+18	7.2E+18	1.4E+19
7.6E+01	9.2E+10	2.2E+11	5.3E+11	1.2E+12	2.9E+12	6.7E+12	1.5E+13	3.5E+13	7.8E+13	1.7E+14	3.8E+14	8.3E+14	1.8E+15	3.8E+15	8.0E+15	1.7E+16	3.5E+16	7.2E+16	1.5E+17	3.0E+17	6.0E+17	1.2E+18	2.4E+18	4.7E+18	9.1E+18
7.7E+01	8.1E+10	1.9E+11	4.5E+11	1.1E+12	2.4E+12	5.5E+12	1.2E+13	2.8E+13	6.2E+13	1.4E+14	2.9E+14	6.2E+14	1.3E+15	2.8E+15	5.7E+15	1.2E+16	2.4E+16	4.9E+16	9.9E+16	2.0E+17	3.9E+17	7.7E+17	1.5E+18	2.9E+18	5.6E+18
7.8E+01	7.0E+10	1.6E+11	3.8E+11	8.7E+11	2.0E+12	4.4E+12	9.9E+12	2.2E+13	4.8E+13	1.0E+14	2.2E+14	4.5E+14	9.5E+14	2.0E+15	4.0E+15	8.1E+15	1.6E+16	3.3E+16	6.5E+16	1.3E+17	2.5E+17	4.8E+17	9.3E+17	1.8E+18	3.4E+18
7.9E+01	6.0E+10	1.4E+11	3.1E+11	7.1E+11	1.6E+12	3.5E+12	7.7E+12	1.7E+13	3.5E+13	7.5E+13	1.6E+14	3.2E+14	6.6E+14	1.3E+15	2.7E+15	5.4E+15	1.1E+16	2.1E+16	4.1E+16	8.0E+16	1.5E+17	2.9E+17	5.6E+17	1.0E+18	2.0E+18
8.0E+01	5.0E+10	1.1E+11	2.5E+11	5.7E+11	1.2E+12	2.7E+12	5.8E+12	1.2E+13	2.6E+13	5.3E+13	1.1E+14	2.2E+14	4.5E+14	8.9E+14	1.8E+15	3.5E+15	6.8E+15	1.3E+16	2.5E+16	4.8E+16	9.1E+16	1.7E+17	3.2E+17	6.0E+17	1.1E+18
8.1E+01	4.1E+10	9.1E+10	2.0E+11	4.4E+11	9.5E+11	2.0E+12	4.2E+12	8.8E+12	1.8E+13	3.7E+13	7.4E+13	1.5E+14	2.9E+14	5.8E+14	1.1E+15	2.2E+15	4.2E+15	7.9E+15	1.5E+16	2.8E+16	5.2E+16	9.7E+16	1.8E+17	3.3E+17	5.9E+17
8.2E+01	3.2E+10	7.1E+10	1.5E+11	3.3E+11	7.0E+11	1.5E+12	3.0E+12	6.1E+12	1.2E+13	2.5E+13	4.9E+13	9.6E+13	1.9E+14	3.6E+14	6.9E+14	1.3E+15	2.5E+15	4.6E+15	8.6E+15	1.6E+16	2.9E+16	5.3E+16	9.6E+16	1.7E+17	3.1E+17
8.3E+01	2.5E+10	5.4E+10	1.2E+11	2.4E+11	5.0E+11	1.0E+12	2.1E+12	4.1E+12	8.1E+12	1.6E+13	3.1E+13	6.0E+13	1.1E+14	2.2E+14	4.1E+14	7.6E+14	1.4E+15	2.6E+15	4.7E+15	8.5E+15	1.5E+16	2.8E+16	4.9E+16	8.7E+16	1.5E+17
8.4E+01	1.9E+10	4.0E+10	8.3E+10	1.7E+11	3.4E+11	6.8E+11	1.4E+12	2.6E+12	5.1E+12	9.9E+12	1.9E+13	3.6E+13	6.7E+13	1.2E+14	2.3E+14	4.2E+14	7.6E+14	1.4E+15	2.5E+15	4.4E+15	7.8E+15	1.4E+16	2.4E+16	4.2E+16	7.2E+16
8.5E+01	1.4E+10	2.8E+10	5.7E+10	1.1E+11	2.3E+11	4.4E+11	8.5E+11	1.6E+12	3.1E+12	5.9E+12	1.1E+13	2.0E+13	3.7E+13	6.8E+13	1.2E+14	2.2E+14	4.0E+14	7.0E+14	1.2E+15	2.2E+15	3.8E+15	6.5E+15	1.1E+16	1.9E+16	3.2E+16
8.6E+01	9.5E+09	1.9E+10	3.8E+10	7.4E+10	1.4E+11	2.7E+11	5.2E+11	9.7E+11	1.8E+12	3.3E+12	6.1E+12	1.1E+13	2.0E+13	3.6E+13	6.3E+13	1.1E+14	2.0E+14	3.4E+14	5.9E+14	1.0E+15	1.7E+15	2.9E+15	4.9E+15	8.2E+15	1.4E+16
8.7E+01	6.3E+09	1.2E+10	2.4E+10	4.5E+10	8.6E+10	1.6E+11	3.0E+11	5.5E+11	1.0E+12	1.8E+12	3.2E+12	5.7E+12	1.0E+13	1.8E+13	3.1E+13	5.3E+13	9.1E+13	1.5E+14	2.6E+14	4.4E+14	7.4E+14	1.2E+15	2.0E+15	3.3E+15	5.5E+15
8.8E+01	4.0E+09	7.6E+09	1.4E+10	2.7E+10	4.9E+10	9.0E+10	1.6E+11	2.9E+11	5.2E+11	9.2E+11	1.6E+12	2.8E+12	4.8E+12	8.2E+12	1.4E+13	2.4E+13	4.0E+13	6.6E+13	1.1E+14	1.8E+14	3.0E+14	4.8E+14	7.8E+14	1.3E+15	2.0E+15
8.9E+01	2.4E+09	4.4E+09	8.1E+09	1.5E+10	2.6E+10	4.7E+10	8.3E+10	1.5E+11	2.5E+11	4.4E+11	7.5E+11	1.3E+12	2.1E+12	3.6E+12	5.9E+12	9.8E+12	1.6E+13	2.6E+13	4.3E+13	6.9E+13	1.1E+14	1.8E+14	2.8E+14	4.4E+14	6.9E+14
9.0E+01	1.3E+09	2.4E+09	4.3E+09	7.6E+09	1.3E+10	2.3E+10	4.0E+10	6.8E+10	1.2E+11	1.9E+11	3.2E+11	5.4E+11	8.8E+11	1.4E+12	2.3E+12	3.8E+12	6.0E+12	9.6E+12	1.5E+13	2.4E+13	3.8E+13	5.9E+13	9.2E+13	1.4E+14	2.2E+14
9.1E+01	7.0E+08	1.2E+09	2.1E+09	3.7E+09	6.2E+09	1.1E+10	1.8E+10	2.9E+10	4.8E+10	7.9E+10	1.3E+11	2.1E+11	3.3E+11	5.3E+11	8.4E+11	1.3E+12	2.1E+12	3.2E+12	5.0E+12	7.7E+12	1.2E+13	1.8E+13	2.7E+13	4.1E+13	6.2E+13
9.2E+01	3.4E+08	5.7E+08	9.6E+08	1.6E+09	2.7E+09	4.4E+09	7.1E+09	1.1E+10	1.8E+10	2.9E+10	4.6E+10	7.3E+10	1.1E+11	1.8E+11	2.7E+11	4.2E+11	6.4E+11	9.7E+11	1.5E+12	2.2E+12	3.3E+12	4.9E+12	7.2E+12	1.1E+13	1.6E+13
9.3E+01	1.5E+08	2.4E+08	3.9E+08	6.4E+08	1.0E+09	1.6E+09	2.6E+09	4.0E+09	6.3E+09	9.7E+09	1.5E+10	2.3E+10	3.4E+10	5.2E+10	7.8E+10	1.2E+11	1.7E+11	2.6E+11	3.8E+11	5.5E+11	8.0E+11	1.2E+12	1.7E+12	2.4E+12	3.5E+12
9.4E+01	5.7E+07	9.1E+07	1.4E+08	2.2E+08	3.5E+08	5.3E+08	8.2E+08	1.2E+09	1.9E+09	2.8E+09	4.2E+09	6.2E+09	9.1E+09	1.3E+10	1.9E+10	2.8E+10	4.0E+10	5.8E+10	8.3E+10	1.2E+11	1.7E+11	2.4E+11	3.3E+11	4.6E+11	6.5E+11
9.5E+01	1.9E+07	3.0E+07	4.5E+07	6.8E+07	1.0E+08	1.5E+08	2.2E+08	3.2E+08	4.7E+08	6.9E+08	9.9E+08	1.4E+09	2.0E+09	2.9E+09	4.0E+09	5.6E+09	7.9E+09	1.1E+10	1.5E+10	2.1E+10	2.9E+10	4.0E+10	5.4E+10	7.3E+10	1.0E+11
9.6E+01	5.5E+06	8.1E+06	1.2E+07	1.7E+07	2.4E+07	3.5E+07	4.9E+07	7.0E+07	9.8E+07	1.4E+08	1.9E+08	2.6E+08	3.6E+08	4.9E+08	6.7E+08	9.1E+08	1.2E+09	1.6E+09	2.2E+09	3.0E+09	3.9E+09	5.2E+09	6.9E+09	9.1E+09	1.2E+10
9.7E+01	1.2E+06	1.7E+06	2.4E+06	3.3E+06	4.5E+06	6.2E+06	8.4E+06	1.1E+07	1.5E+07	2.1E+07	2.7E+07	3.6E+07	4.8E+07	6.3E+07	8.3E+07	1.1E+08	1.4E+08	1.8E+08	2.4E+08	3.0E+08	3.9E+08	5.0E+08	6.3E+08	8.1E+08	1.0E+09
9.8E+01	2.0E+05	2.6E+05	3.5E+05	4.5E+05	5.9E+05	7.7E+05	1.0E+06	1.3E+06	1.6E+06	2.1E+06	2.7E+06	3.4E+06	4.3E+06	5.4E+06	6.8E+06	8.5E+06	1.1E+07	1.3E+07	1.6E+07	2.0E+07	2.5E+07	3.0E+07	3.7E+07	4.5E+07	5.5E+07
9.9E+01	1.9E+04	2.3E+04	2.9E+04	3.6E+04	4.4E+04	5.4E+04	6.6E+04	8.1E+04	9.8E+04	1.2E+05	1.4E+05	1.7E+05	2.0E+05	2.4E+05	2.9E+05	3.4E+05	4.1E+05	4.8E+05	5.7E+05	6.7E+05	7.8E+05	9.2E+05	1.1E+06	1.2E+06	1.5E+06
1.0E+02	6.7E+02	7.7E+02	8.8E+02	1.0E+03	1.1E+03	1.3E+03	1.5E+03	1.6E+03	1.9E+03	2.1E+03	2.3E+03	2.6E+03	2.9E+03	3.2E+03	3.6E+03	4.0E+03	4.4E+03	4.9E+03	5.4E+03	6.0E+03	6.6E+03	7.2E+03	7.9E+03	8.7E+03	9.5E+03

$K_{2}y$	$K_{1}x$ = 51	52	53	54	55	56	57	58	59	60	61	62	63
1.0E+00	1.4E+22	3.8E+22	1.0E+23	2.8E+23	7.7E+23	2.1E+24	5.7E+24	1.5E+25	4.2E+25	1.1E+26	3.1E+26	8.4E+26	2.3E+27
2.0E+00	1.4E+22	3.8E+22	1.0E+23	2.8E+23	7.7E+23	2.1E+24	5.7E+24	1.5E+25	4.2E+25	1.1E+26	3.1E+26	8.4E+26	2.3E+27
3.0E+00	1.4E+22	3.8E+22	1.0E+23	2.8E+23	7.7E+23	2.1E+24	5.7E+24	1.5E+25	4.2E+25	1.1E+26	3.1E+26	8.4E+26	2.3E+27
4.0E+00	1.4E+22	3.8E+22	1.0E+23	2.8E+23	7.7E+23	2.1E+24	5.7E+24	1.5E+25	4.2E+25	1.1E+26	3.1E+26	8.4E+26	2.3E+27
5.0E+00	1.4E+22	3.8E+22	1.0E+23	2.8E+23	7.7E+23	2.1E+24	5.7E+24	1.5E+25	4.2E+25	1.1E+26	3.1E+26	8.4E+26	2.3E+27
6.0E+00	1.4E+22	3.8E+22	1.0E+23	2.8E+23	7.7E+23	2.1E+24	5.7E+24	1.5E+25	4.2E+25	1.1E+26	3.1E+26	8.4E+26	2.3E+27
7.0E+00	1.4E+22	3.8E+22	1.0E+23	2.8E+23	7.7E+23	2.1E+24	5.7E+24	1.5E+25	4.2E+25	1.1E+26	3.1E+26	8.4E+26	2.3E+27
8.0E+00	1.4E+22	3.8E+22	1.0E+23	2.8E+23	7.7E+23	2.1E+24	5.7E+24	1.5E+25	4.2E+25	1.1E+26	3.1E+26	8.4E+26	2.3E+27
9.0E+00	1.4E+22	3.8E+22	1.0E+23	2.8E+23	7.7E+23	2.1E+24	5.7E+24	1.5E+25	4.2E+25	1.1E+26	3.1E+26	8.4E+26	2.3E+27
1.0E+01	1.4E+22	3.8E+22	1.0E+23	2.8E+23	7.7E+23	2.1E+24	5.7E+24	1.5E+25	4.2E+25	1.1E+26	3.1E+26	8.4E+26	2.3E+27
1.1E+01	1.4E+22	3.8E+22	1.0E+23	2.8E+23	7.7E+23	2.1E+24	5.7E+24	1.5E+25	4.2E+25	1.1E+26	3.1E+26	8.4E+26	2.3E+27
1.2E+01	1.4E+22	3.8E+22	1.0E+23	2.8E+23	7.7E+23	2.1E+24	5.7E+24	1.5E+25	4.2E+25	1.1E+26	3.1E+26	8.3E+26	2.3E+27
1.3E+01	1.4E+22	3.8E+22	1.0E+23	2.8E+23	7.7E+23	2.1E+24	5.7E+24	1.5E+25	4.2E+25	1.1E+26	3.1E+26	8.3E+26	2.3E+27
1.4E+01	1.4E+22	3.8E+22	1.0E+23	2.8E+23	7.7E+23	2.1E+24	5.7E+24	1.5E+25	4.2E+25	1.1E+26	3.1E+26	8.3E+26	2.2E+27
1.5E+01	1.4E+22	3.8E+22	1.0E+23	2.8E+23	7.7E+23	2.1E+24	5.7E+24	1.5E+25	4.2E+25	1.1E+26	3.1E+26	8.3E+26	2.2E+27
1.6E+01	1.4E+22	3.8E+22	1.0E+23	2.8E+23	7.7E+23	2.1E+24	5.6E+24	1.5E+25	4.1E+25	1.1E+26	3.0E+26	8.2E+26	2.2E+27
1.7E+01	1.4E+22	3.8E+22	1.0E+23	2.8E+23	7.7E+23	2.1E+24	5.6E+24	1.5E+25	4.1E+25	1.1E+26	3.0E+26	8.2E+26	2.2E+27
1.8E+01	1.4E+22	3.8E+22	1.0E+23	2.8E+23	7.6E+23	2.1E+24	5.6E+24	1.5E+25	4.1E+25	1.1E+26	3.0E+26	8.1E+26	2.2E+27
1.9E+01	1.4E+22	3.8E+22	1.0E+23	2.8E+23	7.6E+23	2.1E+24	5.6E+24	1.5E+25	4.1E+25	1.1E+26	3.0E+26	8.1E+26	2.2E+27
2.0E+01	1.4E+22	3.8E+22	1.0E+23	2.8E+23	7.6E+23	2.1E+24	5.6E+24	1.5E+25	4.1E+25	1.1E+26	3.0E+26	8.0E+26	2.2E+27
2.1E+01	1.4E+22	3.8E+22	1.0E+23	2.8E+23	7.6E+23	2.1E+24	5.6E+24	1.5E+25	4.1E+25	1.1E+26	3.0E+26	7.9E+26	2.1E+27
2.2E+01	1.4E+22	3.8E+22	1.0E+23	2.8E+23	7.6E+23	2.0E+24	5.5E+24	1.5E+25	4.0E+25	1.1E+26	2.9E+26	7.8E+26	2.1E+27
2.3E+01	1.4E+22	3.8E+22	1.0E+23	2.8E+23	7.5E+23	2.0E+24	5.5E+24	1.5E+25	4.0E+25	1.1E+26	2.9E+26	7.7E+26	2.1E+27
2.4E+01	1.4E+22	3.8E+22	1.0E+23	2.8E+23	7.5E+23	2.0E+24	5.5E+24	1.5E+25	4.0E+25	1.1E+26	2.9E+26	7.6E+26	2.0E+27
2.5E+01	1.4E+22	3.8E+22	1.0E+23	2.8E+23	7.5E+23	2.0E+24	5.4E+24	1.5E+25	3.9E+25	1.1E+26	2.8E+26	7.5E+26	2.0E+27
2.6E+01	1.4E+22	3.8E+22	1.0E+23	2.8E+23	7.4E+23	2.0E+24	5.4E+24	1.4E+25	3.9E+25	1.0E+26	2.8E+26	7.4E+26	2.0E+27
2.7E+01	1.4E+22	3.7E+22	1.0E+23	2.7E+23	7.4E+23	2.0E+24	5.3E+24	1.4E+25	3.8E+25	1.0E+26	2.7E+26	7.2E+26	1.9E+27
2.8E+01	1.4E+22	3.7E+22	1.0E+23	2.7E+23	7.3E+23	2.0E+24	5.3E+24	1.4E+25	3.8E+25	1.0E+26	2.7E+26	7.1E+26	1.9E+27
2.9E+01	1.4E+22	3.7E+22	1.0E+23	2.7E+23	7.2E+23	1.9E+24	5.2E+24	1.4E+25	3.7E+25	9.8E+25	2.6E+26	6.9E+26	1.8E+27
3.0E+01	1.4E+22	3.7E+22	9.9E+22	2.7E+23	7.2E+23	1.9E+24	5.1E+24	1.4E+25	3.6E+25	9.6E+25	2.5E+26	6.7E+26	1.8E+27
3.1E+01	1.4E+22	3.7E+22	9.8E+22	2.6E+23	7.1E+23	1.9E+24	5.0E+24	1.3E+25	3.5E+25	9.4E+25	2.5E+26	6.5E+26	1.7E+27
3.2E+01	1.3E+22	3.6E+22	9.7E+22	2.6E+23	6.9E+23	1.9E+24	4.9E+24	1.3E+25	3.5E+25	9.1E+25	2.4E+26	6.3E+26	1.6E+27
3.3E+01	1.3E+22	3.6E+22	9.6E+22	2.6E+23	6.8E+23	1.8E+24	4.8E+24	1.3E+25	3.4E+25	8.8E+25	2.3E+26	6.0E+26	1.6E+27
3.4E+01	1.3E+22	3.5E+22	9.4E+22	2.5E+23	6.7E+23	1.8E+24	4.7E+24	1.2E+25	3.3E+25	8.5E+25	2.2E+26	5.8E+26	1.5E+27
3.5E+01	1.3E+22	3.5E+22	9.3E+22	2.5E+23	6.5E+23	1.7E+24	4.6E+24	1.2E+25	3.1E+25	8.2E+25	2.1E+26	5.5E+26	1.4E+27
3.6E+01	1.3E+22	3.4E+22	9.1E+22	2.4E+23	6.4E+23	1.7E+24	4.4E+24	1.2E+25	3.0E+25	7.8E+25	2.0E+26	5.2E+26	1.3E+27
3.7E+01	1.3E+22	3.4E+22	8.9E+22	2.4E+23	6.2E+23	1.6E+24	4.3E+24	1.1E+25	2.9E+25	7.5E+25	1.9E+26	5.0E+26	1.3E+27
3.8E+01	1.2E+22	3.3E+22	8.7E+22	2.3E+23	6.0E+23	1.6E+24	4.1E+24	1.1E+25	2.8E+25	7.1E+25	1.8E+26	4.7E+26	1.2E+27
3.9E+01	1.2E+22	3.2E+22	8.4E+22	2.2E+23	5.8E+23	1.5E+24	3.9E+24	1.0E+25	2.6E+25	6.7E+25	1.7E+26	4.4E+26	1.1E+27
4.0E+01	1.2E+22	3.1E+22	8.2E+22	2.1E+23	5.6E+23	1.4E+24	3.7E+24	9.7E+24	2.5E+25	6.3E+25	1.6E+26	4.1E+26	1.0E+27
4.1E+01	1.1E+22	3.0E+22	7.9E+22	2.1E+23	5.3E+23	1.4E+24	3.6E+24	9.1E+24	2.3E+25	5.9E+25	1.5E+26	3.8E+26	9.4E+26
4.2E+01	1.1E+22	2.9E+22	7.6E+22	2.0E+23	5.1E+23	1.3E+24	3.4E+24	8.6E+24	2.2E+25	5.5E+25	1.4E+26	3.5E+26	8.6E+26
4.3E+01	1.1E+22	2.8E+22	7.3E+22	1.9E+23	4.8E+23	1.2E+24	3.2E+24	8.0E+24	2.0E+25	5.1E+25	1.3E+26	3.2E+26	7.8E+26
4.4E+01	1.0E+22	2.7E+22	6.9E+22	1.8E+23	4.6E+23	1.2E+24	2.9E+24	7.4E+24	1.9E+25	4.7E+25	1.2E+26	2.9E+26	7.1E+26
4.5E+01	9.9E+21	2.6E+22	6.6E+22	1.7E+23	4.3E+23	1.1E+24	2.7E+24	6.9E+24	1.7E+25	4.3E+25	1.1E+26	2.6E+26	6.3E+26
4.6E+01	9.4E+21	2.4E+22	6.2E+22	1.6E+23	4.0E+23	1.0E+24	2.5E+24	6.3E+24	1.6E+25	3.9E+25	9.5E+25	2.3E+26	5.6E+26
4.7E+01	8.9E+21	2.3E+22	5.8E+22	1.5E+23	3.7E+23	9.3E+23	2.3E+24	5.7E+24	1.4E+25	3.5E+25	8.5E+25	2.1E+26	5.0E+26
4.8E+01	8.4E+21	2.1E+22	5.4E+22	1.4E+23	3.4E+23	8.5E+23	2.1E+24	5.2E+24	1.3E+25	3.1E+25	7.5E+25	1.8E+26	4.3E+26
4.9E+01	7.9E+21	2.0E+22	5.0E+22	1.2E+23	3.1E+23	7.7E+23	1.9E+24	4.6E+24	1.1E+25	2.7E+25	6.6E+25	1.6E+26	3.8E+26
5.0E+01	7.3E+21	1.8E+22	4.6E+22	1.1E+23	2.8E+23	6.9E+23	1.7E+24	4.1E+24	1.0E+25	2.4E+25	5.8E+25	1.4E+26	3.2E+26

$K_{2}y$	$K_{1}x$ = 64	65	66	67	68	69	70	71	72	73	74	75
1.0E+00	6.2E+27	1.7E+28	4.6E+28	1.2E+29	3.4E+29	9.2E+29	2.5E+30	6.8E+30	1.8E+31	5.0E+31	1.3E+32	3.6E+32
2.0E+00	6.2E+27	1.7E+28	4.6E+28	1.2E+29	3.4E+29	9.2E+29	2.5E+30	6.7E+30	1.8E+31	4.9E+31	1.3E+32	3.6E+32
3.0E+00	6.2E+27	1.7E+28	4.6E+28	1.2E+29	3.4E+29	9.2E+29	2.5E+30	6.7E+30	1.8E+31	4.9E+31	1.3E+32	3.6E+32
4.0E+00	6.2E+27	1.7E+28	4.6E+28	1.2E+29	3.4E+29	9.1E+29	2.5E+30	6.7E+30	1.8E+31	4.9E+31	1.3E+32	3.6E+32
5.0E+00	6.2E+27	1.7E+28	4.6E+28	1.2E+29	3.4E+29	9.1E+29	2.5E+30	6.7E+30	1.8E+31	4.9E+31	1.3E+32	3.6E+32
6.0E+00	6.2E+27	1.7E+28	4.6E+28	1.2E+29	3.4E+29	9.1E+29	2.5E+30	6.7E+30	1.8E+31	4.9E+31	1.3E+32	3.5E+32
7.0E+00	6.2E+27	1.7E+28	4.6E+28	1.2E+29	3.3E+29	9.1E+29	2.4E+30	6.6E+30	1.8E+31	4.8E+31	1.3E+32	3.5E+32
8.0E+00	6.2E+27	1.7E+28	4.5E+28	1.2E+29	3.3E+29	9.0E+29	2.4E+30	6.6E+30	1.8E+31	4.8E+31	1.3E+32	3.4E+32
9.0E+00	6.2E+27	1.7E+28	4.5E+28	1.2E+29	3.3E+29	9.0E+29	2.4E+30	6.5E+30	1.8E+31	4.7E+31	1.3E+32	3.4E+32
1.0E+01	6.2E+27	1.7E+28	4.5E+28	1.2E+29	3.3E+29	8.9E+29	2.4E+30	6.5E+30	1.7E+31	4.7E+31	1.3E+32	3.4E+32
1.1E+01	6.1E+27	1.7E+28	4.5E+28	1.2E+29	3.3E+29	8.9E+29	2.4E+30	6.4E+30	1.7E+31	4.6E+31	1.2E+32	3.3E+32
1.2E+01	6.1E+27	1.7E+28	4.5E+28	1.2E+29	3.3E+29	8.8E+29	2.4E+30	6.4E+30	1.7E+31	4.6E+31	1.2E+32	3.2E+32
1.3E+01	6.1E+27	1.6E+28	4.5E+28	1.2E+29	3.2E+29	8.7E+29	2.3E+30	6.3E+30	1.7E+31	4.5E+31	1.2E+32	3.2E+32
1.4E+01	6.1E+27	1.6E+28	4.4E+28	1.2E+29	3.2E+29	8.6E+29	2.3E+30	6.2E+30	1.7E+31	4.4E+31	1.2E+32	3.1E+32
1.5E+01	6.0E+27	1.6E+28	4.4E+28	1.2E+29	3.2E+29	8.5E+29	2.3E+30	6.1E+30	1.6E+31	4.3E+31	1.1E+32	3.0E+32
1.6E+01	6.0E+27	1.6E+28	4.4E+28	1.2E+29	3.1E+29	8.4E+29	2.2E+30	6.0E+30	1.6E+31	4.2E+31	1.1E+32	3.0E+32
1.7E+01	6.0E+27	1.6E+28	4.3E+28	1.2E+29	3.1E+29	8.3E+29	2.2E+30	5.9E+30	1.6E+31	4.1E+31	1.1E+32	2.9E+32
1.8E+01	5.9E+27	1.6E+28	4.3E+28	1.1E+29	3.0E+29	8.1E+29	2.2E+30	5.7E+30	1.5E+31	4.0E+31	1.1E+32	2.8E+32
1.9E+01	5.8E+27	1.6E+28	4.2E+28	1.1E+29	3.0E+29	8.0E+29	2.1E+30	5.6E+30	1.5E+31	3.9E+31	1.0E+32	2.7E+32
2.0E+01	5.8E+27	1.5E+28	4.1E+28	1.1E+29	2.9E+29	7.8E+29	2.1E+30	5.5E+30	1.4E+31	3.8E+31	1.0E+32	2.6E+32
2.1E+01	5.7E+27	1.5E+28	4.1E+28	1.1E+29	2.9E+29	7.6E+29	2.0E+30	5.3E+30	1.4E+31	3.7E+31	9.6E+31	2.5E+32
2.2E+01	5.6E+27	1.5E+28	4.0E+28	1.1E+29	2.8E+29	7.4E+29	2.0E+30	5.2E+30	1.4E+31	3.5E+31	9.2E+31	2.4E+32
2.3E+01	5.5E+27	1.5E+28	3.9E+28	1.0E+29	2.7E+29	7.2E+29	1.9E+30	5.0E+30	1.3E+31	3.4E+31	8.8E+31	2.3E+32
2.4E+01	5.4E+27	1.4E+28	3.8E+28	1.0E+29	2.7E+29	7.0E+29	1.8E+30	4.8E+30	1.2E+31	3.2E+31	8.4E+31	2.2E+32
2.5E+01	5.3E+27	1.4E+28	3.7E+28	9.8E+28	2.6E+29	6.8E+29	1.8E+30	4.6E+30	1.2E+31	3.1E+31	8.0E+31	2.0E+32
2.6E+01	5.2E+27	1.4E+28	3.6E+28	9.5E+28	2.5E+29	6.5E+29	1.7E+30	4.4E+30	1.1E+31	2.9E+31	7.5E+31	1.9E+32
2.7E+01	5.1E+27	1.3E+28	3.5E+28	9.2E+28	2.4E+29	6.3E+29	1.6E+30	4.2E+30	1.1E+31	2.8E+31	7.1E+31	1.8E+32
2.8E+01	4.9E+27	1.3E+28	3.4E+28	8.9E+28	2.3E+29	6.0E+29	1.5E+30	4.0E+30	1.0E+31	2.6E+31	6.6E+31	1.7E+32
2.9E+01	4.8E+27	1.2E+28	3.3E+28	8.5E+28	2.2E+29	5.7E+29	1.5E+30	3.8E+30	9.6E+30	2.4E+31	6.2E+31	1.6E+32
3.0E+01	4.6E+27	1.2E+28	3.1E+28	8.1E+28	2.1E+29	5.4E+29	1.4E+30	3.5E+30	9.0E+30	2.3E+31	5.7E+31	1.4E+32
3.1E+01	4.4E+27	1.2E+28	3.0E+28	7.7E+28	2.0E+29	5.1E+29	1.3E+30	3.3E+30	8.4E+30	2.1E+31	5.3E+31	1.3E+32
3.2E+01	4.3E+27	1.1E+28	2.8E+28	7.3E+28	1.9E+29	4.8E+29	1.2E+30	3.1E+30	7.7E+30	1.9E+31	4.9E+31	1.2E+32
3.3E+01	4.1E+27	1.0E+28	2.7E+28	6.9E+28	1.8E+29	4.5E+29	1.1E+30	2.8E+30	7.1E+30	1.8E+31	4.4E+31	1.1E+32
3.4E+01	3.9E+27	9.9E+27	2.5E+28	6.5E+28	1.6E+29	4.1E+29	1.0E+30	2.6E+30	6.5E+30	1.6E+31	4.0E+31	9.9E+31
3.5E+01	3.7E+27	9.3E+27	2.4E+28	6.0E+28	1.5E+29	3.8E+29	9.6E+29	2.4E+30	5.9E+30	1.5E+31	3.6E+31	8.9E+31
3.6E+01	3.4E+27	8.8E+27	2.2E+28	5.6E+28	1.4E+29	3.5E+29	8.8E+29	2.2E+30	5.4E+30	1.3E+31	3.2E+31	7.9E+31
3.7E+01	3.2E+27	8.2E+27	2.1E+28	5.2E+28	1.3E+29	3.2E+29	8.0E+29	2.0E+30	4.8E+30	1.2E+31	2.9E+31	7.0E+31
3.8E+01	3.0E+27	7.6E+27	1.9E+28	4.7E+28	1.2E+29	2.9E+29	7.2E+29	1.8E+30	4.3E+30	1.1E+31	2.6E+31	6.2E+31
3.9E+01	2.8E+27	7.0E+27	1.7E+28	4.3E+28	1.1E+29	2.6E+29	6.5E+29	1.6E+30	3.8E+30	9.3E+30	2.2E+31	5.4E+31
4.0E+01	2.6E+27	6.4E+27	1.6E+28	3.9E+28	9.7E+28	2.4E+29	5.8E+29	1.4E+30	3.4E+30	8.2E+30	1.9E+31	4.6E+31
4.1E+01	2.3E+27	5.8E+27	1.4E+28	3.5E+28	8.6E+28	2.1E+29	5.1E+29	1.2E+30	3.0E+30	7.1E+30	1.7E+31	3.9E+31
4.2E+01	2.1E+27	5.3E+27	1.3E+28	3.2E+28	7.7E+28	1.9E+29	4.5E+29	1.1E+30	2.6E+30	6.1E+30	1.4E+31	3.3E+31
4.3E+01	1.9E+27	4.7E+27	1.2E+28	2.8E+28	6.8E+28	1.6E+29	3.9E+29	9.3E+29	2.2E+30	5.2E+30	1.2E+31	2.8E+31
4.4E+01	1.7E+27	4.2E+27	1.0E+28	2.5E+28	5.9E+28	1.4E+29	3.4E+29	8.0E+29	1.9E+30	4.3E+30	1.0E+31	2.3E+31
4.5E+01	1.5E+27	3.7E+27	9.0E+27	2.2E+28	5.2E+28	1.2E+29	2.9E+29	6.7E+29	1.6E+30	3.6E+30	8.3E+30	1.9E+31
4.6E+01	1.4E+27	3.3E+27	7.9E+27	1.9E+28	4.4E+28	1.0E+29	2.4E+29	5.6E+29	1.3E+30	3.0E+30	6.9E+30	1.6E+31
4.7E+01	1.2E+27	2.9E+27	6.8E+27	1.6E+28	3.8E+28	8.8E+28	2.0E+29	4.7E+29	1.1E+30	2.5E+30	5.6E+30	1.3E+31
4.8E+01	1.0E+27	2.5E+27	5.8E+27	1.4E+28	3.2E+28	7.3E+28	1.7E+29	3.9E+29	8.8E+29	2.0E+30	4.5E+30	1.0E+31
4.9E+01	9.0E+26	2.1E+27	4.9E+27	1.1E+28	2.6E+28	6.0E+28	1.4E+29	3.1E+29	7.1E+29	1.6E+30	3.6E+30	7.9E+30
5.0E+01	7.6E+26	1.8E+27	4.1E+27	9.5E+27	2.2E+28	4.9E+28	1.1E+29	2.5E+29	5.7E+29	1.3E+30	2.8E+30	6.2E+30

K_2 \ K_1	51	52	53	54	55	56	57	58	59	60	61	62	63	64	65	66	67	68	69	70	71	72	73	74	75
5.1E+01	6.8E+21	1.7E+22	4.2E+22	1.0E+23	2.5E+23	6.2E+23	1.5E+24	3.6E+24	8.7E+24	2.1E+25	5.0E+25	1.2E+26	2.8E+26	6.4E+26	1.5E+27	3.4E+27	7.8E+27	1.8E+28	4.0E+28	9.0E+28	2.0E+29	4.5E+29	9.9E+29	2.2E+30	4.8E+30
5.2E+01	6.2E+21	1.5E+22	3.8E+22	9.3E+22	2.3E+23	5.5E+23	1.3E+24	3.2E+24	7.6E+24	1.8E+25	4.3E+25	1.0E+26	2.3E+26	5.3E+26	1.2E+27	2.8E+27	6.3E+27	1.4E+28	3.2E+28	7.1E+28	1.6E+29	3.5E+29	7.6E+29	1.7E+30	3.6E+30
5.3E+01	5.6E+21	1.4E+22	3.4E+22	8.3E+22	2.0E+23	4.8E+23	1.2E+24	2.8E+24	6.5E+24	1.5E+25	3.6E+25	8.3E+25	1.9E+26	4.4E+26	1.0E+27	2.3E+27	5.1E+27	1.1E+28	2.5E+28	5.6E+28	1.2E+29	2.7E+29	5.8E+29	1.3E+30	2.7E+30
5.4E+01	5.1E+21	1.2E+22	3.0E+22	7.3E+22	1.8E+23	4.2E+23	1.0E+24	2.4E+24	5.6E+24	1.3E+25	3.0E+25	6.9E+25	1.6E+26	3.6E+26	8.0E+26	1.8E+27	4.0E+27	8.9E+27	2.0E+28	4.3E+28	9.4E+28	2.0E+29	4.4E+29	9.5E+29	2.0E+30
5.5E+01	4.6E+21	1.1E+22	2.7E+22	6.4E+22	1.5E+23	3.6E+23	8.6E+23	2.0E+24	4.7E+24	1.1E+25	2.5E+25	5.6E+25	1.3E+26	2.9E+26	6.4E+26	1.4E+27	3.1E+27	6.9E+27	1.5E+28	3.3E+28	7.1E+28	1.5E+29	3.3E+29	7.0E+29	1.5E+30
5.6E+01	4.0E+21	9.8E+21	2.3E+22	5.6E+22	1.3E+23	3.1E+23	7.3E+23	1.7E+24	3.9E+24	8.8E+24	2.0E+25	4.5E+25	1.0E+26	2.3E+26	5.0E+26	1.1E+27	2.4E+27	5.3E+27	1.1E+28	2.5E+28	5.3E+28	1.1E+29	2.4E+29	5.1E+29	1.1E+30
5.7E+01	3.6E+21	8.5E+21	2.0E+22	4.8E+22	1.1E+23	2.6E+23	6.1E+23	1.4E+24	3.2E+24	7.2E+24	1.6E+25	3.6E+25	8.0E+25	1.8E+26	3.9E+26	8.5E+26	1.9E+27	4.0E+27	8.6E+27	1.8E+28	3.9E+28	8.3E+28	1.8E+29	3.7E+29	7.7E+29
5.8E+01	3.1E+21	7.3E+21	1.7E+22	4.1E+22	9.5E+22	2.2E+23	5.0E+23	1.1E+24	2.6E+24	5.7E+24	1.3E+25	2.8E+25	6.3E+25	1.4E+26	3.0E+26	6.5E+26	1.4E+27	3.0E+27	6.4E+27	1.4E+28	2.9E+28	6.0E+28	1.3E+29	2.6E+29	5.4E+29
5.9E+01	2.7E+21	6.3E+21	1.5E+22	3.4E+22	7.9E+22	1.8E+23	4.1E+23	9.1E+23	2.0E+24	4.5E+24	1.0E+25	2.2E+25	4.8E+25	1.0E+26	2.3E+26	4.8E+26	1.0E+27	2.2E+27	4.6E+27	9.8E+27	2.0E+28	4.2E+28	8.8E+28	1.8E+29	3.7E+29
6.0E+01	2.3E+21	5.3E+21	1.2E+22	2.8E+22	6.4E+22	1.4E+23	3.2E+23	7.2E+23	1.6E+24	3.5E+24	7.7E+24	1.7E+25	3.6E+25	7.8E+25	1.7E+26	3.6E+26	7.6E+26	1.6E+27	3.3E+27	6.9E+27	1.4E+28	3.0E+28	6.1E+28	1.2E+29	2.5E+29
6.1E+01	1.9E+21	4.4E+21	1.0E+22	2.3E+22	5.2E+22	1.2E+23	2.6E+23	5.7E+23	1.2E+24	2.7E+24	5.9E+24	1.3E+25	2.7E+25	5.8E+25	1.2E+26	2.6E+26	5.4E+26	1.1E+27	2.4E+27	4.9E+27	1.0E+28	2.0E+28	4.1E+28	8.4E+28	1.7E+29
6.2E+01	1.6E+21	3.6E+21	8.2E+21	1.8E+22	4.1E+22	9.1E+22	2.0E+23	4.4E+23	9.5E+23	2.1E+24	4.4E+24	9.4E+24	2.0E+25	4.2E+25	8.9E+25	1.9E+26	3.8E+26	8.0E+26	1.6E+27	3.3E+27	6.8E+27	1.4E+28	2.8E+28	5.6E+28	1.1E+29
6.3E+01	1.3E+21	2.9E+21	6.5E+21	1.5E+22	3.2E+22	7.0E+22	1.5E+23	3.3E+23	7.2E+23	1.5E+24	3.3E+24	6.9E+24	1.4E+25	3.0E+25	6.3E+25	1.3E+26	2.7E+26	5.5E+26	1.1E+27	2.3E+27	4.6E+27	9.1E+27	1.8E+28	3.6E+28	7.2E+28
6.4E+01	1.0E+21	2.3E+21	5.1E+21	1.1E+22	2.5E+22	5.4E+22	1.2E+23	2.5E+23	5.3E+23	1.1E+24	2.4E+24	4.9E+24	1.0E+25	2.1E+25	4.4E+25	9.0E+25	1.8E+26	3.7E+26	7.5E+26	1.5E+27	3.0E+27	6.0E+27	1.2E+28	2.3E+28	4.5E+28
6.5E+01	8.2E+20	1.8E+21	4.0E+21	8.7E+21	1.9E+22	4.0E+22	8.6E+22	1.8E+23	3.9E+23	8.1E+23	1.7E+24	3.5E+24	7.2E+24	1.5E+25	3.0E+25	6.1E+25	1.2E+26	2.5E+26	4.9E+26	9.8E+26	1.9E+27	3.8E+27	7.4E+27	1.5E+28	2.8E+28
6.6E+01	6.4E+20	1.4E+21	3.0E+21	6.5E+21	1.4E+22	3.0E+22	6.3E+22	1.3E+23	2.8E+23	5.7E+23	1.2E+24	2.4E+24	4.9E+24	1.0E+25	2.0E+25	4.1E+25	8.1E+25	1.6E+26	3.2E+26	6.2E+26	1.2E+27	2.4E+27	4.6E+27	8.9E+27	1.7E+28
6.7E+01	4.9E+20	1.1E+21	2.3E+21	4.8E+21	1.0E+22	2.2E+22	4.5E+22	9.4E+22	1.9E+23	4.0E+23	8.1E+23	1.6E+24	3.3E+24	6.7E+24	1.3E+25	2.6E+25	5.2E+25	1.0E+26	2.0E+26	3.9E+26	7.6E+26	1.5E+27	2.8E+27	5.4E+27	1.0E+28
6.8E+01	3.7E+20	7.9E+20	1.7E+21	3.5E+21	7.4E+21	1.5E+22	3.2E+22	6.5E+22	1.3E+23	2.7E+23	5.5E+23	1.1E+24	2.2E+24	4.3E+24	8.6E+24	1.7E+25	3.3E+25	6.4E+25	1.2E+26	2.4E+26	4.6E+26	8.8E+26	1.7E+27	3.1E+27	5.9E+27
6.9E+01	2.7E+20	5.8E+20	1.2E+21	2.5E+21	5.2E+21	1.1E+22	2.2E+22	4.4E+22	9.0E+22	1.8E+23	3.6E+23	7.1E+23	1.4E+24	2.8E+24	5.4E+24	1.1E+25	2.0E+25	3.9E+25	7.5E+25	1.4E+26	2.7E+26	5.1E+26	9.7E+26	1.8E+27	3.4E+27
7.0E+01	2.0E+20	4.1E+20	8.5E+20	1.8E+21	3.6E+21	7.3E+21	1.5E+22	3.0E+22	5.9E+22	1.2E+23	2.3E+23	4.6E+23	8.9E+23	1.7E+24	3.3E+24	6.4E+24	1.2E+25	2.3E+25	4.4E+25	8.4E+25	1.6E+26	2.9E+26	5.5E+26	1.0E+27	1.9E+27
7.1E+01	1.4E+20	2.9E+20	5.9E+20	1.2E+21	2.4E+21	4.9E+21	9.8E+21	1.9E+22	3.8E+22	7.5E+22	1.5E+23	2.8E+23	5.5E+23	1.1E+24	2.0E+24	3.8E+24	7.2E+24	1.4E+25	2.6E+25	4.8E+25	8.9E+25	1.6E+26	3.0E+26	5.5E+26	1.0E+27
7.2E+01	9.7E+19	2.0E+20	4.0E+20	8.0E+20	1.6E+21	3.2E+21	6.3E+21	1.2E+22	2.4E+22	4.7E+22	9.0E+22	1.7E+23	3.3E+23	6.3E+23	1.2E+24	2.2E+24	4.2E+24	7.7E+24	1.4E+25	2.7E+25	4.9E+25	8.9E+25	1.6E+26	2.9E+26	5.3E+26
7.3E+01	6.6E+19	1.3E+20	2.6E+20	5.3E+20	1.0E+21	2.0E+21	4.0E+21	7.7E+21	1.5E+22	2.8E+22	5.4E+22	1.0E+23	1.9E+23	3.6E+23	6.8E+23	1.3E+24	2.4E+24	4.3E+24	7.8E+24	1.4E+25	2.6E+25	4.7E+25	8.5E+25	1.5E+26	2.7E+26
7.4E+01	4.4E+19	8.7E+19	1.7E+20	3.3E+20	6.5E+20	1.3E+21	2.4E+21	4.6E+21	8.8E+21	1.7E+22	3.2E+22	5.9E+22	1.1E+23	2.0E+23	3.8E+23	6.9E+23	1.3E+24	2.3E+24	4.2E+24	7.5E+24	1.3E+25	2.4E+25	4.3E+25	7.6E+25	1.3E+26
7.5E+01	2.8E+19	5.5E+19	1.1E+20	2.1E+20	4.0E+20	7.6E+20	1.4E+21	2.7E+21	5.1E+21	9.6E+21	1.8E+22	3.3E+22	6.1E+22	1.1E+23	2.0E+23	3.7E+23	6.7E+23	1.2E+24	2.1E+24	3.8E+24	6.8E+24	1.2E+25	2.1E+25	3.7E+25	6.5E+25
7.6E+01	1.8E+19	3.4E+19	6.6E+19	1.3E+20	2.4E+20	4.5E+20	8.4E+20	1.6E+21	2.9E+21	5.4E+21	9.8E+21	1.8E+22	3.3E+22	5.9E+22	1.1E+23	1.9E+23	3.4E+23	6.0E+23	1.1E+24	1.9E+24	3.3E+24	5.8E+24	1.0E+25	1.7E+25	3.0E+25
7.7E+01	1.1E+19	2.1E+19	3.9E+19	7.3E+19	1.4E+20	2.6E+20	4.7E+20	8.7E+20	1.6E+21	2.9E+21	5.2E+21	9.5E+21	1.7E+22	3.0E+22	5.4E+22	9.5E+22	1.7E+23	2.9E+23	5.1E+23	8.9E+23	1.5E+24	2.7E+24	4.6E+24	7.9E+24	1.3E+25
7.8E+01	6.4E+18	1.2E+19	2.2E+19	4.2E+19	7.7E+19	1.4E+20	2.6E+20	4.7E+20	8.4E+20	1.5E+21	2.7E+21	4.8E+21	8.5E+21	1.5E+22	2.6E+22	4.6E+22	8.0E+22	1.4E+23	2.4E+23	4.1E+23	7.0E+23	1.2E+24	2.0E+24	3.4E+24	5.8E+24
7.9E+01	3.7E+18	6.8E+18	1.2E+19	2.3E+19	4.1E+19	7.5E+19	1.3E+20	2.4E+20	4.3E+20	7.6E+20	1.3E+21	2.4E+21	4.1E+21	7.2E+21	1.2E+22	2.1E+22	3.7E+22	6.3E+22	1.1E+23	1.8E+23	3.1E+23	5.1E+23	8.6E+23	1.4E+24	2.4E+24
8.0E+01	2.0E+18	3.7E+18	6.7E+18	1.2E+19	2.2E+19	3.8E+19	6.8E+19	1.2E+20	2.1E+20	3.7E+20	6.4E+20	1.1E+21	1.9E+21	3.3E+21	5.6E+21	9.5E+21	1.6E+22	2.7E+22	4.6E+22	7.6E+22	1.3E+23	2.1E+23	3.5E+23	5.8E+23	9.5E+23
8.1E+01	1.1E+18	1.9E+18	3.4E+18	6.1E+18	1.1E+19	1.9E+19	3.3E+19	5.7E+19	9.9E+19	1.7E+20	2.9E+20	5.0E+20	8.5E+20	1.4E+21	2.4E+21	4.1E+21	6.8E+21	1.1E+22	1.9E+22	3.1E+22	5.1E+22	8.3E+22	1.4E+23	2.2E+23	3.6E+23
8.2E+01	5.5E+17	9.6E+17	1.7E+18	3.0E+18	5.2E+18	8.9E+18	1.5E+19	2.6E+19	4.5E+19	7.6E+19	1.3E+20	2.2E+20	3.6E+20	6.0E+20	1.0E+21	1.7E+21	2.7E+21	4.5E+21	7.3E+21	1.2E+22	1.9E+22	3.1E+22	5.0E+22	8.0E+22	1.3E+23
8.3E+01	2.7E+17	4.6E+17	8.0E+17	1.4E+18	2.4E+18	4.0E+18	6.8E+18	1.1E+19	1.9E+19	3.2E+19	5.3E+19	8.8E+19	1.5E+20	2.4E+20	3.9E+20	6.4E+20	1.0E+21	1.7E+21	2.7E+21	4.3E+21	6.9E+21	1.1E+22	1.7E+22	2.8E+22	4.4E+22
8.4E+01	1.2E+17	2.1E+17	3.6E+17	6.1E+17	1.0E+18	1.7E+18	2.9E+18	4.7E+18	7.8E+18	1.3E+19	2.1E+19	3.4E+19	5.6E+19	9.0E+19	1.5E+20	2.3E+20	3.7E+20	5.9E+20	9.4E+20	1.5E+21	2.3E+21	3.7E+21	5.8E+21	9.0E+21	1.4E+22
8.5E+01	5.5E+16	9.2E+16	1.5E+17	2.5E+17	4.2E+17	6.9E+17	1.1E+18	1.9E+18	3.0E+18	4.9E+18	7.9E+18	1.3E+19	2.0E+19	3.2E+19	5.1E+19	8.0E+19	1.3E+20	2.0E+20	3.1E+20	4.8E+20	7.5E+20	1.2E+21	1.8E+21	2.7E+21	4.2E+21
8.6E+01	2.3E+16	3.7E+16	6.2E+16	1.0E+17	1.6E+17	2.6E+17	4.3E+17	6.8E+17	1.1E+18	1.7E+18	2.8E+18	4.3E+18	6.8E+18	1.1E+19	1.7E+19	2.6E+19	4.0E+19	6.2E+19	9.5E+19	1.5E+20	2.2E+20	3.4E+20	5.2E+20	7.8E+20	1.2E+21
8.7E+01	8.9E+15	1.4E+16	2.3E+16	3.7E+16	5.9E+16	9.4E+16	1.5E+17	2.4E+17	3.7E+17	5.8E+17	9.0E+17	1.4E+18	2.2E+18	3.3E+18	5.1E+18	7.8E+18	1.2E+19	1.8E+19	2.7E+19	4.1E+19	6.2E+19	9.2E+19	1.4E+20	2.1E+20	3.1E+20
8.8E+01	3.2E+15	5.1E+15	8.1E+15	1.3E+16	2.0E+16	3.1E+16	4.8E+16	7.5E+16	1.2E+17	1.8E+17	2.7E+17	4.1E+17	6.3E+17	9.5E+17	1.4E+18	2.1E+18	3.2E+18	4.8E+18	7.1E+18	1.1E+19	1.6E+19	2.3E+19	3.4E+19	5.0E+19	7.3E+19
8.9E+01	1.1E+15	1.7E+15	2.6E+15	4.0E+15	6.2E+15	9.5E+15	1.4E+16	2.2E+16	3.3E+16	5.0E+16	7.5E+16	1.1E+17	1.7E+17	2.5E+17	3.7E+17	5.4E+17	8.0E+17	1.2E+18	1.7E+18	2.5E+18	3.6E+18	5.2E+18	7.6E+18	1.1E+19	1.6E+19
9.0E+01	3.3E+14	5.1E+14	7.7E+14	1.2E+15	1.8E+15	2.6E+15	3.9E+15	5.9E+15	8.7E+15	1.3E+16	1.9E+16	2.8E+16	4.0E+16	5.9E+16	8.6E+16	1.2E+17	1.8E+17	2.6E+17	3.7E+17	5.3E+17	7.5E+17	1.1E+18	1.5E+18	2.2E+18	3.0E+18
9.1E+01	9.3E+13	1.4E+14	2.1E+14	3.0E+14	4.5E+14	6.6E+14	9.6E+14	1.4E+15	2.0E+15	2.9E+15	4.2E+15	6.1E+15	8.7E+15	1.2E+16	1.8E+16	2.5E+16	3.6E+16	5.0E+16	7.1E+16	9.9E+16	1.4E+17	1.9E+17	2.7E+17	3.8E+17	5.2E+17
9.2E+01	2.3E+13	3.3E+13	4.8E+13	7.0E+13	1.0E+14	1.4E+14	2.1E+14	2.9E+14	4.2E+14	5.9E+14	8.4E+14	1.2E+15	1.7E+15	2.3E+15	3.2E+15	4.5E+15	6.2E+15	8.6E+15	1.2E+16	1.6E+16	2.2E+16	3.1E+16	4.2E+16	5.7E+16	7.7E+16
9.3E+01	4.9E+12	7.0E+12	9.9E+12	1.4E+13	2.0E+13	2.8E+13	3.9E+13	5.4E+13	7.4E+13	1.0E+14	1.4E+14	2.0E+14	2.7E+14	3.7E+14	5.0E+14	6.8E+14	9.2E+14	1.2E+15	1.7E+15	2.3E+15	3.0E+15	4.1E+15	5.5E+15	7.3E+15	9.7E+15
9.4E+01	9.0E+11	1.2E+12	1.7E+12	2.4E+12	3.2E+12	4.4E+12	6.0E+12	8.2E+12	1.1E+13	1.5E+13	2.0E+13	2.7E+13	3.6E+13	4.8E+13	6.4E+13	8.6E+13	1.1E+14	1.5E+14	2.0E+14	2.6E+14	3.4E+14	4.5E+14	5.9E+14	7.7E+14	1.0E+15
9.5E+01	1.3E+11	1.8E+11	2.4E+11	3.2E+11	4.3E+11	5.8E+11	7.6E+11	1.0E+12	1.3E+12	1.8E+12	2.3E+12	3.0E+12	3.9E+12	5.1E+12	6.6E+12	8.6E+12	1.1E+13	1.4E+13	1.8E+13	2.4E+13	3.0E+13	3.9E+13	5.0E+13	6.3E+13	8.0E+13
9.6E+01	1.6E+10	2.0E+10	2.6E+10	3.4E+10	4.5E+10	5.7E+10	7.4E+10	9.5E+10	1.2E+11	1.6E+11	2.0E+11	2.5E+11	3.2E+11	4.0E+11	5.1E+11	6.5E+11	8.1E+11	1.0E+12	1.3E+12	1.6E+12	2.0E+12	2.5E+12	3.1E+12	3.8E+12	4.8E+12
9.7E+01	1.3E+09	1.6E+09	2.1E+09	2.6E+09	3.2E+09	4.0E+09	5.0E+09	6.3E+09	7.8E+09	9.6E+09	1.2E+10	1.5E+10	1.8E+10	2.2E+10	2.7E+10	3.3E+10	4.0E+10	4.9E+10	6.0E+10	7.3E+10	8.8E+10	1.1E+11	1.3E+11	1.6E+11	1.9E+11
9.8E+01	6.7E+07	8.2E+07	9.9E+07	1.2E+08	1.4E+08	1.7E+08	2.1E+08	2.5E+08	3.0E+08	3.6E+08	4.3E+08	5.1E+08	6.0E+08	7.1E+08	8.4E+08	1.0E+09	1.2E+09	1.4E+09	1.6E+09	1.9E+09	2.2E+09	2.6E+09	3.1E+09	3.6E+09	4.2E+09
9.9E+01	1.7E+06	2.0E+06	2.3E+06	2.6E+06	3.0E+06	3.5E+06	4.0E+06	4.6E+06	5.2E+06	6.0E+06	6.8E+06	7.8E+06	8.9E+06	1.0E+07	1.1E+07	1.3E+07	1.5E+07	1.7E+07	1.9E+07	2.1E+07	2.4E+07	2.7E+07	3.0E+07	3.4E+07	3.8E+07
1.0E+02	1.0E+04	1.1E+04	1.2E+04	1.3E+04	1.5E+04	1.6E+04	1.7E+04	1.9E+04	2.0E+04	2.2E+04	2.4E+04	2.6E+04	2.8E+04	3.0E+04	3.2E+04	3.4E+04	3.7E+04	4.0E+04	4.3E+04	4.6E+04	4.9E+04	5.2E+04	5.6E+04	6.0E+04	6.4E+04

K_{2y}	K_1x = 76	77	78	79	80	81	82	83	84	85	86	87
1.0E+00	9.8E+32	2.7E+33	7.2E+33	1.9E+34	5.2E+34	1.4E+35	3.7E+35	1.0E+36	2.7E+36	7.2E+36	1.9E+37	5.1E+37
2.0E+00	9.8E+32	2.6E+33	7.1E+33	1.9E+34	5.1E+34	1.4E+35	3.7E+35	9.9E+35	2.6E+36	7.0E+36	1.9E+37	5.0E+37
3.0E+00	9.7E+32	2.6E+33	7.0E+33	1.9E+34	5.1E+34	1.4E+35	3.6E+35	9.7E+35	2.6E+36	6.9E+36	1.8E+37	4.9E+37
4.0E+00	9.6E+32	2.6E+33	7.0E+33	1.9E+34	5.0E+34	1.3E+35	3.6E+35	9.6E+35	2.5E+36	6.7E+36	1.8E+37	4.7E+37
5.0E+00	9.6E+32	2.6E+33	6.9E+33	1.8E+34	4.9E+34	1.3E+35	3.5E+35	9.4E+35	2.5E+36	6.6E+36	1.7E+37	4.6E+37
6.0E+00	9.5E+32	2.5E+33	6.8E+33	1.8E+34	4.9E+34	1.3E+35	3.4E+35	9.2E+35	2.4E+36	6.4E+36	1.7E+37	4.5E+37
7.0E+00	9.4E+32	2.5E+33	6.7E+33	1.8E+34	4.8E+34	1.3E+35	3.4E+35	8.9E+35	2.4E+36	6.2E+36	1.6E+37	4.3E+37
8.0E+00	9.2E+32	2.5E+33	6.6E+33	1.8E+34	4.7E+34	1.2E+35	3.3E+35	8.7E+35	2.3E+36	6.1E+36	1.6E+37	4.2E+37
9.0E+00	9.1E+32	2.4E+33	6.5E+33	1.7E+34	4.6E+34	1.2E+35	3.2E+35	8.5E+35	2.2E+36	5.9E+36	1.5E+37	4.0E+37
1.0E+01	9.0E+32	2.4E+33	6.4E+33	1.7E+34	4.5E+34	1.2E+35	3.1E+35	8.2E+35	2.2E+36	5.6E+36	1.5E+37	3.8E+37
1.1E+01	8.8E+32	2.3E+33	6.2E+33	1.6E+34	4.4E+34	1.2E+35	3.0E+35	7.9E+35	2.1E+36	5.4E+36	1.4E+37	3.7E+37
1.2E+01	8.6E+32	2.3E+33	6.1E+33	1.6E+34	4.2E+34	1.1E+35	2.9E+35	7.7E+35	2.0E+36	5.2E+36	1.3E+37	3.5E+37
1.3E+01	8.5E+32	2.2E+33	5.9E+33	1.6E+34	4.1E+34	1.1E+35	2.8E+35	7.4E+35	1.9E+36	5.0E+36	1.3E+37	3.3E+37
1.4E+01	8.3E+32	2.2E+33	5.8E+33	1.5E+34	4.0E+34	1.0E+35	2.7E+35	7.1E+35	1.8E+36	4.7E+36	1.2E+37	3.1E+37
1.5E+01	8.0E+32	2.1E+33	5.6E+33	1.5E+34	3.8E+34	1.0E+35	2.6E+35	6.7E+35	1.7E+36	4.5E+36	1.1E+37	2.9E+37
1.6E+01	7.8E+32	2.1E+33	5.4E+33	1.4E+34	3.7E+34	9.6E+34	2.5E+35	6.4E+35	1.6E+36	4.2E+36	1.1E+37	2.8E+37
1.7E+01	7.6E+32	2.0E+33	5.2E+33	1.4E+34	3.5E+34	9.1E+34	2.4E+35	6.1E+35	1.6E+36	4.0E+36	1.0E+37	2.6E+37
1.8E+01	7.3E+32	1.9E+33	5.0E+33	1.3E+34	3.4E+34	8.7E+34	2.2E+35	5.7E+35	1.5E+36	3.7E+36	9.5E+36	2.4E+37
1.9E+01	7.1E+32	1.8E+33	4.8E+33	1.2E+34	3.2E+34	8.2E+34	2.1E+35	5.4E+35	1.4E+36	3.5E+36	8.8E+36	2.2E+37
2.0E+01	6.8E+32	1.8E+33	4.6E+33	1.2E+34	3.0E+34	7.8E+34	2.0E+35	5.0E+35	1.3E+36	3.2E+36	8.1E+36	2.0E+37
2.1E+01	6.5E+32	1.7E+33	4.3E+33	1.1E+34	2.9E+34	7.3E+34	1.9E+35	4.7E+35	1.2E+36	3.0E+36	7.5E+36	1.9E+37
2.2E+01	6.2E+32	1.6E+33	4.1E+33	1.0E+34	2.7E+34	6.8E+34	1.7E+35	4.4E+35	1.1E+36	2.7E+36	6.9E+36	1.7E+37
2.3E+01	5.9E+32	1.5E+33	3.9E+33	9.9E+33	2.5E+34	6.3E+34	1.6E+35	4.0E+35	1.0E+36	2.5E+36	6.3E+36	1.5E+37
2.4E+01	5.6E+32	1.4E+33	3.6E+33	9.2E+33	2.3E+34	5.9E+34	1.5E+35	3.7E+35	9.2E+35	2.3E+36	5.7E+36	1.4E+37
2.5E+01	5.2E+32	1.3E+33	3.4E+33	8.6E+33	2.2E+34	5.4E+34	1.4E+35	3.4E+35	8.4E+35	2.1E+36	5.1E+36	1.3E+37
2.6E+01	4.9E+32	1.2E+33	3.1E+33	7.9E+33	2.0E+34	5.0E+34	1.2E+35	3.1E+35	7.6E+35	1.9E+36	4.6E+36	1.1E+37
2.7E+01	4.6E+32	1.2E+33	2.9E+33	7.3E+33	1.8E+34	4.5E+34	1.1E+35	2.8E+35	6.8E+35	1.7E+36	4.1E+36	9.9E+36
2.8E+01	4.2E+32	1.1E+33	2.7E+33	6.7E+33	1.7E+34	4.1E+34	1.0E+35	2.5E+35	6.1E+35	1.5E+36	3.6E+36	8.7E+36
2.9E+01	3.9E+32	9.8E+32	2.5E+33	6.1E+33	1.5E+34	3.7E+34	9.1E+34	2.2E+35	5.4E+35	1.3E+36	3.2E+36	7.6E+36
3.0E+01	3.6E+32	9.0E+32	2.2E+33	5.5E+33	1.4E+34	3.3E+34	8.2E+34	2.0E+35	4.8E+35	1.2E+36	2.8E+36	6.6E+36
3.1E+01	3.3E+32	8.2E+32	2.0E+33	5.0E+33	1.2E+34	3.0E+34	7.2E+34	1.8E+35	4.2E+35	1.0E+36	2.4E+36	5.6E+36
3.2E+01	3.0E+32	7.4E+32	1.8E+33	4.5E+33	1.1E+34	2.6E+34	6.4E+34	1.5E+35	3.6E+35	8.6E+35	2.0E+36	4.8E+36
3.3E+01	2.7E+32	6.6E+32	1.6E+33	4.0E+33	9.6E+33	2.3E+34	5.6E+34	1.3E+35	3.1E+35	7.4E+35	1.7E+36	4.1E+36
3.4E+01	2.4E+32	5.9E+32	1.4E+33	3.5E+33	8.4E+33	2.0E+34	4.8E+34	1.1E+35	2.7E+35	6.3E+35	1.5E+36	3.4E+36
3.5E+01	2.2E+32	5.3E+32	1.3E+33	3.1E+33	7.3E+33	1.7E+34	4.1E+34	9.7E+34	2.3E+35	5.3E+35	1.2E+36	2.8E+36
3.6E+01	1.9E+32	4.6E+32	1.1E+33	2.7E+33	6.3E+33	1.5E+34	3.5E+34	8.2E+34	1.9E+35	4.4E+35	1.0E+36	2.3E+36
3.7E+01	1.7E+32	4.1E+32	9.7E+32	2.3E+33	5.4E+33	1.3E+34	3.0E+34	6.9E+34	1.6E+35	3.7E+35	8.4E+35	1.9E+36
3.8E+01	1.5E+32	3.5E+32	8.3E+32	2.0E+33	4.6E+33	1.1E+34	2.5E+34	5.7E+34	1.3E+35	3.0E+35	6.9E+35	1.6E+36
3.9E+01	1.3E+32	3.0E+32	7.1E+32	1.7E+33	3.8E+33	8.9E+33	2.1E+34	4.7E+34	1.1E+35	2.5E+35	5.6E+35	1.3E+36
4.0E+01	1.1E+32	2.6E+32	6.0E+32	1.4E+33	3.2E+33	7.4E+33	1.7E+34	3.9E+34	8.8E+34	2.0E+35	4.5E+35	1.0E+36
4.1E+01	9.2E+31	2.2E+32	5.0E+32	1.2E+33	2.6E+33	6.1E+33	1.4E+34	3.1E+34	7.1E+34	1.6E+35	3.5E+35	7.9E+35
4.2E+01	7.8E+31	1.8E+32	4.1E+32	9.5E+32	2.2E+33	4.9E+33	1.1E+34	2.5E+34	5.6E+34	1.3E+35	2.8E+35	6.2E+35
4.3E+01	6.5E+31	1.5E+32	3.4E+32	7.8E+32	1.8E+33	4.0E+33	8.9E+33	2.0E+34	4.4E+34	9.8E+34	2.2E+35	4.8E+35
4.4E+01	5.3E+31	1.2E+32	2.8E+32	6.3E+32	1.4E+33	3.2E+33	7.1E+33	1.6E+34	3.5E+34	7.6E+34	1.7E+35	3.7E+35
4.5E+01	4.4E+31	9.9E+31	2.2E+32	5.0E+32	1.1E+33	2.5E+33	5.5E+33	1.2E+34	2.7E+34	5.9E+34	1.3E+35	2.8E+35
4.6E+01	3.5E+31	7.9E+31	1.8E+32	4.0E+32	8.8E+32	2.0E+33	4.3E+33	9.4E+33	2.0E+34	4.4E+34	9.6E+34	2.1E+35
4.7E+01	2.8E+31	6.3E+31	1.4E+32	3.1E+32	6.9E+32	1.5E+33	3.3E+33	7.2E+33	1.5E+34	3.3E+34	7.2E+34	1.5E+35
4.8E+01	2.2E+31	5.0E+31	1.1E+32	2.4E+32	5.3E+32	1.2E+33	2.5E+33	5.4E+33	1.2E+34	2.5E+34	5.3E+34	1.1E+35
4.9E+01	1.8E+31	3.9E+31	8.5E+31	1.8E+32	4.0E+32	8.7E+32	1.9E+33	4.0E+33	8.6E+33	1.8E+34	3.8E+34	8.1E+34
5.0E+01	1.4E+31	3.0E+31	6.5E+31	1.4E+32	3.0E+32	6.5E+32	1.4E+33	2.9E+33	6.2E+33	1.3E+34	2.8E+34	5.8E+34

K_{2y}	K_1x = 88	89	90	91	92	93	94	95	96	97	98	99	100
1.0E+00	1.3E+38	3.6E+38	9.5E+38	2.5E+39	6.6E+39	1.7E+40	4.5E+40	1.2E+41	3.1E+41	8.0E+41	2.1E+42	5.4E+42	1.4E+43
2.0E+00	1.3E+38	3.5E+38	9.2E+38	2.4E+39	6.4E+39	1.7E+40	4.3E+40	1.1E+41	2.9E+41	7.6E+41	2.0E+42	5.1E+42	1.3E+43
3.0E+00	1.3E+38	3.4E+38	8.9E+38	2.3E+39	6.1E+39	1.6E+40	4.2E+40	1.1E+41	2.8E+41	7.3E+41	1.9E+42	4.8E+42	1.2E+43
4.0E+00	1.2E+38	3.3E+38	8.6E+38	2.3E+39	5.9E+39	1.5E+40	4.0E+40	1.0E+41	2.7E+41	6.9E+41	1.8E+42	4.5E+42	1.2E+43
5.0E+00	1.2E+38	3.2E+38	8.3E+38	2.2E+39	5.7E+39	1.5E+40	3.8E+40	9.8E+40	2.5E+41	6.5E+41	1.7E+42	4.2E+42	1.1E+43
6.0E+00	1.2E+38	3.1E+38	8.0E+38	2.1E+39	5.4E+39	1.4E+40	3.6E+40	9.3E+40	2.4E+41	6.1E+41	1.6E+42	4.0E+42	1.0E+43
7.0E+00	1.1E+38	2.9E+38	7.7E+38	2.0E+39	5.2E+39	1.3E+40	3.4E+40	8.8E+40	2.2E+41	5.7E+41	1.5E+42	3.7E+42	9.3E+42
8.0E+00	1.1E+38	2.8E+38	7.3E+38	1.9E+39	4.9E+39	1.3E+40	3.2E+40	8.3E+40	2.1E+41	5.4E+41	1.4E+42	3.4E+42	8.6E+42
9.0E+00	1.0E+38	2.7E+38	7.0E+38	1.8E+39	4.6E+39	1.2E+40	3.0E+40	7.7E+40	2.0E+41	5.0E+41	1.3E+42	3.2E+42	7.9E+42
1.0E+01	9.9E+37	2.6E+38	6.6E+38	1.7E+39	4.4E+39	1.1E+40	2.8E+40	7.2E+40	1.8E+41	4.6E+41	1.2E+42	2.9E+42	7.3E+42
1.1E+01	9.5E+37	2.4E+38	6.3E+38	1.6E+39	4.1E+39	1.0E+40	2.7E+40	6.7E+40	1.7E+41	4.3E+41	1.1E+42	2.7E+42	6.6E+42
1.2E+01	9.0E+37	2.3E+38	5.9E+38	1.5E+39	3.8E+39	9.7E+39	2.5E+40	6.2E+40	1.6E+41	3.9E+41	9.8E+41	2.4E+42	6.0E+42
1.3E+01	8.5E+37	2.2E+38	5.6E+38	1.4E+39	3.6E+39	9.0E+39	2.3E+40	5.7E+40	1.4E+41	3.6E+41	8.9E+41	2.2E+42	5.4E+42
1.4E+01	8.0E+37	2.0E+38	5.2E+38	1.3E+39	3.3E+39	8.4E+39	2.1E+40	5.3E+40	1.3E+41	3.3E+41	8.1E+41	2.0E+42	4.9E+42
1.5E+01	7.5E+37	1.9E+38	4.8E+38	1.2E+39	3.1E+39	7.7E+39	1.9E+40	4.8E+40	1.2E+41	2.9E+41	7.3E+41	1.8E+42	4.4E+42
1.6E+01	7.0E+37	1.8E+38	4.5E+38	1.1E+39	2.8E+39	7.1E+39	1.8E+40	4.4E+40	1.1E+41	2.7E+41	6.5E+41	1.6E+42	3.9E+42
1.7E+01	6.5E+37	1.6E+38	4.1E+38	1.0E+39	2.6E+39	6.4E+39	1.6E+40	3.9E+40	9.7E+40	2.4E+41	5.8E+41	1.4E+42	3.4E+42
1.8E+01	6.0E+37	1.5E+38	3.8E+38	9.5E+38	2.4E+39	5.8E+39	1.4E+40	3.6E+40	8.7E+40	2.1E+41	5.1E+41	1.2E+42	3.0E+42
1.9E+01	5.6E+37	1.4E+38	3.5E+38	8.6E+38	2.1E+39	5.3E+39	1.3E+40	3.2E+40	7.7E+40	1.9E+41	4.5E+41	1.1E+42	2.6E+42
2.0E+01	5.1E+37	1.3E+38	3.2E+38	7.8E+38	1.9E+39	4.7E+39	1.2E+40	2.8E+40	6.8E+40	1.6E+41	3.9E+41	9.4E+41	2.2E+42
2.1E+01	4.7E+37	1.2E+38	2.9E+38	7.0E+38	1.7E+39	4.2E+39	1.0E+40	2.5E+40	6.0E+40	1.4E+41	3.4E+41	8.1E+41	1.9E+42
2.2E+01	4.2E+37	1.0E+38	2.6E+38	6.3E+38	1.5E+39	3.7E+39	9.0E+39	2.2E+40	5.2E+40	1.2E+41	2.9E+41	6.9E+41	1.6E+42
2.3E+01	3.8E+37	9.4E+37	2.3E+38	5.6E+38	1.4E+39	3.3E+39	7.9E+39	1.9E+40	4.5E+40	1.1E+41	2.5E+41	5.9E+41	1.4E+42
2.4E+01	3.4E+37	8.4E+37	2.1E+38	5.0E+38	1.2E+39	2.9E+39	6.8E+39	1.6E+40	3.9E+40	9.1E+40	2.1E+41	5.0E+41	1.2E+42
2.5E+01	3.1E+37	7.5E+37	1.8E+38	4.3E+38	1.0E+39	2.5E+39	5.9E+39	1.4E+40	3.3E+40	7.7E+40	1.8E+41	4.2E+41	9.8E+41
2.6E+01	2.7E+37	6.6E+37	1.6E+38	3.8E+38	9.0E+38	2.1E+39	5.1E+39	1.2E+40	2.8E+40	6.5E+40	1.5E+41	3.5E+41	8.1E+41
2.7E+01	2.4E+37	5.7E+37	1.4E+38	3.3E+38	7.7E+38	1.8E+39	4.3E+39	1.0E+40	2.3E+40	5.4E+40	1.3E+41	2.9E+41	6.7E+41
2.8E+01	2.1E+37	5.0E+37	1.2E+38	2.8E+38	6.6E+38	1.6E+39	3.6E+39	8.4E+39	2.0E+40	4.5E+40	1.0E+41	2.4E+41	5.4E+41
2.9E+01	1.8E+37	4.3E+37	1.0E+38	2.4E+38	5.6E+38	1.3E+39	3.0E+39	7.0E+39	1.6E+40	3.7E+40	8.5E+40	1.9E+41	4.4E+41
3.0E+01	1.6E+37	3.7E+37	8.6E+37	2.0E+38	4.7E+38	1.1E+39	2.5E+39	5.8E+39	1.3E+40	3.1E+40	6.9E+40	1.6E+41	3.6E+41
3.1E+01	1.3E+37	3.1E+37	7.3E+37	1.7E+38	3.9E+38	9.1E+38	2.1E+39	4.8E+39	1.1E+40	2.5E+40	5.6E+40	1.3E+41	2.8E+41
3.2E+01	1.1E+37	2.6E+37	6.1E+37	1.4E+38	3.3E+38	7.5E+38	1.7E+39	3.9E+39	8.8E+39	2.0E+40	4.5E+40	1.0E+41	2.2E+41
3.3E+01	9.5E+36	2.2E+37	5.1E+37	1.2E+38	2.7E+38	6.1E+38	1.4E+39	3.1E+39	7.1E+39	1.6E+40	3.6E+40	7.9E+40	1.8E+41
3.4E+01	7.9E+36	1.8E+37	4.2E+37	9.6E+37	2.2E+38	5.0E+38	1.1E+39	2.5E+39	5.6E+39	1.3E+40	2.8E+40	6.2E+40	1.4E+41
3.5E+01	6.6E+36	1.5E+37	3.4E+37	7.8E+37	1.8E+38	4.0E+38	8.9E+38	2.0E+39	4.5E+39	9.9E+39	2.2E+40	4.8E+40	1.1E+41
3.6E+01	5.4E+36	1.2E+37	2.8E+37	6.3E+37	1.4E+38	3.2E+38	7.1E+38	1.6E+39	3.5E+39	7.7E+39	1.7E+40	3.7E+40	8.0E+40
3.7E+01	4.4E+36	9.9E+36	2.2E+37	5.0E+37	1.1E+38	2.5E+38	5.5E+38	1.2E+39	2.7E+39	5.9E+39	1.3E+40	2.8E+40	6.1E+40
3.8E+01	3.5E+36	7.9E+36	1.8E+37	4.0E+37	8.8E+37	2.0E+38	4.3E+38	9.5E+38	2.1E+39	4.5E+39	9.8E+39	2.1E+40	4.5E+40
3.9E+01	2.8E+36	6.3E+36	1.4E+37	3.1E+37	6.9E+37	1.5E+38	3.3E+38	7.2E+38	1.6E+39	3.4E+39	7.3E+39	1.6E+40	3.4E+40
4.0E+01	2.2E+36	5.0E+36	1.1E+37	2.4E+37	5.3E+37	1.2E+38	2.5E+38	5.5E+38	1.2E+39	2.5E+39	5.4E+39	1.2E+40	2.5E+40
4.1E+01	1.7E+36	3.9E+36	8.5E+36	1.9E+37	4.1E+37	8.8E+37	1.9E+38	4.1E+38	8.8E+38	1.9E+39	4.0E+39	8.5E+39	1.8E+40
4.2E+01	1.4E+36	3.0E+36	6.5E+36	1.4E+37	3.1E+37	6.6E+37	1.4E+38	3.0E+38	6.5E+38	1.4E+39	2.9E+39	6.1E+39	1.3E+40
4.3E+01	1.0E+36	2.3E+36	4.9E+36	1.1E+37	2.3E+37	4.9E+37	1.0E+38	2.2E+38	4.7E+38	1.0E+39	2.1E+39	4.4E+39	9.1E+39
4.4E+01	7.9E+35	1.7E+36	3.7E+36	7.9E+36	1.7E+37	3.6E+37	7.7E+37	1.6E+38	3.4E+38	7.1E+38	1.5E+39	3.1E+39	6.4E+39
4.5E+01	6.0E+35	1.3E+36	2.7E+36	5.8E+36	1.2E+37	2.6E+37	5.5E+37	1.2E+38	2.4E+38	5.0E+38	1.0E+39	2.2E+39	4.4E+39
4.6E+01	4.4E+35	9.5E+35	2.0E+36	4.3E+36	9.0E+36	1.9E+37	3.9E+37	8.2E+37	1.7E+38	3.5E+38	7.3E+38	1.5E+39	3.0E+39
4.7E+01	3.3E+35	6.9E+35	1.5E+36	3.1E+36	6.4E+36	1.3E+37	2.8E+37	5.7E+37	1.2E+38	2.4E+38	5.0E+38	1.0E+39	2.1E+39
4.8E+01	2.4E+35	5.0E+35	1.0E+36	2.2E+36	4.5E+36	9.4E+36	1.9E+37	4.0E+37	8.1E+37	1.7E+38	3.4E+38	6.8E+38	1.4E+39
4.9E+01	1.7E+35	3.5E+35	7.4E+35	1.5E+36	3.2E+36	6.5E+36	1.3E+37	2.7E+37	5.5E+37	1.1E+38	2.2E+38	4.5E+38	9.1E+38
5.0E+01	1.2E+35	2.5E+35	5.1E+35	1.1E+36	2.2E+36	4.4E+36	9.0E+36	1.8E+37	3.7E+37	7.4E+37	1.5E+38	3.0E+38	5.9E+38

		$K_{1}x$																								
		76	77	78	79	80	81	82	83	84	85	86	87	88	89	90	91	92	93	94	95	96	97	98	99	100
K_{2y}	5.1E+01	1.0E+31	2.3E+31	4.9E+31	1.0E+32	2.2E+32	4.8E+32	1.0E+33	2.1E+33	4.5E+33	9.4E+33	2.0E+34	4.1E+34	8.4E+34	1.7E+35	3.5E+35	7.2E+35	1.5E+36	3.0E+36	6.0E+36	1.2E+37	2.4E+37	4.8E+37	9.6E+37	1.9E+38	3.8E+38
	5.2E+01	7.9E+30	1.7E+31	3.6E+31	7.7E+31	1.6E+32	3.5E+32	7.3E+32	1.5E+33	3.2E+33	6.6E+33	1.4E+34	2.8E+34	5.8E+34	1.2E+35	2.4E+35	4.9E+35	9.9E+35	2.0E+36	4.0E+36	7.9E+36	1.6E+37	3.1E+37	6.2E+37	1.2E+38	2.4E+38
	5.3E+01	5.9E+30	1.3E+31	2.7E+31	5.6E+31	1.2E+32	2.5E+32	5.2E+32	1.1E+33	2.2E+33	4.6E+33	9.5E+33	1.9E+34	3.9E+34	8.0E+34	1.6E+35	3.2E+35	6.5E+35	1.3E+36	2.6E+36	5.1E+36	1.0E+37	2.0E+37	3.9E+37	7.6E+37	1.5E+38
	5.4E+01	4.3E+30	9.2E+30	1.9E+31	4.1E+31	8.5E+31	1.8E+32	3.7E+32	7.5E+32	1.5E+33	3.2E+33	6.5E+33	1.3E+34	2.6E+34	5.3E+34	1.1E+35	2.1E+35	4.2E+35	8.4E+35	1.7E+36	3.3E+36	6.4E+36	1.2E+37	2.4E+37	4.7E+37	9.1E+37
	5.5E+01	3.1E+30	6.6E+30	1.4E+31	2.9E+31	6.0E+31	1.2E+32	2.5E+32	5.2E+32	1.1E+33	2.1E+33	4.3E+33	8.7E+33	1.7E+34	3.5E+34	6.9E+34	1.4E+35	2.7E+35	5.3E+35	1.0E+36	2.0E+36	4.0E+36	7.7E+36	1.5E+37	2.9E+37	5.5E+37
	5.6E+01	2.3E+30	4.7E+30	9.8E+30	2.0E+31	4.1E+31	8.5E+31	1.7E+32	3.5E+32	7.1E+32	1.4E+33	2.9E+33	5.7E+33	1.1E+34	2.2E+34	4.4E+34	8.7E+34	1.7E+35	3.3E+35	6.5E+35	1.3E+36	2.4E+36	4.7E+36	8.9E+36	1.7E+37	3.2E+37
	5.7E+01	1.6E+30	3.3E+30	6.8E+30	1.4E+31	2.8E+31	5.7E+31	1.2E+32	2.3E+32	4.7E+32	9.4E+32	1.9E+33	3.7E+33	7.3E+33	1.4E+34	2.8E+34	5.4E+34	1.1E+35	2.0E+35	4.0E+35	7.6E+35	1.5E+36	2.8E+36	5.3E+36	1.0E+37	1.9E+37
	5.8E+01	1.1E+30	2.3E+30	4.6E+30	9.4E+30	1.9E+31	3.8E+31	7.7E+31	1.5E+32	3.1E+32	6.0E+32	1.2E+33	2.3E+33	4.6E+33	8.9E+33	1.7E+34	3.3E+34	6.5E+34	1.2E+35	2.4E+35	4.5E+35	8.6E+35	1.6E+36	3.1E+36	5.8E+36	1.1E+37
	5.9E+01	7.6E+29	1.5E+30	3.1E+30	6.3E+30	1.3E+31	2.5E+31	5.0E+31	9.9E+31	2.0E+32	3.8E+32	7.5E+32	1.5E+33	2.8E+33	5.5E+33	1.1E+34	2.0E+34	3.9E+34	7.4E+34	1.4E+35	2.6E+35	5.0E+35	9.4E+35	1.8E+36	3.3E+36	6.1E+36
	6.0E+01	5.1E+29	1.0E+30	2.1E+30	4.1E+30	8.2E+30	1.6E+31	3.2E+31	6.3E+31	1.2E+32	2.4E+32	4.6E+32	8.9E+32	1.7E+33	3.3E+33	6.3E+33	1.2E+34	2.3E+34	4.3E+34	8.1E+34	1.5E+35	2.8E+35	5.3E+35	9.8E+35	1.8E+36	3.4E+36
	6.1E+01	3.4E+29	6.8E+29	1.3E+30	2.7E+30	5.2E+30	1.0E+31	2.0E+31	3.9E+31	7.6E+31	1.5E+32	2.8E+32	5.4E+32	1.0E+33	2.0E+33	3.7E+33	7.0E+33	1.3E+34	2.5E+34	4.6E+34	8.5E+34	1.6E+35	2.9E+35	5.4E+35	9.9E+35	1.8E+36
	6.2E+01	2.2E+29	4.4E+29	8.6E+29	1.7E+30	3.3E+30	6.4E+30	1.2E+31	2.4E+31	4.6E+31	8.8E+31	1.7E+32	3.2E+32	6.0E+32	1.1E+33	2.1E+33	4.0E+33	7.4E+33	1.4E+34	2.6E+34	4.7E+34	8.7E+34	1.6E+35	2.9E+35	5.3E+35	9.6E+35
	6.3E+01	1.4E+29	2.8E+29	5.4E+29	1.0E+30	2.0E+30	3.9E+30	7.5E+30	1.4E+31	2.7E+31	5.2E+31	9.8E+31	1.8E+32	3.5E+32	6.5E+32	1.2E+33	2.2E+33	4.1E+33	7.6E+33	1.4E+34	2.6E+34	4.7E+34	8.5E+34	1.5E+35	2.8E+35	5.0E+35
	6.4E+01	8.9E+28	1.7E+29	3.3E+29	6.4E+29	1.2E+30	2.3E+30	4.5E+30	8.4E+30	1.6E+31	3.0E+31	5.6E+31	1.0E+32	1.9E+32	3.6E+32	6.6E+32	1.2E+33	2.2E+33	4.1E+33	7.4E+33	1.3E+34	2.4E+34	4.4E+34	7.9E+34	1.4E+35	2.5E+35
	6.5E+01	5.4E+28	1.0E+29	2.0E+29	3.8E+29	7.3E+29	1.4E+30	2.6E+30	4.9E+30	9.1E+30	1.7E+31	3.1E+31	5.8E+31	1.1E+32	2.0E+32	3.6E+32	6.5E+32	1.2E+33	2.2E+33	3.9E+33	7.0E+33	1.3E+34	2.2E+34	4.0E+34	7.1E+34	1.3E+35
	6.6E+01	3.3E+28	6.2E+28	1.2E+29	2.2E+29	4.2E+29	7.9E+29	1.5E+30	2.7E+30	5.1E+30	9.4E+30	1.7E+31	3.2E+31	5.8E+31	1.0E+32	1.9E+32	3.4E+32	6.2E+32	1.1E+33	2.0E+33	3.5E+33	6.3E+33	1.1E+34	2.0E+34	3.5E+34	6.1E+34
	6.7E+01	1.9E+28	3.6E+28	6.8E+28	1.3E+29	2.4E+29	4.4E+29	8.2E+29	1.5E+30	2.8E+30	5.1E+30	9.2E+30	1.7E+31	3.0E+31	5.4E+31	9.8E+31	1.8E+32	3.1E+32	5.6E+32	9.8E+32	1.7E+33	3.1E+33	5.4E+33	9.4E+33	1.6E+34	2.9E+34
	6.8E+01	1.1E+28	2.1E+28	3.9E+28	7.2E+28	1.3E+29	2.4E+29	4.4E+29	8.1E+29	1.5E+30	2.7E+30	4.8E+30	8.7E+30	1.6E+31	2.8E+31	4.9E+31	8.7E+31	1.5E+32	2.7E+32	4.8E+32	8.4E+32	1.5E+33	2.5E+33	4.4E+33	7.6E+33	1.3E+34
	6.9E+01	6.3E+27	1.2E+28	2.1E+28	3.9E+28	7.1E+28	1.3E+29	2.4E+29	4.3E+29	7.7E+29	1.4E+30	2.5E+30	4.4E+30	7.8E+30	1.4E+31	2.4E+31	4.2E+31	7.4E+31	1.3E+32	2.3E+32	3.9E+32	6.8E+32	1.2E+33	2.0E+33	3.4E+33	5.9E+33
	7.0E+01	3.4E+27	6.3E+27	1.1E+28	2.1E+28	3.8E+28	6.8E+28	1.2E+29	2.2E+29	3.9E+29	6.9E+29	1.2E+30	2.1E+30	3.8E+30	6.6E+30	1.2E+31	2.0E+31	3.5E+31	6.0E+31	1.0E+32	1.8E+32	3.0E+32	5.2E+32	8.9E+32	1.5E+33	2.6E+33
	7.1E+01	1.8E+27	3.3E+27	6.0E+27	1.1E+28	1.9E+28	3.4E+28	6.1E+28	1.1E+29	1.9E+29	3.4E+29	5.9E+29	1.0E+30	1.8E+30	3.1E+30	5.3E+30	9.2E+30	1.6E+31	2.7E+31	4.6E+31	7.9E+31	1.3E+32	2.3E+32	3.8E+32	6.4E+32	1.1E+33
	7.2E+01	9.6E+26	1.7E+27	3.1E+27	5.4E+27	9.6E+27	1.7E+28	3.0E+28	5.2E+28	9.1E+28	1.6E+29	2.8E+29	4.8E+29	8.2E+29	1.4E+30	2.4E+30	4.1E+30	7.0E+30	1.2E+31	2.0E+31	3.4E+31	5.7E+31	9.5E+31	1.6E+32	2.6E+32	4.4E+32
	7.3E+01	4.8E+26	8.6E+26	1.5E+27	2.7E+27	4.7E+27	8.1E+27	1.4E+28	2.5E+28	4.2E+28	7.3E+28	1.3E+29	2.1E+29	3.6E+29	6.2E+29	1.0E+30	1.8E+30	3.0E+30	5.0E+30	8.4E+30	1.4E+31	2.3E+31	3.9E+31	6.4E+31	1.1E+32	1.7E+32
	7.4E+01	2.4E+26	4.1E+26	7.2E+26	1.3E+27	2.2E+27	3.8E+27	6.5E+27	1.1E+28	1.9E+28	3.2E+28	5.5E+28	9.3E+28	1.6E+29	2.6E+29	4.4E+29	7.4E+29	1.2E+30	2.0E+30	3.4E+30	5.6E+30	9.2E+30	1.5E+31	2.5E+31	4.1E+31	6.6E+31
	7.5E+01	1.1E+26	1.9E+26	3.4E+26	5.8E+26	9.9E+26	1.7E+27	2.9E+27	4.9E+27	8.3E+27	1.4E+28	2.3E+28	3.9E+28	6.5E+28	1.1E+29	1.8E+29	3.0E+29	4.9E+29	8.1E+29	1.3E+30	2.2E+30	3.5E+30	5.7E+30	9.3E+30	1.5E+31	2.4E+31
	7.6E+01	5.1E+25	8.8E+25	1.5E+26	2.6E+26	4.3E+26	7.3E+26	1.2E+27	2.1E+27	3.5E+27	5.8E+27	9.6E+27	1.6E+28	2.6E+28	4.3E+28	7.1E+28	1.2E+29	1.9E+29	3.1E+29	5.0E+29	8.0E+29	1.3E+30	2.1E+30	3.4E+30	5.4E+30	8.6E+30
	7.7E+01	2.3E+25	3.9E+25	6.5E+25	1.1E+26	1.8E+26	3.1E+26	5.1E+26	8.4E+26	1.4E+27	2.3E+27	3.8E+27	6.2E+27	1.0E+28	1.6E+28	2.7E+28	4.3E+28	7.0E+28	1.1E+29	1.8E+29	2.9E+29	4.6E+29	7.3E+29	1.2E+30	1.8E+30	2.9E+30
	7.8E+01	9.7E+24	1.6E+25	2.7E+25	4.5E+25	7.4E+25	1.2E+26	2.0E+26	3.3E+26	5.4E+26	8.8E+26	1.4E+27	2.3E+27	3.7E+27	6.0E+27	9.6E+27	1.5E+28	2.5E+28	3.9E+28	6.2E+28	9.8E+28	1.6E+29	2.4E+29	3.8E+29	6.0E+29	9.4E+29
	7.9E+01	4.0E+24	6.5E+24	1.1E+25	1.8E+25	2.9E+25	4.7E+25	7.6E+25	1.2E+26	2.0E+26	3.2E+26	5.2E+26	8.3E+26	1.3E+27	2.1E+27	3.3E+27	5.3E+27	8.3E+27	1.3E+28	2.1E+28	3.2E+28	5.0E+28	7.8E+28	1.2E+29	1.9E+29	2.9E+29
	8.0E+01	1.5E+24	2.5E+24	4.1E+24	6.6E+24	1.1E+25	1.7E+25	2.8E+25	4.4E+25	7.1E+25	1.1E+26	1.8E+26	2.8E+26	4.4E+26	7.0E+26	1.1E+27	1.7E+27	2.7E+27	4.2E+27	6.4E+27	1.0E+28	1.5E+28	2.4E+28	3.6E+28	5.6E+28	8.5E+28
	8.1E+01	5.8E+23	9.3E+23	1.5E+24	2.4E+24	3.8E+24	6.0E+24	9.6E+24	1.5E+25	2.4E+25	3.7E+25	5.9E+25	9.2E+25	1.4E+26	2.2E+26	3.4E+26	5.3E+26	8.2E+26	1.3E+27	1.9E+27	2.9E+27	4.5E+27	6.8E+27	1.0E+28	1.6E+28	2.4E+28
	8.2E+01	2.0E+23	3.2E+23	5.1E+23	8.1E+23	1.3E+24	2.0E+24	3.1E+24	4.9E+24	7.6E+24	1.2E+25	1.8E+25	2.8E+25	4.3E+25	6.6E+25	1.0E+26	1.5E+26	2.4E+26	3.6E+26	5.4E+26	8.2E+26	1.2E+27	1.9E+27	2.8E+27	4.2E+27	6.2E+27
	8.3E+01	6.9E+22	1.1E+23	1.7E+23	2.6E+23	4.1E+23	6.3E+23	9.7E+23	1.5E+24	2.3E+24	3.5E+24	5.4E+24	8.2E+24	1.2E+25	1.9E+25	2.8E+25	4.3E+25	6.4E+25	9.6E+25	1.4E+26	2.1E+26	3.2E+26	4.7E+26	7.0E+26	1.0E+27	1.5E+27
	8.4E+01	2.2E+22	3.4E+22	5.2E+22	7.9E+22	1.2E+23	1.9E+23	2.8E+23	4.3E+23	6.5E+23	9.8E+23	1.5E+24	2.2E+24	3.3E+24	5.0E+24	7.4E+24	1.1E+25	1.6E+25	2.4E+25	3.6E+25	5.3E+25	7.7E+25	1.1E+26	1.7E+26	2.4E+26	3.5E+26
	8.5E+01	6.4E+21	9.8E+21	1.5E+22	2.2E+22	3.4E+22	5.1E+22	7.7E+22	1.1E+23	1.7E+23	2.6E+23	3.8E+23	5.6E+23	8.3E+23	1.2E+24	1.8E+24	2.6E+24	3.9E+24	5.7E+24	8.2E+24	1.2E+25	1.7E+25	2.5E+25	3.6E+25	5.2E+25	7.6E+25
	8.6E+01	1.8E+21	2.7E+21	4.0E+21	5.9E+21	8.8E+21	1.3E+22	1.9E+22	2.9E+22	4.2E+22	6.2E+22	9.0E+22	1.3E+23	1.9E+23	2.8E+23	4.1E+23	5.9E+23	8.5E+23	1.2E+24	1.8E+24	2.5E+24	3.6E+24	5.2E+24	7.4E+24	1.0E+25	1.5E+25
	8.7E+01	4.5E+20	6.7E+20	9.8E+20	1.4E+21	2.1E+21	3.1E+21	4.5E+21	6.6E+21	9.5E+21	1.4E+22	2.0E+22	2.9E+22	4.1E+22	5.9E+22	8.4E+22	1.2E+23	1.7E+23	2.4E+23	3.4E+23	4.9E+23	6.9E+23	9.7E+23	1.4E+24	1.9E+24	2.7E+24
	8.8E+01	1.1E+20	1.5E+20	2.2E+20	3.2E+20	4.7E+20	6.7E+20	9.6E+20	1.4E+21	2.0E+21	2.8E+21	4.0E+21	5.6E+21	8.0E+21	1.1E+22	1.6E+22	2.2E+22	3.1E+22	4.4E+22	6.1E+22	8.5E+22	1.2E+23	1.6E+23	2.3E+23	3.2E+23	4.4E+23
	8.9E+01	2.2E+19	3.2E+19	4.6E+19	6.5E+19	9.2E+19	1.3E+20	1.8E+20	2.6E+20	3.7E+20	5.1E+20	7.2E+20	1.0E+21	1.4E+21	1.9E+21	2.7E+21	3.7E+21	5.1E+21	7.1E+21	9.7E+21	1.3E+22	1.8E+22	2.5E+22	3.4E+22	4.7E+22	6.4E+22
	9.0E+01	4.3E+18	6.0E+18	8.4E+18	1.2E+19	1.6E+19	2.3E+19	3.2E+19	4.4E+19	6.1E+19	8.4E+19	1.2E+20	1.6E+20	2.2E+20	3.0E+20	4.0E+20	5.5E+20	7.5E+20	1.0E+21	1.4E+21	1.9E+21	2.5E+21	3.4E+21	4.5E+21	6.1E+21	8.2E+21
	9.1E+01	7.2E+17	9.9E+17	1.4E+18	1.9E+18	2.6E+18	3.5E+18	4.8E+18	6.5E+18	8.8E+18	1.2E+19	1.6E+19	2.2E+19	2.9E+19	4.0E+19	5.3E+19	7.1E+19	9.5E+19	1.3E+20	1.7E+20	2.2E+20	3.0E+20	3.9E+20	5.2E+20	6.9E+20	9.1E+20
	9.2E+01	1.0E+17	1.4E+17	1.9E+17	2.6E+17	3.5E+17	4.6E+17	6.2E+17	8.3E+17	1.1E+18	1.5E+18	2.0E+18	2.6E+18	3.4E+18	4.5E+18	6.0E+18	7.8E+18	1.0E+19	1.3E+19	1.8E+19	2.3E+19	3.0E+19	3.9E+19	5.1E+19	6.6E+19	8.6E+19
	9.3E+01	1.3E+16	1.7E+16	2.3E+16	3.0E+16	3.9E+16	5.2E+16	6.8E+16	8.9E+16	1.2E+17	1.5E+17	2.0E+17	2.6E+17	3.3E+17	4.3E+17	5.6E+17	7.2E+17	9.3E+17	1.2E+18	1.5E+18	2.0E+18	2.5E+18	3.2E+18	4.1E+18	5.2E+18	6.7E+18
	9.4E+01	1.3E+15	1.7E+15	2.2E+15	2.8E+15	3.6E+15	4.7E+15	6.0E+15	7.7E+15	9.8E+15	1.3E+16	1.6E+16	2.0E+16	2.6E+16	3.3E+16	4.2E+16	5.3E+16	6.7E+16	8.4E+16	1.1E+17	1.3E+17	1.7E+17	2.1E+17	2.6E+17	3.3E+17	4.1E+17
	9.5E+01	1.0E+14	1.3E+14	1.6E+14	2.1E+14	2.6E+14	3.3E+14	4.1E+14	5.2E+14	6.4E+14	8.1E+14	1.0E+15	1.3E+15	1.6E+15	1.9E+15	2.4E+15	3.0E+15	3.7E+15	4.5E+15	5.6E+15	6.9E+15	8.5E+15	1.0E+16	1.3E+16	1.6E+16	1.9E+16
	9.6E+01	5.9E+12	7.3E+12	9.0E+12	1.1E+13	1.4E+13	1.7E+13	2.0E+13	2.5E+13	3.1E+13	3.7E+13	4.5E+13	5.5E+13	6.7E+13	8.1E+13	9.9E+13	1.2E+14	1.4E+14	1.7E+14	2.1E+14	2.5E+14	3.0E+14	3.6E+14	4.4E+14	5.2E+14	6.3E+14
	9.7E+01	2.3E+11	2.7E+11	3.3E+11	3.9E+11	4.7E+11	5.6E+11	6.6E+11	7.9E+11	9.4E+11	1.1E+12	1.3E+12	1.6E+12	1.9E+12	2.2E+12	2.6E+12	3.1E+12	3.6E+12	4.2E+12	5.0E+12	5.8E+12	6.9E+12	8.0E+12	9.4E+12	1.1E+13	1.3E+13
	9.8E+01	4.9E+09	5.7E+09	6.6E+09	7.7E+09	8.9E+09	1.0E+10	1.2E+10	1.4E+10	1.6E+10	1.8E+10	2.1E+10	2.4E+10	2.8E+10	3.2E+10	3.6E+10	4.2E+10	4.8E+10	5.5E+10	6.2E+10	7.1E+10	8.1E+10	9.2E+10	1.1E+11	1.2E+11	1.4E+11
	9.9E+01	4.3E+07	4.8E+07	5.4E+07	6.0E+07	6.7E+07	7.5E+07	8.4E+07	9.3E+07	1.0E+08	1.2E+08	1.3E+08	1.4E+08	1.6E+08	1.8E+08	1.9E+08	2.1E+08	2.4E+08	2.6E+08	2.9E+08	3.2E+08	3.5E+08	3.9E+08	4.3E+08	4.7E+08	5.1E+08
	1.0E+02	6.8E+04	7.3E+04	7.8E+04	8.3E+04	8.8E+04	9.4E+04	1.0E+05	1.1E+05	1.1E+05	1.2E+05	1.3E+05	1.3E+05	1.4E+05	1.5E+05	1.6E+05	1.7E+05	1.8E+05	1.9E+05	2.0E+05	2.1E+05	2.2E+05	2.3E+05	2.4E+05	2.6E+05	2.7E+05